Evaluation of the Rheological Properties of Recovered Seal Binders

by

Tanya Lingenfelder

Thesis presented in partial fulfilment of the requirements for the degree of Master of Engineering in the Faculty of Engineering at Stellenbosch University

Supervisor: Prof. K.J Jenkins
Co-Supervisor: Dr. E.S Goosen

April 2022

Declaration

By submitting this thesis electronically, I declare that the entirety of the work contained therein is my own, original work, that I am the sole author thereof (save to the extent explicitly otherwise stated), that reproduction and publication thereof by Stellenbosch University will not infringe any third party rights and that I have not previously in its entirety or in part submitted it for obtaining any qualification.

Date : .....April 2022....

Abstract

Bitumen is a complex material that behaves differently depending on the temperature and loading conditions. The ageing of bitumen is an important consideration that influences the durability of a pavement structure. The South African pavement industry is currently transitioning towards a Performance Grade (PG) specification. The PG specifications were developed in the USA and only provide requirements for the evaluation of bitumen performance in asphalt layers. In South Africa, seals are used more frequently than asphalt. Therefore, there is a necessity to develop a seal binder recovery procedure, to gain insight regarding the rheology of South African seal binders and determine to what extent the PG requirements must be altered in order to be applied to seal binders. This study utilises a recommended seal binder recovery procedure and aim to evaluate the consistency of the rheological properties of the recovered seal binders

The recommended seal binder recovery method was used to extract bitumen from in-situ seal samples. Various laboratory test, such as the Dynamic Shear Rheometer (DSR), Bending Beam Rheometer (BBR), and Fourier-Transform Infrared Spectroscopy (FTIR), were performed to gain an understanding of the physical and chemical performance of the recovered binders. The precision values for penetration and softening point, provided in EN 12697-3 (2013), were used to compare the durability parameters (G-R, G_{vet}, T_{vet}, T_{max}, and ΔT_c) of binders recovered from the same seal.

The durability parameters of younger binders (less than 6 years old) revealed that G-R and T_{vet} experienced the most variability and did not comply with the recommended specifications. The durability parameters of the older binders (6 years +) experienced less variability, since all complied with the recommended specifications. Where variability is present in the 8 mm DSR data, the G-R and T_{vet} did not comply with the proposed evaluation criteria. Similarly, variability in the 25 mm DSR and BBR data corresponded with inconsistencies in T_{max} and ΔT_c values, respectively.

The FTIR absorbance revealed that all of the recovered binders had distinct peaks at two wave numbers (1030 cm^{-1} and 1460 cm^{-1}). The peak areas at 1030 cm^{-1} appeared to correlate for both repeatability and reproducibility samples. The heights of the peaks at 1460 cm^{-1} varied, where binders recovered with a toluene-ethanol blend experienced a lower peak, while binders recovered with trichloroethylene, experienced higher peaks. Binders recovered with the toluene-ethanol blend experienced a peak at 1700 cm^{-1} and a more distinct peak at 1600 cm^{-1}. The wave numbers where binders, recovered using trichloroethylene, experienced peaks varied between 1720 cm^{-1} and 1560 cm^{-1}.

Opsomming

Bitumen is 'n komplekse materiaal wat die vermoë het om verskillend op te tree, afhangende van die temperatuur en ladingstoestand waaraan die materiaal blootgestel is. Die veroudering van bitumen is 'n belangrike faktor wat die duursaamheid van 'n plaveiselstruktuur beïnvloed. Die Suid-Afrikaanse plaveiselbedryf is besig om oor te skakel na 'n Werksverrigtingspesifikasies. Hierdie spesifikasies is in die VSA ontwikkel en verskaf slegs vereistes vir die evaluering van bitumenprestasie in asfaltlae. In Suid-Afrika word seëls meer gereeld as asfalt gebruik. Daarom is daar 'n noodsaaklikheid om 'n seëlbindmiddelherwinningsprosedure te ontwikkel om insig te verkry rakende die reologie van Suid-Afrikaanse seëlbinders en te bepaal tot watter mate die nuwe spesifikasie verander moet word sodat dit op seëlbinders toegepas kan word. Hierdie studie gebruik 'n aanbevole seëlbindmiddelherwinningsprosedure en het ten doel om die konsekwentheid van die reologiese eienskappe van herwonne seëlbinders te evalueer

Die aanbevole seëlbindmiddelherwinningsmetode is gebruik om bitumen uit in-situ seëlmonsters te onttrek. Verskeie laboratoriumtoetse, soos die *Dynamic Shear Rheometer* (DSR), *Bending Beam Rheometer* (BBR), en *Fourier-Transform Infrared Spectroscopy* (FTIR), is uitgevoer om 'n beter begrip van die fisiese en chemiese werkverrigting van die herwonne bindmiddels te verkry. Die evalueringskriteria vir penetrasie en versagtingspunt, soos verskaf in EN 12697-3 (2013), is gebruik om die duursaamheidsparameter (G-R, G_{vet}, T_{vet}, T_{max} en ΔT_c) van bindmiddels, wat van dieselfde seël herwin is, te vergelyk.

Die duursaamheidsparameters van jonger bindmiddels (jonger as 6 jaar oud) toon aan dat G-R en T_{vet} die meeste variasie ervaar het en nie aan die aanbevole spesifikasies voldoen het nie. Dit blyk dat die duursaamheidsparameters van ouer bindmiddels (6 jaar +) minder variasie ervaar, aangesien al die duursaamheidsparameters aan die aanbevole spesifikasies voldoen het. Waar wisselvalligheid in die 8 mm DSR-data voorkom, het G-R en T_{vet} nie aan die aanbevole spesifikasie voldoen nie. Variasie in die 25 mm DSR data stem ooreen met verskille in T_{max}, terwyl variasie in die BBR data korreleer met ΔT_c wat nie aan die aanbevole spesifikasie voldoen nie.

Die FTIR-absorbansie het aangedui dat al die herwonne bindmiddels duidelike pieke by twee golflengtes (1030 cm^{-1} en 1460 cm^{-1}) ervaar. Die piekareas by 1030 cm^{-1} korreleer goed. Die hoogtes van die pieke by 1460 cm^{-1} varieer. Bindmiddels wat met 'n tolueen-etanolmengsel herwin is, ervaar laer pieke, terwyl bindmiddels wat met trichlooretileen herwin is, hoër pieke ervaar. Bindmiddels wat met die tolueen-etanolmengsel herwin is, het 'n piek by 1700 cm^{-1} en 'n meer duidelike piek by 1600 cm^{-1}. Die golfgetalle waar bindmiddels wat met trichlooretileen herwin is, pieke ervaar, wissel tussen 1720 cm^{-1} en 1560 cm^{-1}.

Acknowledgements

The author would like to express sincere gratitude and appreciation to the following people who contributed towards the completion of this thesis:

- Prof Kim Jenkins
- Dr Elaine Goosen
- Much Asphalt for allowing use of their equipment and their Central Laboratory Staff
  (Mr Colin Brooks, Mr Morné Labuschagne, Mrs Firyaal Moos, Mr Siya Sidinile)
- Pavement Laboratory Staff
  (Mr Guillaume Nel and Mr Gaven Williams)

Table of Content

List of Figures

List of Tables

List of Abbreviations

AASHTO	The American Association of State Highway and Transportation Officials
ASTM	American Society for Testing and Materials
BBR	Bending Beam Rheometer
CA	Christensen-Anderson
CAM	Christensen-Anderson-Marasteanu
CSIR	Council of Scientific and Industrial Research
DSR	Dynamic Shear Rheometer
EC	Eastern Cape
FTIR	Fourier-Transform Infrared Spectroscopy
FS	Free-State
GL	Generalised Logistic
G-R	Glower-Rowe parameter
KZN	Kwa-Zulu Natal
LT	Low Temperature Grade
LVE	Linear Viscoelastic
MSCR	Multi-Stress Creep Recovery
NC	Northern Cape
PAV	Pressure Ageing Vessel
Pen	Penetration
PG	Performance Grade

PMB	PolymerModified Binder
PP	Parallel Plate
RTFO	Rolling Thin Film Oven
SABITA	Southern African Bitumen Association
SABS	South African Bureau of Standards
SANRAL	South African National Roads Authority
SANS	South African National Standards
SARA	Saturates, Aromatics, Resins and Asphaltenes
SBR	Styrene-Butadiene-Rubber
SBS	Styrene-Butadiene-Styrene
SS	Standard Sigmoidal
TG	Technical Guideline
TMH	Technical Methods for Highways
TRH	Technical Recommendation for Highways
TTSP	Time Temperature Superposition Principle
USA	United States of America
VET	Viscoelastic Transition
WC	Western Cape
WLF	Williams, Landel and Ferry

List of Symbols

α_T	Horizontal shift factor
β_T	Vertical shift factor
δ (°)	Phase angle
η* (Pa.s)	Complex shear viscosity
η_0 (Pa.s)	Steady state viscosity
ω (rad/s)	Angular frequency
ω_c (rad/s)	Crossover frequency
ω_r (rad/s)	Reduced frequency
v, w	CAM fitting parameters
γ (Pa)	Shear strain
ΔT_c (°C)	Critical low temperature difference
C_1	Arrhenius / WLF/ Kaelble constant
C_2	Arrhenius / WLF/ Kaelble constant
f (Hz)	Loading frequency
f_r (Hz)	Reduced frequency
G (Pa)	Shear relaxation modulus
G" (Pa)	Loss modulus
G* (Pa)	Complex shear modulus
G’ (Pa)	Storage modulus
G_e (Pa)	Equilibrium complex shear modulus
G_g (Pa)	Glassy modulus [Pa]
G-R (kPa)	Glower-Rowe parameter

G_{VET} (Pa)	Viscoelastic transition stiffness
J* (Pa)	Complex shear compliance modulus
J_{nr} (kPa^{-1})	Non-recoverable Creep Compliance
m(t) (Pa/s)	Slope of BBR logarithm stiffness at time (t)
RMSE (%)	Root Mean Square Error
S(t) (Pa)	BBR flexural creep modulus at time (t)
t (s)	Loading time
T (°C)	Testing temperature
T_c (°C)	Critical temperature
T_d (°C)	Defining temperature
T_g (°C)	Glass transition temperature
T_{int} (°C)	Intermediate temperature
T_{max} (°C)	Maximum temperature
T_{min} (°C)	Minimum temperature
T_{ref} (°C)	Reference temperature
T_{VET} (°C)	Viscoelastic transition temperature

Chapter 1: Introduction

1.1 Background

In South Africa, a seal or asphalt is used as a road surfacing. For both seals and asphalt, bitumen is the most essential binding component. At low temperatures and high frequencies, bitumen behaves like an elastic solid, while more liquid, viscous behaviour is experienced at high temperatures and low frequencies. This complex material behaviour is related to the different molecular structures that form the chemical composition of bitumen. Over its lifetime, bitumen is susceptible to ageing, resulting in a harder, more brittle binder, that is prone to cracking. Therefore, it is important to monitor the ageing susceptibility of bitumen, as this contributes towards the service life of the road surface.

Bitumen ageing can be determined from physical or chemical binder properties. Physical properties include penetration, softening point, viscosity, complex modulus, and phase angle. Chemical techniques, such as infra-red analysis, gel permeation chromatography, and SARA (Saturates, Aromatics, Resins and Asphaltenes), are used to link the chemical composition of bitumen to its performance characteristics. By combining both physical and chemical binder properties, the rate and extent of ageing can be monitored, which is useful for pavement management, especially in a country that has a declining road budget. (Connell and Steyn, 2017)

Over the years, various methods have been developed to simulate the field ageing of binders in a laboratory. The goal of these simulations is to predict the chemical and physical changes that bitumen will experience after being exposed to different traffic and climatic conditions. The Rolling Thin-Film Oven (RTFO) test has been proven useful in predicting the short-term ageing, that is typically associated with constructing the road surface. The Pressure Aging Vessel (PAV) is used for long-term ageing. During this ageing test, bitumen is exposed to temperatures and pressures that are much higher than the ambient in-situ conditions. It is possible that these severe conditions cause a chemical reaction to alter the chemical composition of the binder, which would not occur in the field. Therefore, despite various investigations, there is still not sufficient field data available to confirm whether the artificial ageing in the laboratory properly predict the natural ageing that occurs in the field. However,

the required field data can be obtained when in-situ binders are recovered. (Lu, Talon and Redelius, 2008)

The introduction of polymer modified bitumen, technological advances relating to rheological test methods, and changes in traffic volumes and loads, have played a significant role in the evolution of the South African pavement industry. From various premature pavement failures, it soon became clear that the Penetration Grade Specifications was unable to comply with the current industry needs (Bredenhann *et al.*, 2019) . These shortcomings gave rise to the development of a Performance Grade (PG) Specification for bituminous binders in South Africa (SATS 3208), which was introduced in 2016. The PG Specification rely on fundamental engineering properties to determine the actual pavement performance. However, these performance parameters and compliance limits were developed in the United States of America (USA) and only consider the requirements of binder performance in asphalt layers. The challenge is that in South Africa, seals are more commonly used than asphalt. (Bredenhann *et al.*, 2019)

1.2 Problem Statement and Significance

The current performance classification system used in South Africa does not account for seal binders, or South African binders in general. There is a necessity to investigate the rheological performance of South African seal binders, to determine to what extent SATS 3208 must be adjusted and amended, so that the performance requirements can cater for binders used in seals. It is also important to bridge the gap between natural in-situ binder ageing and artificial ageing. In order for this to happen, a seal binder recovery method is needed.

1.3 Goals and Objectives

The primary goal of this study is to evaluate the consistency of rheological properties of recovered seal binders in order to:

- Evaluate acceptable variability in parameters derived from the performance grade specifications,
- Expand standards and specifications specifically for seal binder performance.
- Investigate the relationship between artificial laboratory and in-field ageing, with the intention of gaining beneficial insights of the comparative results.

To achieve this goal, the following objectives need to be satisfied:

1. Recover seal binders from existing road surfaces, in order to understand the rate of ageing of bitumen and its influence on changes in rheology.
2. Conduct rheological tests to obtain the relevant performance data to assist in developing durability parameters.
3. Evaluate the consistency of the results by comparing performance properties of samples recovered from the same study and samples recovered from previous studies, using a chosen repeatability and reproducibility criteria.
4. Assess the variation in durability parameters to establish benchmarks for performance related parameters.
5. Analyse the molecular changes due to ageing and the impact of the extraction-recovery process by conducting FTIR analysis of recovered binders, with the intention of using these tools to gain improved insights based on chemistry principles.

1.4 Scope and Limitations

The seal samples that were used were retrieved before the commencement date of this study. These seal samples vary in terms of surfacing type (single, double, multiple and Cape seals), binder type (70/100, S-E1, and SC-E2), and surfacing age. Traffic and climate variability are not considered.

The extent of rheological testing is mainly dependent on the amount of binder recovered during the seal binder recovery procedure. The availability of equipment and seal specifications and guidelines are also identified as factors to influence the outcome of this study. The scope of rheological testing is developed to include physical tests (Dynamic Shear Rheometer and Bending Beam Rheometer), chemical analysis (Fourier-Transform Infrared Spectroscopy), and quality control tests (mass change and Ash Content). Due to time and test constraints, it was not possible to determine the ash content of each recovery.

Five durability parameters, namely the G-R parameter, G_{vet}, T_{vet}, ΔT_c, and T_{max}, are used to evaluate the rheology of the recovered binders. The evaluation of the seal binder recovery procedure is not limited to indicators and parameters that are only used in the PG Specifications.

1.5 Thesis Overview and Layout

This thesis comprises of 5 chapters, with each chapter contributing towards achieving the goals and objectives, as mentioned in Chapter 1.3. An overview of each chapter is given below:

1. Introduction: Indicated the circumstances that led to the significance of this research. The scope of the investigation is determined from the goals, objectives, and limitations.
2. Literature Study: Introduces concepts relating to bitumen, seals, and the PG Specification. Background relating to binder recovery, testing, and modelling is examined and linked to durability parameters.
3. Methodology: Explains the procedures followed in order to complete this study. Actions, decisions, and reasoning regarding the execution of tests, the calculation of the durability parameters, as well as the sequence in which the data will be presented, is also provided.
4. Results and Discussion: Provides, presents, and analyses the results obtained from the tests. The results from the quality control tests will be used to determine the efficiency of the seal binder recovery method, while the durability parameters will consider the variability within the data. The FTIR analysis will consider any molecular changes that could result from the extraction-recovery process.
5. Conclusion and Recommendations: The conclusions drawn from pertinent findings, including recommendations for future research is presented.

A summary of the appendices:

A. Repeatability and Reproducibility Analysis: The repeatability and reproducibility of binders not explicitly discussed in the main document are presented. The variability of the durability parameters (G-R parameter, G_{vet}, T_{max}, ΔT_c, and T_{vet}), shift factor models, and master curve models are considered. The raw data is presented in Black Space.
B. FTIR Analysis: The FTIR absorbance of binders not explicitly discussed in the main document, are evaluated at three critical ranges. The FTIR absorbance is plotted against the wave number. Binders are evaluated in terms of the variability of the peak areas within the critical ranges.
C. Ash Content: A recommended procedure to determine the ash content of the recovered seal binders. The constraints that were encountered are also discussed. Visual documentation of the testing apparatus is included.
D. Data Modelling from RHEA Software: Present the shift factor and master curve models obtained from RHEA Software.

Chapter 2: Literature Study

To comply with the objectives of this thesis, a thorough review of the performance of seals is needed. The behaviour of bitumen within seals is also examined. This Chapter introduces performance grade (PG) specifications, as well as the methods and procedures used to determine and model the relevant rheological properties. Durability parameters used to evaluate the rheological properties, are also revealed.

2.1 Overview of Bitumen

Bitumen is a dark brown to black viscous liquid or solid, comprising of complex hydrocarbons (SABITA, 2019b). Bitumen is a residual by-product obtained from petroleum refining. During the refining proses, crude oil is distilled to remove the lighter fractions. As seen in Figure 2.1, the lighter fractions include liquid petroleum gas, petrol, and diesel. The remaining compounds have relatively high molecular weight with low volatility.

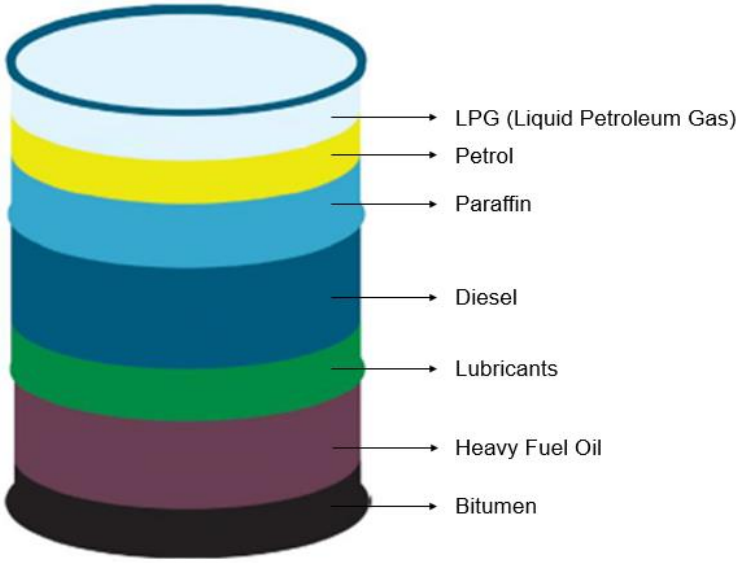

Figure 2.1 Products yielded from the distillation of crude oil (SABITA, 2019b)

At ambient temperatures bitumen has a solid or semi-solid consistency that will soften when heated. When dissolving bitumen in petroleum solvents or emulsifying it in water, bitumen can be liquefied. Due to its remarkable characteristics, bitumen is considered the oldest known engineering material. Bitumen is frequently used to construct and maintain pavement

structures because of its versatility to serve as a strong, readily adhesive, highly waterproof, and durable material (SABITA, 2014).

2.1.1 Composition and Structure

The physical and chemical properties of bitumen are typically similar. Variation is experienced depending on the crude oil source from which it was derived, as well as the processes used during refining and blending. The typical chemical elements of bitumen are illustrated in Figure 2.2. It can be seen that bitumen primarily comprise of hydrocarbons. Small trace amounts of metals such as vanadium, magnesium, iron, and nickel are also present (Hunter *et al.,* 2015).

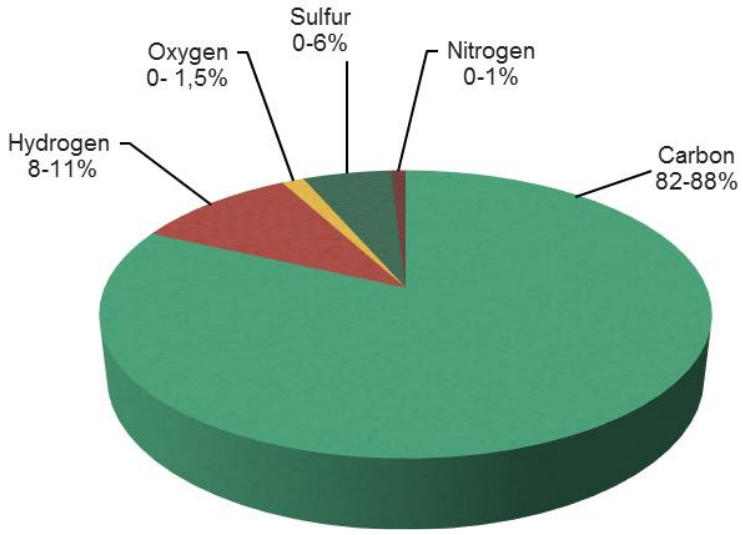

Figure 2.2: Typical Chemical Elements of Bitumen (adapted from (Hunter *et al*., 2015)

Despite the fact that the chemical composition of bitumen can become quite intricate, two chemical groups, asphaltenes and maltenes, have been identified to aid in the categorisation of bitumen. Maltenes can further be divided into saturates, aromatics and resins, based on molecular mass. Although some overlap exists between these groups, the following characteristics are associated with each (Hunter *et al*., 2015):

- Asphaltenes are n-heptane insoluble, highly polar and have a relatively high molecular weight. Bitumen with high asphaltene content is typically harder and has a higher softening point which will result in an increase in viscosity.
- Maltenes are soluble in n-heptane, have lower molecular weight and will determine the viscosity of the bitumen.

- Saturates are non-polar viscous oils that comprise of straight and branched aliphatic hydrocarbons with ring structured aliphatic compounds. The saturates content will influence the softening point of the bitumen.
- Aromatics comprise of non-polar carbon chains connected to unsaturated ring systems. Bitumen with increased aromatics will be less susceptible to shear.
- Resins are solid or semi-solid and mainly comprise of carbon and hydrogen, with a small number of nitrogen, sulphur, and oxygen atoms. Resins function as a dispersing agent for asphaltenes and due to their polar nature, resins are strongly adhesive.

Simple colloidal models are used to imitate the structure of bitumen. Bitumen is considered a colloidal arrangement of asphaltene micelles dispersed in maltenes. The micelles comprise of asphaltenes and an absorbed layer of aromatic resins. These polar molecules will provide bitumen with elastic properties, while the non-polar molecules will be responsible for the viscous properties. A homogeneous mixture with visco-elastic properties is obtained. The visco-elastic behaviour of bitumen will be discussed further in Chapter 2.1.3.3.

This dual structure will allow the saturates and aromatics to provide a body that will transfer the asphaltenes and resins. Where a sufficient quantity of resins and aromatics are present, the asphaltenes will be fully dispersed. This will allow the micelles to have good mobility within the bitumen and is referred to as a solution (SOL) type bitumen. A lack of sufficient quantities of aromatics and resins will result in irregular structures of connected micelles since the micelles are not fully peptised. This type of bitumen is known as gelatinous (GEL). Figure 2.3 show the structural difference between SOL and GEL type bitumen. (SABITA, 2014)

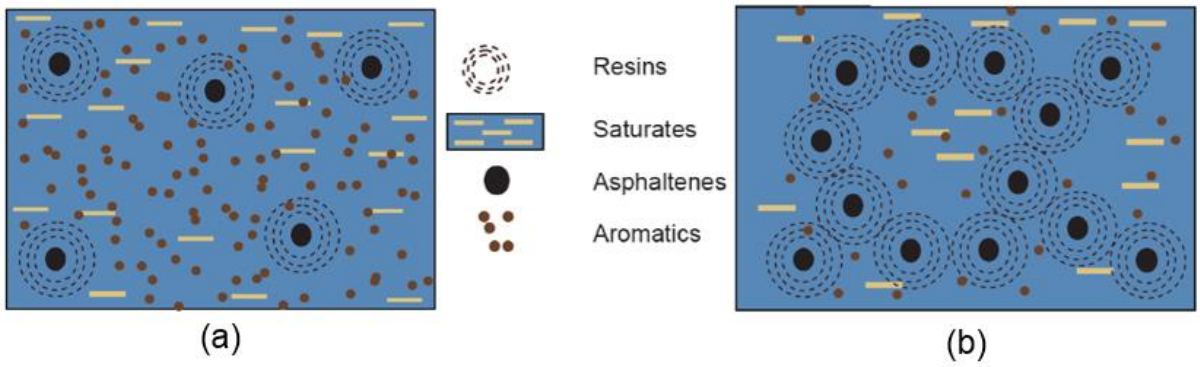

Figure 2.3: Bitumen Structure (a) SOL Type Bitumen and (b) GEL Type Bitumen (SABITA, 2014)

Theoretically, GEL bitumen display non-Newtonian behaviour, while the SOL-type will display Newtonian behaviour. When the GEL type bitumen is heated to high temperatures, the non-

Newtonian behaviour will decrease. Research found that bitumen generally has an intermediate character because of the SOL-GEL structure (Lesueur, 2009).

2.1.2 Bitumen Types

The bitumen that is directly obtained from the distillation process without undergoing additional modification, is referred to as straight-run bitumen. In this simple form, straight-run bitumen might not be able to meet all of the requirements that it is intended for in pavement systems (Hunter *et al*., 2015). This basic form can be enhanced to a sufficient specification grade either by further refining or by blending two different components to create penetration grade bitumen. Penetration grade bitumen is differentiated using the penetration tests and serve as a base to manufacture cutback bitumen, modified binders and bitumen emulsions (SABITA, 2014). Figure 2.4 shows the available bituminous binders in South Africa.

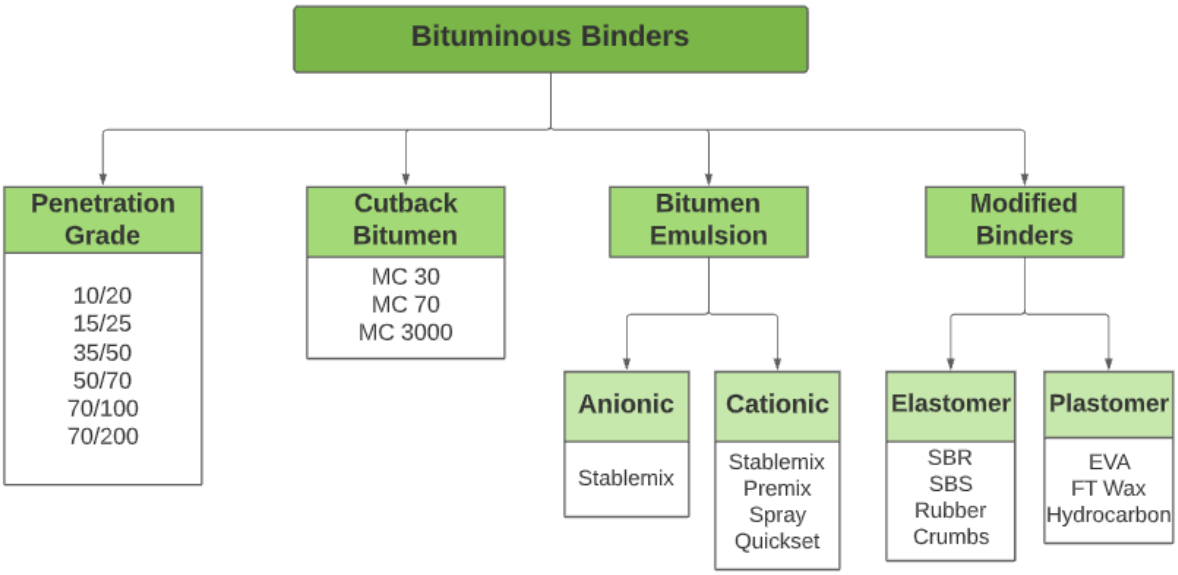

Figure 2.4:Types of bitumen available in South Africa *(SABITA, 2019b)*

Cutback bitumen is manufactured when a volatile solvent is added to penetration grade bitumen. Once the solvent evaporates, only the original penetration grade bitumen will remain. The addition of a solvent will reduce the viscosity of the bitumen, which will allow the cutback bitumen to be placed at lower temperatures (Hunter *et al*., 2015).

Bitumen emulsions comprise of heated bitumen droplets that are dispersed in water as discrete globules. The water will contain an emulsifying agent to stabilise the emulsion. The emulsification process will reduce the viscosity of the bitumen, which will allow the emulsion to act as a fluid while being applied. Bitumen emulsions are categorised based on the electrical

charge of the bitumen particles. An anionic emulsion will contain negatively charged particles, whereas cationic emulsions will contain positively charged particles. (SABITA, 2014)

The addition of modifiers, elastomers or plastomers, to conventional binders will produce a more durable binder with enhanced rheological properties, also referred to as polymer modified binders (PMB). Elastomers will typically improve the strength and elastic behaviour of the binder, while plastomers will increase the viscosity of the bitumen (SABITA, 2016). Enhanced rheological properties are experienced over an extended range of temperatures and loading times. Due to the significant increase in stiffness modulus and elasticity of PMBs, they have greater resistance against rutting, abrasion, cracking, fatigue, stripping, and bleeding. PMBs are prone to less ageing at high temperatures and do not experience brittle facture at low temperatures (Yusoff *et al*., 2005). In South Africa the most common types of modifiers used in seal construction are (SABITA, 2016):

Styrene-butadiene-rubber (SBR) latex is a copolymer comprising of butadiene and styrene monomers. SBR is commonly used as a cold applied bitumen emulsion in spray seals and micro-surfacing but can also be used as a hot applied binder in spray seals and asphalt. Improvements in flexibility, elasticity and adhesion are yielded.

Styrene-butadiene-styrene (SBS) is a thermoplastic block copolymer of butadiene and styrene. This polymer will increase the softening point, cohesive strength, and elasticity of the binder. The binder will have improved low temperature flexibility and greater resistance to permanent deformation, resulting in the overall enhancement of the performance characteristics of the binder.

Rubber crumb is derived from recycled rubber tyres. Although bitumen rubber is much more viscous than unmodified binders, it has a limited shelf life of approximately six hours. Since bitumen rubber is not a homogeneous binder, it requires specific equipment to be applied. The reduction in temperature susceptibility allows for improved resistance to crack reflection and flushing.

2.1.3 Bitumen Rheology

The Greek word rheology comprises of the terms *rheos* (flow) and *logy* (science), thus translating to the *study of flow*. The rheology of bitumen considers both the flow and deformation characteristics of bitumen. It is important to have a good understanding of the rheology of bitumen, since these characteristics are vital for optimal pavement performance.

2.1.3.1 Principles of Elasticity

According to Hooke's Law, when a uniaxial load is applied to a homogeneous, isotropic material, the material will exhibit linear stress-strain behaviour. The load will elastically deform or strain the material, which will develop stresses within the material. The linear relationship between stress and strain can be formulated as follows (e.g. Craig, 2003):

$$\sigma = E\,\varepsilon \tag{2.1}$$

Where σ = normal stress

E = Young's Modulus

ε = normal strain

Similarly, if a shear load is applied to a homogeneous, isotropic material, the shear stress can also be related to the shear stain:

$$\tau = G\,\gamma \tag{2.2}$$

Where τ = shear stress

G = shear stiffness modulus

γ = shear strain

The following equation can be used to translate from the normal stress state to the shear stress state:

$$G = \frac{E}{2(1+\upsilon)} \tag{2.3}$$

Where ν = Poisson's Ratio

Hooke's Law is only valid within the elastic region. Within this region, recoverable deformation takes place and the material will recover to its equilibrium state. When the elastic limit is exceeded, permanent strain accumulates within the material. Ductile materials are able to absorb loads until a yield point is reached. Here, large deformations are experienced before failure occurs. Brittle materials will not display any yielding before failure, resulting in complete fracture beyond the yield point. (Craig, 2003)

2.1.3.2 Principles of Viscosity

Viscosity is used to measure a fluid's resistance to flow. Some fluids resist flow more efficiently than others. A fluid with a low viscosity will flow more easily than a fluid with a higher viscosity.

The shear stress that causes Newtonian fluids to flow, is directly proportional to the rate of deformation (rate of shear strain). The direct proportionality is referred to as the absolute or dynamic viscosity. The absolute viscosity indicates the fluid's internal resistance to flow. (Britannica, 2018)

Newton's law of viscosity can be rearranged in order to express absolute viscosity as (Fox *et al.*, 2011):

$$\mu = \tau \,/\, \frac{du}{dy} \tag{2.4}$$

Where μ = absolute or dynamic viscosity (Pa.s)

τ = shear stress

du/dy = rate of deformation or shear strain rate

The ratio of the absolute viscosity of the fluid to the fluid mass density can also be obtained. This ratio is referred to as the kinematic viscosity of the material. No forces are involved with this quantity. The kinematic viscosity can be calculated as (Fox *et al.*, 2011):

$$\upsilon = \frac{\mu}{\rho} \tag{2.5}$$

Where v = kinematic viscosity (m^2/s)

ρ = fluid density (kg/m^3)

For some fluids, the shear stress is not directly proportional to the deformation rate. These fluids are referred to as non-Newtonian since they do not comply with Newton's law of viscosity. The majority of non-Newtonian fluids have an apparent viscosity (η) that is relatively high when compared to the viscosity of water. The power law model is used to represent the flow of non-Newtonian fluids as (Fox *et al.*, 2011):

$$\tau = k \left(\frac{du}{dy}\right)^n \tag{2.6}$$

Where k = consistency index

n = flow behaviour index

Equation 2.6 can be altered to obtain the apparent viscosity of the fluid (Fox *et al.*, 2011):

$$\tau = k \left|\frac{du}{dy}\right|^{n-1} \frac{du}{dy} = \eta \frac{du}{dy} \tag{2.7}$$

Where η = apparent viscosity

The behaviour of non-Newtonian fluids is considered to be either time-dependent or time-independent. Fluids that exhibit time-independent behaviour are termed pseudoplastic or dilatant. Pseudoplastic or shear thinning fluids will experience a decrease in apparent viscosity when the deformation rate is increased (n<1), while apparent viscosity of dilatant or shear thickening fluids will increase with an increase in deformation rate (n>1). Figure 2.5 indicates the different material behaviour for each of these non-Newtonian fluids. Ideal or Bingham plastics will behave as a solid. Once the minimum yield stress is exceeded, a linear relationship will be observed between the shear stress and the deformation rate. (Fox *et al.*, 2011)

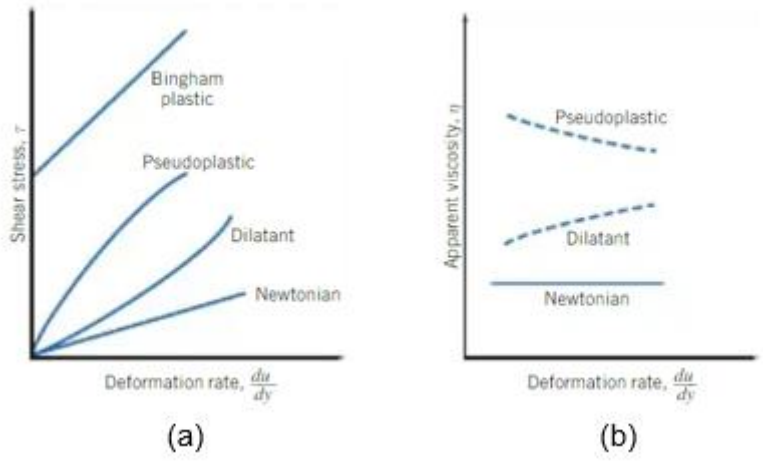

Figure 2.5: Difference between Newtonian and non-Newtonian fluids in terms of shear stress (a) and apparent viscosity (b)

It is also possible for the apparent viscosity of fluids to be time dependant. These fluids are referred to as thixotropic or rheopectic fluids. Thixotropic, also known as shear thinning, is a phenomenon where the apparent viscosity of a fluid decreases with time under a constant applied shear stress. An exact opposite reaction is observed in Rheopectic fluids, where the apparent viscosity of the fluid will increase with time, which is also referred to as shear thickening. (Fox *et al.*, 2011)

2.1.3.3 Visco-Elastic Behaviour of Bitumen

Bitumen is a thermoplastic, visco-elastic material, which implies that the behaviour of bitumen is influenced by temperature and loading time. An elastic material response governs at low temperatures and short loading times. Once the load is removed the material will recover to its original state. This is a complete contrast to the viscous behaviour that dominates at high

temperature and slow loading rates. In this state, the material will not recover to its original state because permanent deformation took place. (Hunter *et al.,* 2015)

Figure 2.6 is an idealised representation of the modulus-temperature curve of a visco-elastic material. The figure illustrates the four regions of visco-elastic behaviour, as identified by Shaw and MacKnight (2005). Figure 2.6 shows that the shear modulus is decreasing function of temperature. At low temperatures and shear modulus values greater than 10^9 Pa, the material is hard and brittle. This region is referred to as the glassy region. The material behaviour is considered to be purely elastic, since the chemical structure of the material is fixed, due to the lack of thermal energy. An increase in temperature will result in a decrease in stiffness and allow the material to become more resilient. This transition zone ranges from 5°C to 20°C. The rubbery plateau region will follow if the temperature is increased further. Within the rubbery plateau, the changes in modulus are insignificant when compared to the glassy region. At high temperatures the material will enter the flow region, where the material will behave as a viscous liquid. At temperatures beyond the flow region, purely viscous material response governs. (Shaw and MacKnight, 2005)

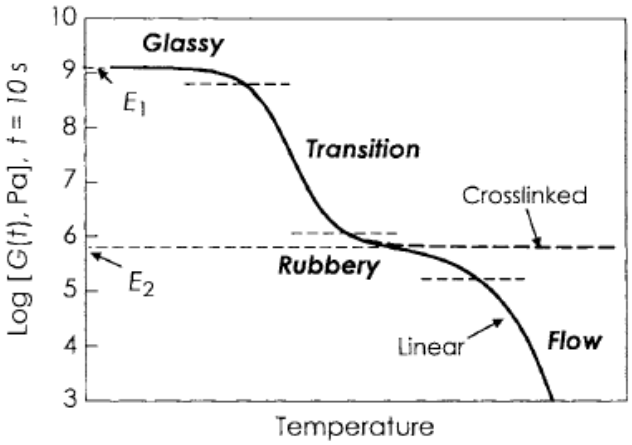

Figure 2.6: Regions of Visco-Elastic Behaviour (Shaw and MacKnight, 2005)

Shaw and MacKnight (2005) identified mechanical models to accurately predict the visco-elastic response of materials. The models combine various elements, such as springs and dashpots. These models include:

- Maxwell Model
- Voigt Model
- Generalised Maxwell Model
- Voigt-Kelvin Model

2.2 Introduction to Seals

Nearly 80% of South Africa's surfaced roads are covered with various types of seals, either as initial surfacing or as a reseal (SABITA, 2019a). A seal comprises of a coat of bituminous binder sprayed onto a clean road surface, followed by a layer of aggregate. While the binder is still in its hot fluid state, the aggregate is rolled to ensure that the particles are positioned into a compacted matrix (Hoffmann, 2007). The binder will fill the voids between the aggregate particles to create a dense and relatively impermeable pavement structure (TRH 3, 2007).

2.2.1 Aggregate

The structural and functional performance of a seal is highly influenced by the choice of aggregate. The choice of aggregate will be influenced by various factors, including the traffic volume, design life, noise level requirements and skid-resistance of the pavement structure. The aggregate must allow for the following functions to be met (TRH 3, 2007):

- The aggregate must be able to transfer the wheel loads to the underlaying pavement structure, while resisting the abrasion caused by the moving wheel loads.
- The aggregate must deliver a skid-resistant road surface.
- The aggregate must provide a structure to prevent the elastic and impermeable bituminous binder from flushing to the surface when exposed to loading.
- The aggregate must protect the binder form the ultra-violet rays of the sun.

The aggregate size used in seals vary from 6.7 mm to 19.0 mm and the selection of stone size will depend on the type of seal that is being constructed (Distin, 2008). The aggregate must consist of particles of identical shape and size, derived from hard and durable stone. Angular particles have a larger contact area than flat elongated particles, which allow these particles to create good interlock. By incorporating uniform size particles, the friction area between the tyre load and the road surface will be optimised to create an interlocked matrix. This will increase skid-resistance and reduce noise levels. The grading specification of aggregate is indicated in Table 2.2.

The shape and size of the aggregate will also influence the ability of the seal to disperse surface water, as well as the void content of the seal (TRH 3, 2007). The aggregate must not contain dust, deleterious minerals, or inferior material. The crushing strength of the aggregate must be sufficient to prevent weathering during rolling and traffic loading. The use of porous material should be limited, since the lighter fractions of the binder could be absorbed by the aggregate. Consequently, the binder will be too brittle to retain the aggregate on the road.

Table 2.1 show the specifications that aggregate properties must comply with in order to be used in surfacing seals.

Table 2.1: Properties of Aggregates for Surfacing Seals (TRH 3, 2007)

PROPERTY	GRADE OF AGGREGATE	
	GRADE 1	GRADE 2 & 3
Flakiness Index [%] (max)		
19,0 mm nominal size	25	30
13,2 mm nominal size	25	30
9,5 mm nominal size	30	35
6,7 mm nominal size	30	35
10% FACT [kN] (min)	210	210
Wet to Dry Ratio [%]	75	75
Aggregate Crushing Value (ACV) [%] (max)	21	21
Polished Stone Value (PSV) (min)	50	50

Table 2.2: Grading of Aggregate for Surfacing Seals (TRH 3, 2007)

SIEVE SIZE (mm)	GRADE	PERCENTAGE PASSING BY MASS						
		26,5 mm nominal size	19,0 mm nominal size	13,2 mm nominal size	9,5 mm nominal size	6,7 mm nominal size	4,75 mm nominal size	2,36 mm nominal size
37,50	**Grade 1 & 2**	100	–	–	–	–	–	–
26,50		85 – 100	100	–	–	–	–	–
19,00		0 – 30	85 – 100	100	–	–	–	–
13,20		0 – 50	0 – 30	85 – 100	100	–	–	–
9,50		–	0 – 5	0 – 30	85 – 100	100	–	–
6,70		–	–	0 – 5 **	0 – 30	85 – 100	100	–
4,75		–	–	–	0 – 5 **	0 – 30 *	85 – 100	100
3,35		–	–	–	–	–	0 – 30	–
2,36		–	–	–	–	0 – 5	0 – 5	0 – 100
	Grade 3	Grading shall comply with the requirements for grade 1 and 2 with the following exceptions * 0 – 50 ** 0– 10						
Fines Content [1]	**Grade 1**	0,5	0,5	0,5	0,5	0,5	1,0	15,0
	Grade 2	1,5	1,5	1,5	1,5	2,0	2,5	15,0
	Grade 3	N/A	N/A	2,0	2,0	3,0	3,5	15,0
Dust Content [2]	**Grade 1**	N/A	N/A	N/A	N/A	N/A	N/A	2,0
	Grade 2	0,5	0,5	0,5	0,5	1,0	1,0	2,0
	Grade 3	N/A	N/A	1,5	1,5	1,5	1,5	2,0

[1] Fines Content: Material passing a 0,425 mm sieve (max)
[2] Dust Content: Material passing a 0,075 mm sieve (max)

2.2.2 Function of Seals

A seal is relatively thin compared to the other layers in the pavement structure. Despite not being a load distribution layer, the seal must still be able to provide strength to the road surface in order to withstand the stresses associated with traffic loading (Texas Department of Transporation, 2010).

In South Africa, the functions of a surface seal include (Hoffmann, 2007):

- An impermeable layer to protect the underlaying pavement structure against the intrusion of water and air.
- A safe, durable, all-weather, dust-free road surface that offers sufficient skid resistance and a desired surface texture.
- Protect the underlaying material from the damaging and abrasive forces associated with traffic loading and the environment.
- A Stress Absorbing Membrane Interlayer (SAMI) that will prevent the cracks of the underlaying layers from rising through new surfacing or overlays.

2.2.3 Type of Seals

In South Africa, various seal types are used. These seals could either be sprayed seals, slurry seals or combination seals (Van Zyl and Jenkins, 2015). The selection of seals varies between agencies and is also influenced by factors such as environmental conditions, traffic volume and road gradient. Double seals are mainly used on National Roads, since these roads carry the majority of freight movement, while Provincial Roads use single seals for resealing and Cape seals for new construction works.

Figure 2.7 shows the structure of a single seal (S1). A single seal is the most basic form of a spray seal and consists of a tack coat of bituminous binder and a single application of aggregate. The tack coat will ensure that the surface is impermeable to moisture and to bond the aggregate to the surface.

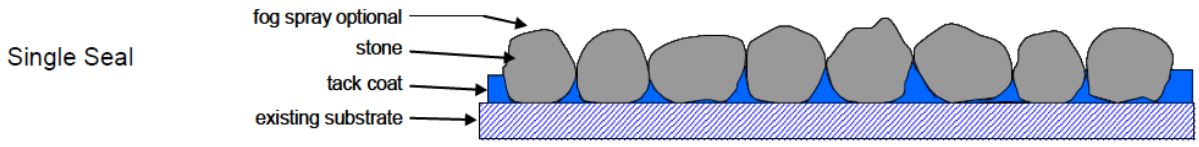

Figure 2.7: Structure of a Single Seal (TRH 3, 2007)

The structure of a double seal (S2) is indicated in Figure 2.8. A double seal is similar to a single seal but contains an additional penetration coat and layer of aggregate. The first layer of aggregate comprises of large size aggregates, while the aggregate size of the second layer is reduced to approximately half the nominal size of the first layer.

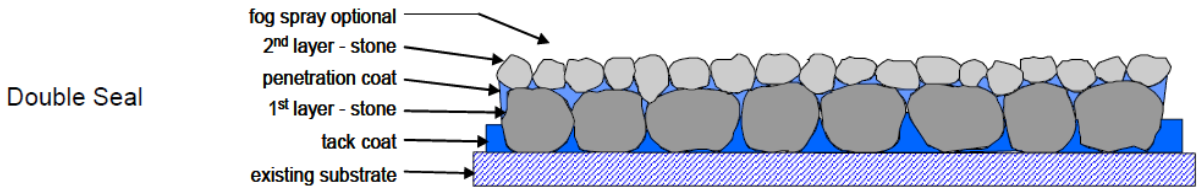

Figure 2.8: Structure of a Double Seal (TRH 3, 2007)

As seen in Figure 2.9, the difference between a Cape seal and a single seal, is the addition of a slurry layer. A slurry is a mixture of bitumen emulsion, water, hydrated lime or cement, and a suitably graded fine aggregate, (SANRAL, 2014). Typically, the fine slurry is applied by hand to force the slurry into the voids between the surfacing aggregate. The slurry serves as a micro-surfacing that will provide a smooth finished surface that binds any loose aggregate to prevent stone loss.

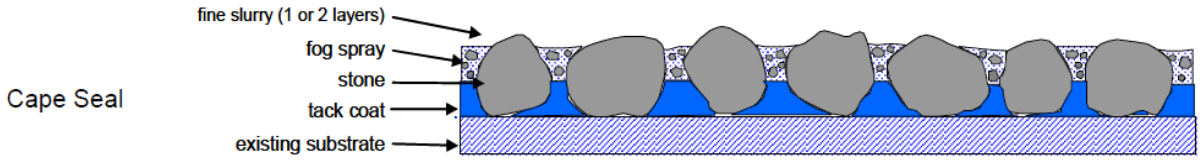

Figure 2.9: Structure of a Cape Seal (TRH 3, 2007)

It should be noted that for these types of seals a fog spray could be added to the top layer of aggregate. The purpose of the diluted bitumen emulsion is to ensure adhesion of the aggregate to obtain a dense, impermeable surface. A prime coat is applied to the to the base layer to ensure sustained adhesion between the base and the surfacing layer. The prime may also prevent the surfacing binder from being absorbed by the base (SANRAL, 2014).

2.2.4 Factors that Influence the Performance of Seals

When the performance of seals are evaluated, it is important to consider the degree to which the functions of the seal are fulfilled and the effective service life of the surfacing. A variety of factors can influence the short- and long-term performance of seals. These factors are summarised as construction and design, maintenance, traffic, and environment (TRH 3, 2007).

2.2.4.1 Design and Construction

It is important that a thorough design process should take place before the seal is constructed. A pre-design investigation will allow for a proper design that will ensure that the seal performance is optimal. The following factors must be considered:

Road space - The gradient of the road, sharp curves, intersections and the road width can escalate the deterioration of the surfacing seal. Where steep gradients are present, the wheel friction can cause debonding or flushing of the surface. Similar forms of distress are experienced when sharp curves, braking or acceleration induces high horizontal stresses in the seal.

Structural adequacy of the underlaying pavement structure – The flexural stiffness of the pavement structure will contribute to the fatigue experienced in the surfacing. The choice of base material and degree of compaction will determine the ability of the aggregate to resist penetration into the base. If the aggregate is submerged into the base, skidding problems will be experienced.

Choice of aggregate – The shape, nominal size and grading must be considered. Aggregate properties, including dust content, porosity, adhesion characteristics, spread rate, strength durability, cleanness, and resistance to wearing will also affect the performance of seals. These properties were discussed in Chapter 2.2.1.

Type and Quantity of binder – Typically modified binders are used in surfacing seals for their enhanced performance in terms of adhesion, elasticity, reduced sensitivity to bleeding and increased durability, especially at sub-zero temperatures. The binder selection criteria will be discussed further in Chapter 2.2.6.

During the construction process good construction practices must be followed, this includes adequate supervision and continual evaluation of progress. The conditions must be inspected to ensure that a clean, dense surface is provided on which the seal can be constructed, otherwise insufficient bonding will exist between the seal and the underlaying layer. The binder and stone must be applied uniformly, and plant and equipment must be calibrated correctly. It is vital that repairs must be completed before constructing the seal to ensure that the treatments have stabilised. Pre-treatments can be used to remove texture irregularities from the surface to ensure that a smooth riding surface is constructed. Treatments for both dry and porous surfaces include the spraying of a rejuvenator or diluted emulsion or the application of a sand or small aggregate seal.

2.2.4.2 Maintenance

Some seals require more timely maintenance than others. The service life of a pavement can be drastically extended if suitable maintenance takes place. A visual inspection in accordance with TMH 9 (2008) can be used to evaluate the condition of the surface. The following factors must be considered:

- Texture depth – Variations in texture depth will indicate that texture treatment is needed and suggest the amount of additional binder required.
- Permeability – Will indicate whether additional binder should be added to the existing surfacing.
- Expected embedment of stone - Should be considered to indicate the number of voids within the seal that will be lost if the aggregate gets embedded into the existing surface.
- Degree and extent of cracking – Will suggest whether the cracks will reflect through the new surfacing. These cracks will also be an indication of the loss of flexibility or the relative brittleness of the existing surfacing, that the new seal must supply.

Maintenance actions can include diluted emulsion sprayed onto the surface to rejuvenate the existing binder and prevent loss of aggregate. Where debonding occurs in small areas, these problem areas can be patched. A fine slurry can also be applied to specific areas where ravelling is present.

2.2.4.3 Traffic

The performance of a seal is significantly influenced by the number, type, and combination of vehicles. The effect of a single heavy vehicle is considered equivalent to 40 light vehicles (TRH 3, 2007). The following traffic parameters are considered:

- Volume – Friction between the tyres and surface will weather the stone, reduce the voids in the seal and will lead to flushing and loss of skid resistance. For the binder to remain flexible, it is required that the seal be exposed to a minimum number of vehicles each day. Conventional binders require at least 50 vehicles per day to remain “alive” (TRH 3, 2007).
- Loading – Heavy vehicles will expedite aggregate embedment into the existing surface more than light vehicle loads.
- Tyre pressure – Large tyre pressure induce vertical stresses much higher than the tyre inflation pressure. Therefore, tyre pressure is a major contributor towards bleeding and flushing.

- Axle – Vehicles with tandem or tridem axles cause severe damage to seal surfaces. Associated forms of distress include slippage, debonding and ravelling.
- Speed – Seals typically perform better when trafficked by fast-moving vehicles because of shorter loading periods and higher horizontal stresses caused by traction.

2.2.4.4 Environment

The climatic conditions must be considered when the type and grade of binder is determined, since variable weather and temperature will affect seal performance. Seals in regions with extremely hot temperatures will experience reduced cohesion, while cold weather will make the binder hard and brittle and result in stone loss and cracks. Ultra-violet radiation from sun rays will accelerate the ageing of the binder and volatiles will evaporate in humid conditions. Wind conditions must also be assessed, because dust and transported sand will cause poor adhesion between freshly laid binder and stone.

2.2.5 Failure Mechanism of Seals

The deterioration of a pavement is not only caused by substandard design and defective construction. The inevitable wear and tear, varying climatic conditions and increase in traffic loading contribute significantly to the weakening of the pavement. Routine maintenance must take place to ensure that the functional requirements of the pavement are met. Insufficient maintenance will ultimately result in pavement failure. For the purpose of this study, pavement failure is regarded as the decrease in serviceability caused by the development of surface distress.

The two main failure mechanisms of seals are cohesive failure and adhesive failure (Alaamri *et al.*, 2017). From Figure 2.10 it can be seen that cohesive failure presents as cracks within the binder, while adhesive failure exists between the binder and the aggregate.

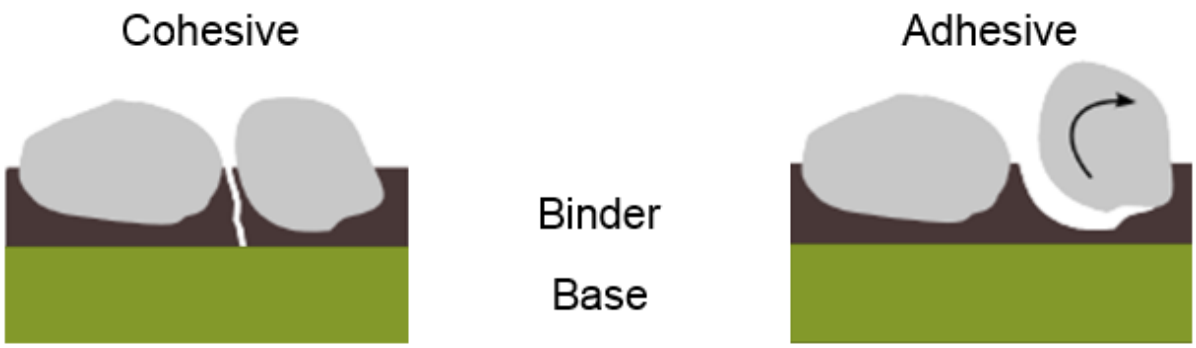

Figure 2.10: Failure Mechanism of Seals (Gerber, 2016)

2.2.5.1 Adhesive Failure

Adhesive strength refers to the potential of the binder to retain the aggregate. Aggregate loss occurs when the aggregate is detached from the seal due to the eroding effect of traffic. In some cases, early stone loss is experienced directly after construction. The reason being faulty binders, cold temperatures, too low application rates or extreme delays in the placement of aggregate (TRH 3, 2007).

Aggregate loss will allow for bleeding or flushing to occur. Typically, bleeding will occur when the binder moves upwards relative to the aggregate, until a layer of free binder accumulate on the pavement surface. Bleeding can also occur when the aggregate penetrates into the base course. Since bleeding reduces the surface texture depth, a decrease in skid resistance will also take place (SANRAL, 2009). Where thin surface treatments, like single seals, are used, attention should be paid to aggregate loss, since the underlaying pavement structure will be exposed. This could lead to structural failure and have detrimental consequences.

The composition of the bitumen and aggregate, as well as moisture conditions will influence the adhesive strength of the seal. Moisture damage refers to the premature distress of the seal due to the presence of moisture. Studies have identified stripping and ravelling as moisture damage mechanisms (Caro *et al.*, 2008).

Stripping refers to the loss of bonding between the binder and the aggregate in the presence of moisture. This will result in the physical separation of the binder and stone and prevent the seal from acting as a structural unit. Aggregate surface characteristics, such as chemical stability, polarity, surface energy and pore size distribution, are considered the main factors to influence stripping. (Bagampadde *et al.*, 2005)

Ravelling is regarded as the progressive disintegration of the layer due to the dislodgement of aggregate particles from the surface. Usually only the tack layer remains. Other causes of ravelling include wearing due to traffic, surfacing in cold weather, ageing of the binder or when the seal is opened to traffic too soon and the bitumen still has to set. (SANRAL, 2009)

2.2.5.2 Cohesive Failure

Cohesion refers to the tensile stress needed to break the bond between the molecules of a bituminous binder (SABITA, 2019). As bitumen ages the binder oxidises, becomes harder and more brittle, resulting in a binder that is more prone to cracking. Cracks are considered the main contributor of cohesive failure, followed by repetitive mechanical loading and

temperature changes. Therefore, cohesive failure is affiliated with mechanical and environmental fatigue cracking.

Cracks can be distinguished as passive or active . Active cracks are considered reflection cracks since they originate from levels below the surface. Passive cracks apply to the surfacing itself due to binder fatigue. Passive cracks are typically caused by (SANRAL, 2009):

- Surface cracks - overstressing of the surfacing layer that is not limited to the wheel tracks.
- Single cracks - long, transverse, and random cracks
- Crocodile cracking - overstressing of the base or subbase. These cracks are associated with rutting and limited to the wheel tracks.

2.2.6 Binder Selection Criteria

Figure 2.11 indicates the process followed to select the ideal binder. The objective is to select a binder that will perform optimally under the prevailing conditions. First the seal type will be determined, followed by the binder type and finally the binder grade. The workability and stiffness (hardness) of the binder are considered during binder grade classification.

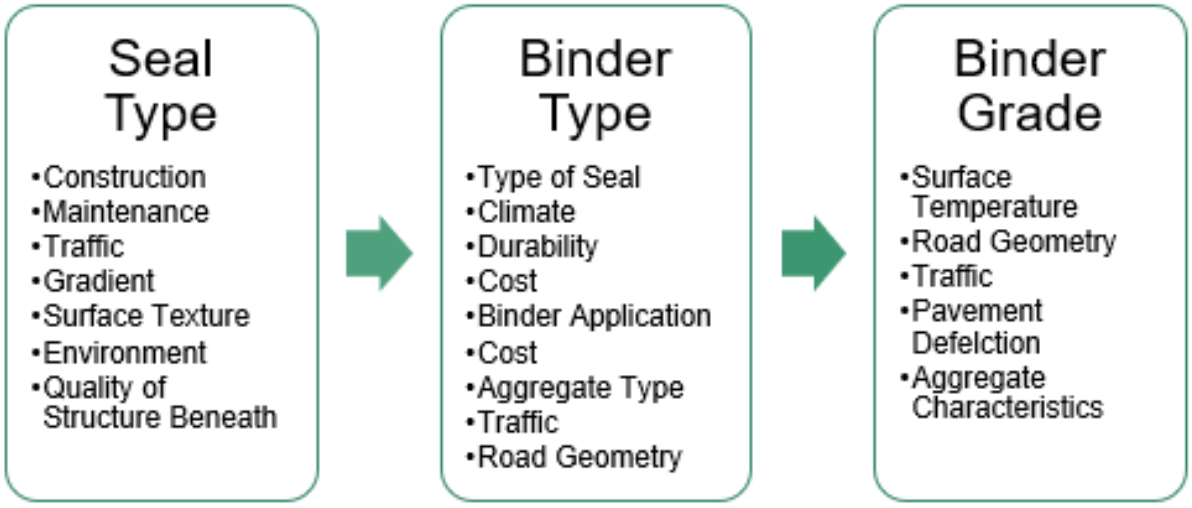

Figure 2.11: Binder Selection Criteria

There are three properties that are typically used to designate a binder grade. These properties are the softening point, penetration, and viscosity of the binder (Hunter *et al.,* 2015). A short summary is provided as to how these properties are obtained:

- During the penetration test a bitumen sample of 25°C will be loaded with a 100g needle for 5 seconds. The penetration value (dmm) refers to the depth to which the needle

penetrated the bitumen. Therefore, a harder bitumen will correspond to a smaller penetration value

- Since bitumen is a viscoelastic material, it will become softer and less viscous when heated. The ring and ball test is used to verify the temperature at which the ball flows through the ring and reaches the bottom disk of the apparatus. This temperature is known as the softening point (°C).
- Dynamic and kinematic viscosity were already discussed in Chapter 2.1.2.2.

In South Africa, the published specifications regarding binder grade are also based on above mentioned properties. The SANS 4001 specifications and the Technical Guideline (TG1) specifies the grades for the types of bitumen mentioned in Section 2.1.2. The provisions are as follows:

- SANS 4001-BT1: penetration grade bitumen (SANS 4001, 2016)
- SANS 4001-BT2: cutback bitumen (SANS 4001, 2012)
- SANS 4001-BT3: anionic bitumen road emulsion (SANS 4001, 2014a)
- SANS 4001-BT4: cationic bitumen road emulsion (SANS 4001, 2014b)
- SANS 4001-BT5: inverted bitumen road emulsion (SANS 4001, 2014c)
- Technical Guideline (TG1): The Use of Modified Bituminous Binders in Road Construction

The TG 1 (SABITA, 2019) identified four criteria to differentiate between different classes of modified binders. The criteria consider the type of binder system, type of application, level of modification and the predominant type of modifier used. The different level of application are asphalt (A), crack sealant (C), and spray seal (S). If an emulsion is used as a type of binder system, a letter C will display after the letter indicating the type of application. Where a letter is omitted after the type of application, hot applied is used. The predominant type of modifiers could either be Rubber (R), Elastomer (E), Plastomer (P), or Hydrocarbon (H). A numerical value is used to indicate the level of modification. A higher number will suggest that the binder has a higher softening point. An additional code (t) can also be added at the end of the classification to indicate whether the use of fluxing agent or cutter is allowed. A visual representation of the modified binder classification system can be seen in Figure 2.12. The introduction of modifiers has altered the pavement industry, which will be discussed further in Chapter 2.3. (SABITA, 2019)

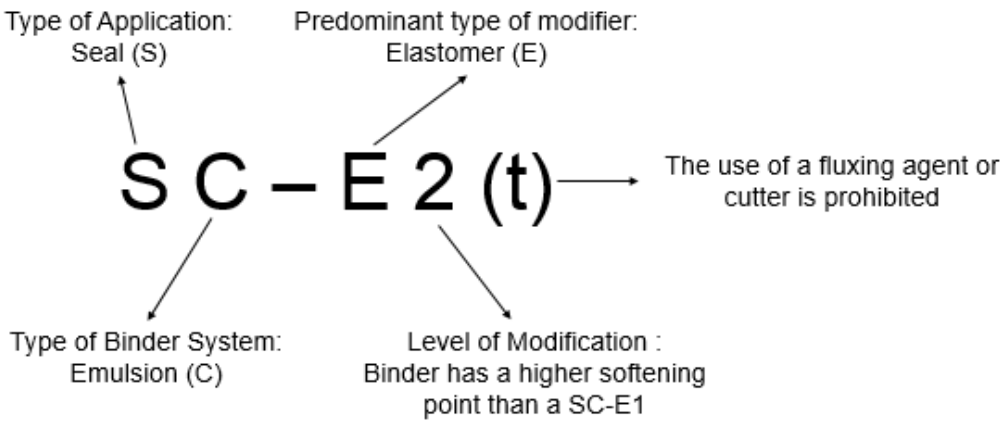

Figure 2.12: Modified Binder Classification (SABITA; 2019)

2.2.7 Seals v Asphalt

Most international sources refer to asphalt, while local sources consider seals, as well as asphalt. For research purposes, it is important to distinguish between these two materials. Asphalt is defined as the upper part of the pavement structure comprising of bitumen and aggregate. From this definition it appears that asphalt and seals are similar, therefore various standards that were developed for asphalt can be slightly modified and also used for seals. Cognisance must be given to the discrepancies between these materials, as they will serve as a reference point for various decisions.

Seals and asphalt differ in functionality due to their thicknesses. For pavement design, the TG 2 (SABITA, 2020) limits the thickness of a seal to 10mm, while the layer thickness of asphalt ranges from 20 mm to 100 mm. This difference in thickness allows for an asphalt layer to serve as a load distributing layer and seals will merely serve as a surfacing layer.

Seals and asphalt also have different construction methods. For seal construction, a bituminous binder is sprayed onto a road at a specific rate, covered with aggregate and finished with a roller mechanically compacting the surfacing. For asphalt construction, asphalt is prepared at an asphalt plant. Here bitumen and aggregate are heated and mixed at temperatures typically above 160^{o}C and then transported to site where the mixture will be compacted. The properties of the asphalt mixture are influenced by factors such as the volume of air within the compacted asphalt mixture (void content) and the volume of bitumen expressed as a percentage of the asphalt mixture (binder content), which are not considered for seal performance.

Due to the functional differences between seals and asphalt, the failure mechanisms also differ. The main failures associated with asphalt failure include fatigue cracking, rutting, thermal cracking, and moisture induced failure. Fatigue cracks result from tensile strains at the bottom of the asphalt layer. Rutting refers to the permanent deformation of the asphalt layer, which is typically experienced at hight to intermediate temperatures where the behaviour is more viscous than elastic. Moisture-induced damage result in loss of bond, either within the asphalt binder itself (cohesive failure) or at the asphalt binder-aggregate interface (adhesive failure) (Howson et al., 2009).

2.3 Performance Grading (PG) Specifications

The South African Penetration Grade Specifications (SANS 4001-BT1) incorporates empirical tests, namely softening point and penetration, as well as fundamental properties such as kinematic and dynamic viscosity. Throughout South Africa premature road pavement failures are experienced. Various limitations were identified within the Penetration Grade Specifications. These limitations suggest that the method is unable to convert test results to actual pavement performance, due to the evolution of applicable traffic volume and loading. The limitations associated with these empirical tests are (SABITA, 2016):

- The tests do not measure fundamental material stresses and strains, therefore, cannot characterise the rheological properties of polymer modified binders.
- The viscosity of the binder is only described in terms of substitute properties, such as softening point, penetration, and dynamic viscosity at temperatures between 25°C and 135°C.
- No provision is made to determine the long-term ageing characteristics of the binder. The influence of traffic speed and volumes, climate and other critical performance characteristics cannot be considered to assess the durability of the binder.

These limitations demand that an enhanced, less empirical characterisation system be developed in order to comprehensively characterise the performance of bitumen. Therefore, a performance grade (PG) specification came about. This system is similar to the Superpave PG Specification used in the USA. The USA developed their performance grade system in 1995. Some of the benefits that the system has yielded include (SABITA, 2016):

- The system is developed to minimise pavement distress that result from permanent deformation (rutting at high temperatures), fatigue cracks (repeated loading at inter-mediate temperatures), and thermal fractures (shrinkage cracks at low temperatures).

- A refined relationship between material properties and pavement performance, making these results more accurate than the penetration grade specifications.
- Not only can different binder ages be tested, binder performance can also be tested over a wide range of temperatures. Consequently, the bitumen performance can be related to field performance.
- Binder classification is based on fundamental engineering properties. The impact of climatic conditions, traffic and ageing is considered as these factors will influence the binder performance.

In 2018, SABS, with assistance from COTO, SANRAL, SABITA and the CSIR, published the Performance Grade (PG) specifications for bitumen in South Africa (SATS 3208, 2019). The Performance Grade Specifications can be viewed in Table 2.4. Since SATS 3208 is based on local conditions, traffic and climate serve as a basis for binder selection.

2.3.1 Traffic

The PG Specifications evaluates traffic in terms of speed and the severity of the traffic loading conditions. This approach considers the fact that slow moving traffic will apply more extreme loading conditions. Four categories of binder grades are available based on the expected design traffic in cumulative standard (E80) axles and speed of travel. As seen from Table 2.3, these categories are Extreme (E), Very Heavy (V), Heavy (H), and Standard (S) conditions. (SATS 3208, 2019)

Table 2.3: Binder Grade Selection Categories (SATS 3208, 2019)

Design Traffic (million E80)	**Binder Grade Requirement**		
	Traffic Speed (km/h)		
	< 20	**20 - 80**	**> 80**
<0.3	S	S	S
0.3 – 3	H	S	S
> 3 – 10	V	H	S
> 10 – 30	E	V	H
> 30	E	E	V

Table 2.4: SATS 3208 (2019): Performance Grade (PG) specifications for bitumen in South Africa

Test Properties	Note	South African Performance Grades												Test Method
		58S-22	64S-16	70S-10	58H-22	64H-16	70H-10	58V-22	64V-16	70V-10	58E-22	64E-16	70E-10	
Max pavement design temperature (°C)		58	64	70	58	64	70	58	64	70	58	64	70	
Minimum grading temperature (°C)		-22	-16	-10	-22	-16	-10	-22	-16	-10	-22	-16	-10	
		Unaged												
G* and δ @ [(T_{max} + T_{min})/2+4] (°C) [a]	1.10	Compulsory report only – see detail description of report only item												ASTM D7175
G*/sinδ @10rad/s (kPa) @ T=T_{max} [b]	1.2	Compulsory report only												ASTM D7175
Viscosity at 165°C (Pa.s) ≥ 30 sec^{-1} [c]	1.3	< 0.9												ASTM D4402
Storage Stability at 180°C (%diff in G* at T_{max})	1.4	< 15												ASTM D7175
Flash Point (°C)		≥ 230												ASTM D92b

[a] DSR tests as follows:
1) for homogeneous binders with a stiffness greater than 100 kPa use PP8 spindle with 2 mm gap;
2) for homogeneous binders with a stiffness equal to or less than 100 kPa use PP25 spindle with 1 mm gap; and
3) for non-homogeneous binders (until further notice) use PP8 and PP25 spindles with 2 mm gap

[b] G*/sinδ has been retained for unaged binder as a quick test and may be used as a quality control measure, but not as a rutting compliance requirement. Also report G* and δ separately.

[c] An indication of pump-ability only.

Table 2.4: SATS 3208 (2019): Performance Grade (PG) specifications for bitumen in South Africa (continued)

Test Properties	**Note**	**South African Performance Grades**												**Test Method**
		58S-22	**64S-16**	**70S-10**	**58H-22**	**64H-16**	**70H-10**	**58V-22**	**64V-16**	**70V-10**	**58E-22**	**64E-16**	**70E-10**	
Max pavement design temperature (°C)		58	64	70	58	64	70	58	64	70	58	64	70	
Minimum grading temperature (°C)		-22	-16	-10	-22	-16	-10	-22	-16	-10	-22	-16	-10	
	1.5	After RFTO Ageing												ASTM D2872 TG1 MB3
G* and δ @ [(T_{max} + T_{min})/2+4] (°C) [b]	1.10	Compulsory report only – see detail description of report only item												ASTM D7175
Mass Change (% m/m) [a]		≤ 0.1												< 1.0
J_{nr} at T_{max} (kPa^{-1})		≤ 4.5	≤ 4.5	≤ 4.5	≤ 2.0	≤2.0	≤ 2.0	≤ 1.0	≤ 1.0	≤ 1.0	≤ 0.5	≤ 0.5	≤ 0.5	< 4.5
Ageing ratio [G^*_{RFTO} /$G^*_{Original}$] [c]	1.8	≤ 3.0												ASTM D7175

[a] The specimen is aged prior to testing as described in ASTM D2872 for PG58S, PG58H and PG64S, and TG1 MB-3 for other binders.
[b] DSR tests as follows:
1) for homogeneous binders with a stiffness greater than 100 kPa use 8mm PP8 spindle with 2 mm gap;
2) for homogeneous binders with a stiffness equal to or less than 100 kPa use 25mm PP25 spindle with 1 mm gap; and
3) for non-homogeneous binders (until further notice) use 25 mm PP25 spindle with 2 mm gap.
[c] The ageing ratio gives an indication of the sensitivity of the binder to short term ageing after RTFO.

Table 2.4: SATS 3208 (2019): Performance Grade (PG) specifications for bitumen in South Africa (continued)

Test Properties	Note	South African Performance Grades												
		58S-22	64S-16	70S-10	58H-22	64H-16	70H-10	58V-22	64V-16	70V-10	58E-22	64E-16	70E-10	
Max pavement design temperature (°C)		58	64	70	58	64	70	58	64	70	58	64	70	
Minimum grading temperature (°C)		-22	-16	-10	-22	-16	-10	-22	-16	-10	-22	-16	-10	
		After RFTO and PAV Ageing [a]												
G* and δ @ [(T_{max} + T_{min})/2+4] (°C) [b]	1.10	Compulsory report only – see detail description of report only item												ASTM D7175
S(60s) at T_{min} + 10°C, MPa		≤ 300 @ - 12°C	≤ 300 @ - 6°C	≤ 300 @ 0°C	≤ 300 @ - 12°C	≤ 300 @ - 6°C	≤ 300 @ 0°C	≤ 300 @ - 12°C	≤ 300 @ - 6°C	≤ 300 @ 0°C	≤ 300 @ - 12°C	≤ 300 @ - 6°C	≤ 300 @ 0°C	ASTM D6648
m(60s) at T_{min} + 10°C		≥ 0.3 @ - 12°C	≥ 0.3 @ - 6°C	≥ 0.3 @ 0°C	≥ 0.3 @ - 12°C	≥ 0.3 @ - 6°C	≥ 0.3 @ 0°C	≥ 0.3 @ - 12°C	≥ 0.3 @ - 6°C	≥ 0.3 @ 0°C	≥ 0.3 @ - 12°C	≥ 0.3 @ - 6°C	≥ 0.3 @ 0°C	ASTM D6648
ΔT_c (°C) = $T_{c,s}$ – $T_{c,m}$ [c]	1.7	≥ -5												ASTM D7643
Ageing ratio [G^*_{RFTO} /$G^*_{Original}$] [d]	1.8	≤ 6.0												ASTM D7175

[a] The specimen is aged prior to testing as described in ASTM D2872 (RTFO) and then ASTM D6521-13 (PAV).
[b] DSR tests as follows:
1) for homogeneous binders with a stiffness greater than 100 kPa use 8mm PP with 2 mm gap;
2) for homogeneous binders with a stiffness equal to or less than 100 kPa use 25mm PP with 1 mm gap; and
3) for non-homogeneous binders (until further notice) use 25 mm PP with 2 mm gap.
[c] T_C.S is the critical temperature at which S (60 s) = 300 MPa and T_C.m is the critical temperature at which m (60 s) = 0,3 MPa/s. S (60 s) and m (60 s) are determined at more than one temperature until S (60 s) = 300 and m (60 s) = 0,3 are bracketed and the bracketed regions for S and m may differ. S (60 s) = 300 and m 60 s) = 0,3 may only be calculated by interpolation. Extrapolation is not allowed. Bracketed means that values of S(60) and m(60) are determined at values lower and higher than 300 and 0,3 respectively and are interpolated from these values. For example S(60) values were determined at 275 and 365 and the value at 300 was interpolated from these two values.
[d] The ageing ratio gives an indication of the sensitivity of the binder to short term ageing after RTFO and PAV.

2.3.2 Climate

Three categories of temperature are considered to examine the effect of climate. These temperatures are minimum temperature, intermediate temperature, and maximum temperature. The maximum pavement temperature refers to the maximum annual 7-day average temperature in an asphalt layer at a depth of 20 mm. From Figure 2.13, it can be seen that a thick red line divides South Africa into two distinct temperature zones. The maximum pavement design temperature for the North-Western region is 64°C and 58°C for the South-Eastern region. (Bredenhann *et al.*, 2019)

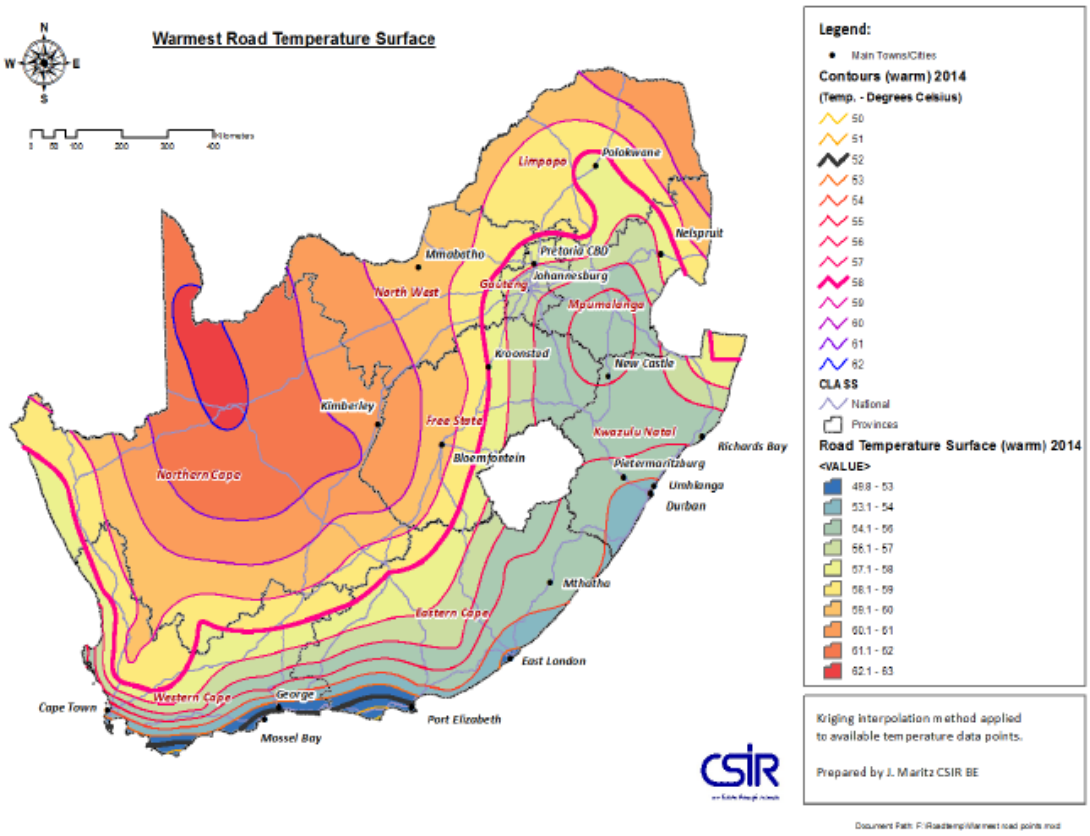

Figure 2.13: Maximum pavement temperatures in South Africa (O'Connell et al., 2015)

The minimum temperature refers to the minimum temperature at the road surface, as presented in Figure 2.14. Although temperatures below -10°C rarely occurs in South Africa, lower minimum pavement design temperatures were assigned in order to align the standards to the US PG Specifications.

The minimum temperatures associated with 64°C and 58°C are -16°C and -22°C. The choice in temperatures allows for South African binders to have good durability because a temperature difference of 80°C is maintained. It should be noted that if the actual minimum

pavement design temperatures were adopted, it would not be possible to perform minimum temperature testing, since the samples would deform at these high minimum temperatures (Bredenhann *et al.*, 2019). The intermediate temperature refers to the average of the minimum and maximum pavement design temperature plus 4°C. The traffic experienced at this operating temperature would result in fatigue (durability) cracks

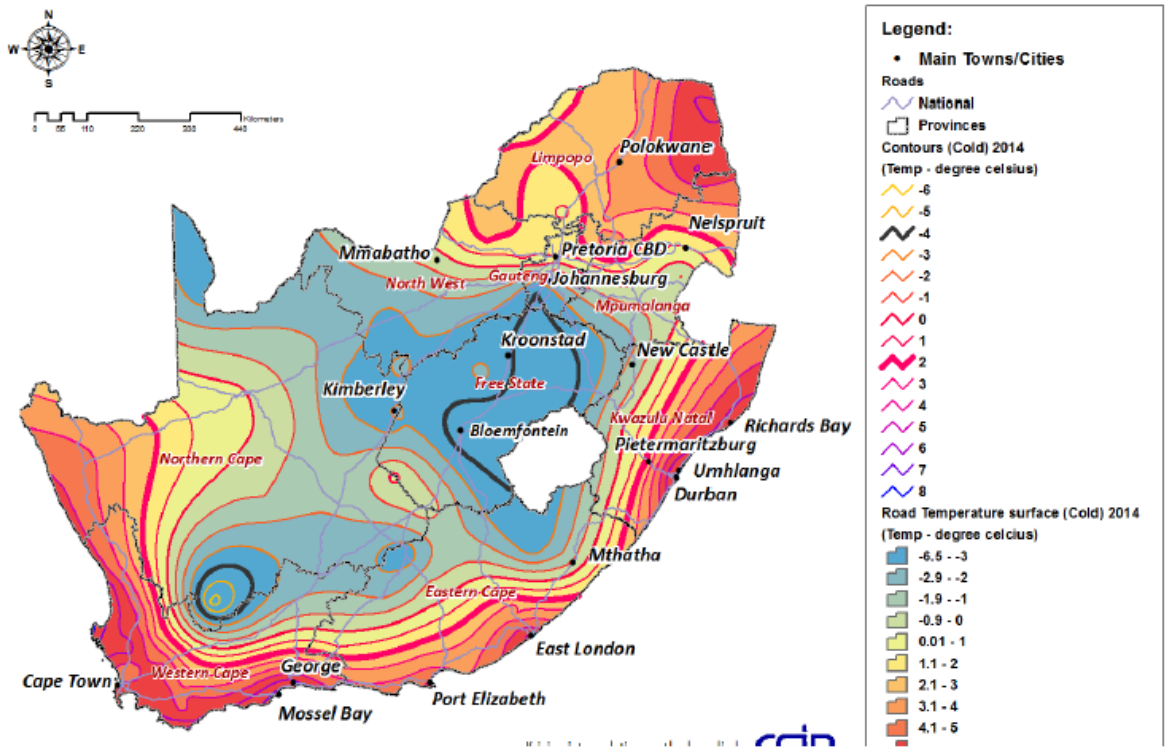

Figure 2.14: Minimum pavement temperatures in South Africa *(O'Connell et al., 2015)*

2.3.3 Correlation between Pen Grade and PG Specifications

The Penetration Grade Specifications rely on empirical tests to measure the consistency and quality of bitumen, with the penetration test being the most commonly used method. The PG Specification uses rheological properties obtained from the Dynamic Shear Rheometer (DSR) and Bending Beam Rheometer (BBR). This section considers possible correlations between the parameters obtain from the different specifications.

Saal and Labout (1958) established a correlation between the penetration test and bitumen stiffness. The complex modulus (G*) was calculated at the following test conditions: temperature = 25°C, frequency =0.4 Hz, and equivalent loading time = 0.4 seconds. A linear

relationship was formulated, as seen from Equation 2.8, which performed well for both modified and unmodified binders.

$$\log(G^*) = 2.923 - 1.9\log(Pen) \tag{2.8}$$

A study by Lee *et al.* (2004) identified a good correlation between the Brookfield viscosity and G*/sinδ at 60°C, while strong correlation was found between penetration and G*sinδ (loss modulus) at 25°C. The relationship between penetration and G*sinδ is illustrated in Figure 2.15. It can be seen that G*sinδ increases as the penetration decreases.

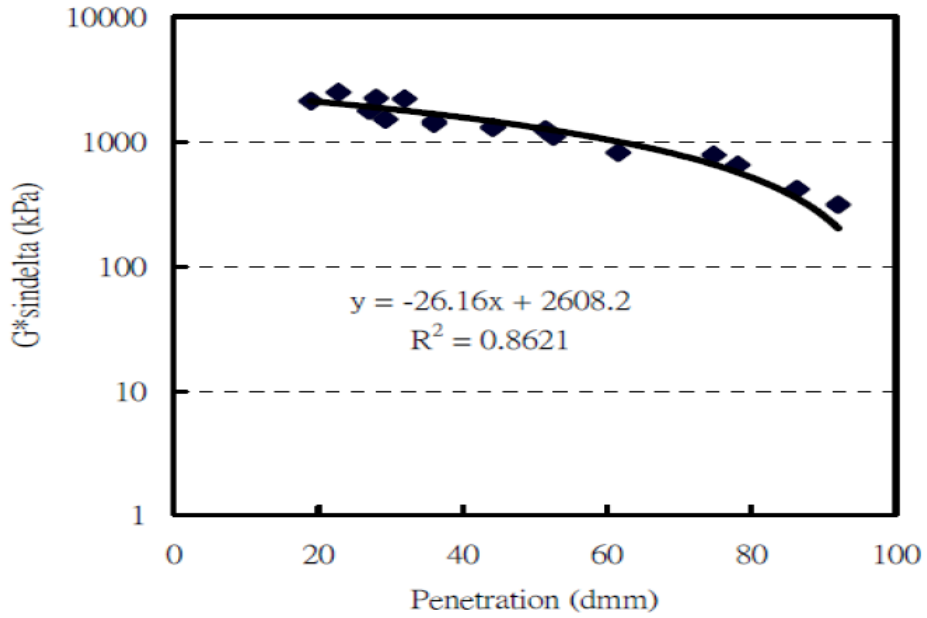

Figure 2.15: Relationship between penetration and G*sinδ at 25℃ (Lee et al., 2004))

In a more recent study, Van Heerden *et al.* (2011) used 80/100 penetration grade bitumen samples to determine a correlation between the results from the DSR and the penetration test. The results revealed that G* increases as the penetration values decreases, implying an increase in stiffness. Since the penetration values correlated well with G* at 25°C, the study concluded that it is possible to predict penetration values from G*, using Equation 2.9.

$$\log(Pen) = 2.971 - 0.381\log(G^*) \tag{2.9}$$

2.3.4 Repeatability and Reproducibility

As mentioned in Chapter 1.3, the goal of this study is to evaluate the consistency of rheological properties of recovered seal binders. The suggested seal binder recovery method must be validated to ensure that the test procedure performs within acceptable standards of accuracy, precision, and reliability for its intended purpose. For this study, there will be focussed on

precision. Precision measures the method's ability to generate reproducible results and is evaluated in terms of repeatability and reproducibility. (Lister, 2005)

Lister (2005) defines repeatability as the ability of a method to generate similar results for multiple preparations of the same sample, when the test is carried out by a single analyst. Reproducibility differs from repeatability, as the test is carried out by various analysts.

The PG Specification does not contain any requirements relating to precision. EN12697- 3 (2013) provides precision values for the penetration and softening point of recovered bitumen. These values are applicable to hot mix asphalt. As seen in Table 2.5, there is a distinction between repeatability and reproducibility.

Table 2.5: EN 12697-3 (2013): Precision Values for Recovered Binders

	Repeatability	Reproducibility
Softening Point (°C)	1,9	3,4
Penetration (mm)	0,10 x	0,27 x

Where x is the average of the results being compared

2.4 Rheological Tests

There are various procedures available which can determine the performance properties of recovered seal binders as stated in the Performance Grade Specifications (Table 2.4). This section will elaborate on the methods for recovering binder from seal samples and discuss the DSR (Dynamic Shear Rheometer) and BBR (Bending Beam Rheometer) testing apparatus. Standard testing methods based on existing American and European procedures are considered and where available, substituted with South African standards.

2.4.1 Binder Recovery Process

Due to evolving technological advances, numerous quality control and assurance procedures require the properties of the binder in order to evaluate the performance of the binder mixture. Therefore, the binder has to be separated from the aggregate. The binder recovery process can be divided into three phases: extraction, aggregate removal, and distillation. As seen from Figure 2.16, various methods are available for aggregate removal and distillation. The combination of methods must be carefully considered since these methods can impact or modify the characteristics of the binder. (Mikhailenko and Baaj, 2017)

Figure 2.16: Binder Recovery Process

There are four key aspects that will influence the repeatability and reproducibility of the binder recovery process. In order to prevent poor technical performance, the binder recovery process must account for (Mturi *et al.*, 2015):

- The binder hardening effect caused by the solvent
- The presence of solvent in the recovered binder
- The presence of aggregate fines in the recovered binder
- The extent to which binder is removed from aggregate

2.4.1.1 Extraction

In order to separate the binder from the aggregate, the sample is submerged in solvent. EN- 12697-3 (2013) recommend 1500 ml solvent for every 120 - 150 g estimated recoverable binder. The choice of solvent determines the extraction and distillation conditions. These conditions ensure that the properties of the recovered binder correspond to the in-situ binder properties. Table 2.6 shows the type of solvents that are available for extraction, together with the corresponding distillation conditions.

Table 2.6: Solvents and Distillation Conditions (EN-12697-3, 2013)

Name	Chemical Formula	Boiling Point (ºC)	Temp T_1 (ºC)	Pressure P_1 (kPa)	Temp T_2 (ºC)	Pressure P_2 (kPa)	Temp T_3 (ºC)
Dichloromethane	CH_2Cl_2	40.1	85	85	150	2.0	175
1.1.1-Trichlorethane	CH_3Cl_3	74.1	80	30	160	2.0	185
Benzene	C_6H_6	80.1	80	30	160	2.0	185
Trichlorethylene	C_2HCl_3	90	90	40	160	2.0	185
Xylene	C_8H_{10}	120	120	30	180	2.0	205
Toluene	C_7H_8	110	110	40	160	2.0	185
Tetrachloroethylene	C_2Cl_4	110	110	40	160	2.0	180

The solvent selection has an influence on the physical properties of the recovered binder as a result of variation in the amount of residual solvent remaining after recovery, age hardening and fines retention. Therefore, the choice of solvent dictates the extraction and recovery conditions, to ensure that the recovered binder's properties represent the in-situ binder properties. (SANS 3001, 2011)

Mturi *et al.*(2015) describes binder hardening as the process where a binder that is dissolved in a solvent, will present higher stiffness properties after recovery when compared to the stiffness properties before being dissolved in the solvent. Stiffness increases varying from 5 – 300% can be experienced. Bur et al (1991) found that two chemical processes, oxidation and molecular weight increase, occur during the hardening process. The oxidation process corresponds to normal ageing of bitumen and can be limited by preventing exposure to the partial pressure of oxygen.

The degree of binder hardening is influenced by (Mturi *et al.*, 2015):

- Solvent type: Van Assen (1997) assessed binder extraction methodologies for South African binders and aggregate and established that using benzene and toluene as solvents delivered good technical performance. Despite the higher solvency power, the hardening effect of chlorinated solvents was much higher than that of toluene and benzene. Another finding was that pure toluene is prone to remain in the bitumen for longer periods. In an attempt to prevent the toluene from compromising the binder properties, ethanol can be added to the toluene. The addition of 15% ethanol to an existing solvent has been found to deliver more accurate and repeatable binder properties.
- Exposure time between the binder and solvent: There is a direct correlation between the exposure time of the solvent-binder solution and the hardening effect. The recovery time varies depending on the method used. A recovery time is not specified for ASTM D5404, while EN 12697-3 allows for a maximum exposure time of 24 hours. According to the ASTM D1856 the entire recovery process must be completed within 8 hours. Although AASHTO T319 does not specify a time limit for the entire recovery process, the time limit placed on each stage of the recovery process will allow for the entire process to be completed within 8 hours.
- Temperature when the binder is exposed to solvent: When the solvent-binder solution is exposed to high temperatures, greater binder hardening will take place than at room temperature. The temperature the solution will be exposed to will depend on the boiling temperature of the solvent type used. These temperatures can be viewed in Table 2.6.

- Exposure to light and oxygen: In order to reduce binder hardening, the exposure of the solvent-binder solution to light and oxygen pressure must be limited.
- Binder-aggregate type: Despite similar extraction conditions, the degrees of binder hardening varies depending on the binder-aggregate type.

The solvent chosen must have sufficient solvency power to ensure that the binder is completely removed from the aggregate. Pyridine, that is recognised as the solvent with the highest solvency power, will succeed in removing all of the binder from aggregate but because of its highly toxic nature, this solvent cannot be used. Therefore, one might have to sacrifice the solvency power of the solvent, resulting in incomplete removal of binder from the aggregate, to ensure the health and safety of the person conducting the test.

Research has shown that regardless of the solvent used, aggregate is never completely free of binder. The residual binder will either be highly oxidized (aged) causing the polar frictions of the binder to be strongly associated with the aggregate or it has been absorbed by the porous aggregate. Because of the close association between the remaining binder and aggregate, the residual binder must be considered as an integral part of the aggregate, rather than a function of binder. (Mturi *et al.*, 2015)

2.4.1.2 Centrifuge

A centrifuge can be used to separate the suspended particles within a liquid by utilising the principle of sedimentation. The centrifuge has a metal cup (rotor) that rotates about a central axis to generate a centrifugal force that will push the particles away from the rotating axis. The particles with a density higher than the solvent will sink, while the lighter particles will rise to the top.

Once the extraction phase is completed, the content comprising of aggregate, fines, and solvent-binder solution will be poured through a sieve into the funnel of the centrifuge. Various sieves can be placed on top of the funnel to ease with the washing of the aggregate, but a single 0.064 mm sieve would also be sufficient. The washing of the aggregate will continue until the solvent runs effectively colourless from the centrifuge. SANS 3001 (2011) suggest that re-centrifuging must take place where the mass of fine minerals in the cup exceeds 50g. The presence of fines within the recovered binder will contaminate the binder, resulting in stiffer performance properties. As a quality control measure, the ash content can be used to determine the amount of fines present in the recovered binder.

2.4.1.3 Distillation

The goal of the distillation process is to remove the solvent from the recovered binder. Failure to remove the solvent from the recovered binder will result in reduced binder stiffness. Various methods are available to evaluate whether residual solvent is present within the recovered binder (Mturi *et al.*, 2015):

- Gas chromatography
- Infrared Spectroscopy
- Gel permeation chromatography
- High performance liquid chromatography

Mturi et al. (2015) recognises two distillation methods, the Abson (Figure 2.17) and Rotary Evaporator methods (Figure 2.18). The intuitive nature and the low distillation conditions, makes the Rotary Evaporator method very popular, despite accounts of poor repeatability and consistency. Research suggest that recovered binder from the Abson method contains more residual binder than binders recovered from the Rotary Evaporator method.

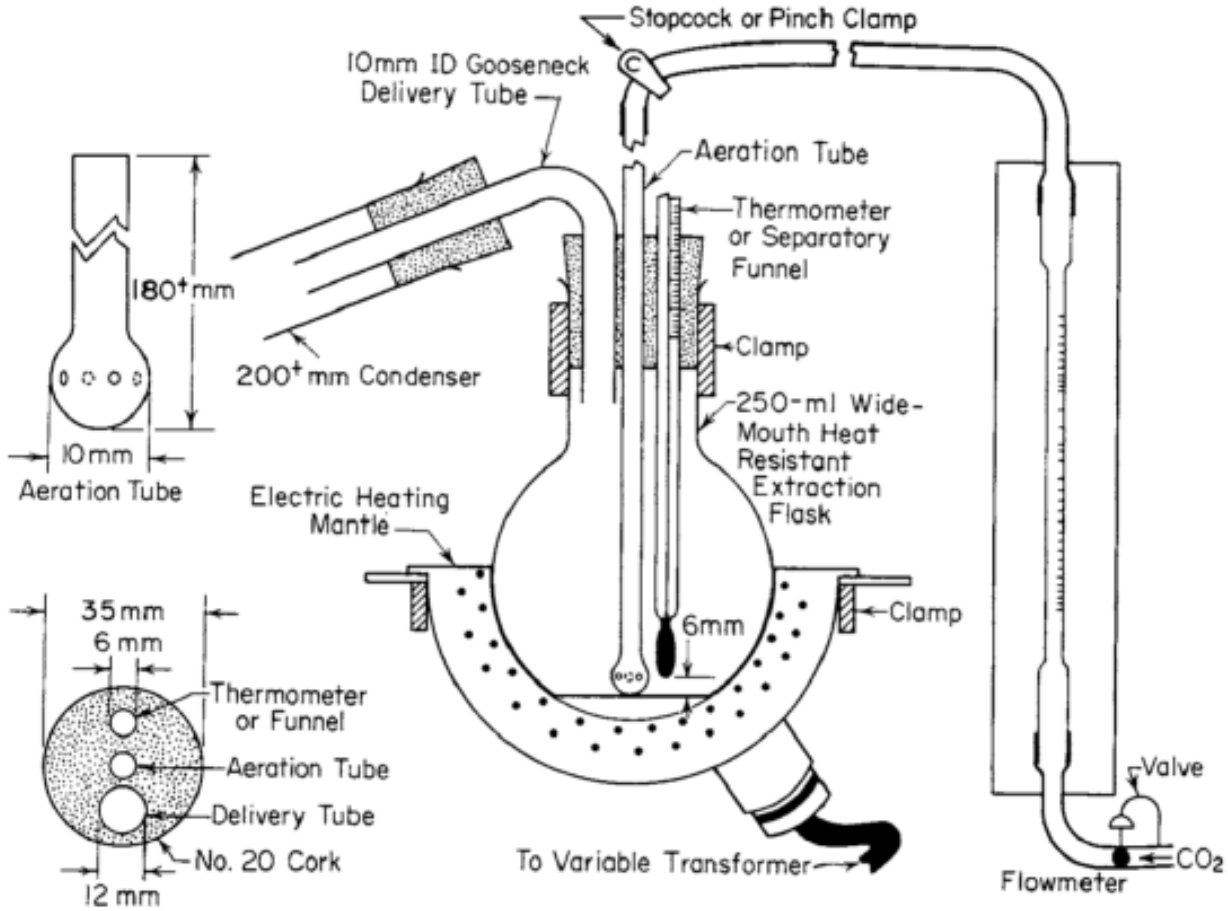

Figure 2.17: Abson Method Illustration (ASTM D 1856, 2009)

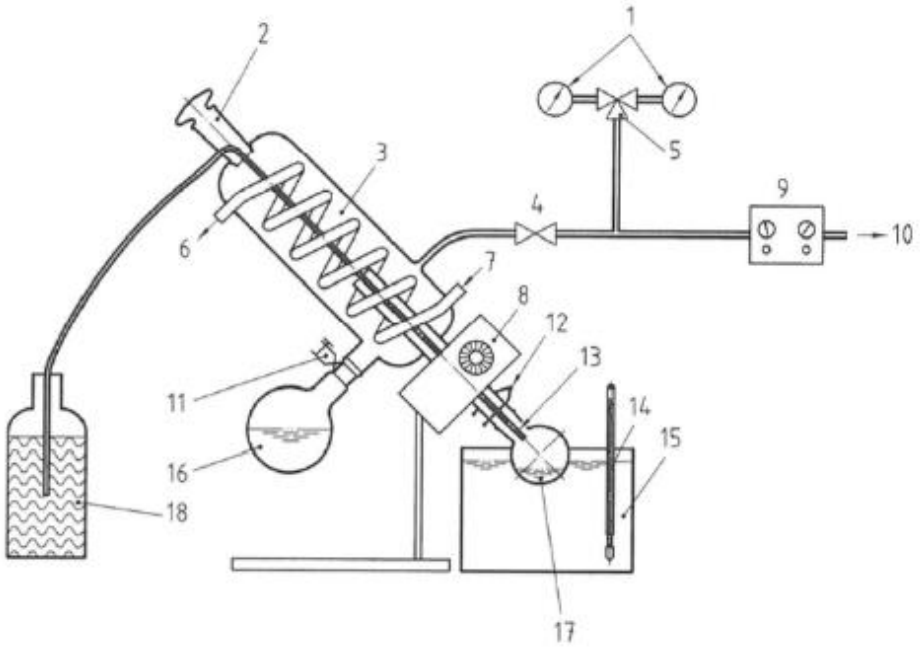

Key

1	vacuum gauge	8	rotary drive motor	14	thermometer
2	induction stopcock	9	vacuum regulator	15	oil bath
3	condenser	10	to vacuum pump	16	receiving flask
4	auxiliary air inlet	11	screw clip	17	rotating evaporating flask
5	change-over valve	12	spring clip	18	bitumen solution
6	water outlet	13	delivery tube (end approximately 1/3 of way into flask)		
7	water inlet				

Figure 2.18: Rotary Evaporator Illustration (EN-12697-3, 2013)

2.4.2 Dynamic Shear Rheometer (DSR)

A dynamic shear rheometer test system comprises of parallel metal plates, a loading device, a temperature controlling device, and a control and data acquisition system. The two parallel test plates can either be 8 mm in diameter or 25 mm in diameter. The plate dimensions can be viewed in Figure 2.19.

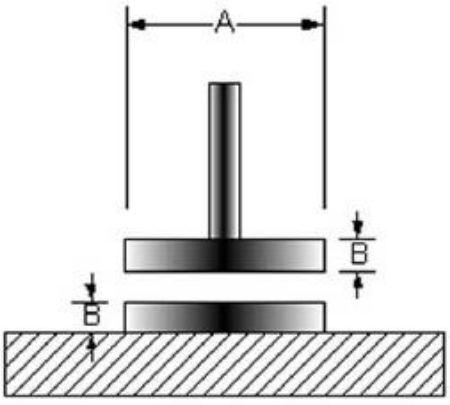

Dimension	8-mm Nominal	25-mm Nominal
A	8 ± 0.1 mm	25 ± 0.5 mm
B	> 1.5 mm	> 1.5 mm

Figure 2.19: Plate Dimensions (ASTM 7175, 2001)

When performing a DSR test, the dynamic mechanical analysis can either be strain-controlled or stress-controlled. During a strain-controlled analysis a sinusoidal strain is applied to the bitumen sample to obtain a stress that is presented as a function of frequency, while a stress-controlled analysis measures the strain response of a sinusoidally varying stress. Figure 2.20 shows a typical stress-strain response for a dynamic sinusoidal load. When a strain-control analysis is conducted, the operator will provide a target strain percentage and the DSR will determine the torque (T) and the phase angle (δ). (Mturi et al., 2011)

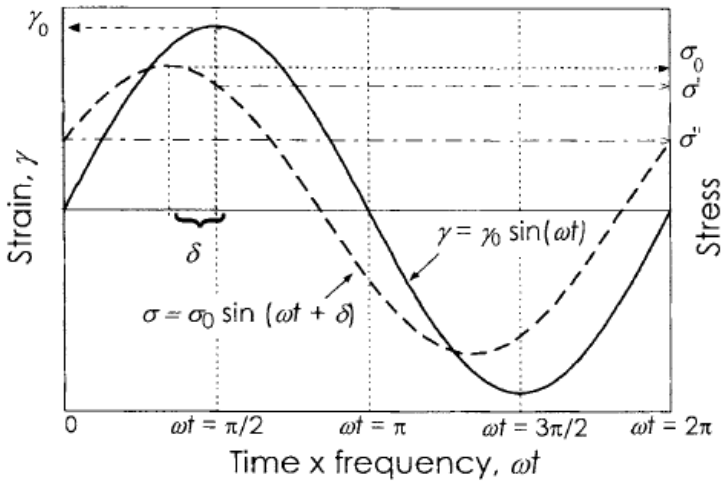

Figure 2.20: Measured Stress-Strain Material Response (Shaw and MacKnight, 2005)

From the measured torque and phase angle (δ), the complex shear modulus (G*) is calculated. These parameters measure the viscous and elastic behaviour of the binder. G* indicates the resistance of the binder to deformation under shear load pulses, as seen in Equation 2.10. δ suggests the relative proportion of recoverable and non-recoverable deformation. Figure 2.20 shows that δ can be visually represented as the time lag between the maximum applied shear stress and the corresponding maximum shear strain resultant. (SABITA, 2016)

$$G^*(\omega) = \frac{|\tau(\omega)|}{|\gamma(\omega)|} \tag{2.10}$$

Where G*(ω) = Complex Shear Modulus at frequency ω (Pa)

|τ(ω)| = Absolute magnitude of the dynamic shear response (Pa)

|Y(ω)| = Absolute magnitude of the applied dynamic shear strain (m/m)

Once G* and δ has been obtained, other reporting parameters, such as the loss modulus (G'') and the storage modulus (G'), can be calculated. G' (Equation 2.11) portrays the in-phase component of G*, and G'' (Equation 2.12) portrays the out-of-phase component of G*. (Mturi et al., 2011)

$$G'(\omega) = G^*(\omega)\ \cos\delta \tag{2.11}$$

$$G''(\omega) = G^*(\omega)\ \sin\delta \tag{2.12}$$

Where G' = Dynamic Storage Modulus at frequency ω (Pa)

G'' = Dynamic Loss Modulus at frequency ω (Pa)

δ = Phase angle (°)

G' and G'' should not be interpreted as elastic or viscous moduli. As seen in Figure 2.21, the elastic behaviour only represents part of G', while the viscous behaviour presents part of the G''. As mentioned earlier, real viscoelastic materials display a remarkable amount of delayed elastic response. This response is time-dependent but completely recoverable. Therefore, G' and G'' represent a portion of the delayed elastic response. For purely elastic materials δ = 0°, while δ = 90° for purely viscous materials. When binders are compared in terms of phase angles, a smaller phase angle implies that the material has a larger elastic component, allowing the material to recover better from an applied load. (Mturi et al., 2011)

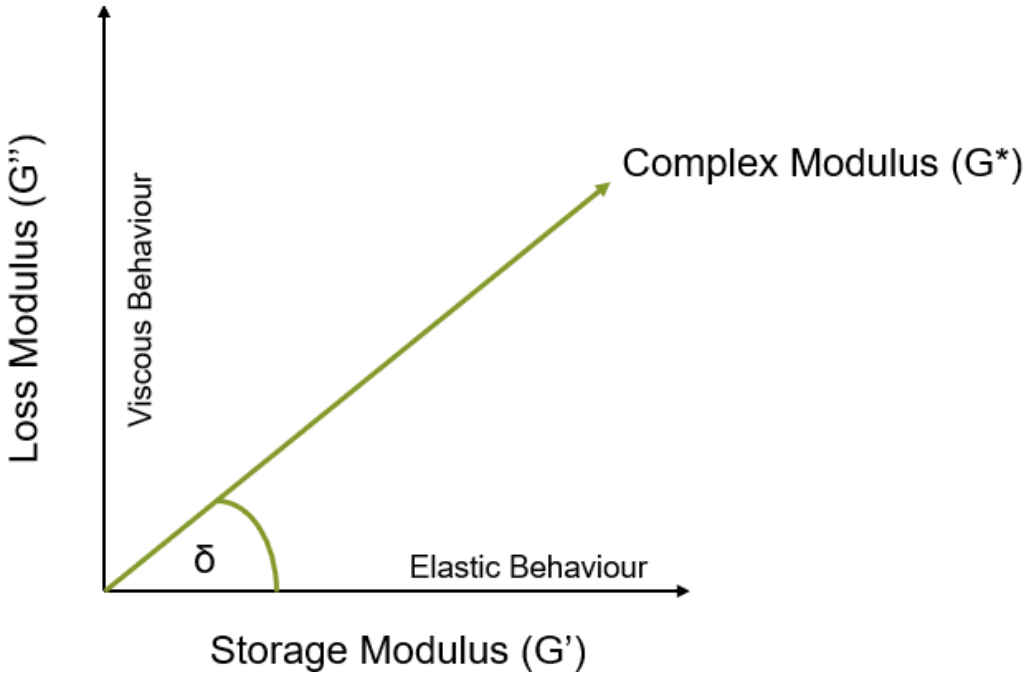

Figure 2.21: Viscoelastic Behaviour from Dynamic Mechanical Properties

Other viscoelastic parameters can be obtained from G* and δ. These parameters include the dynamic compliance in shear (J*), as seen from Equation 2.13, and the dynamic complex viscosity in shear (η*), as calculated in Equation 2.14.

$$\eta^* = \frac{G^*}{\omega} \quad (2.13)$$

$$J^* = \frac{1}{G^*} \quad (2.14)$$

Where η* = Dynamic Complex Viscosity in shear

J* = Dynamic Complex Compliance in shear

The following factors can influence the repeatability and reproducibility of the test method (ASTM 7175, 2001):

- Dynamic Shear Modulus: The test method is suitable for binders having a dynamic shear modulus between 100 Pa and 10 MPa. The dynamic shear modulus is typically achieved at temperatures in the range of 4ºC and 88 ºC at 10 rad/s. The binder grade, test temperature and ageing of the binder will play a role here.
- Particulate Material: The largest dimension of binder particles must be less than 0.250 mm. Where two-phase material is tested, the thickness of the test specimen must be at least four times the maximum particle size.
- Steric Hardening: the time-dependent effect of molecular association that occurs when binder is stored at ambient temperature. Binder should be heated until sufficiently fluid in order to remove the effects of steric hardening.
- Thermal History: the number of times that binder has been heated before testing commences should be limited to one heating cycle if possible.
- Trimming: excess binder must be removed from the test specimen to ensure that the test specimen is flush with the outer diameter of the top and bottom plate. Improper trimming will change the sample geometry and result in discrepancies.

Typically, three types of tests can be performed on the DSR: strain sweeps, frequency sweeps and multiple stress creep and recovery (MSCR). For the purpose of this study, MSCR is not performed. Therefore, only strain sweeps and frequency sweeps will be discussed.

2.4.2.1 Strain Sweep

The strain sweep is conducted at a constant temperature and frequency, while an increasing strain percentage is applied to the bitumen sample. The goal of the strain sweep is to determine the region of linear behaviour (LVE). Within this region G* is independent of stress or strain. As seen from Figure 2.22, the position where the complex modulus decreases to 95% of the initial modulus, defines the upper limit LVE. (Mturi et al., 2011)

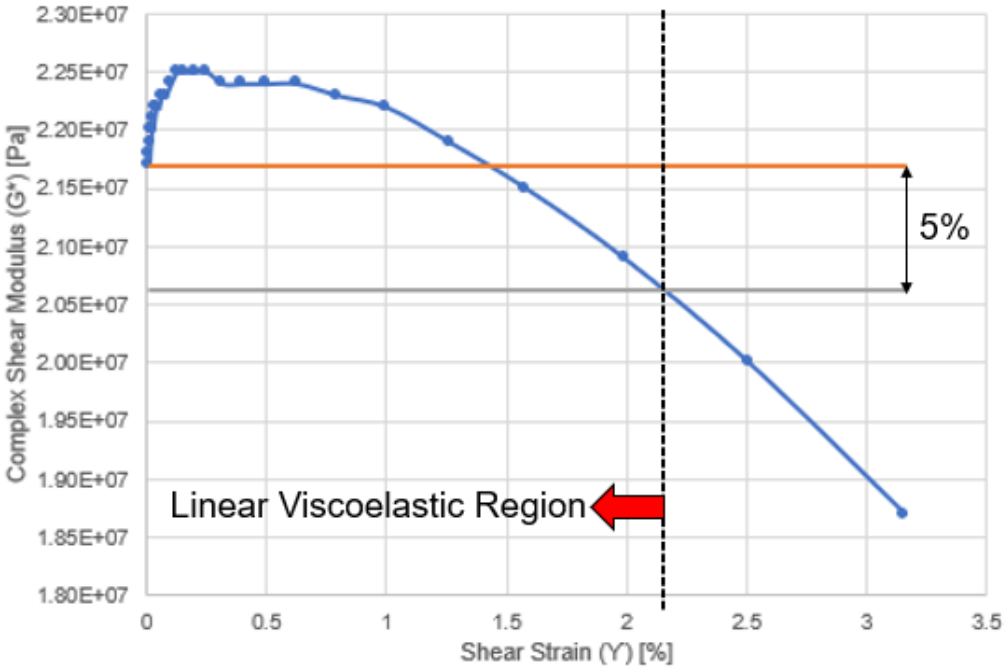

Figure 2.22: Linear Viscoelastic Region

A study lead by Airey et al. (2002) considered the LVE range of conventional and modified binders over a range of temperatures and frequencies. A strain dependent LVE criteria between 2% and 6% was discovered for both conventional and modified binders at low temperatures. It was also found that modified binders have narrower LVE ranges because of the increase in stiffness that is associated with modification.

Another study was conducted by Mturi et al. (2011) to determine the effect of temperature and ageing conditions on G*. The key findings were that the LVE limit tend to increase when temperature is increased; and an increase in test frequency, results in an increase of both G* and G' that will reduce the LVE limit. It was concluded that a reduction in temperature or loading time will cause a reduction in the LVE limits.

2.4.2.2 Frequency Sweep

During the frequency sweep a variety of load frequencies are applied while the temperature and strain remains constant. The strain sweep is conduced beforehand to certify that the applicable strain is within the LVE range. Since frequency is the inverse value of time, the frequency sweep allows for the time-dependant shear behaviour of the binder to be examined. From the frequency sweep a stiffness isotherm is obtained. The process is repeated at a variety of temperatures in order to evaluate the specific behaviour of the binder over a wide temperature range.

2.4.3 Bending Beam Rheometer (BBR)

A Bending Beam Rheometer comprises of a loading frame, a data acquisition system, and a temperature-controlled liquid bath. Figure 2.23 shows a schematic representation of the loading frame. The liquid bath has the following two functions: (1) maintain the bitumen specimen at the test temperature and (2) provide a buoyant force to counterbalance the force resulting from the mass of the test specimen. (ASTM D 6648, 2008)

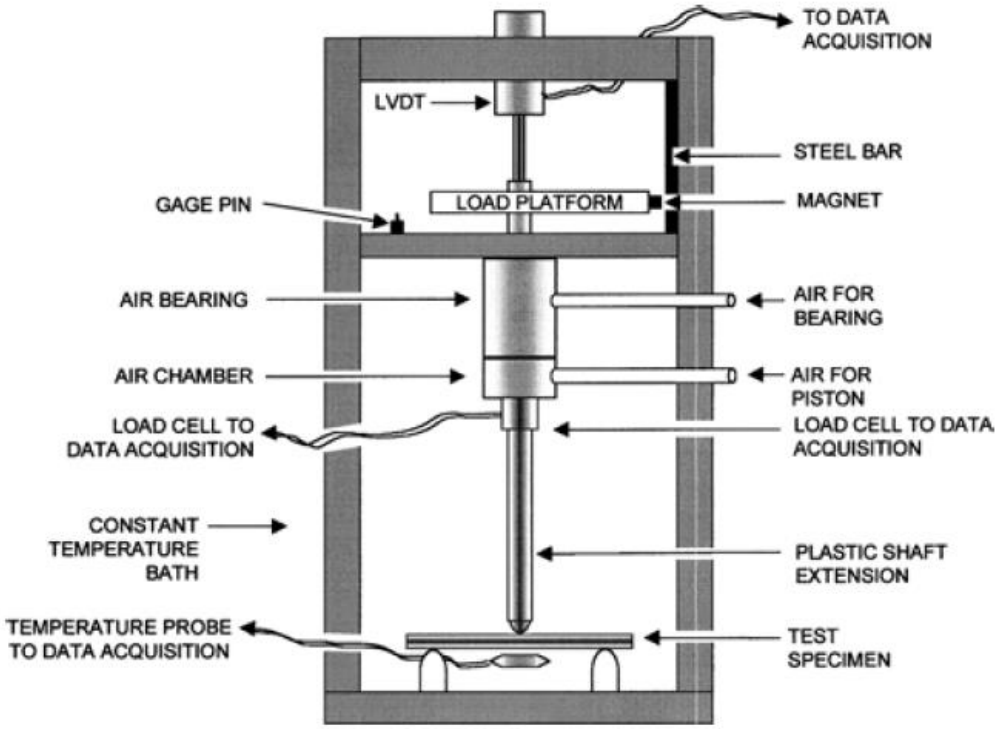

Figure 2.23: Schematic Representation of the BBR Loading Frame *(ASTM D 6648, 2008)*

The purpose of the BBR is to determine the amount of permanent deformation a binder is exposed to at a given temperature. The BBR test is conducted at low temperatures between 0°C and -36 °C, where the binder tends to behave as an elastic solid. The low temperature rheological properties will be used to evaluate the tendency of the binder becoming brittle and determine the binder's stiffness and relaxation abilities at low temperatures. (SABITA, 2016)

During the BBR test, a constant test load is applied to the mid-point of a simply supported bitumen beam for 240 seconds. The load will simulate the stresses that gradually build up in a layer at low temperatures. The central deflection is measured at various time intervals, as seen from Figure 2.24(a).

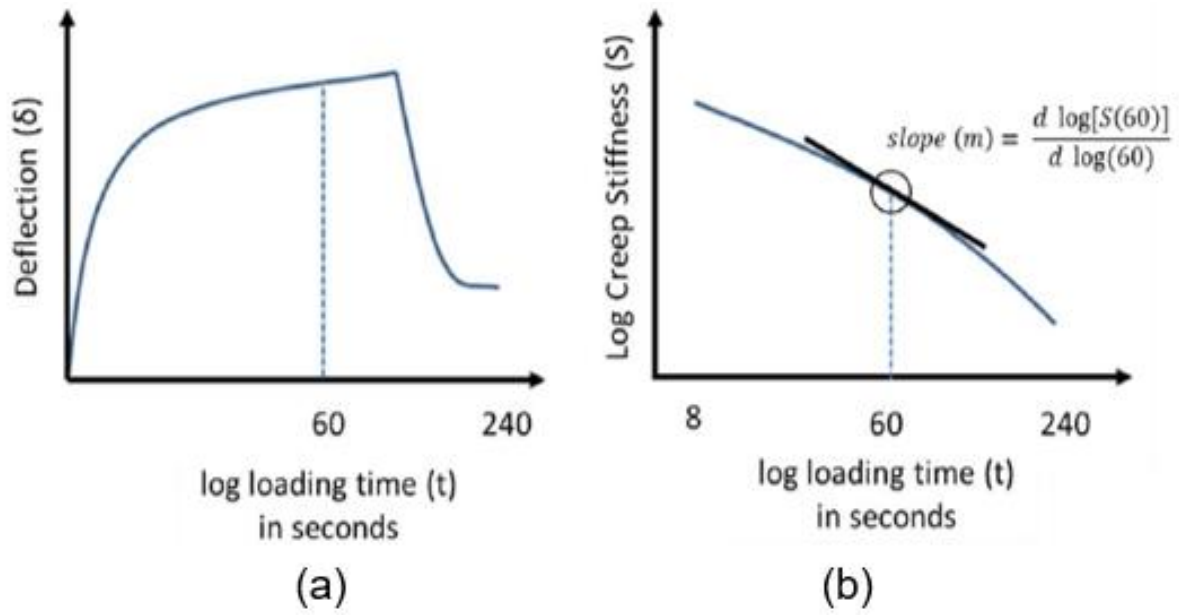

Figure 2.24: BBR Output (SABITA, 2016)

Principles of linear elastic beam theory is used determine the flexural creep stiffness (Equation 2.15) and creep rate (Equation 2.16) (Figure 2.24(b)) of the binder, from the measured deflections. The flexural creep stiffness of the bitumen measures the binder's resistance to creep loading, while the creep rate describes the change in binder stiffness with time during loading. (SABITA, 2016)

$$S(t) = \frac{PL^3}{4bh^3\delta(t)} \tag{2.15}$$

Where S(t) = flexural creep stiffness at time t (MPa)

P = constant creep load (mN)

L = distance between the beam supports (mm)

b = bitumen bean width (mm)

h = bitumen beam depth (mm)

δ(t) = beam deflection at time t (mm)

t = loading time (s)

$$m(t) = \left|\frac{d\log[S(t)]}{d\log(t)}\right| \tag{2.16}$$

Where m(t) = stress relaxation factor = slope of the log [S(t)]

log[S(t)] = logarithm stiffness function (MPa)

log(t) = logarithm of loading time (s)

The following factors can influence the repeatability and reproducibility of the test method (ASTM 7175, 2001):

- Physical hardening: a time-dependent increase in stiffness that occur at low temperatures. Since excessive cooling will create unwanted hardening, the conditioning time must be monitored to prevent variability.
- Beam geometry: as seen from Equation 2.13, the dimensions of the bitumen beam are used to determine the beam stiffness. Therefore, care should be taken to prevent deformation of the beam during demoulding.
- Initial conditioning load: deflection due to the initial 8 second conditioning load must be discarded since load stabilisation has not yet taken place.
- Deflections: the test method does not allow for deflections more than 4 mm or less than 0.08 mm.

2.4.4 Fourier-Transform Infrared Spectroscopy (FTIR)

Various methods, such as the Gas or Gel Permeation Chromatography, Fourier Transform Infrared Spectroscopy (FTIR), and Corbett chromatography, are available to analyse the chemistry of bitumen. From these methods, FTIR is a popular choice to examine the effect that oxidative ageing has on the chemical composition of bitumen.

The chemical composition of a material is established from the bond energy between the components of the material. FTIR considers the interaction between infrared light and the bonds within a material. An infrared light beam is introduced to the material. At distinct frequencies, the active bonds within the material will absorb the energy of the infrared light. A detector is used to identify these absorbed frequencies in order to determine the absorbance of the sample. The absorbance is calculated as the difference between the light intensity entering and leaving the sample. (Van Den Bergh, 2011)

For the molecular analysis of bitumen, the mid-infrared region (400 to 4000 cm^{-1}) is relevant. Information regarding oxidative ageing will reflect in the compounds containing oxygen, namely the carbonyls and sulfoxides, and the aliphatic hydrocarbons. Therefore, ageing is typically observed between 600 to 1800 cm^{-1}. Since the composition of bitumen varies based on its origin, Van Den Bergh (2011) suggest that ranges of wavenumbers be used to evaluate the ageing components. Figure 2.25 contains the FTIR absorbance of three different bitumen types. The ranges of primary concern, aliphatic hydrocarbons at approximately 1460 cm^{-1}, carbonyls near 1700 cm^{-1}, and sulfoxides near 1030 cm^{-1}, are also indicated.

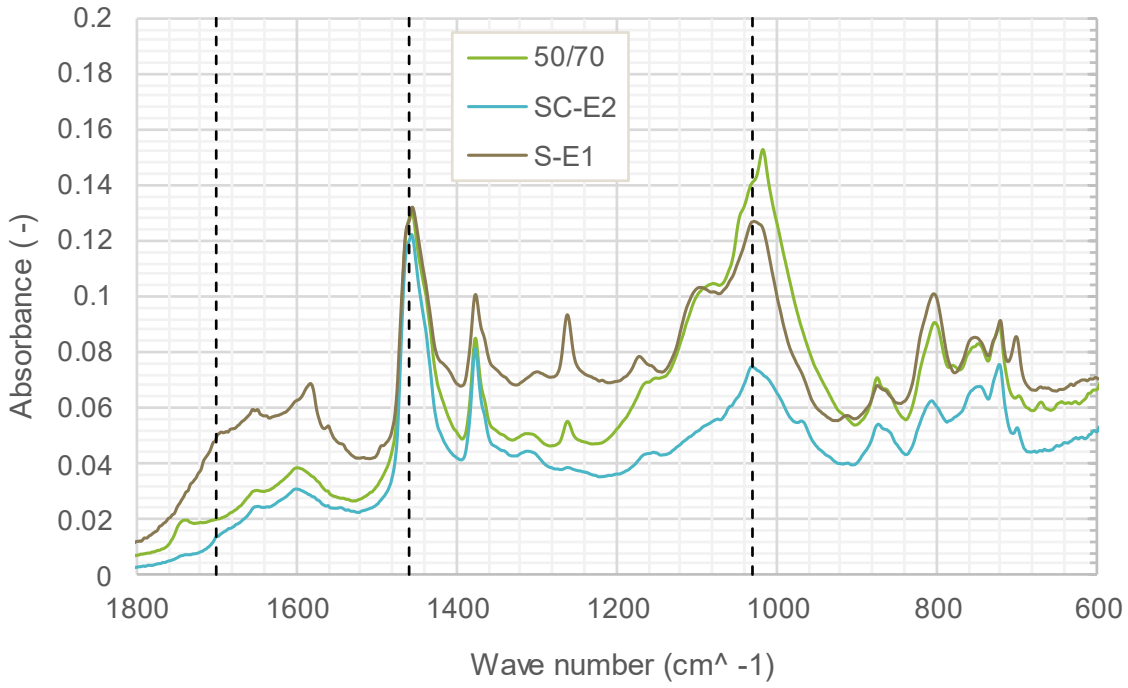

Figure 2.25: FTIR Absorption and Peaks for Bitumen

FTIR can also be extended to solvents. This is useful in binder recoveries, since the functional groups of the solvent and binder can be analysed to determine the existence of solvent within the binder. Figure 2.26 contains the FTIR absorbance of three different solvents. The following peaks are identified for each solvent: Trichloroethylene near 840 and 930 cm^{-1}, Toluene near 690 and 730 cm^{-1}, and ethanol near 1040 cm^{-1}.

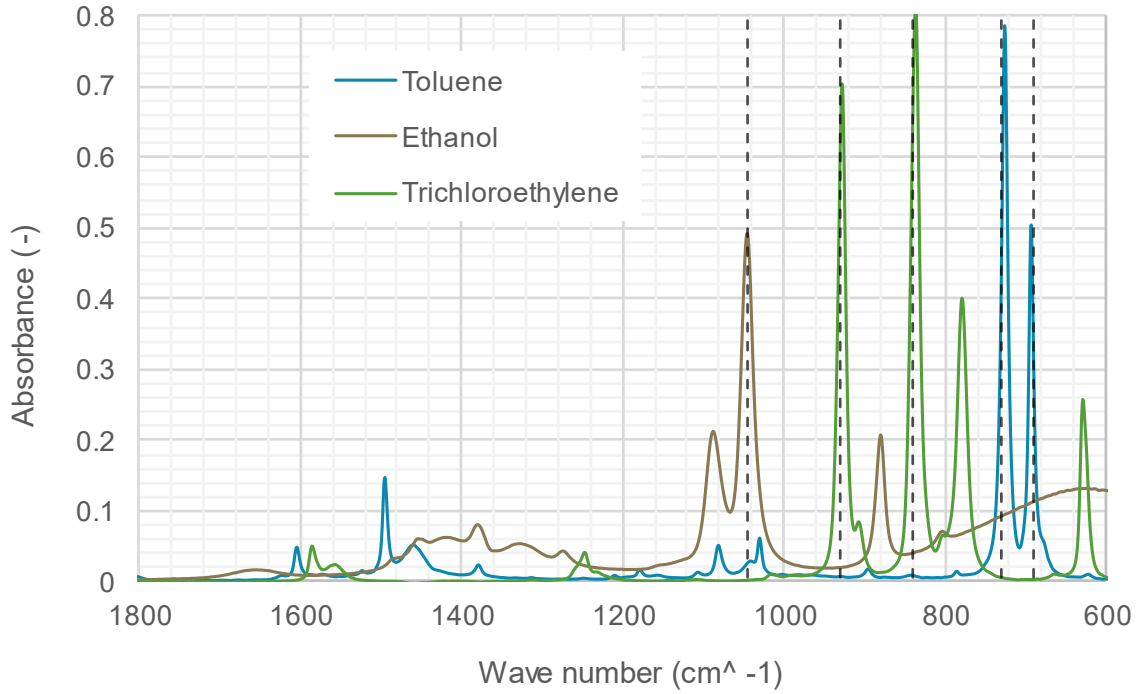

Figure 2.26: FTIR Absorption and Peaks for Solvents

2.5 Modelling of Rheological Properties

As explained in Chapter 2.1.3, bitumen is a viscoelastic material, therefore the performance of the binder is influenced by both loading rate and temperature. It is important to understand the rheological properties of binders since these properties are directly related to the in-situ behaviour of actual pavement mixtures. Models are used to explain the rheological performance of the binder and will allow analysts to predict and evaluate the behaviour of a binder under certain conditions.

In the 1950's LVE rheological properties of bitumen were portrayed by using nonlinear multivariable methods, called nomographs. Unmodified binders were used to develop this model, rendering it not suitable for polymer-modified bitumen. Nomographs rely on temperature, softening point, loading time and penetration index (PI). The PI and softening point of the binder are properties that are typically associated with the previous Penetration Grade Specifications. The development of computational methods, empirical algebraic equations and mechanical element approaches have provided alternative means for representing rheological properties. The incorporation of the PG Specifications has also contributed to the decline in use of nomographs. (Yusoff, Shaw and Airey, 2011)

Two of the primary analytical tools used for examining the rheological properties of binders include the construction of master curves and Black Space diagrams. Master curves of G* versus ω is used to model the material response to loading. Black Space diagrams, where G* is plotted against δ, indicate the durability of the binder by considering age and temperature related behaviour.

In Chapter 2.4.2 it was mentioned that viscoelastic parameters such as G*, δ, G', and G'', must be obtained under linear viscoelastic (LVE) conditions. The reason being that within this region, the stress-strain response is only affected by temperature and loading rate and not by the degree of stress or strain. It is very difficult to model the non-linear response of viscoelastic materials. By limiting the testing conditions to within the LVE range, the material response can be simplified by applying the principles of time temperature superposition.

2.5.1 Time-Temperature Superposition Principle (TTSP)

The interrelationship between frequency and temperature within the LVE range allows for the time-temperature shift factors to be applied to measurements taken at different temperatures, to create a continuous graph at a reduced frequency. This graph, also referred to as a master curve, will represent the behaviour of the binder at a given temperature over a wide range of

frequencies. The principle used to relate the equivalency between temperature and frequency in order to construct master curves, is called the time-temperature superposition principle. (Yusoff, Shaw and Airey, 2011)

Dynamic data is collected at a various temperature and frequency ranges, as seen in Figure 2.27. A standard reference temperature (T_{ref}) is selected and all of the other temperature isotherms are shifted with respect to frequency until the curves merge into a single, smooth curve, as represented in Figure 2.28. Given that no phase transformations or structural rearrangements in terms of temperature or time took place, the TTSP is valid, meaning that all other viscoelastic properties can also form continuous functions after shifting. Although the TTSP cannot be applied to data obtained outside the LVE range, master curves can still be constructed over different viscoelastic regions. (Christensen and Anderson, 1992)

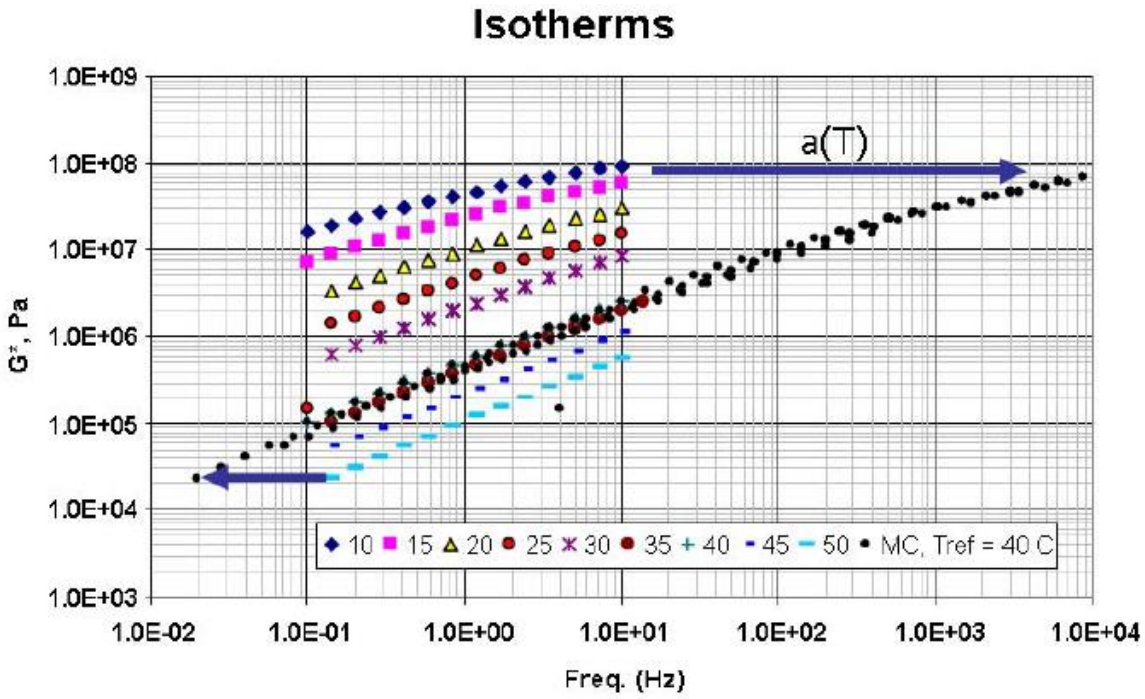

Figure 2.27: Isotherms of G* (Rowe and Sharrock, 2011)

Shift factors (α_T) are used to determine the extent to which isotherms must be shifted. In conjunction with the master curve, a plot of α_T versus temperature is constructed based on the reference temperature. At T_{ref} the value of α_T is equal to one and log α_T is equal to zero. The location and shape of the master curve represents the time dependency of the binder, while the plot of the shift factor indicates the temperature dependency. Temperature dependency is crucial in determining the relaxation of the binder due to a change in temperature. (Yusoff, Chailleux and Airey, 2011)

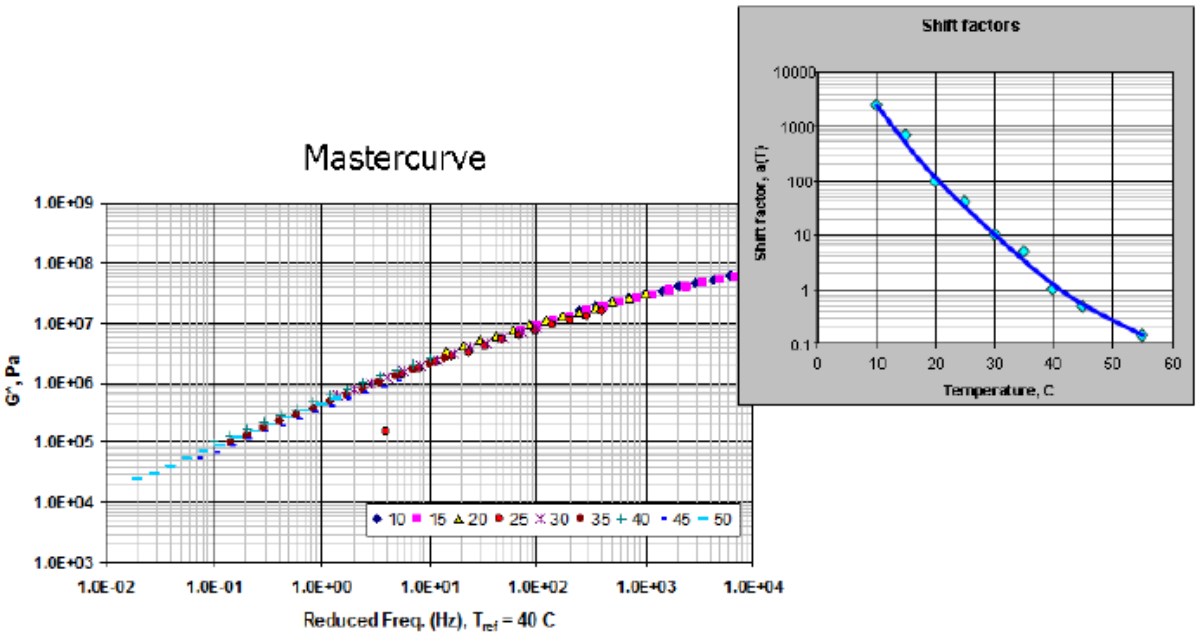

Figure 2.28: Corresponding Master Curve and Shift Factor (Rowe and Sharrock, 2011)

From the shift factors, the reduced frequency is calculated as seen from Equation 2.17. The master curve typically comprises of G* plotted against the reduced frequency (ω_r (rad/s) or f_r (Hz)). (Yusoff, Chailleux and Airey, 2011)

$$f_r = \alpha_T * f \tag{2.17}$$

Where f_r = reduced frequency at reference temperature (Hz)

α_T= shift factor

f = tested frequency

Two approaches, namely free shifting and constrained shifting can be used to construct shift factors. Free shifting refers to the manual approach where the shift factors are independently obtained for each isotherm, while constrained shifting uses an underlaying model to convert the data into fitting a predefined functional form. Where the degree of temperature or frequency susceptibility is unknown, a free shifting approach should be used to ensure that the shape of the individual isotherms determine the shape of the master curve. (Rowe and Sharrock, 2011)

Various shifting techniques are available to construct G* master curves when applying the TTSP. The following shift factors are typically used (Yusoff, Chailleux and Airey, 2011):

- Arrhenius
- William, Landel and Ferry (WLF)

- Kaelble
- Modified Kaelble

These empirical methods can deliver different results. It should be noted that these shift functions only account for horizontal movement. Vertical shifting represents temperature induced density changes. Research found that since vertical shifting is reliant on the thermal history of the binder, vertical shifts do not deliver accurate temperature adjustments. (Yusoff, Chailleux and Airey, 2011)

The **Arrhenius** equation is accurate where the temperature is below the glassy transition temperature (T_g) and within the Newtonian region (Yusoff, Shaw and Airey, 2011). The purpose of the constant within the Arrhenius equation (Equation 2.18) is to ensure a linear relation between the shift factor and reciprocal of temperature (Rowe and Sharrock, 2011).

$$\log \alpha_T = C \left(\frac{1}{T} - \frac{1}{T_{ref}}\right) \tag{2.18}$$

Where C = Constant

The **WLF** equation (Equation 2.19) is based on the free volume theory and it has been shown to provide adequate representation where the temperature is above T_g (Rowe and Sharrock, 2011). The incorporation of the temperature differences allows for the practical manipulation of the equation (Hunter et al., 2015) .

$$\log \alpha_T = \frac{-C_1(T - T_{ref})}{C_2(T - T_{ref})} \tag{2.19}$$

Where C1, C2 = Constants

Since both the WLF and Arrhenius equations are derived from theoretical analysis, the input parameters can shed light on the molecular structure of the bitumen (Marasteanu and Anderson, 1996). Where binders behave as visco-elastic solids, neither Arrhenius nor WLF will adequately shift the data sets (Rowe, Baumgardner and Sharrock, 2009)

The defining temperature (T_d) refers to the transition point that distinguished the temperature regions where the Arrhenius (below T_g) and WLF (above T_g) equations better describes the generated shift factors. T_d is similar in nature to T_g (Rowe and Sharrock, 2011).

The **Kaelble** shift equation (Equation 2.20) incorporates an inflection point at T_d, where the shape of the curve changes from hyperbolic to sigmoidal. Above the inflection point

temperature the curve is equivalent to a WLF curve, while below the inflection point temperature the curve slowly proceeds towards a horizontal asymptote. (Rowe and Sharrock, 2011)

$$\log \alpha_T = \frac{-C_1(T-T_d)}{C_2(T-T_d)} \quad (2.20)$$

Where T_d = Defining Temperature

Unfortunately, the Kaelble equation is difficult to apply since the form of the equation suggest that T_{ref} and T_d are similar. In order to address the difficulty, the **Modified Kaelble** equation (Equation 2.21) was developed. This equation introduces an additional constant to separate T_{ref} and T_d. (Rowe and Sharrock, 2011)

$$\log \alpha_T = -C_1 \left(\frac{T-T_d}{C_2|T-T_d|} - \frac{T_{ref}-T_d}{C_2|T_{ref}-T_d|} \right) \quad (2.21)$$

Rowe, Baumgardner and Sharrock (2009) analysed various functional forms for master curves. Where shift factors are extended to lower temperatures, Figure 2.29 shows that Arrhenius and WLF approaches high values. This observation is consistent with the fact that the WLF method is most accurate above T_g. The sigmoidal behaviour of the Kaelble method prevent excessively high values as the temperature decreases.

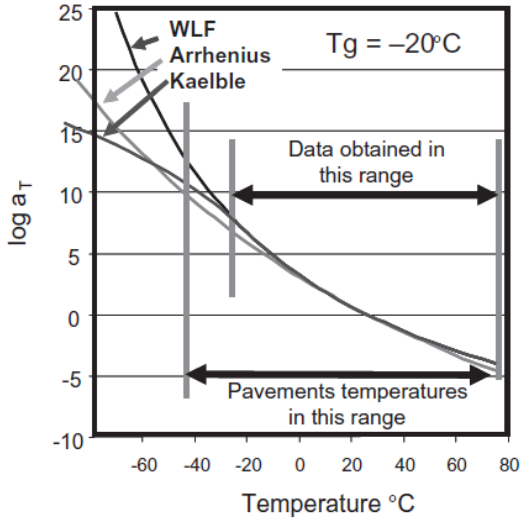

Figure 2.29: Shift Function with Cold Temperature Extension (Rowe, Baumgardner and Sharrock, 2009)

Rowe and Sharrock (2011) evaluated alternative shift factors to describe the temperature dependency of viscoelastic behaviour of asphalt materials and ranked the shifting equations in terms of the root mean square error. This study also confirms, as seen in Figure 2.30, that the Kaelble equation is the best fit at lower temperatures, followed by the WLF.

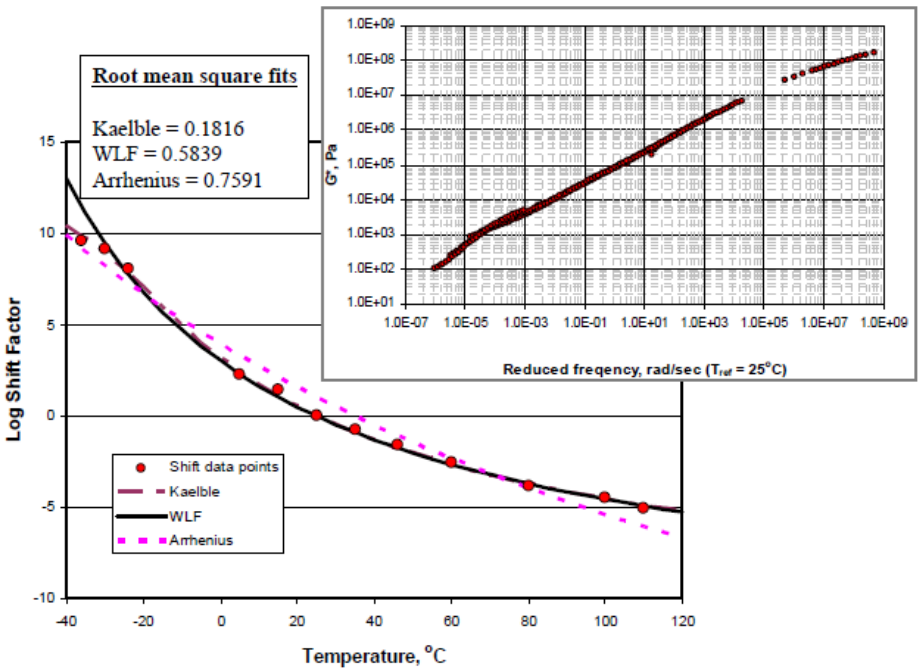

Figure 2.30: Comparing Shift Factors (Rowe and Sharrock, 2011)

2.5.2 Rheological Models for Seal Binder Performance

Mathematical models comprising of empirical algebraic equations are used to describe the linear viscoelastic rheological properties of bitumen. Each model has advantages and disadvantages that should be considered when choosing a suitable model. In order to characterise the rheological properties, various parameters have been identified. Figure 2.31 schematically represents the four primary parameters that are used to distinguish the viscoelastic properties of binders.

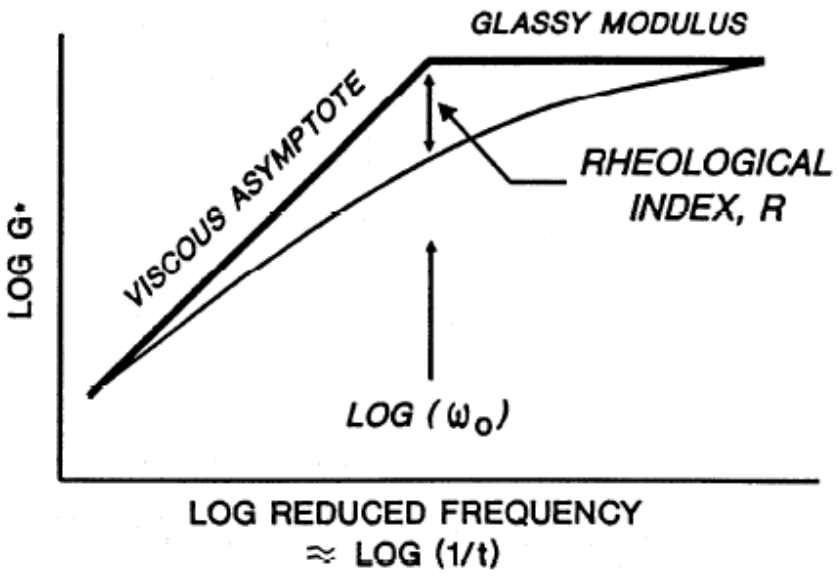

Figure 2.31:Parameters used to Characterise Master Curves (Christensen and Anderson, 1992)

These parameters can be defined as follows (Christensen and Anderson, 1992):

- Glassy modulus (G_g): refers to the asymptote that G*, G' and G'' will strive towards at low temperatures and high frequencies or short loading times. The value of G_g will range between 0.6 and 1.5 GPa, but typically 1 GPa will prove sufficient for analytical purposes.
- Steady-state viscosity (η_o): describes the limit of the dynamic viscosity as δ approaches 90^o. Within this region the viscous material response will govern.
- Crossover frequency (ω_c): the frequency where tan δ = 1, in other words where the G' is equal to G''. ω_c should be considered a hardness parameter that specifies the consistency of the binder at a certain temperature.
- Rheological index (R): is the difference between G_g and G*(ω_c). A larger R-value will result in a wider relaxation spectrum. The R-value is also proportional to the asphaltene content of the binder.

The **Standard Sigmoidal (SS)** Model assumes a symmetrical sigmoidal shape around a midpoint. The input parameters are defined in Figure 2.32. The SS model was widely used for asphalt mixes (Yusoff *et al.*, 2013).

$$\log|G^*| = \upsilon + \frac{\alpha}{1+ e^{\beta+\gamma\{\log(\omega)\}}} \tag{2.22}$$

Where v = value of lower asymptote

α = the difference between the upper and lower asymptote

β = determines the horizontal location of the inflection point

ϒ = influences the shape of the curve

ω = reduced frequency

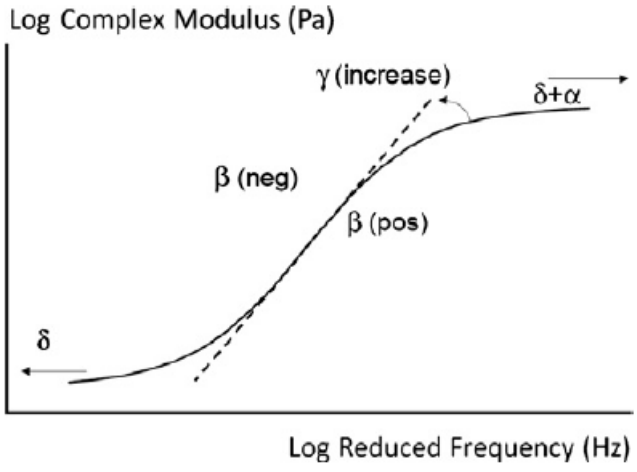

Figure 2.32: Standard Sigmoidal Modal (Yusoff *et al.*, 2013)

In order to model the data, Yusoff *et al.* (2013) decided on initial values of β = -1, δ = 1 and ϒ = 1. It was discovered that all of the δ values were negative, which implied that at high temperatures and/or low frequencies, G* was very small. Furthermore, the value of ϒ for modified and unmodified binders remained consistent despite ageing, while the β value for both modified and unmodified binder decreased with ageing. This is expected since ageing creates harder binders due to the increase in asphaltene content.

It was concluded that the SS model could not accurately fit the rheological properties of highly modified binders. Not all binders exhibit symmetric sigmoidal properties as required by the SS model, hence the **Generalised Logistic Sigmoidal (GLS)** model was developed to account for the effect of non-symmetry.

$$\log|G^*| = \upsilon + \frac{\alpha}{[1+\lambda e^{(\beta+\gamma\{\log(\omega)\})}]^{1/\lambda}} \qquad 2.23$$

Where λ = coefficient accounting for the effect of non-symmetry in the function

When modelling the data, Yusoff *et al.* (2013) selected initial values of β = λ = ϒ = 1. Findings similar to the SS model was experienced. From unaged to aged, the value of λ increased, suggesting that ageing will impact the bitumen microstructure.

Christensen and Anderson (1992) developed the **Christensen Anderson (CA)** model, which comprises of a diagonal, viscous asymptote, and a horizontal, glassy asymptote. The model is suitable for modelling the simple S-shaped master curves of unmodified binders but is unable to model the plateau zone associated with modified binders (Asgharzadeh et al., 2015).

It was found that the model can be utilised at various temperatures and frequencies ranges, especially extending well into the glassy region. The accuracy of the model decreases as viscous flow is approached at hight temperatures and loading rates (Christensen and Anderson, 1992).

$$|G^*(\omega)| = G_g \left[1 + \left(\frac{\omega_c}{\omega}\right)^{\log 2/R}\right]^{-R/\log 2} \qquad (2.24)$$

$$\delta(\omega) = \frac{90}{1+\left(\frac{\omega}{\omega_c}\right)^{\log 2/R}} \qquad (2.25)$$

$$R = \frac{(\log 2)\log\left[\frac{G^*(\omega)}{G_g}\right]}{\log(1-\frac{\delta}{90})} \qquad (2.26)$$

The **Christensen Anderson and Marasteanu (CAM)** model was developed to address the shortcomings of the CA model by improving the fitting of the curve for both modified and unmodified binders. The CAM model introduced an additional parameter, w, that considers the rate at which the phase angle data approaches the asymptotic values from zero to 90 degrees (Da Silva *et al.*, 2004).

$$|G^*(\omega)| = G_g \left[1 + \left(\frac{\omega_c}{\omega}\right)^{\upsilon}\right]^{-w/\upsilon} \quad (2.27)$$

$$\delta(\omega) = \frac{90\omega}{\left[1+\left(\frac{\omega_c}{\omega}\right)^{\upsilon}\right]} \quad (2.28)$$

Where v = log 2 / R

w = determines the arc length between the asymptotes

Da Silva *et al.* (2004) studies the rheological properties of modified and unmodified binders. The study concluded that within intermediate frequencies, both the CA and CAM models accurately describes the viscoelastic behaviour of unmodified binder but at higher and lower frequency ranges, both models perform inadequate. It was also found that a single parameter (R for the CA model and v for the CAM model) is not sufficient to determine the shape of the relaxation spectrum to adequately describe the viscoelastic behaviour of the binder.

The study conducted by Yusoff *et al.* (2013) found that in terms of the sum of square error (SSE) the GLS method presents the best fit between measured and modelled data, followed by the SS model, CAM model and CA model. Based on measured errors, it is suggested that GLS model, CAM model and CA model be used for temperature ranges between 10 and 75^{o}C and the SS model is suitable between 15 and 75^{o}C. In terms of unaged modified binders, the GLS and SS models far outperforms the CA and CAM models.

2.5.3 Discrete Spectrum Modelling

Another method that can be used to model the rheological properties of bitumen, is discrete spectrum mathematics. Rheological indicators are expressed as a sum of discrete terms, with each term having a characteristic time constant (λ_i). There are positive gaps between these discrete terms, therefore, they are not connected. (Baumgaertel and Winter, 1992)

The model does not require any material specific input values, other than the G' and G'' data set. As seen in Equation 2.29 and Equation 2.30, Baumgaertel and Winter (1989) used the discrete spectrum to formulate equations for the complex modulus components.

$$G'(\omega) = G_e + \sum_{i=1}^{N} g_i \frac{(\omega\lambda_i)^2}{1+(\omega\lambda_i)^2} \quad (2.29)$$

$$G''(\omega) = \sum_{i=1}^{N} g_i \frac{\omega\lambda_i}{1+(\omega\lambda_i)^2} \quad (2.30)$$

Where G_e = equilibrium modulus

N = number of relaxation times/elements

g_i = relaxation strength

λ_i = relaxation time

The variables in Equation 2.29 and 2.30 are calculated by using a nonlinear regression to simultaneously adjust the variables until a good fit for G' and G'' is found. N will typically aim to model the linear viscoelastic indicators with the smallest possible number of times, while g_i and λ_i are considered to be freely adjustable. The time domain in which the discrete spectrum is valid, depends on the frequency domain of the input data. Data can easily be converted between these two domains. From above mentioned equations, G* and λ can be obtained. Due to its ability to predict a wide range of linear viscoelastic material functions, discrete spectrum modelling has been used extensively in flow modelling. (Baumgaertel and Winter, 1989)

2.5.4 Black Space Diagrams

By plotting G* against the δ, a Black Space Diagram can evaluate the stiffness and elasticity of the binder. A Black Space diagram is further distinguished from a master curve, as the principle of time-temperature superposition is not needed to transform data to the reduced frequency domain. (Vega, 2016)

As mentioned earlier, the overall performance of a seal is determined from the combined interaction of the binder and the aggregate. At higher temperatures, the binder will exhibit low stiffness and viscous flow. Hence the aggregate structure will dominate the behaviour. At low temperatures, the binder will be stiffer and more elastic which will reduce the relaxation capabilities of the binder. Since the phase angle demonstrates the relaxation capabilities of the binder, the Black Space diagram is considered a low temperature feature due to the incorporation of the phase angle. (Mensching *et al.*, 2015)

Figure 2.33 is used to indicate how a Black Space diagram is interpreted. At low phase angle values, the binder will be more elastic, in comparison to high phase angle values, where the binder will be more viscous. Higher dynamic modulus values indicate a stiffer binder. As a

binder ages, G* will increase, while δ decreases. This will allow for the use of Black Space diagrams to monitor the effect of ageing on the rheological characteristics of a binder (Rowe, King and Anderson, 2014).

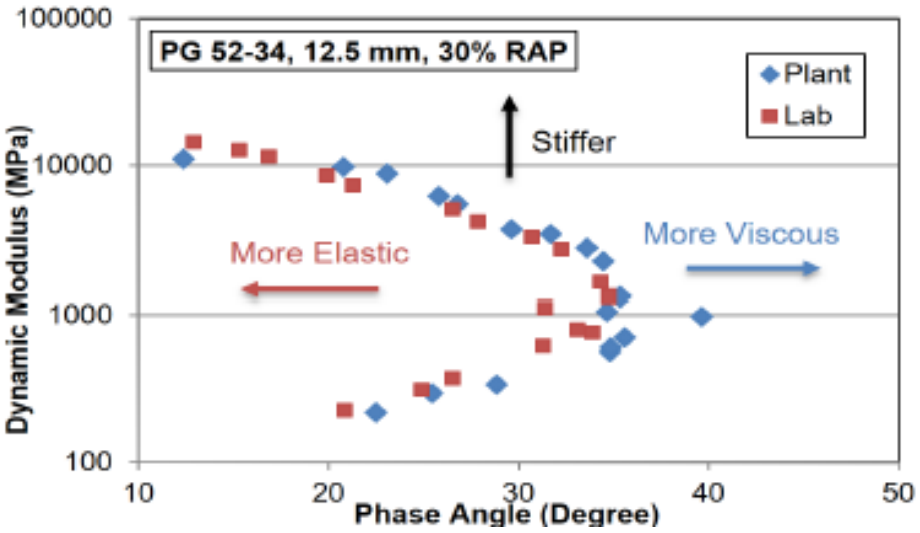

Figure 2.33: Black Space Diagram (Rastegar, 2016)

2.6 Durability Parameters

Scholz (1995) defines the term durability as the ability of the binder to resist the effects of ageing, water, and temperature variation when exposed to traffic loadings without significant deterioration for an extended period of time. Durability parameters are used to describe binder performance by considering the retention of desirable serviceability characteristics and the resistance to the negative influence of ageing. Frequently used durability parameters include:

- Glover-Rowe (G-R, kPa) parameter
- Difference in critical low temperatures (ΔTc, °C)
- Viscoelastic transition (VET) temperature (T_{VET}) and stiffness (G_{VET})

2.6.1 Glover-Rowe parameter

The ductility of recovered binders has shown to correlate well with cracking failure experienced in pavement surfaces. ASTM D113 (2007) defines ductility as the distance to which a bitumen sample will elongate before breaking when pulled apart at a specified speed and temperature. Since ductility measurement is an extensive process, an ideal temperature and elongation rate could ease the process. Glover *et al.* (2001) considered various literature reports and concluded that ductility measured at 15°C at an elongation rate of 1cm/min is a good indicator of the cracking condition of binders.

Glover *et al.* (2001) also examined the effect of ageing on the rheological properties of binders. At intermediate temperatures, it was found that the ageing increased the dynamic viscosity (η') and G'. Since G' increased more rapidly than G'', δ decreased with ageing to ultimately have a substantial effect on the durability. Furthermore, a Maxwell model comprising of a spring and dashpot element was used to represent the elastic and viscous material response during a ductility test. From the model it became clear that the ductility of a binder is reliant on the value of G', as well as the ratio between η' and G'. This led to the development of the Glover Parameter, as defined in Equation 2.31.

$$Glover\ Parameter = \frac{G'}{\eta'/G'} \tag{2.31}$$

The η' and G' used in Equation 2.31 is obtained from the DSR at 15°C and a frequency of 0.005 rad/s, which is equivalent to an elongation rate of 1cm/minute. The Glover parameter is limited to 3 and 90 kPa/s, which correlates to the ductility cracking limits of 3 and 5 cm. From Figure 2.34(a) it appears that there is a general correlation between ductility and the Glover parameter for unmodified binders. Figure 2.34(b) show that for ductility values less than 10 cm, a linear relationship exist between the variables, which is why for conventional binders, the Glover parameter is considered a surrogate for ductility. Glover *et al.* (2001)

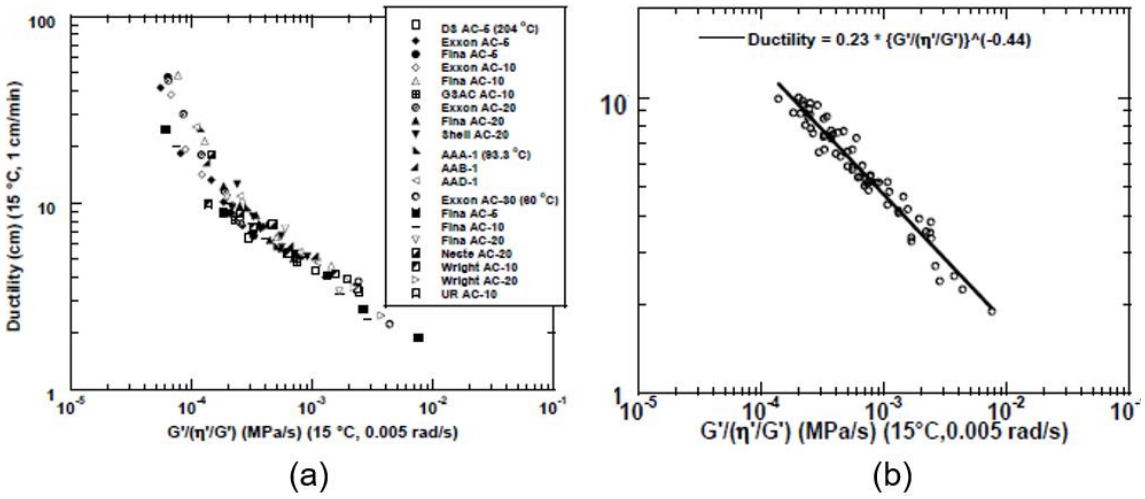

Figure 2.34: Graph of Ductility and Glover Parameter for Unmodified Binders (Glover et al., 2005)

When considering the ductility and Glover parameter for modified binders, Figure 2.35(a) show that the data is significantly more scattered than the unmodified results (Figure 2.34). Within the low ductility region there is also no linear relationship between the ductility and Glover parameter. Despite the lack of correlation, Figure 2.35(a) show that when modified binders are group according to type of modification, the correlation improves. The discrepancies between Figure 2.34 and Figure 2.35 is understandable, since the behaviour associated with

modified binders vastly differ from the behaviour associated with unmodified binders. Figure 2.35(b) shows that the ductility of all of the modified binders outperforms the unmodified binder.

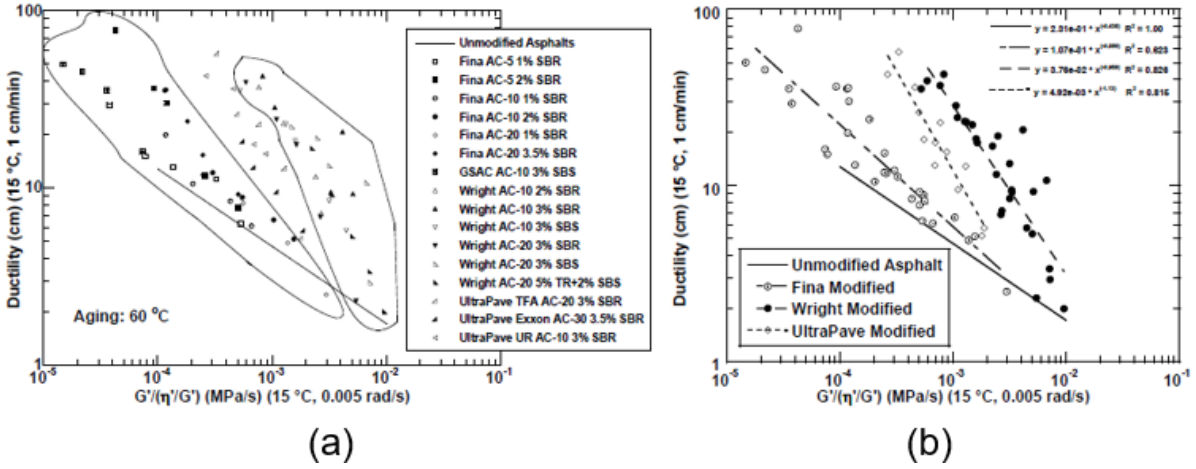

Figure 2.35: Graph of Ductility and Glover Parameter of Modified Binders (Glover *et al.*, 2005)

Rowe et al. (2014) modified the Glover parameter as follows:

$$\eta' = \frac{G''}{\omega}$$

$$G' = \frac{G''}{\tan\delta}$$

Hence, $$\frac{\eta'}{G'} = \frac{G''}{\omega} * \frac{1}{G'} = \frac{\tan\delta}{\omega}$$

Therefore $$\frac{G'}{\left(\frac{\eta'}{G'}\right)} = \frac{G'}{\left(\frac{\tan\delta}{\omega}\right)} = \frac{G'\,\omega}{\tan\delta} = \frac{G^*\cos\delta\,\omega}{\tan\delta} = \frac{G^*\cos^2\delta\,\omega}{\sin\delta}$$

Since the frequency has a fixed value of 0.005 rad/s, it can be ignored to create the Glover-Rowe (G-R) parameter as defined in Equation 2.32:

$$G - R = \frac{G^*\cos^2\delta}{\sin\delta} \qquad (2.32)$$

The Glover-Rowe parameter is also subject to the ductility limitations of 3 and 5 cm, which is equivalent to 180 and 600 kPa. Below 180 kPa no damage is expected but within these boundaries cracking could be present. Since the G-R parameter is expressed in terms of G* and δ, data analysis on Black Space diagrams are possible. These Black Space diagrams can be used to monitor the changes in stiffness and relaxation properties as the binder ages. (Rowe, King and Anderson, 2014)

2.6.2 Critical low temperatures difference

At low temperatures, a binder will approach its limiting stiffness, hence the need to quantify the low-temperature cracking resistance of a binder. The critical low temperature difference (ΔT_c) has been identified as a second parameter to relate ductility and loss of flexibility with ageing. As seen from Equation 2.33, ΔT_c quantifies the difference in continuous grade temperature for stiffness and relaxation properties.

$$\Delta T_c = T_{c,S(60)} - T_{c,m(60)} \tag{2.33}$$

Where ΔT_c = critical low temperature difference

$T_{c,S(60)}$ = stiffness critical temperature at 60 seconds

$T_{c,m(60)}$ = relaxation critical temperature at 60 seconds

Through BBR testing at various temperatures, values for S(60) and m(60) are obtained until the specifications, as required in SATS 3208 (2019), are reached. The specifications include $T_{c,S}$ (Equation 2.34) as the temperature where S(60) = 300 MPa and $T_{c,m}$ (Equation 2.35) as the temperature where m(60) =0.3. Since data extrapolation is prohibited, values of S(60) and m(60) are determined at values lower and higher than 300 and 0,3 respectively in order to interpolate from these values. T_1 and T_2 refer the testing temperatures between which interpolation takes place.

$$T_{c,S(60)} = T_1 + \left[\frac{\log 300 - \log S(60)_1}{\log S(60)_1 - \log S(60)_2} (T_1 - T_2)\right] - 10 \tag{2.34}$$

$$T_{c,m(60)} = T_1 + \left[\frac{0.3 - m(60)_1}{m(60)_1 - m(60)_2} (T_1 - T_2)\right] - 10 \tag{2.35}$$

ΔT_c will indicate whether the binder is m-controlled or S-controlled. For S-controlled binders, $T_{c,S}$ is greater than $T_{c,m}$, resulting in a positive ΔT_c, while a m-controlled binder will have a negative ΔT_c. Anderson *et al.* (2011) found that as ΔT_c increases, the binder becomes more m-controlled which decreases the ductility of the binder. Therefore, a S-controlled binder is preferred. As seen from Table 2.4, SATS 3208 requires $\Delta T_c \geq -5$. Although ΔT_c and G-R measure both stiffness (S and G) and relaxation (m and δ), the temperature at which they operate differ. G-R is more suitable for intermediate temperatures, while ΔT_c operates better at low temperatures. Rowe (2014) found that the Superpave low temperature specifications ($S(60) \leq 300$ MPa and $m \geq 0.3$) can be converted to Black Space variables ($G^* \leq 111$ MPa and $\delta \geq 26.6°$) (Mensching *et al.*, 2015).

2.6.3 Viscoelastic transition temperature and stiffness

The Viscoelastic Transition temperature (T_{VET}) refers to the temperature where the value of δ is 45° and the elastic component of the complex modulus (G') is equal to the elastic component (G'') at a specified frequency. Initially a frequency of 7.8 Hz was used but Widyatmoko, Elliott, Heslop and Williams (2002) opted for a lower frequency of 0.4 Hz (2.56 rads). Since T_{VET} has the ability to quantify the capacity of a binder to heal or dissipate stress, this parameter correlates well to surface cracking. (Rowe and Sharrock, 2017)

The corresponding stiffness, G_{VET}, has also proven useful in assessing the ageing of binders. Since G'' = G', G_{VET} is considered independent of the viscous or elastic response of the binder which suggest that G_{VET} is influenced by the rheological characteristics of the binder.

Figure 2.36 illustrates the change in G_{VET} for a 15pen and 50pen binder at the corresponding T_{VET}. As the binder ages, T_{VET} increases while G_{VET} decreased, resulting in a decrease in the cracking resistance of the binder. Figure 2.36 confirms that G_{VET} is dependent on the bitumen grade and the production route. A harder grade bitumen has a higher T_{VET} and a lower G_{VET}.

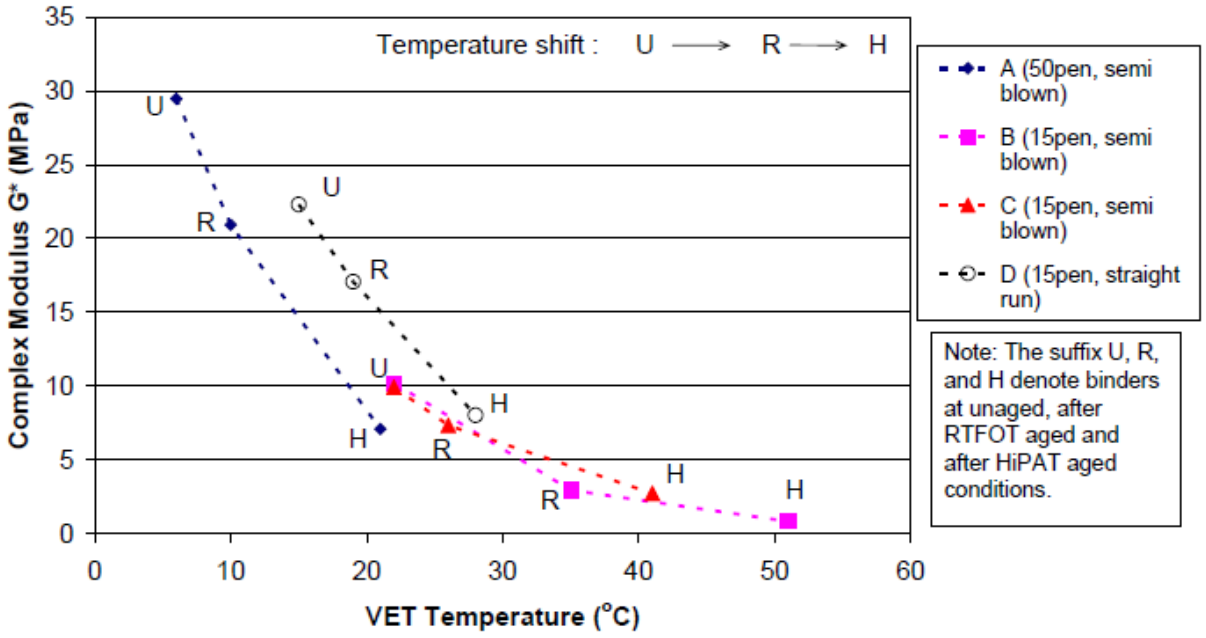

Figure 2.36: G*VET for Different Levels of Ageing at 0.4 Hz *(Widyatmoko et al., 2005)*

Widyatmoko et al. (2005) managed to compile a tentative specification for bituminous binders to minimise the crack susceptibility. The specifications are as follows:

- For 15pen grade bitumen: T_{VET} (0.4 Hz) < 35°C and G_{VET} (0.4 Hz) > 5 MPa.
- For 50pen grade bitumen: T_{VET} (0.4Hz) < 20°C and G_{VET} (0.4 Hz) > 10 MPa.

2.7 Summary

Bitumen is considered a viscoelastic material. At low temperatures, bitumen is hard at brittle since the elastic material response governs. In this state the binder is able to recover to its original state once the load is removed. At high temperatures, the stiffness of the binder will decrease, the viscous material response governs, and permanent deformation will take place. Due to the viscoelastic material response, it is important to conduct rheological tests within the linear viscoelastic (LVE) range of the binder, since within this region the stiffness is independent of stress or strain. The results will indicate the influence that frequency and temperature have on the behaviour of bitumen.

The time-temperature superposition principle can be applied when testing is conducted within the LVE range and no phase or structural changes to the binder take place. This implies that all of the viscoelastic properties can be shifted to form a continuous function. Shift factors are used to shift data from various temperature isotherms to a single master curve at a specified reference temperature. The following discoveries were made with regard to shift factors:

- The Arrhenius equation is accurate where $T < T_{g.}$
- The William, Landel and Ferry (WLF) equation is accurate where $T > T_{g.}$
- The Modified Kaeble equation incorporates T_d and is regarded as the transition between the Arrhenius and WLF equation.

Various rheological models are available to reproduce the change in stiffness associated with a change in frequency. The following findings were relevant to identifying a suitable model to the rheological properties:

- The Standard Sigmoidal (SS) model: not accurate for highly modified binders.
- The Christensen Anderson (CA) model: at high temperatures and loading rates accuracy decreased.
- The Christensen Anderson and Marasteanu (CAM) model: at high temperatures and loading rates accuracy decreased.

Durability parameters are available to indicate the binder's resistance to withstand the effect of ageing. These parameters are:

- G-R parameter: measures the relationship between the G* and δ at 0.005 rad/s.
- ΔTc: the difference in grade temperature for stiffness and relaxation properties
- TVET and GVET: temperature and stiffness where G' = G" and δ = 45°, which is associated with the crossover frequency (ω_C)

Chapter 3: Methodology

The goal of this study is to evaluate the consistency of rheological properties of recovered seal binders. Various test methods and modelling equations that are relevant to this study were introduced in Chapter 2. This chapter will specify all of the equipment and test procedures that will be used to achieve the objectives as stated in Chapter 1.3. Based on the availability of the required equipment, testing was performed at two different laboratories. The binder recovery process took place at Much Asphalt, while other rheological tests were performed at Stellenbosch University.

3.1 Experimental Design

Since there is no formal procedure available to prescribe a seal binder recovery method, thorough planning is needed to ensure that the laboratory work conducted in this study took place in a precise and orderly manner. Therefore, an experimental design was developed. From the experimental design, as illustrated in Figure 3.1, five categories can be distinguished and are discussed further in this Chapter. These categories are:

- Material Selection (Chapter 3.2): The procedure followed to select a variety of road segments.
- Material Retrieval (Chapter 3.3): The extraction and recovery procedure followed to obtain the binder that will be tested.
- Material Testing (Chapter 3.4 to Chapter 3.6): Various tests that will be performed on the recovered binder, as well as the quality control tests.
- Rheological Modelling and Analysis (Chapter 3.7 to Chapter 3.9): An indication of how data was processed to obtain durability parameters that will aid in analysing the results.
- FTIR Analysis (Chapter 3.10): The manner in which the FTIR data will be analysed.

3.2 Material Selection

Material must be carefully selected, since the results obtained from the tests conducted on these samples must aid in evaluating the consistency of rheological properties of the recovered seal binders. Two main requirements are identified. The first requirement, addressing repeatability, was that sufficient material of that road section must be available; and the second requirement, addressing reproducibility, was that the material must have been used in previous studies. The reproducibility of this study will be evaluated against the results

obtained by two other students, Tredoux (2020) and Goosen (2021). As part of Stellenbosch University's ongoing research into seal rheology and performance, seals from various sources have been retrieved. These seal samples were obtained in two forms, either as slabs or in fragmented form. To assure that the seal binder recovery method is not biased towards certain conditions, a second requirement was established to ensure that the method can be applied to a variety of cases. The following factors were considered for the criteria:

- Seal type: single seal (S1), double seal (S2), Cape seal (S4), and multiple seal (M)
- Binder type: unmodified binder (70/100), hot applied elastomer modified binder (S-E1) and emulsion elastomer modified (SC-E2)
- Provincial Region: Western Cape (WC), KwaZulu-Natal (KZN), Eastern Cape (EC), Free State (FS). Each province experiences different climatic conditions.
- Seal age: Two age groups are considered, 0-6 years and 6+ years.
- Road type: National Road (N), Regional Road (R), Divisional Road (DR), and Main Road (MR). Each road type is exposed to different traffic conditions.

Table 3.1 provides a summary the road sections that were selected based on the abovementioned criteria. The table shows how many repetitions are done on each sample to evaluate repeatability, as well as the source used to evaluate the reproducibility. When considering MR265 km 12, three uniform samples were identified. The binder from each sample is recovered, tested, and modelled separately. These three samples will first be compared with one another, and next to a fourth sample, which was recovered by a different tester, in order to gain insight regarding the reproducibility of the seal recovery method.

Table 3.1: Summary of Selected Materials

Sample	Seal	Binder	Prov	Age	Repeatability	Reproducibility
MR265 km12	S1	S-E1	WC	1	3	Goosen (2021)
DR2216 km1	S1	70/100	WC	10	-	-
N8/8 km5.6	S2	S-E1	NC	7	2	-
N2/31 km3.6	S2	S-E1	KZN	12	-	Goosen (2021)
N2/32 km21	S2	S-E1	KZN	6	-	Goosen (2021)
R61/6 km 88	S4	SC-E1	EC	1	2	Tredoux (2020)
R61/8 km51	S4	SC-E2	EC	1	3	Tredoux (2020)
MR265 km41	S4[3]	70/100	WC	1	3	Goosen (2021)
MR174 km9	S4[4]	70/100	WC	9	-	Tredoux (2020)
N2/16 km71	M[5]	S-E1	FS	2	-	Tredoux (2020)
N6/4 km87	M	S-E1	EC	9	-	-

[3] S4 (13mm)
[4] S4 (19mm)
[5] M (20/7/7)

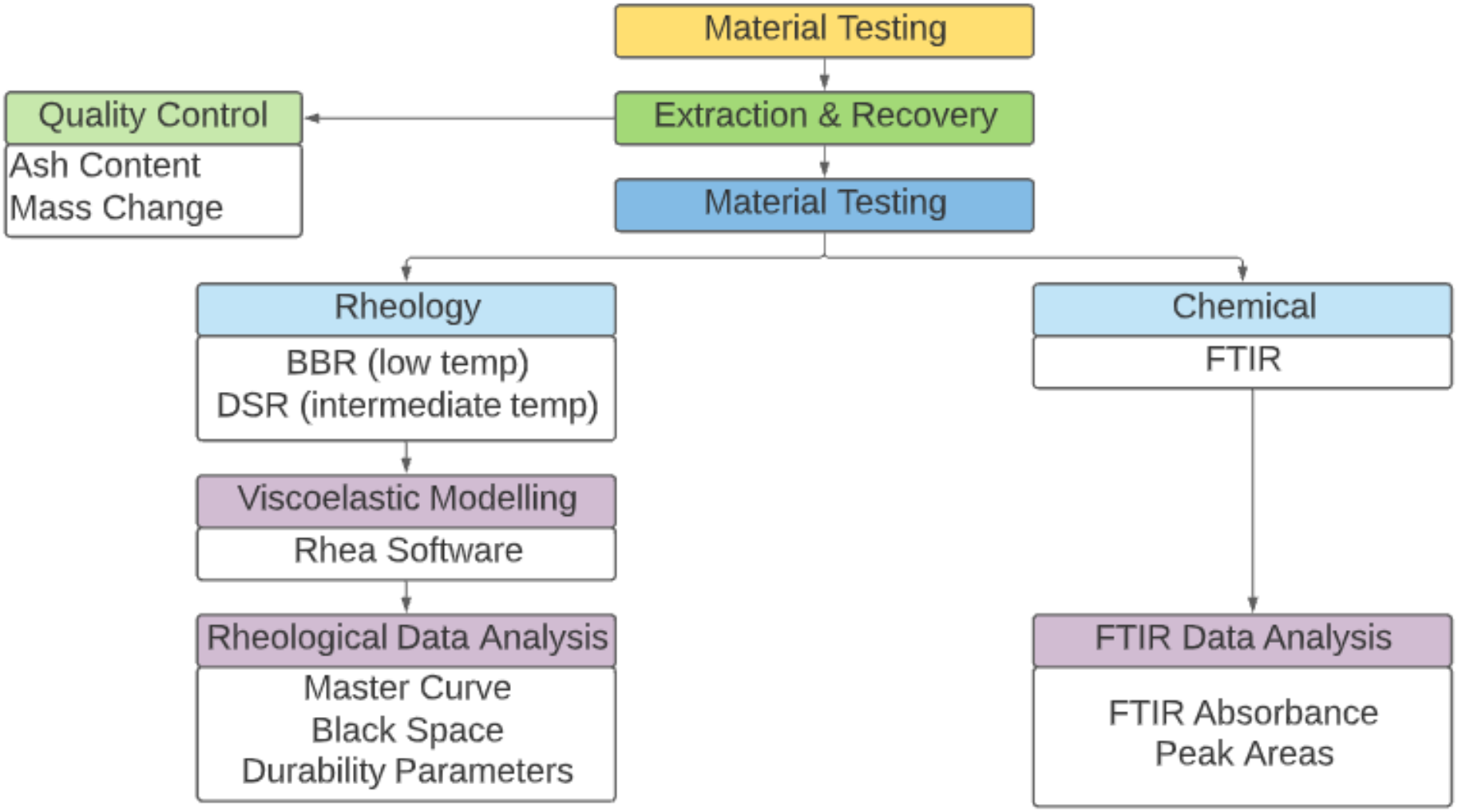

Figure 3.1: Experimental Design Flow Chart

3.3 Extraction and Recovery Procedure

The selected seals were either stored as a slab or fragmented in bags, as shown in Figure 3.2. The dimensions of the slabs were approximately 300 x 300mm. Previous studies found that one slab provided sufficient binder, therefore a single slab was used per recovery. Where the content was fragmented in bags, the dimensions of the fragments varied. The slabs were weighed and served as a reference to determine the mass of fragmented material needed for the recovery. It was found that 4 kg of the fragmented material was sufficient.

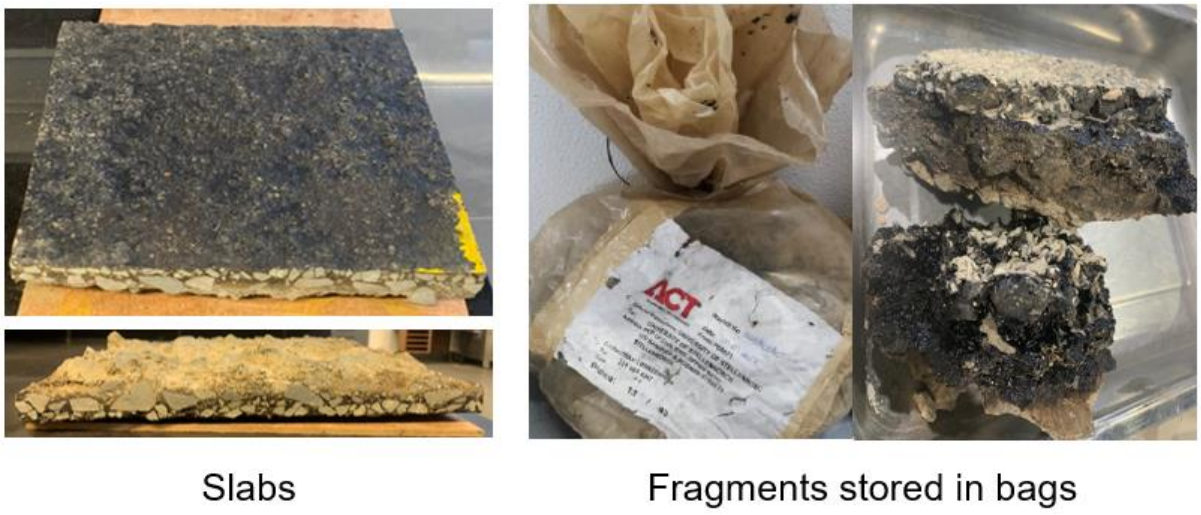

Figure 3.2: Retrieved Seals Used

The procedure as set out in EN 12697-3 (2013), with adjustments as recommended in Goosen and Jenkins (2019), was used as a reference for the seal binder recovery process used in this study. As discussed in Chapter 2.4.1, the binder recovery process comprises of three distinct phases: extraction, aggregate removal, and distillation.

The material was preheated at 60^{o}C for 60 minutes. This makes the binder more viscous, allowing for the material to be fragmented into smaller segments. These smaller segments will ensure that most of the binder is exposed, which will allow for the extraction process to take place more effectively. The fragmented material was weighed to ensure that the sample size is sufficient.

A blend comprising of 85% Toluene (C_7H_6) and 15% Ethanol (C_2H_5OH) was selected as the solvent to remove the binder from the aggregate. Although this blend does not contain any corrosive chemicals and has no severe health hazards, the correct personal protective equipment (PPE) was worn at all times. For the duration of the extraction phase, the sample was submerged in solvent. Approximately 1500 ml of solvent was added to the sample. Where

1500 ml was not sufficient to submerge the sample, additional solvent was added. Caution must be taken when adding additional solvent, since this will extend the duration of the distillation phase.

The time required to dissolve the binder from the solvent will depend on the age of the binder. For younger binders (0-6 years) three hours was sufficient to dissolve the binder, while older binders (6+ years) were soaked overnight for approximately 12 hours. Where a younger binder was involved, the sample was agitated every hour and the entire recovery was completed within an eight hour work day, compared to an older binder where the sample was agitated after the solvent was added and before the next phase commenced the following day. Figure 3.3 provides an overview of the entire extraction phase.

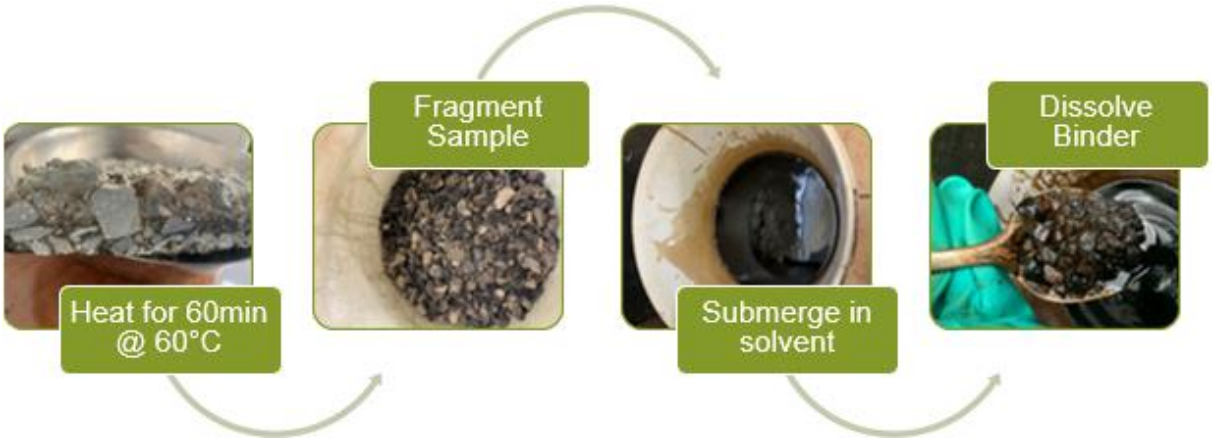

Figure 3.3: Extraction Phase

The centrifuge was used to remove the aggregate from the solvent-binder solution. Although EN 12697-3 (2013) only suggest a 0.063 mm sieve be used to remove the insoluble material, it was decided to protect the 0.063 mm sieve by adding two additional sieves (2.36 mm and 0.075 mm). As a safety precaution, the centrifuge is operated within a fume tight cupboard containing an extractor fan to remove any hazardous fumes associated with the solvent.

The three sieves were assembled on top of the funnel that feeds the content to the centrifuge. The solvent-binder solution containing fines ran through the sieves into the rotating metal cup, where the fines gathered and only solvent and binder exited through the outlet drainpipe and accumulated in a container. Additional solvent was used to wash the aggregate and remove any binder still remaining with the aggregate.

Once the solvent ran colourless from the outlet drainpipe, the washing of the aggregate was suspended. SANS 3001 (2011) states that the solvent binder solution must be re-centrifuged

if the mass collected in the cup exceeds 50 g. In this case, all solutions were re-centrifuged three times in an attempt to ensure that all of the fines were removed, since the actual mass of fines accumulated in the cup can only be determined once the cup has been dried overnight. The entire centrifuge process was completed within an hour. The aggregate accumulated in the sieves and the cups were placed in the oven to dry. Figure 3.4 provide a summary of the centrifugation phase.

Figure 3.4: Centrifugation Phase

The rotary evaporator, as shown in Figure 3.5, was used for the distillation phase. The Heidolph Rotary Evaporator (Hei-VAP Core HL G3) was also operated from a fume tight cupboard containing an extraction fan to remove the fumes. As mentioned in Chapter 2.4.1, the choice of solvent determines the distillation condition. A tolerance of ± 5°C was allowed for the recovery temperatures (T_1=110 °C; T_2=160 °C; T_3= 185 °C), as well as a tolerance of ± 5kPa for the recovery pressure (P_1=40 kPa; P_2=2 kPa). It should be noted that silica gel and nitrogen gas were not present within the system.

The evaporating flask rotated at 75±15 r/min, while the temperature of the oil bath was set to T_1 and the pressure within the apparatus was set to P_1. The solvent-binder solution was fed into the system at a rate equal to the rate at which the distillate flowed into the receiving flask. It was also suggested that the solvent-binder solution not exceed 2/3 of the capacity of the evaporating flask, to prevent the backwash of binder into the receiving flask. (EN 12697-3, 2013)

Figure 3.5: Rotary Evaporator

Figure 3.6 provides an overview of the entire distillation phase, which will aid in explaining the process followed during phase two of distillation, which commences once all of the solvent binder solution has been fed into the evaporating flask. The induction stopcock was closed, and the temperature of the oil bath was set to T_2. If the bubbling of the bitumen within the evaporating flask ceases before the temperature of the oil bath reached T_2, the pressure was immediately lowered to P_2, otherwise the pressure was gradually lowered to P_2.

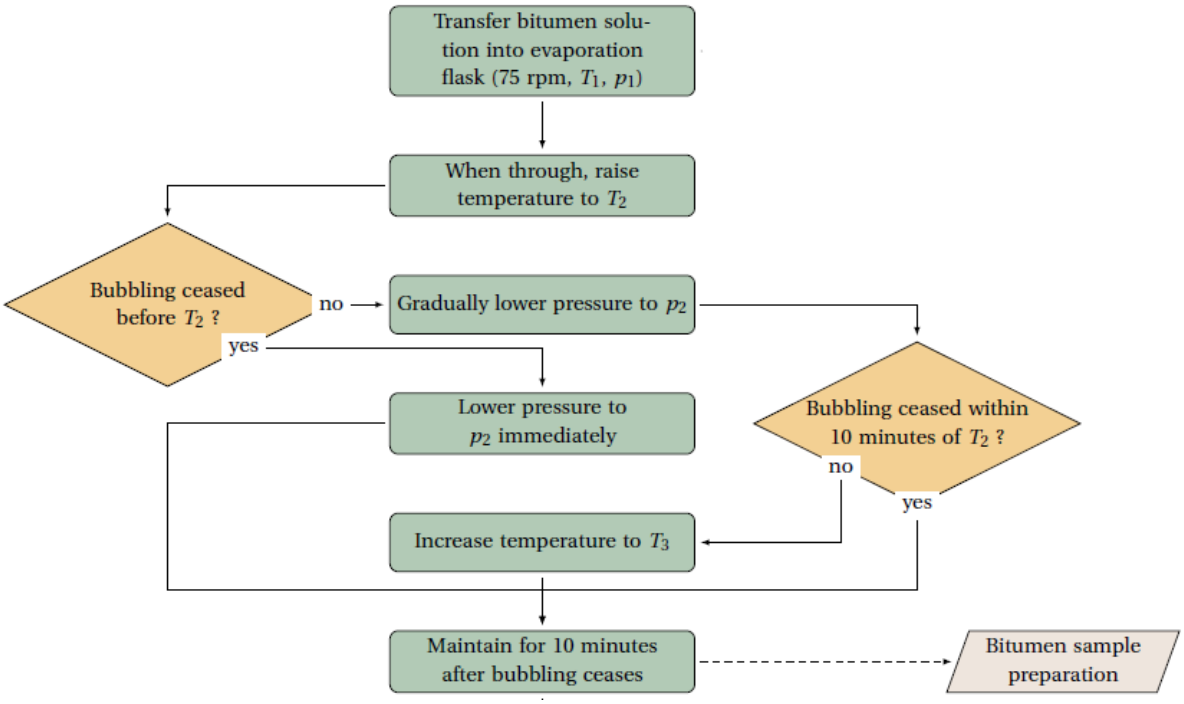

Figure 3.6: Summary of the Distillation Phase (Goosen and Jenkins, 2019)

It was decided that a rate should be used to define gradually. This will ensure that the same procedure is followed for all recoveries and limit variation. For this study gradually was defined as 50 millibar (5 kPa) per minute (Figure 3.7). This rate allowed for the pressure to reach P_2 within 10 minutes of changing the temperature to T_2 and prevented backwash of binder into the receiving flask. In most cases, the bubbling of the bitumen ceased within 10 minutes of T_2. Therefore, T_2 and P_2 were maintained for a further 10 minutes. The rotation of the evaporating flask was stopped, the pressure was increased to atmospheric, and the recovered binder was portioned into glass containers.

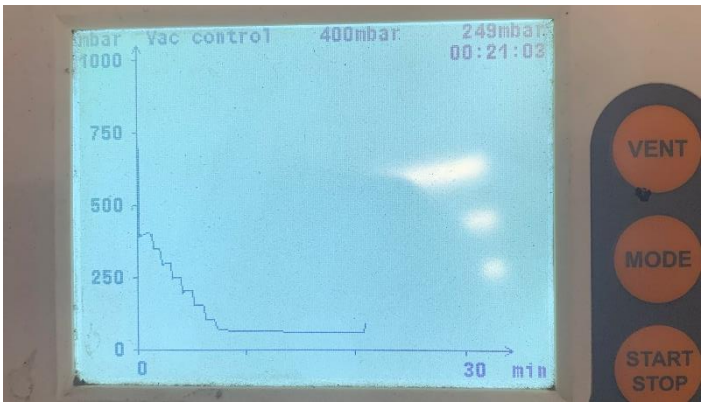

Figure 3.7: Gradually Lower Pressure to P_2

By portioning approximately 25 g of the recovered binders into a container, one will ensure that the obtained rheological properties are not compromised, since a sample will only be reheated once before subsequent testing. Remaining binder from that cup will be discarded. If further testing is needed a second cup will be heated and used.

3.4 Quality Control

As explained in Chapter 2.4.1, the presence of solvent and fines within the recovered binder will influence the repeatability and reproducibility of the binder recovery method. Therefore, two tests were identified that can compare the properties of the recovered binder against the actual in-situ performance of the binder. Mass change can be used to determine the percentage of solvent present within the binder, while the ash content can indicate the amount of fines present in the binder.

3.4.1 Mass Change

When solvent is present within the binder, the stiffness of the bitumen will be softer than it actually is. The binder was placed in the oven for 30 minutes at 160 ^{o}C. At 160 ^{o}C, the binder will be sufficiently fluid, and the temperature is also higher than the boiling point of the solvent. Therefore, any residual solvent will evaporate from the binder, ensuring that only bitumen

remain for testing. The cup containing the binder was weighed before and after being placed in the oven.

$$mass\ change\ (\%) = \frac{m_{initial} - m_{final}}{m_{initial}} * 100$$

Where $m_{initial}$ = mass before heated

m_{final} = mass after heated

3.4.2 Fourier-Transform Infrared Spectroscopy

The Perkin Elmer ATR Spectrometer was used to measure the absorbance between 400 and 4000 cm^{-1}. A cold sampling method was used to remove a fragment of binder from the storage container. The size of the binder fragment varied. The only sample size requirement is that the fragment must be large enough to cover the entire crystal.

Before testing commenced, the spectrometer was calibrated by conducting a background scan to self-regulate the instrument and check for contaminants. The bitumen fragment was rolled into a ball and placed on the crystal. The spindle was lowered to a constant height and the test execution started. Figure 3.8 provides a summary of the sample preparation.

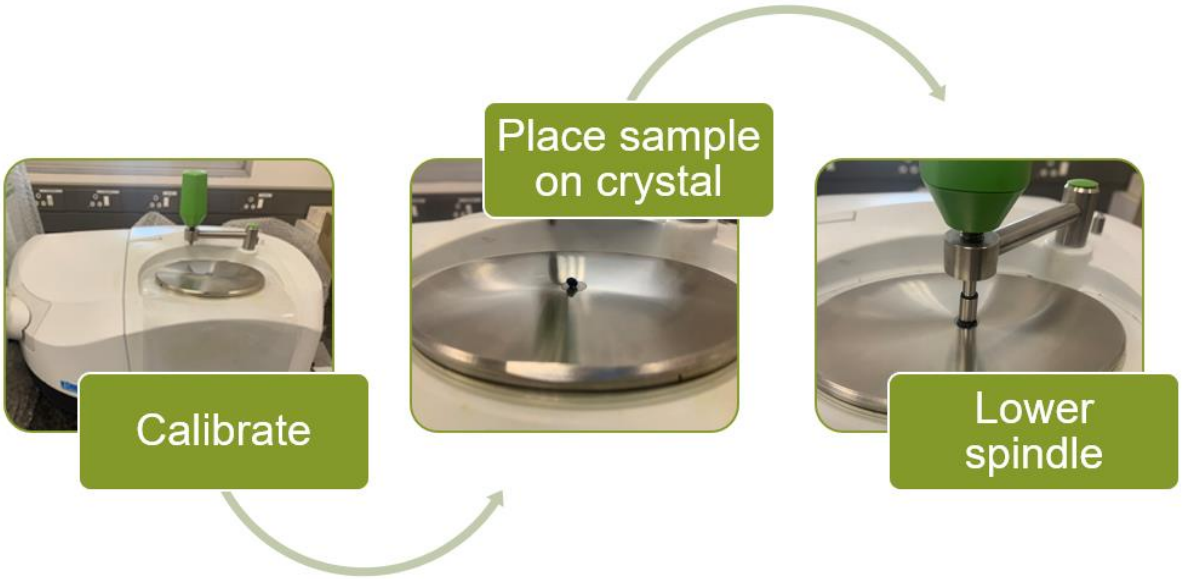

Figure 3.8: FTIR Sample Preparation

3.4.3 Ash Content

When fines are present within the binder, the stiffness of the binder will be harder than it actually is. ASTM D482 (2019) provides the following procedure:

- Heat a crucible in a furnace at 700 °C for 10 minutes. Remove the crucible from the furnace and place in a desiccator to cool to room temperature. Weigh the crucible.
- Heat the bitumen until sufficiently mobile and pour binder into a crucible. The amount of binder will depend on the expected ash content of the binder. The weight of the crucible containing bitumen must also be noted.
- Place the crucible on a Bunsen burner until the content can be ignited. Maintain the temperature until the burning ceases.
- Heavy samples, such as marine fuels and bitumen, tend to form a crust over the unburnt material. Apply additional heat and break the crust with a rod.
- Heat the residue in the furnace at 775 °C ± 25 °C until all of the carbonaceous material has disappeared. Cool the crucible in a desiccator to room temperature and weigh.
- Reheat the residue in the furnace at 775 °C ± 25 °C for 20 minutes, allow to cool and weigh. Repeat this process until consecutive weighing differ by no more than 0.5mg.

Preliminary testing was conducted but due to time and test constraints the ash content of all of the recovered binders were not determined. Refer to Appendix C for a visual documentation of the procedure, as well as further discussion.

3.5 Dynamic Shear Rheometer

The Anton Paar Modular Compact Rheometer 302 (Software: RheoCompass 1.25) was used to determine the rheological properties of the recovered binder at intermediate temperatures. The procedure followed was based on the ASTM D7175 (2008). As mentioned in Chapter 2.4.2, both 8 mm and 25 mm parallel plates (PP) will be incorporated into the test method. Therefore, test specimen for both sizes had to be prepared.

Silicone moulds were created by combining a silicone elastomer and a silicone activator (catalyst). Once the elastomer and activator were sufficiently mixed, it was poured into the moulding plate and left overnight to dry. The silicone moulds were removed from the moulding plate and cleaned with soap and water to ensure that no other material that can influence the rheology of the binder, is present on the moulding surface. Figure 3.9 provides an overview of the silicone mould preparation.

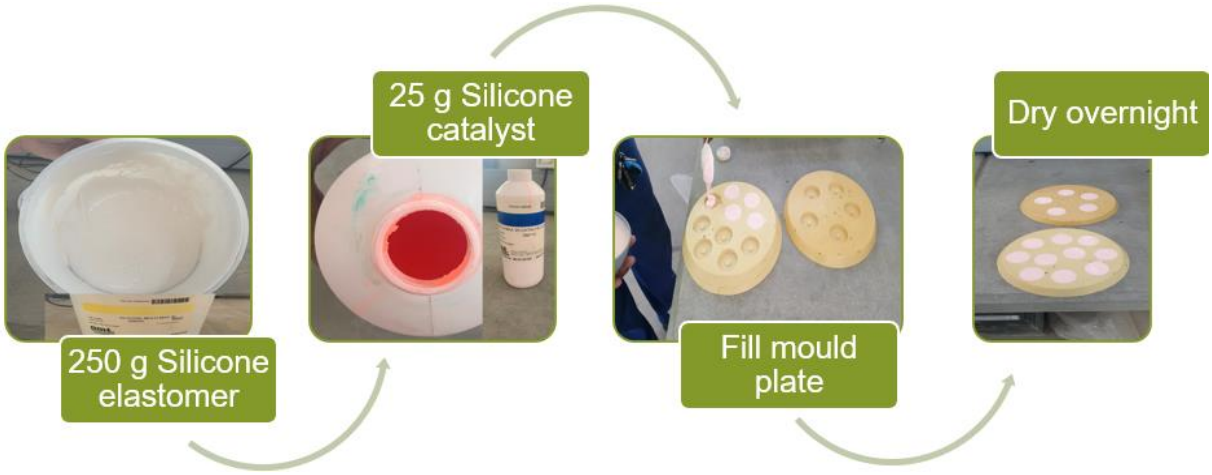

Figure 3.9: Silicone Mould Preparation

ASTM D7175 (2008) prescribes that the binder must be heated until sufficiently fluid in order to be poured into the DSR moulds, but the temperature of the binder may not exceed 163°C. ASTM D7175 (2008) does not place a time constraint on the annealing process, it only advises that the heating and exposure time must be minimised to prevent binder hardening. Therefore, it was decided that the binder will be heated at 160 °C for 30 minutes before being poured into the DSR moulds. The test specimen was left at room temperature to cool for 60 minutes after which testing commenced. Figure 3.10 indicates the process followed to create the test specimen.

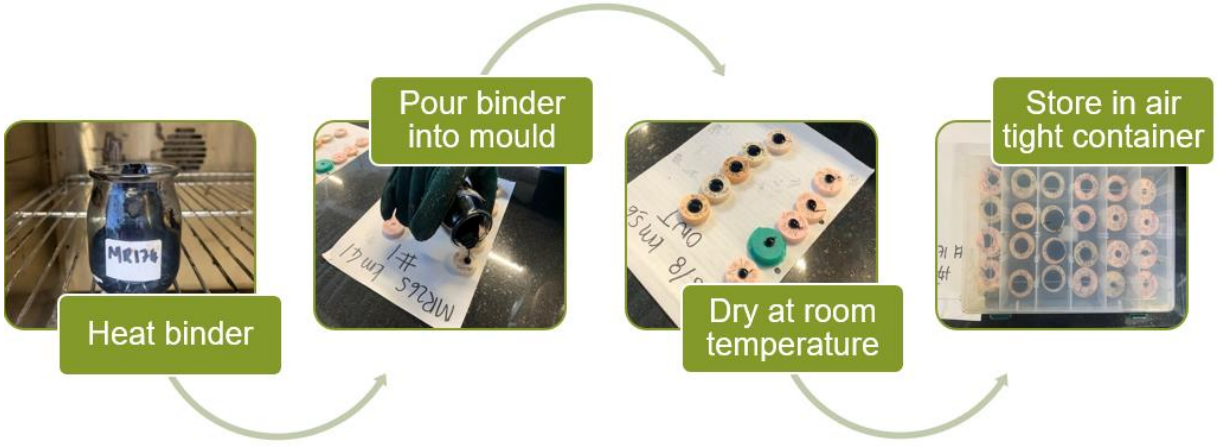

Figure 3.10: DSR Specimen Preparation

ASTM D7175 (2008) also requires that the testing of the samples must be completed within two hours of pouring. Since limited binder was recovered, this time restraint could not be met. Once a container of bitumen was heated, all of the content was utilised, hence six test specimen (3 x 25 mm and 3 x 8 mm) were casted. The specimens were allowed to cool at room temperature for an hour, after which they were stored in an airtight container to prevent

oxidisation of the bitumen. This deviation from the time constraint was the only way to ensure that the integrity of the binder remained, without comprising the availability of the recovered binder. However, before testing, the binder was heated to ensure annealing takes place to minimise steric hardening effects.

The same apparatus set-up was followed, regardless of whether a strain sweep or frequency sweep was conducted. The compressor was set to operate at 5 bars, while the cooling unit was set to 5°C. The PP were initialised, and the zero gap was set depending on the plate geometry. A 2 mm gap was set at 20°C for the 8 mm PP and a 1 mm gap was set at 50°C for the 25 mm PP. The plates were heated to 60°C to ensure sufficient bonding between the plates and the specimen. The top plate was lowered to the trimming position where excess binder was removed around the edges of the plate to ensure that the bitumen specimen is flush with the outside edge. The testing procedure will follow next, which is dependent on the type of test, strain sweep or frequency sweep, that is conducted.

3.5.1 Strain Sweep

The test conditions for the strain sweep are constant temperature (15 °C for 8 mm and 45 °C for 25 mm), constant frequency (10 rad/s), and increasing strain percentage (between 0.01 and 10%). For the 25 mm geometry, strain sweeps were conducted at 45 °C. Previous studies found that strain sweeps for the 8 mm geometry conducted at 5 °C did not fall within the LVE range (Goosen and Jenkins, 2019; Tredoux, 2020; Engelbrecht, 2018). Since the goal is to test within the LVE range, it was decided that the 8 mm strain sweeps will be performed at 15 °C. It is also believed that testing at 5 °C should rather be classified as low temperature performance, rather than intermediate temperature performance. This implies that if BBR testing equipment allowed for testing at this temperature, these results could be more representative. From the strain sweep results, the LVE limit is identified as the position where G* reduces below 95% of its initial value. If the strain percentage at the LVE limit is less than 1%, that strain percentage will be applied during the frequency sweep, otherwise 1% will be used.

3.5.2 Frequency Sweep

The test conditions for the frequency sweep are constant strain percentage (as determined from the strain sweep), constant temperature and various load frequencies (between 0.251 and 25.1 rad/s). This process was repeated at various temperatures in order to obtain stiffness isotherms over a wide range of intermediate temperatures. The test temperatures vary depending on the plate geometry. The 8 mm diameter PP was used to test the specimen at

35, 25, 15 and 5°C, while the 25 mm diameter PP test at 35, 45, 60 and 70°C. It can be seen that both 8 mm and 25 mm PP were tested at 35°C. This overlapping will ensure that the two data sets correlate.

3.6 Bending Beam Rheometer

The Cannon Thermoelectric Bending Beam Rheometer (Software: BBRw) was used to determine the rheological properties of the recovered binders at cold temperatures. The procedure followed was based on the ASTM D 6648 (2008). Metal moulds were used to prepare the test specimen. The interior face of the three metal sections were covered in a thin layer of grease. A thin plastic film was placed on the greased surface, which was rubbed firmly to remove any air bubbles that can distort the beam geometry. The sections were assembled using rubber O-rings. The recovered bitumen was heated at 160 °C for 30 minutes and then poured into the metal mould. The mould was slightly overfilled. The filled mould cooled at room temperature for 45 to 60 minutes. After cooling the excess binder was trimmed using a heated spatula. Prior to demoulding, the filled mould was placed in a climate chamber for 5 minutes at a temperature exceeding 10 °C of the test temperature. This allowed the bitumen to stiffen so that the mould can be removed without deforming the beam. The demoulded beam was placed in the test bath for 30 minutes to condition the beam to the testing temperature, after which the seating load was applied. Figure 3.11 provides a summary of the procedure followed to prepare the test specimen.

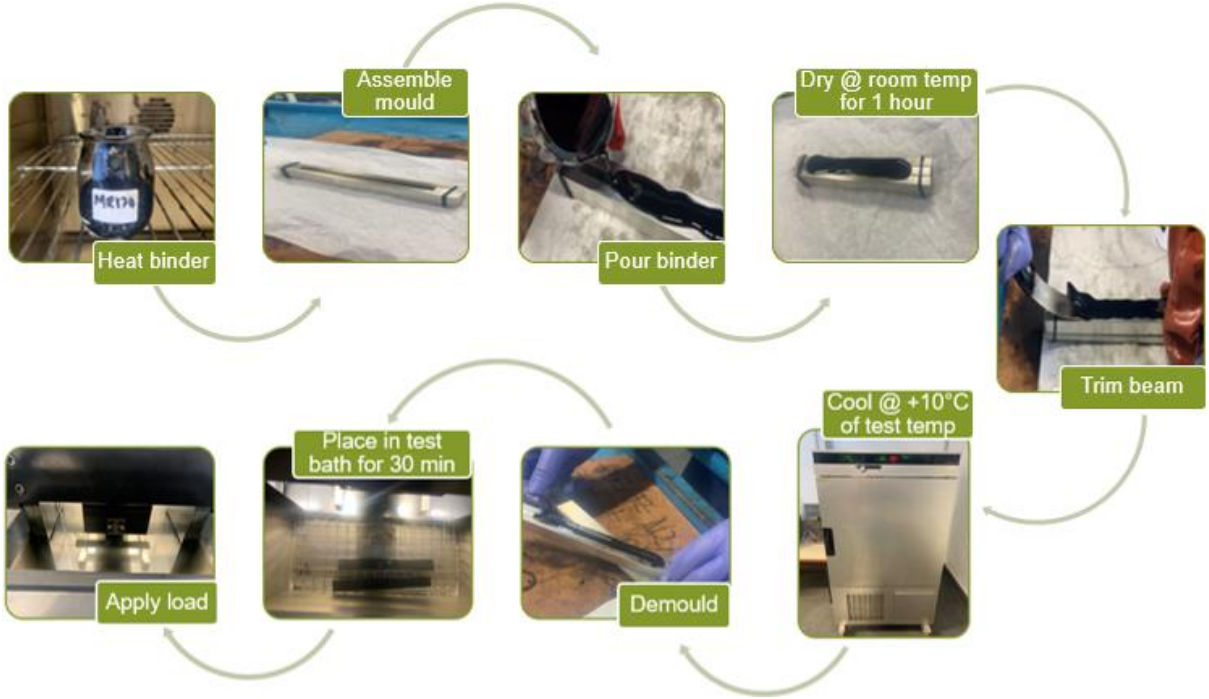

Figure 3.11: BBR Specimen Preparation

3.7 Data Modelling

Abatech RHEA Software was used to analyse the viscoelastic behaviour of the binder over a range of temperatures and frequencies. Apart from the DSR and BBR results, the software requires additional input parameters. One of these parameters was the reference temperature. A reference temperature of 15°C was used in this study, the same reference temperature as used by Goosen (2021) and Tredoux (2020). The values suggested by the RHEA User Manuel was used for the other parameters. These parameters were:

- Glassy temperature = -20°C
- Expansion coefficient below the glassy temperature = 0.00017
- Expansion coefficient below the glassy temperature = 0.00020

From the DSR data, the frequency, G' and G'' for each temperature isotherm was provided as input data. As mentioned in Chapter 3.5.2, both the 8mm and 25mm test procedures were executed at 35°C. The average complex modulus of each 35°C isotherm was calculated in order to determine which data set is more appropriate. Where the average G* was equal or less than 10^5 Pa, the 25 mm data set was used, otherwise if G* was greater than 10^5 Pa, the 8 mm data set was used.

From the BBR data, the stiffness at certain time intervals was provided as input data. The bending stiffness was converted to shear stiffness using the assumption that $S \approx 3G^*$ and the time domain was converted to the frequency domain using $\omega t = 2\pi$.

It is required that the provided data must be within the LVE range, otherwise the master curves cannot be determined. Combining the DSR and BBR data, revealed that some of the 5°C isotherms did not follow the trend that is typically observed. In these cases, it is assumed that the data was affected by machine compliance. The G* values of the 5°C isotherm correspond to the BBR stiffness range. In these cases, data from the 5°C isotherms are omitted.

RHEA incorporates the Gordon and Shaw (1994) free shifting method to shift each isotherm to the reference temperature. As illustrated in Figure 3.12, a pairwise shift was completed for G', G'' and G*.

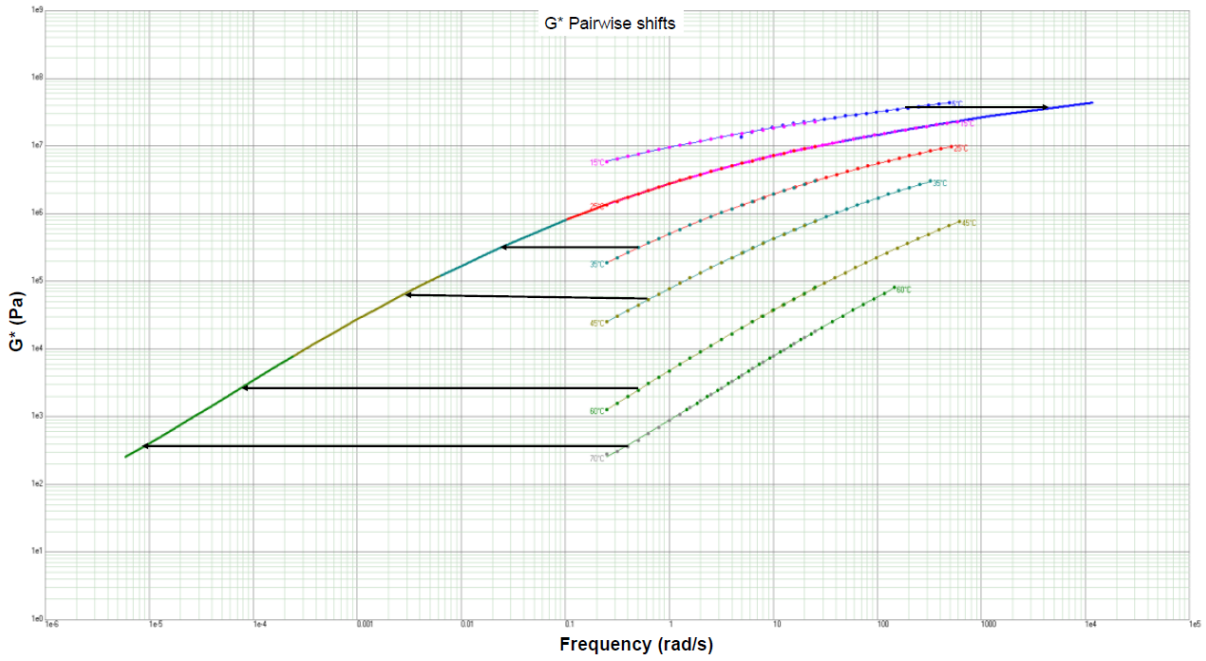

Figure 3.12: G* Pairwise Shift (Tredoux, 2020)

RHEA considers three shift factor equations. The root mean square error (RMSE) of each equation was calculated. The root mean square error (Equation 3.1) measures the accuracy of observed and predicted values. Therefore, the function containing the lowest RMSE was selected to shift the data.

$$RMSE(\%) = \sqrt{\frac{1}{n}\sum\left(\frac{x_{model} - x_{data}}{x_{data}}\right)^2} * 100 \quad (3.1)$$

Where x_{model} = predicted value

x_{data} = observed/measured value

n = number of data points

The available shift factors include:

- Modified Kaelble

$$\log \alpha_T = -C_1\left(\frac{T - T_d}{C_2|T - T_d|} - \frac{T_{ref} - T_d}{C_2|T_{ref} - T_d|}\right) \quad (3.2)$$

- WLF

$$\log \alpha_T = \frac{-C_1(T - T_{ref})}{C_2(T - T_{ref})} \quad (3.3)$$

- Arrhenius

$$\log \alpha_T = C\left(\frac{1}{T} - \frac{1}{T_{ref}}\right) \tag{3.4}$$

RHEA considers various models to predict the values of G* and δ, and also calculate the RMSE of each model. The models include:

- Discrete modelling

$$G'(\omega) = G_e + \sum \frac{g_i(\omega\lambda_i)^2}{(1+(\omega\lambda_i)^2)} \tag{3.5}$$

$$G''(\omega) = G_e + \sum \frac{g_i\lambda_i}{(1+(\omega\lambda_i)^2)} \tag{3.6}$$

- CAM Model:

$$|G^*(\omega)| = G_g\left[1+\left(\frac{\omega_c}{\omega}\right)^{\upsilon}\right]^{-\frac{w}{\upsilon}} \tag{3.7}$$

$$\delta(\omega) = \frac{90\omega}{\left[1+\left(\frac{\omega_c}{\omega}\right)^{\upsilon}\right]} \tag{3.8}$$

- GLS Model:

$$\log|G^*| = \upsilon + \frac{\alpha}{[1+\lambda e^{(\beta+\gamma\{\log(\omega)\})}]^{1/\lambda}} \tag{3.9}$$

If one wants to compare model parameters, the same models must be used. However, it is possible to compare results calculated from different models if their RMSE is within acceptable limits, because one will be comparing accurate stiffness and deflection calculations. The models obtained in this study and Goosen (2021) varied between discrete modelling and CAM. Therefore, the model with the lowest RMSE for the combination of samples was used. Tredoux (2020) did not complete BBR testing and the resulting G* values were typically lower than 10^4, hence GLS modelling was mostly used. Therefore, discrete modelling was only mutual model between this study and Tredoux (2020).

3.8 Durability Parameters

The consistency of the rheological properties of the recovered seal binders were evaluated by using durability parameters. The durability parameters were determined as follows:

- G-R Parameter: From the best fit rheological model, RHEA calculated the values of G* and δ at 15°C and 0.005 rad/s. The limits of the G-R parameter is 180 kPa for onset cracking and 600 kPa for significant cracking.

$$G - R = \frac{G^* \cos^2 \delta}{\sin \delta} \tag{3.10}$$

- ΔTc: The low temperature cracking resistance of the recovered binders were calculated in Excel using the stiffness and slope of the stiffness curve obtained from the BBR results. SATS 3208 recommend that the value of ΔT_c be greater or equal to - 5°C.

$$\Delta T_c = T_{c,S(60)} - T_{c,m(60)} \tag{3.11}$$

- T_{VET}: T_{VET} is the temperature where ω_c is equal to 0.4 Hz (2.51 rad/s). In order to shift from T_{ref} to T_{VET}, the shift from ω_c to 2.51 rad/s is needed. This shift was then substituted into the Modified Kaelble shift factor (Equation 3.2) to solve T_{VET}.

$$\log \omega_C - \log 2.51 = \log \alpha_T = -C_1 \left(\frac{T - T_d}{C_2 | T - T_d|} - \frac{T_{ref} - T_d}{C_2 | T_{ref} - T_d|} \right) \tag{3.12}$$

Rowe (2014) also developed an equation for T_{VET} using parameters from the CAM model.

$$T_{VET} = T_d + \chi \left(\frac{C_2}{1 - |\chi|} \right) \tag{3.13}$$

Where,

$$\chi = \frac{T_{ref} - T_d}{C_2 + |T_{ref} - T_d|} - \frac{\log \omega_C - \log \omega_{VET}}{C1} \tag{3.14}$$

- G_{VET}: From the frequency sweep results, the value of G* that correlates to δ = 45° was calculated using interpolation.
- T_{max}: T_{max} refers to the maximum temperature at which the binder can be used and was calculated based on the equation below :

$$\frac{G^*_{10\,rad/s}}{\sin \delta_{10\,rad/s}} = 1 \; @ \; T_{max} \tag{3.15}$$

- The 60 °C (T_1) and 70 °C (T_2) frequency sweep isotherms were used to obtain G* and δ at 10 rad/s. T_{max} was calculated by interpolating as follow:

$$T_{max} = T_1 + \left(\frac{1 - \left(\frac{G^*}{\sin\delta}\right)_1}{\left(\frac{G^*}{\sin\delta}\right)_1 - \left(\frac{G^*}{\sin\delta}\right)_2} \right) * (T_1 - T_2) \quad (3.16)$$

3.9 Repeatability and Reproducibility Analysis

For the repeatability and reproducibility analysis, each of the seals identified in Table 3.1, will be considered separately. Table 3.1 also indicates whether the seal will be used to evaluate repeatability, reproducibility, or both. Each seal was considered separately by using the durability parameters from each recovery.

As mentioned earlier, G-R and T_{vet} is calculated from modelled data, while T_{max}, G_{vet} and ΔT_c is calculated from raw data obtained as output from the rheological tests. Where the parameters using modelled data varies, the inconsistencies can either be due to binder rheology or the degree of fit provided by the shift factor model and rheological model. The RMS error of the shift factor model and the master curve model is used to confirm whether or not the variation is a shifting or modelling error. Based on observations made by Goosen (2021), a classification criteria is chosen. Table 3.2 shows the chosen classification criteria for shift factors models.

Table 3.2: Classification of Shift Factor's RMS Error

RMS Error	Classification
x < 10	Very Good (VG)
10 ≤ x <20	Good (G)
x ≥ 20	Poor (P)

Similarly, Table 3.3 shows the chosen classification criteria for the master curve models. It can be seen that the master curve models are subject to a stricter criterion than the shift factors models. The reason is related to the number of data points used to determine the shift factor or master curve model. Less data points are used to populate the equations of the shift factor model. A single outlier would have a large effect on the accuracy of the shift factor equation, resulting in a higher RMS Error. The master curve models are populated with multiple data points. The effect of a single outlier would be insignificant in comparison with an outlier present in the shift factor. Therefore, a stricter criterion is used to evaluate the master curve models.

Table 3.3: Classification of Master Curve Model's RMS Error

RMS Error	Classification
x < 3	Very Good (VG)
3 ≤ x <7	Good (G)
7 ≤ x <15	Fair (F)
15 ≤ x <20	Poor (P)
x ≥ 20	Unacceptable (U)

Regardless of experimental precision, a degree of variability is expected and accepted. The acceptable degree of variability should be established based on the intended use. As explained in Chapter 2.3.4, the only repeatability and reproducibility criteria available, are for softening point (°C) and penetration (dmm) (EN12697-3, 2013). The precision values are compiled in Table 3.4.

Table 3.4: Repeatability and Reproducibility Criteria (EN12697-3, 2013)

	Repeatability	Reproducibility
Softening Point (°C)	1,9	3,4
Penetration (dmm)	0,10 x	0,27 x

Where x is the average of the results being compared.

For this study, it is evaluated whether the same degree of variability would apply to all temperature parameters. Therefore, the requirement for softening point, in Table 3.4, is used to evaluate the precision of the temperature parameters of the recovered binders. Temperature parameters may not differ by more than 1,9 °C for repeatability or 3,4 °C for reproducibility.

In Chapter 2.3.3, it was mentioned that Saal and Labout (1958) and Van Heerden *et al.* (2011) confirmed a linear relationship between penetration and G* on a log scale. This linear relationship does not necessarily imply that the precision values that are applicable to penetration, can automatically be applied to stiffness parameters. The illustration in Figure 3.13 will be used to confirm whether the penetration precision values can be applied to the stiffness parameters. The graph represents the linear relationship between log(pen) and log(G*). Two points on the graph, with coordinates (G*;pen) and (y_f G*;x_f pen), are identified. The two factors y_f and x_f are factors that account for the changes of both variables.

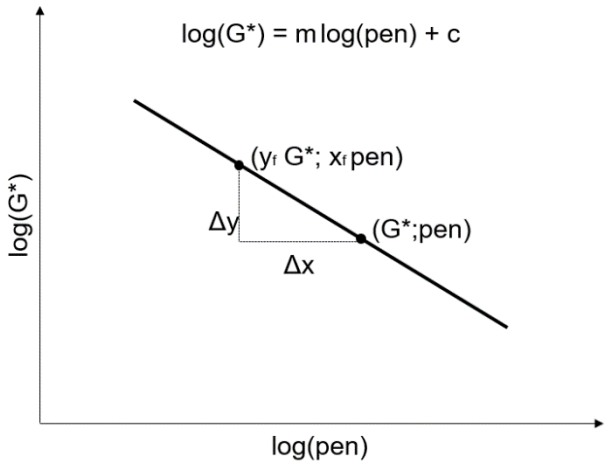

Figure 3.13: Illustration of the Linear Relationship between Penetration and G*

A relationship between y_f and x_f is calculated from the two coordinate points, as follows:

$$\Delta y = \log(y_f\, G^*) - \log(G^*) = \log\left(\frac{y_f G^*}{G^*}\right) = \log(y_f)$$

$$\Delta x = \log(x_f\, pen) - \log(pen) = \log\left(\frac{x_f pen}{pen}\right) = \log(x_f)$$

From

$$\left|\frac{\Delta y}{\Delta x}\right| = |m|$$

$$\Delta y = m\Delta x$$

$$\log(y_f) = m\, \log(x_f) \tag{3.17}$$

$$10^{\log(y_f)} = \left[10^{\log(x_f)}\right]^m$$

$$y_f = \left(x_f\right)^m \tag{3.18}$$

Equation 3.18 shows that if the penetration value changes with a factor x_f, the stiffness will change with a factor $(x_f)^m$. Saal and Labout (1958) found that m = -1.9, while the study by Van Heerden *et al.* (2011) revealed that m = -2.625. Substituting these values for m and the allowable repeatability and reproducibility for penetration from Table 3.4 for x_f into Equation 3.17 and Equation 3.18, the corresponding factor of variability of G*:

- if $x_f = 1 \pm 0.1$ (repeatability): $0.08 < |\log(y_f)| < 0.12$, thus $0.8 < y_f < 1.32$
- if $x_f = 1 \pm 0.27$ (reproducibility): $0.26 < |\log(y_f)| < 0.36$, thus $0.53 < yf < 2.28$

The factors in Table 3.4 for repeatability and reproducibility are thus investigated for the evaluation of variability of log stiffenss values. Therefore, the precision of the stiffness parameters of the recovered binders will be evaluated in terms of the penetration values in Table 3.4.

The provided precision values will be applied to the parameters of the recovered binders. Where the durability parameters of two recoveries are analysed, the difference is calculated by subtracting the two parameters from one another. Where more than two recoveries are being analysed, a conservative approach is followed. The critical difference is identified as the combination that delivers the largest difference between any two samples, which is then compared to the requirements provided in Table 3.4.

In order to gain a comprehensive understanding of the variability in durability parameter, it was decided that the precision requirements would also be applied to evaluate intermediate factors that are used to calculate the durability parameters. The intermediate factors are $T_{c,S}$ and $T_{c,m}$ for ΔT_c , and G* and δ for G-R.

3.10 FTIR Analysis

From the procedure explained in Chapter 3.4.2, the FTIR absorbance of each seal was obtained. These absorbance values are plotted against the corresponding wave number. Depending on the binder type, an unaged bitumen sample is also presented. The unaged sample is used as a reference to indicate the typical absorbance that the binder will experience. This will allow for the identification of peaks that could possibly indicate the presence of solvent. Literature suggests three primary areas that correspond to bitumen ageing. These areas are :

- Aliphatic hydrocarbons near 1460 cm^{-1};
- Carbonyls near 1700 cm^{-1}, and
- Sulfoxides near 1030 cm^{-1}.

The samples are compared in terms of the peaks situated at each of the abovementioned wave numbers. In order to quantify the differences between the peaks of each sample, the area of each peak is calculated. The Perken Elmer Software was used to determine the peak areas for the ranges as indicated in Table 3.5. The purpose of this section is to investigate possible links between the performance parameters and the corresponding chemical composition.

Table 3.5: Ranges Used to Calculate Peak Areas

Range	Wave number (cm^{-1})
A	1640 – 1560
B	1490 - 1330
C	1060 – 960

3.11 Summary

Within this Chapter, a thorough description of the procedures that were followed throughout the experimental design was provided. Figure 3.14 provides a summary of the start-to-end procedure that was followed in order to analyse the physical performance properties and the chemical composition of the recovered binders.

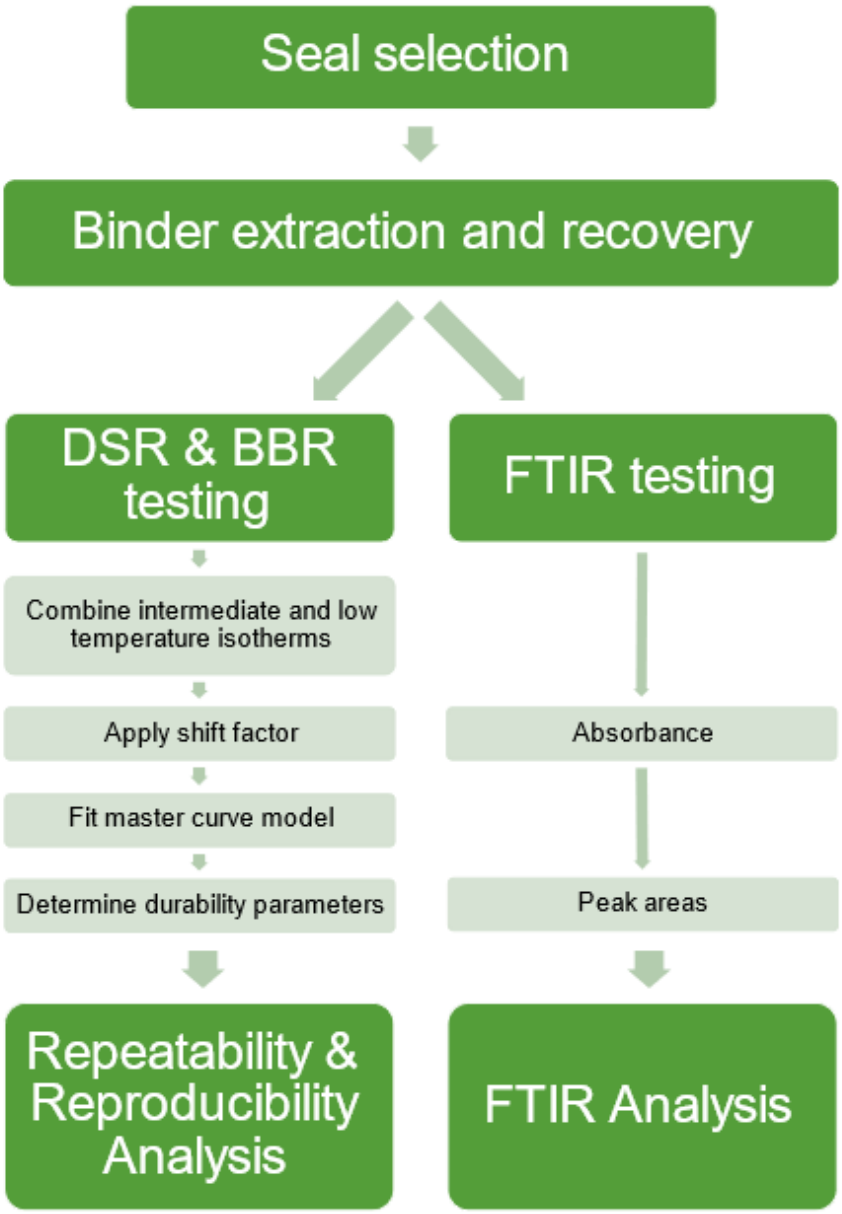

Figure 3.14: Summary of Chapter 3

Chapter 4: Results and Discussion

The purpose of this chapter is to present, interpret and analyse the results obtained from the procedures explained in Chapter 3. Initially, data from each recovery will be considered individually and finally related binders will be grouped accordingly to allow for relevant evaluation. In this chapter the following outcomes will be discussed:

- Observations made during the extraction and recovery procedure, which could possibly influence the efficiency of the method.
- Raw data obtained from DSR and BBR rheometry testing.
- Utilisation of shift factors and rheological models in order to identify the most suitable model to present processed data.
- Calculation of durability parameters to provide insight into the behaviour of the binder.
- Evaluation of durability parameters of recovered binders from the same source to determine the repeatability and reproducibility of the binder recovery procedure.
- Possible trends in Black Space when considering the type and age of the recovered binder.
- Evaluate the absorbance of recovered binders from the same source to determine the effect of the extraction and recovery process on the chemical composition of the binder.
- A summary of the pertinent findings.

4.1 Extraction and Recovery

No results are obtained from the extraction and recovery process, only binder is recovered. As explained in Chapter 3.3, SANS 3001 (2011) require that the solvent-binder solution be re-centrifuged if the mass of fines accumulated in the cup exceeds 50 g. Table 4.1 shows that after the first round of centrifugation, all of the samples retained more than 50 g of fines. After re-centrifugation, the mass of fines significantly decreased. No sample had more than 50 g of fines after re-centrifugation, which means that the specification was met.

Table 4.2 shows the amount of binder recovered from each seal sample. For quality control purposes, the mass change of the recovered binder was also calculated. From Table 4.2 it can be seen that the mass change for all of the samples did not exceed 0.075%.

Table 4.1: Fines Retrieved from Centrifugation

Name	Fines from Centrifugation (g)	Fines from Re-Centrifugation (g)
MR265 km12 #1	59.7	3
MR265 km12 #2	63	0.8
MR265 km12 #3	57.4	4.2
DR2216 km1	7.2	1.3
N8/8 km5.6 OWT	151.7	2
N8/8 km5.6 SHDR	135.5	0.9
N2/31 km3.6	196.8	2.2
N2/32 km21	127	1.8
R61/6 km88.05 #1	81.2	2
R61/6 km88.05 #2	68.9	0.7
R61/8 km51.01 #1	9.7	0.5
R61/8 km51.01 #2	37.5	1.2
R61/8 km51.01 #3	43.5	1.7
MR265 km41 #1	2771.5	24
MR265 km41 #2	249.2	2
MR265 km41 #3	310.5	2.2
MR174 km9	180.6	2.4
N2/16 km71.5 #1	73.8	2.9
N2/16 km71.5 #2	70.7	2.6
N2/16 km71.5 #3	40.8	1.2
N6/4 km87.4	208.7	2

Table 4.2: Mass of Recovered Binder and accompanying Mass Change

Name	Binder (g)	Mass Change (%)
MR265 km12 #1	233	0.045
MR265 km12 #2	224	0.057
MR265 km12 #3	230	0.045
DR2216 km1	137.17	0.049
N8/8 km5.6 OWT	210.89	0.058
N8/8 km5.6 SHDR	224.42	0.047
N2/31 km3.6	140.75	-
N2/32 km21	158.83	0.03
R61/6 km88.05 #1	114.13	-
R61/6 km88.05 #2	95.59	-
R61/8 km51.01 #1	108.07	0.074
R61/8 km51.01 #2	121.14	0.074
R61/8 km51.01 #3	133.99	0.061
MR265 km41 #1	197.29	0.045
MR265 km41 #2	168.18	0.059
MR265 km41 #3	184.98	0.048
MR174 km9	154.55	0.049
N2/16 km71.5 #1	174.82	0.068
N2/16 km71.5 #2	170.5	0.066
N2/16 km71.5 #3	180.89	0.073
N6/4 km87.4	153.27	0.075

All of the binders used for rheometry testing was initially heated at 160°C for 30 minutes. Therefore, it is expected that the stiffness parameters will not be negatively affected due to the presence of solvent, since only trace amounts of solvent was present and that solvent evaporated during the initial heating of the binder. For samples R61/6 km88.05 #1, R61/6 km88.05 #2 and N2/31 km3.6 there was not sufficient binder available to determine the mass change percentage.

4.2 DSR

During a strain sweep, an increasing strain percentage is applied, while the temperature and frequency remain constant. For each strain percentage value, the accompanying shear stress, storage modulus, loss modulus, loss factor, torque and complex shear modulus is received as output values. In determining the LVE, only the strain percentage and complex modulus are used, as depicted in Figure 4.1.

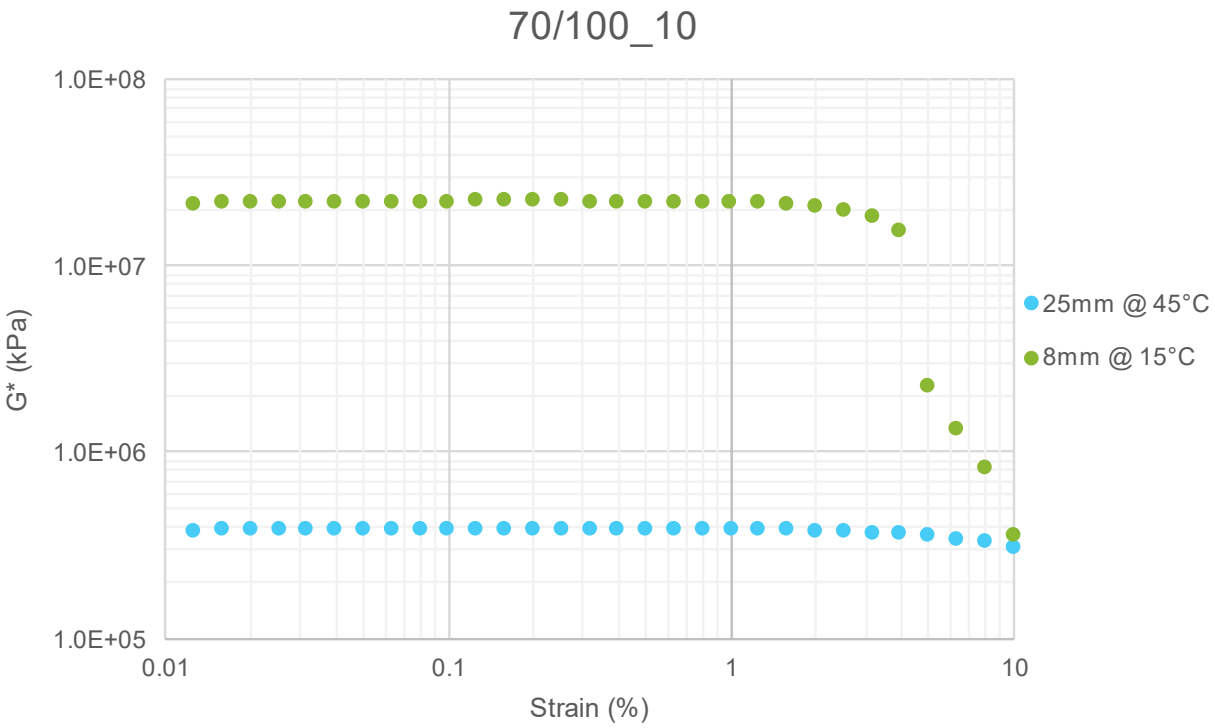

Figure 4.1: Strain Sweep Output

For the specific binder presented in Figure 4.1, deviation from the initial G* values occur at strain percentage values much higher than 1%. Specifically, the 8 mm deviates from the LVE range for strain percentages greater than 4%. Therefore, a constant strain percentage of 1% will be applied during the frequency sweep for both 8 mm and 25 mm geometry. The strain sweeps showed that 1% strain can be used for all binders at both configurations.

Table 4.3 shows the frequency sweep output for a single temperature isotherm. As explained in Chapter 3.7, a frequency sweep is conducted at 35°C for both the 8 mm and 25 mm spindle geometry. From Table 4.3 it can be seen that the average G* is greater than 10^5, which suggests that the 35°C isotherm from the 8 mm geometry be used when combining the DSR and BBR data.

Table 4.3: Frequency Sweep Output of DR2216 km1 (25mm PP)

	Temp [°C]	ω [rad/s]	G' [Pa]	G'' [Pa]	Loss Factor	Ɣ [%]	T [Pa]	Torque [nM.m]	δ [°]	G* [Pa]
1	35	0.251	71528	1.49E+05	2.08	1	1652.4	7.5886	64.33	1.65E+05
2	35	0.316	87470	1.75E+05	2	1	1957.3	8.9888	63.44	1.96E+05
3	35	0.398	1.06E+05	2.05E+05	1.93	1	2309.2	10.605	62.59	2.31E+05
4	35	0.501	1.28E+05	2.39E+05	1.86	1	2714	12.464	61.75	2.71E+05
5	35	0.63	1.55E+05	2.78E+05	1.8	1	3182.3	14.615	60.91	3.18E+05
6	35	0.794	1.85E+05	3.22E+05	1.74	1	3719.3	17.081	60.09	3.71E+05
7	35	0.999	2.21E+05	3.72E+05	1.68	1	4338.2	19.924	59.27	4.33E+05
8	35	1.26	2.63E+05	4.29E+05	1.63	1	5045.5	23.172	58.46	5.03E+05
9	35	1.58	3.12E+05	4.93E+05	1.58	1	5844.4	26.841	57.68	5.83E+05
10	35	1.99	3.69E+05	5.65E+05	1.53	1	6756.3	31.029	56.89	6.75E+05
11	35	2.51	4.35E+05	6.46E+05	1.49	1	7819.6	35.912	56.08	7.79E+05
12	35	3.16	5.11E+05	7.37E+05	1.44	1	8959.5	41.147	55.24	8.97E+05
13	35	3.98	5.99E+05	8.38E+05	1.4	1	10319	47.389	54.46	1.03E+06
14	35	5.01	6.99E+05	9.51E+05	1.36	1	11840	54.378	53.7	1.18E+06
15	35	6.3	8.14E+05	1.08E+06	1.32	1	13534	62.155	52.91	1.35E+06
16	35	7.94	9.45E+05	1.21E+06	1.29	1	15361	70.546	52.12	1.54E+06
17	35	9.99	1.09E+06	1.37E+06	1.25	1	17506	80.396	51.36	1.75E+06
18	35	12.6	1.26E+06	1.54E+06	1.22	1	19937	91.563	50.58	1.99E+06
19	35	15.8	1.45E+06	1.72E+06	1.18	1	22575	103.68	49.81	2.25E+06
20	35	19.9	1.67E+06	1.92E+06	1.15	1	25488	117.06	49.04	2.55E+06
21	35	25.1	1.91E+06	2.14E+06	1.12	1	28706	131.83	48.27	2.87E+06
									Average	1.04E+06

4.3 BBR

BBR testing was performed at -24°C, -18°C, and -12°C. Table 4.5 shows the typical BBR output of DR2216 km1 at -12°C. From these output values the stiffness and relaxation critical temperature at 60 seconds is calculated. Where the S(60) and m(60) values do not comply with the requirements, testing at an additional temperature was performed. A summary of S(60) and m(60) values are presented in Table 4.4. The majority of the binders have a negative ΔT_c which implies that these binders are m-controlled. For binders that are m-controlled the relaxation potential of the binder has decreased from the original unaged state. When considering the SATS 3208 requirement that the value of ΔTc must be greater than or equal to - 5°C, it can be seen that only three binders have a ΔTc value less than -5°C. Since these binders are relatively old (6 years +), it is expected that they may not comply, as the requirement is for PAV aged binders

Table 4.4: Summary of S(60). m(60) and corresponding low temperature parameters

Name	Age	-18		-12		-6		Ts (°C)	Tm (°C)	ΔTc (°C)	LTc (°C)
		S(60) (MPa)	m(60)	S(60) (MPa)	m(60)	S(60) (MPa)	m(60)				
MR265 km12 #1	1	361.490	0.275	167.067	0.340	100.502	0.413	-26.55	-15.73	-0.82	-25.73
MR265 km12 #2	1	385.599	0.272	205.351	0.334	88.681	0.403	-25.61	-25.27	-0.34	-25.27
N8/8 km5.6 OWT	7	325.940	0.271	178.618	0.311	88.380	0.373	-27.17	-23.68	-3.49	-23.68
N2/31 km3.6	12	498.103	0.209	264.642	0.253	156.252	0.322	-23.19	-17.92	-5.27	-17.92
		-24		-18		-12		Ts (°C)	Tm (°C)	ΔTc (°C)	LTc (°C)
		S(60) (MPa)	m(60)	S(60) (MPa)	m(60)	S(60) (MPa)	m(60)				
MR265 km12 #3	1	513.228	0.232	293.030	0.303	150.122	0.353	-28.25	-28.23	-0.02	-28.23
DR2216 km1	10	459.185	0.234	277.331	0.257	171.786	0.302	-28.93	-22.22	-6.72	-22.22
N8/8 km5.6 SHDR	7	486.974	0.240	267.918	0.297	158.828	0.335	-29.14	-27.49	-1.65	-27.49
N2/32 km21	6	606.634	0.225	355.506	0.254	204.290	0.306	-26.16	-22.72	-3.44	-22.72
R61/6 km88.05 #1	1	400.229	0.290	214.227	0.321	97.039	0.391	-31.23	-32.08	0.85	-31.23
R61/6 km88.05 #2	1	407.900	0.262	247.774	0.312	114.246	0.380	-30.30	-29.44	-0.86	-29.44
R61/8 km51.01 #1	1	660.683	0.257	305.883	0.310	146.408	0.375	-27.84	-28.95	1.11	-27.84
R61/8 km51.01 #2	1	397.324	0.250	291.110	0.303	146.942	0.374	-28.58	-28.34	-0.24	-28.34
R61/8 km51.01 #3	1	473.773	0.270	248.403	0.298	129.068	0.389	-29.75	-27.88	-1.87	-27.88
MR265 km41 #1	1	423.530	0.258	258.099	0.311	119.604	0.371	-29.82	-29.29	-0.54	-29.29
MR265 km41 #2	1	586.249	0.232	359.627	0.253	132.060	0.339	-26.91	-24.73	-2.18	-24.73
MR265 km41 #3	1	469.012	0.209	349.899	0.258	132.606	0.345	-27.05	-25.10	-1.95	-25.10
MR174 km9	9	475.505	0.251	306.511	0.278	166.548	0.330	-34.29	-25.45	-8.84	-25.45
N2/16 km71.5 #1	2	483.013	0.271	251.382	0.312	116.398	0.373	-29.62	-29.73	0.11	-29.62
N2/16 km71.5 #2	2	457.032	0.275	219.070	0.298	118.721	0.373	-30.57	-27.83	-2.74	-27.83
N6/4 km87.4	-	543.783	0.245	335.587	0.256	191.711	0.315	-26.80	-23.50	-3.30	-23.50
		-30		-24		-18		Ts (°C)	Tm (°C)	ΔTc (°C)	LTc (°C)
		S(60) (MPa)	m(60)	S(60) (MPa)	m(60)	S(60) (MPa)	m(60)				
N2/16 km71.5 #3	2	1069.027	0.224	346.217	0.302	161.718	0.355	-32.87	-34.12	1.25	-32.87

Table 4.5: BBR Output of DR2216 km1 at -12°C

Time (s)	Force (mN)	Deflection (mm)	Measured Stiffness (MPa)	m-value
8	1002	0.279	297.160	0.241
15	1001	0.327	253.287	0.26
30	1001	0.395	209.683	0.281
60	1003	0.482	172.179	0.301
120	1003	0.599	138.548	0.322
240	1000	0.754	109.738	0.343

The bending stiffness data is converted to shear stiffness. This will allow for the results from BBR testing to be combined with DSR results. Figure 4.2 is a typical plot of G* against frequency for all of the temperature isotherms.

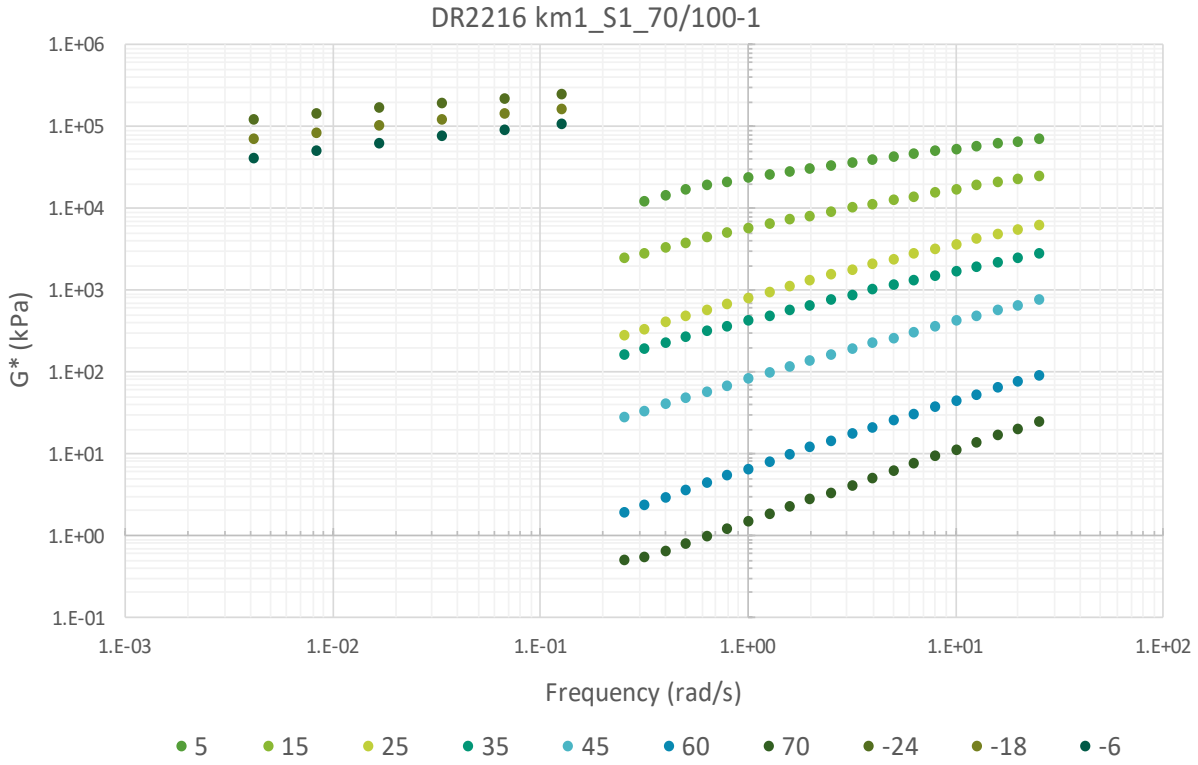

Figure 4.2: Combined Isotherm Data

4.4 Shift Factors

As explained in Chapter 3.7, the Gordon and Shaw free shifting method was used to shift each isotherm to the reference temperature. RHEA software provided the free shift factors for G' and G", as shown in Table 4.6. The average of the G' and G" components is calculated and is presented as the combined shift results. Since 15°C is used as the reference temperature, the shift factors are zero for this isotherm.

Table 4.6 Free Shift Factors for DR2216 km1

Isotherm (°C)	G'	G''	Combined Shift Results
-24	6,152	6,027	6.09
-18	5,204	5,088	5.146
-12	4,414	4,298	4.356
5	1,302	1,290	1.296
15	0	0	0
25	-1,360	-1,327	-1.344
35	-1,695	-1,877	-1.786
45	-2,733	-2,898	-2.815
60	-4,128	-4,263	-4.196
70	-4,888	-5,002	-4.945

The RHEA software applies abovementioned factors to the shift factor models and determines the constants for the shift factor equations. Figure 4.3 illustrates the correlation between the combined shift results and the two available shift factor models, the Modified Kaelble model and the WLF model.

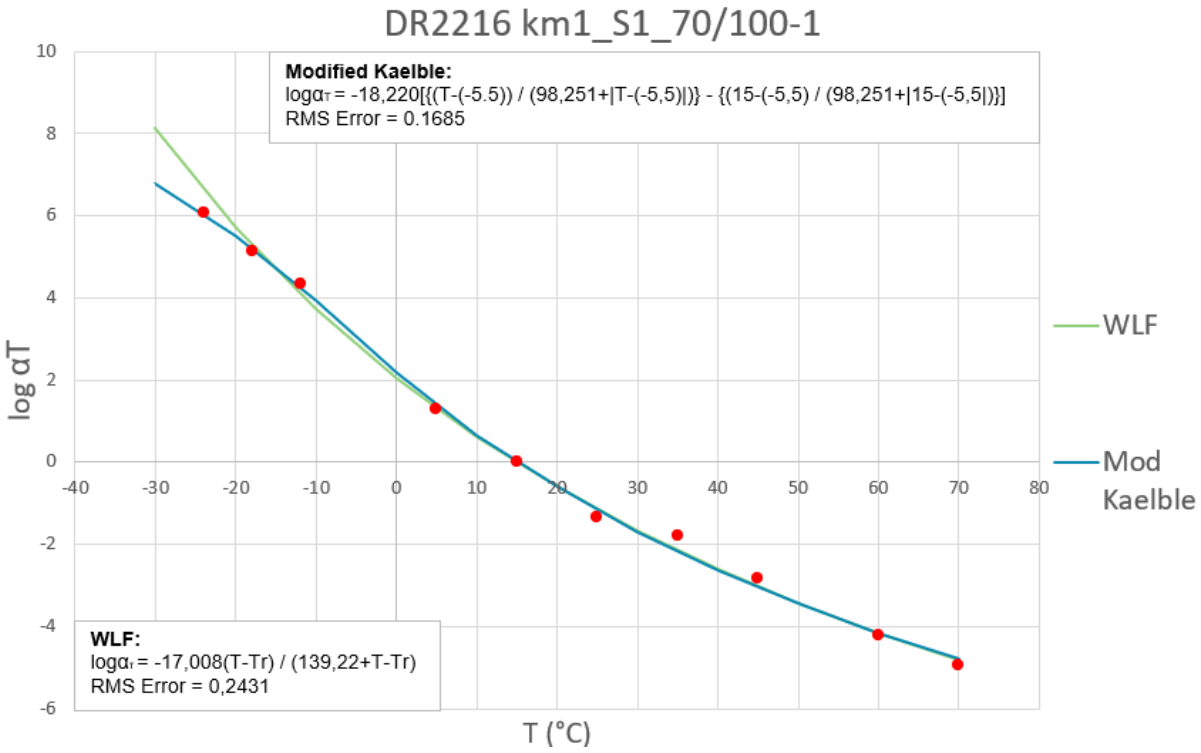

Figure 4.3: Typical Shift Factor Equations

From Figure 4.3, it can be observed that at the low temperatures the WLF model deviates from the data point and tends toward higher values. Rowe, Baumgardner and Sharrock (2009) also recognised this tendency. Despite this observation, the RMS error was still used to

confirm that the equation that yields the lowest RMS error, be used to shift the data to the reference temperature. Table 4.7 and Table 4.8 summarises the shift factor parameters used for each binder. In most cases the Modified Kaelble model was used as the preferred model. The RHEA software was unable to apply the data of binder MR265 km41 #3 to the Modified Kaelble model, therefore the WLF model was used instead.

Table 4.7: Summary of Modified Kaelble Shift Factor Parameters at Tref = 15°C

MODIFIED KAELBLE				
logαT=-C1([{T-Tk}/{C2+|T-Tk|}]-[{Tr-Tk}/{C2+|Tr-Tk|}])				
Name	**C1**	**C2**	**Tk**	**rms error**
MR265 km12 #1	45.928	356.640	5.000	0.160
MR265 km12 #2	30.345	179.440	-7.000	0.106
MR265 km12 #3	37.762	237.420	-11.000	0.115
MR265 km12 EG	15.410	29.925	-5.500	0.375
DR2216 km1	18.220	98.251	-5.500	0.169
N8/8 km5.6 OWT	28.228	167.130	-1.000	0.073
N8/8 km5.6 SHDR	17.619	83.199	2.500	0.082
N2/31 km3.6	20.895	106.010	4.500	0.123
N2/31 km3.6 EG	33.262	186.810	-6.000	0.048
N2/32 km21	13.767	35.732	1.500	0.228
N2/32 km21 EG	27.031	117.800	-18.000	0.091
R61/6 km88.05 #1	24.989	138.640	-8.000	0.073
R61/6 km88.05 #2	25.529	143.190	-8.000	0.077
R61/6 km88.05 CT	6.591	31.699	28.000	0.159
R61/8 km51.01 #1	25.619	130.780	-14.000	0.087
R61/8 km51.01 #2	22.228	125.420	-3.500	0.101
R61/8 km51.01 #3	23.478	133.760	-5.500	0.080
R61/8 km51.01 CT	13.100	99.764	16.000	0.012
MR265 km41 #1	25.528	149.870	-6.000	0.094
MR265 km41 #2	33.128	183.390	-15.000	0.156
MR265 km41 EG	10.691	48.867	-2.500	0.248
MR174 km9	27.668	158.050	-5.500	0.075
MR174 km9 CT	16.897	122.290	20.000	0.024
N2/16 km71.5 #1	26.492	145.720	-10.000	0.069
N2/16 km71.5 #2	25.923	120.640	-17.000	0.187
N2/16 km71.5 #3	30.249	137.500	-30.000	0.178
N2/16 km71.5 CT	19.022	114.200	23.000	0.344
N6/4 km87.4	27.737	147.060	-5.500	0.118

Table 4.8: Summary of WLF Shift Factor Parameters at Tref = 15°C

WLF			
logαT=a(T-Tr)/(b+T-Tr)			
Name	**a**	**b**	**rms error**
MR265 km41 #3	-41.935	289.970	0.272

4.5 Rheological Modelling

The RHEA Software uses the time-temperature superposition principle to model the experimental data in rheological models. Literature revealed that for cases where the stiffness values exceed 10^5 Pa, the CAM model is typically the most ideal rheological model to predict the stiffness values. However, it is important to use the model that has the lowest error. Therefore, the RMS error for both G* and δ should be considered.

In Figure 4.4, the values of G* and δ are plotted against the reduced frequency. The figure illustrates how each isotherm contributes toward the construction of the master curve. The G* data points correlate well to the modelled master curve. When considering the data points from the δ plot, it can be seen that discrepancies exist in the region where the 25°C and 35°C isotherms are supposed to link. This deviation will influence the accuracy of the model.

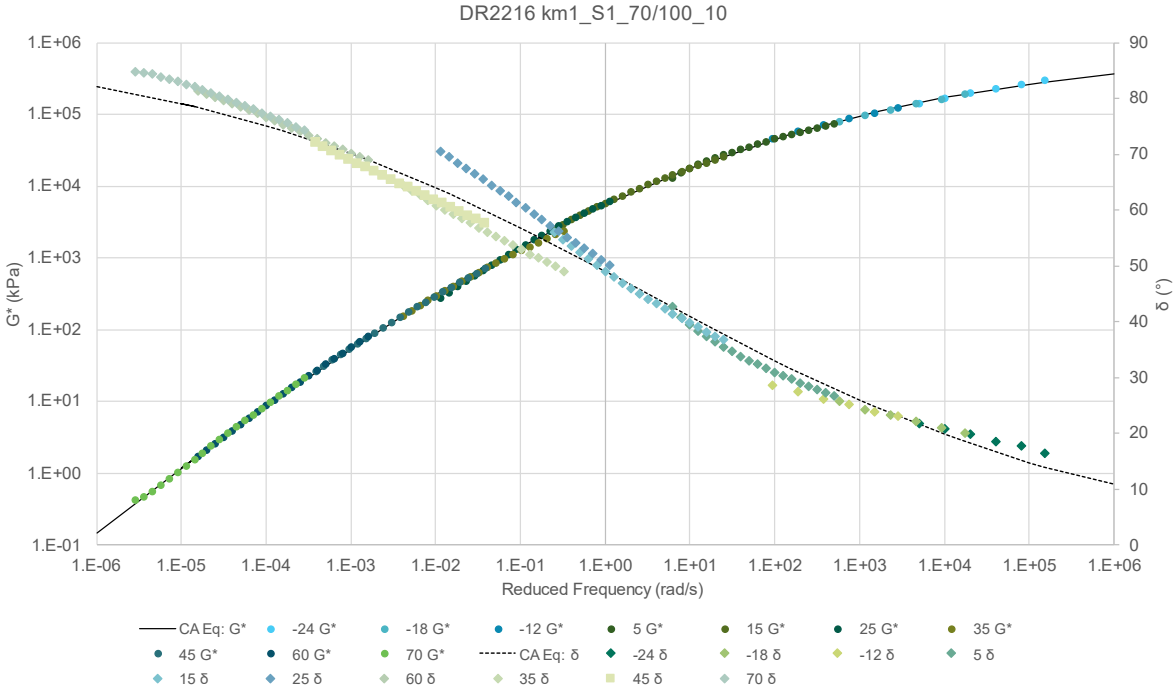

Figure 4.4: CAM Model

For all of the modelled data, RHEA software also determines equations for G' and G'' by following a discrete modelling approach. Values for G* and δ are calculated from the G' and G" equations that contain the variables that are provided in Table 4.9.

Table 4.9: Discrete Modelling Variables for DR2216 km1

i	g_i (kPa)	λ_i (sec)
1	2.53E+05	2.11E-08
2	6.40E+04	2.68E-07
3	7.22E+04	1.15E-06
4	1.11E+05	8.99E-06
5	6.19E+04	5.00E-05
6	4.44E+04	2.01E-04
7	3.56E+04	7.74E-04
8	2.87E+04	3.53E-03
9	2.01E+04	1.64E-02
10	1.10E+04	7.54E-02
11	5.44E+03	3.34E-01
12	2.62E+03	1.30E+00
13	1.12E+03	5.48E+00
14	2.91E+02	5.07E+01
15	6.66E+01	3.08E+02
16	1.39E+01	1.76E+03
17	2.54E+00	8.99E+03
18	4.07E-01	5.45E+04
19	2.77E-02	1.23E+06
20	2.28E-03	1.21E+07

Figure 4.5 shows the values of G* and δ plotted against the reduced frequency when using discrete modelling. There appears to be a good correlation between the G* data and the master curve. Since RHEA also provides an RMS error for each model, the model yielding the lowest RMS error will be used to model G* and δ data. The best fit model will be used to obtain the input values needed to determine the durability parameters.

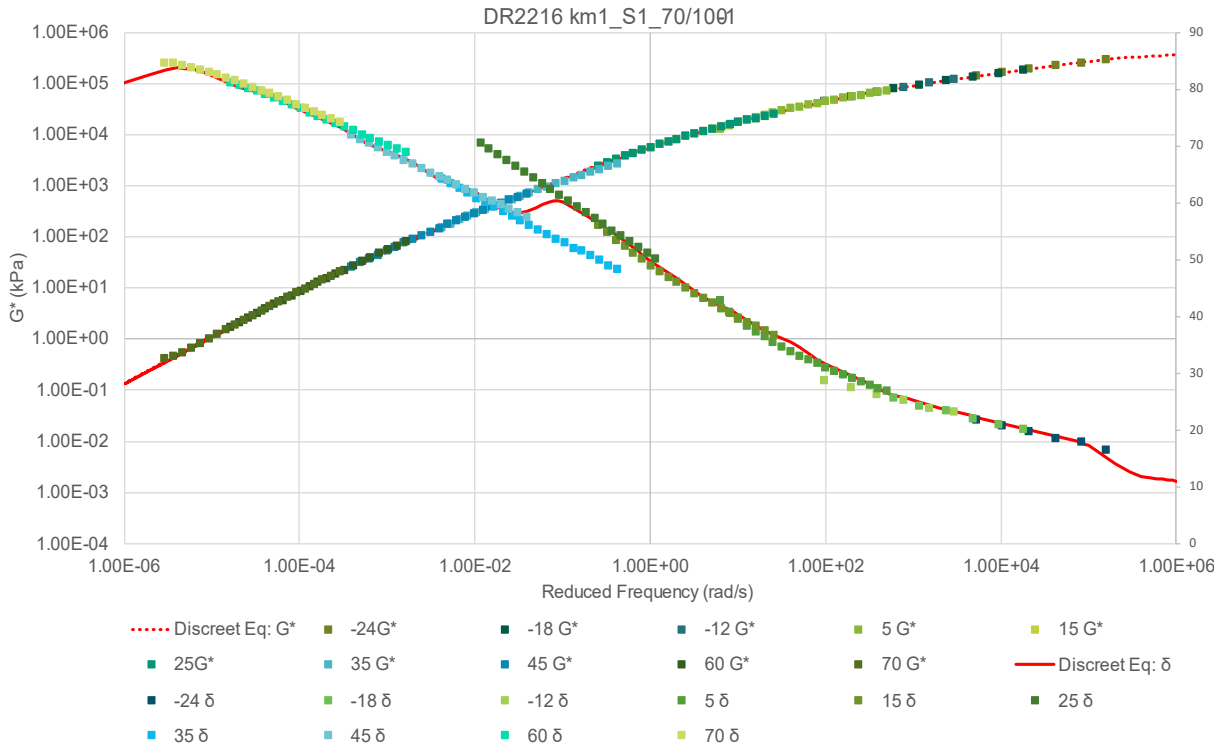

Figure 4.5: Discrete Modelling

4.6 Durability Parameters

Table 4.10 provides a summary of all of the durability parameters that were calculated as explained in Chapter 3.8. The ΔT_c parameters were already briefly discussed in Chapter 4.3. When considering the G-R parameters, only the N2/31 km3.6 binder exceeds the 600 kPa limit. All of the T_{max} values exceed 70°C. The maximum temperature at which DSR testing took place was 70°C, which means that the DSR data was extrapolated in order to determine T_{max}. For data analysis interpolation is preferred. The values of T_{vet} range between 6°C and 28°C, while the G_{vet} value varies between 4160 kPa and 16538 kPa. At first glance, there appears to be no distinct ranges for T_{vet} and G_{vet} when binders of the same age are grouped together. In the next section the durability parameters will be discussed in more depth.

Table 4.10: Summary of Durability Parameters

Name	Binder Type	Age	G-R (kPa)	G_{vet} (kPa)	ΔT_c (°C)	T_{vet} (°C)	T_{max} (°C)
MR265 km12 #1	S-E1	1	46.676	9313	-0.824	15.617	99.884
MR265 km12 #2	S-E1	1	39.330	10300	-0.336	15.062	79.333
MR265 km12 #3	S-E1	1	34.547	10027	-0.018	14.486	78.475
MR265 km12 C	S-E1	1	11.670	14257	0.015	11.308	78.273
MR265 km41 #1	70/100	1	6.224	9650	-0.535	12.651	73.654
MR265 km41 #2	70/100	1	18.694	9545	-2.184	16.006	73.654
MR265 km41 #3	70/100	1	179.809	4160	-1.948	23.855	73.605
MR265 km41 C	70/100	1	21.935	16538	0.363	15.086	75.303
R61/6 km88 #1	SC-E2	1	10.729	7349	0.849	13.138	74.205
R61/6 km88 #2	SC-E2	1	11.600	8512	-0.858	12.626	74.807
R61/6 km88 C	SC-E2	1	3.489	11640	-	9.231	72.766
R61/8 km51 #1	SC-E2	1	4.014	13848	1.112	11.462	72.604
R61/8 km51 #2	SC-E2	1	4.453	12913	-0.242	11.150	72.506
R61/8 km51 #3	SC-E2	1	3.569	14484	-1.874	10.145	71.992
R61/8 km51 C	SC-E2	1	3.241	13414	-	7.212	71.418
N2/16 km71.5 #1	S-E1	2	12.872	10292	0.107	12.928	75.717
N2/16 km71.5 #2	S-E1	2	11.012	8587	-2.737	14.810	75.588
N2/16 km71.5 #3	S-E1	2	4.285	11969	1.247	6.530	72.586
N2/16 km71.5 C	S-E1	2	40.277	12569	-	16.801	79.652
N2/32 km21	S-E1	6	41.518	6947	-3.437	19.881	80.274
N2/32 km21 C	S-E1	6	74.718	11315	-1.510	18.399	82.860
N8/8 km5.6 OWT	S-E1	7	150.951	6139	-3.491	23.795	81.417
N8/8 km5.6 SHDR	S-E1	7	79.773	6201	-1.645	22.659	80.278
MR174 km9	70/100	9	77.351	6888	-8.840	19.935	80.489
MR174 km9 C	70/100	9	47.678	7100	-	17.812	80.071
N6/4 km87.4	S-E1	9	62.946	6069	-3.296	19.366	76.061
DR2216 km1	70/100	10	40.923	9367	-6.718	14.241	87.639
N2/31 km3.6	S-E1	12	833.572	5490	-5.274	28.496	87.195
N2/31 km3.6 C	S-E1	12	1218.287	8072	-3.998	28.529	88.884

4.7 Repeatability and Reproducibility Analysis

Four seals that represent the most significant observations have been identified and will be discussed in order of binder age:

- 1 year old S-E1 single seal;
- 1 year old 70/100 Cape seal;
- 1 year old SC-E1 Cape seal, and
- 9 year old 70/100 Cape seal.

G-R and Gvet are compared to evaluate the consistency in measured behaviour in different G* and δ ranges. Similarly, ΔT_c, T_{vet} and T_{max} are analysed to determine possible differences in rheology at distinct temperatures. The shift and master curve model errors are also presented, as poorly fitted models may contribute to variability in calculated parameters. Additionally, the raw test data and the optimised models are presented in Black Space. These may assist in:

- identification of specific stiffness and delta ranges where variability may be observed;
- pinpointing likely causes in these observed variabilities; and
- visually representing calculated durability parameter differences.

4.7.1 Young, modified single seal

MR265 km 12 is a S-E1 modified binder recovered from a 1 year old single seal. Figure 4.6 illustrates the stiffness parameter of MR265 km12. It can be seen that all of the parameters appear to be in a similar range, although the compare sample has a much lower G-R value and a slightly elevated G_{vet} value. This implies that compare sample experienced less hardening than the other samples.

Figure 4.6: Stiffness Parameters of MR265 km12

Table 4.11 contains the RMS Error values of the shift factor models and the master curve models. It can be seen that test 1 has the highest RMS Error value for both the shift factor model and master curve model. The shift factor model and the master curve model of test 1 is classified as poor. The RMS Error value of the other samples correlate well, and the corresponding shift factor models and master curve models are classified as good.

Table 4.11: RMS Error of Fitted Data of MR265 km12

Name	Shift Factor	RMS Error	Master Curve	RMS Error
Test #1	Modified Kaelble	0.160	CAM Model	0.187
Test #2	Modified Kaelble	0.106	CAM Model	0.035
Test #3	Modified Kaelble	0.115	CAM Model	0.039
Compare	Modified Kaelble	0.117	CAM Model	0.045

Table 4.12 contains the recommended repeatability and reproducibility requirements for the stiffness parameters. The G_{vet} values perform well in terms of repeatability and reproducibility. Although the δ and G* values that form the G-R parameter, comply with the recommended repeatability and reproducibility limits, when combining these input values to determine G-R, it appears that the G-R parameter does not perform well in terms of repeatability.

Since the shift factor model and the master curve model of test 1 is classified as poor, it was decided to reconsider the reproducibility by omitting test 1. This creates a critical difference (Δlog(G-R)) of 0.528 and a specification of 0.378. The G-R parameter still did not meet the recommended repeatability requirements, which suggest that the G-R value is too low and that test 1 is not the reason for the lack of reproducible results.

Table 4.12: Repeatability and Reproducibility of Stiffness Parameters of MR265 km12

	Test #1	Test #2	Test #3	Compare
δ (°)	67.336	69.339	69.668	73.118
G* (kPa)	290.102	295.594	268.330	132.418
G-R (kPa)	46.676	39.330	34.547	11.670
Gvet (kPa)	9312.500	10300.000	10027.391	14257.143
	Repeatability		**Reproducibility**	
Δδ	2.332		5.782	
Recommended	6.878		18.864	
Δlog(G*)	0.042		0.349	
Recommended	0.245		0.640	
Δlog(G-R)	0.131		0.602	
Recommended	0.160		0.396	
Δlog(Gvet)	0.044		0.185	
Recommended	0.399		1.089	

The temperature parameters are shown in Figure 4.7. The ΔT_c values remain very close to zero, which is a critical point is determining whether the binder is S-controlled or m-controlled.

The three test samples have a negative ΔT_c (-0.824°C; -0.336°C; -0.018°C), making these binders m-controlled. The compare sample has a positive ΔT_c (0.015°C), hence the binder is S-controlled. In terms of repeatability, having the same binder with different low temperature classification could be problematic.

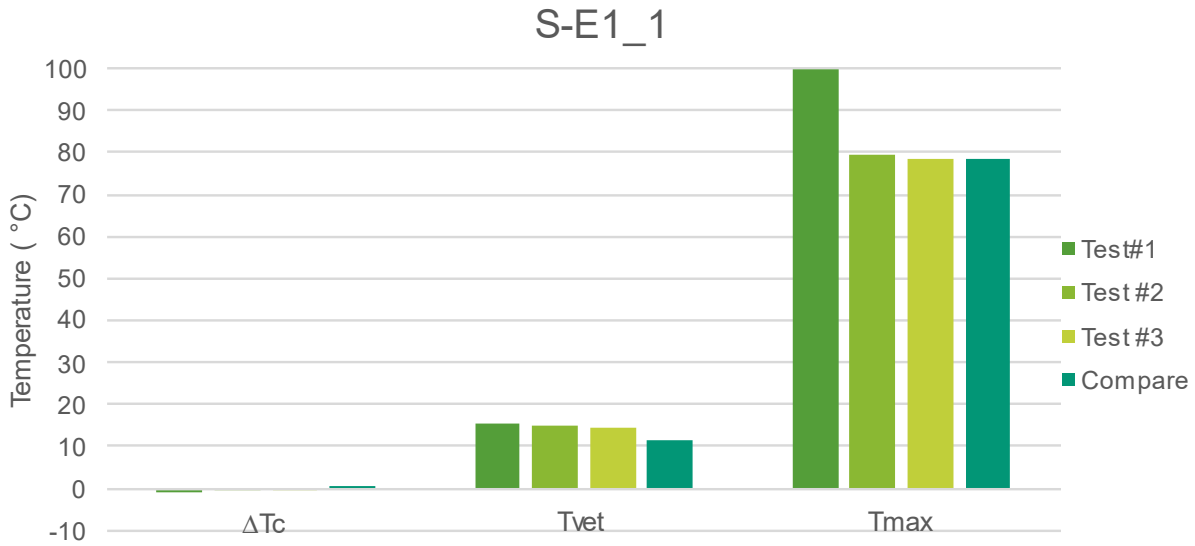

Figure 4.7: Temperature Parameters of MR265 km12

Table 4.13 considers the recommended repeatability and reproducibility requirements for all of the temperature parameters. The T_{vet} values comply with the recommended repeatability limit but exceed the recommended reproducibility limit. The values of T_{max} does not comply with either of the recommended limits. The deviation is expected, as Figure 4.7 showed that the value of T_{max} of test 1 differs vastly from the other samples.

Table 4.13: Repeatability and Reproducibility of Temperature Parameters of MR265 km12

	Test #1	Test #2	Test #3	Compare
Tc,s	-26.551	-25.610	-28.252	-26.771
Tc,m	-25.727	-25.274	-28.233	-26.786
ΔTc	-0.824	-0.336	-0.018	0.015
Tmax	99.884	79.333	78.475	78.273
Tvet	15.617	15.062	14.486	11.308
	Repeatability		**Reproducibility**	
ΔTc,s	2.642		1.481	
ΔTc,m	2.960		1.512	
Δ (ΔTc)	0.806		0.839	
ΔTmax	21.4		21.6	
ΔTvet	1.132		4.309	
Recommended	1.9		3.4	

From Table 4.13, it can be seen that $\Delta T_{c,s}$ and $\Delta T_{c,m}$ exceeds the recommended limit for repeatability. As explained in Chapter 2.4.3, physical hardening and beam geometry are some

of the factors that contribute towards the variability experienced in BBR data. Since the ΔT_c complies with the recommended requirement, the failure of $\Delta T_{c,s}$ and $\Delta T_{c,m}$ to meet the requirements might be insignificant , as it does not appear to influence the calculation of ΔT_c or the low temperature grade

Figure 4.8 contains the Black Space diagram of all 4 samples using the CAM model. There is a strong correlation between the models and the raw data. Where δ>75°, the compare sample's data points deviate from the other data points. The G-R parameters are plotted in the range 67°<δ<73°, where all of the models tend to deviate from the raw data points. It can be seen that the compare sample's G-R is not positioned close to the model, but it does fall on the data, which means that G-R is accurate for the specimen. The G-R value of test 1 is positioned close to the model but does not appear close to the raw data points. This explains the poor RMS error values of test 1. Although the values of δ, that G-R comprises of, met the proposed repeatability requirements in Table 4.12, the visual inspection of Figure 4.8 reveal that this deviation is not acceptable.

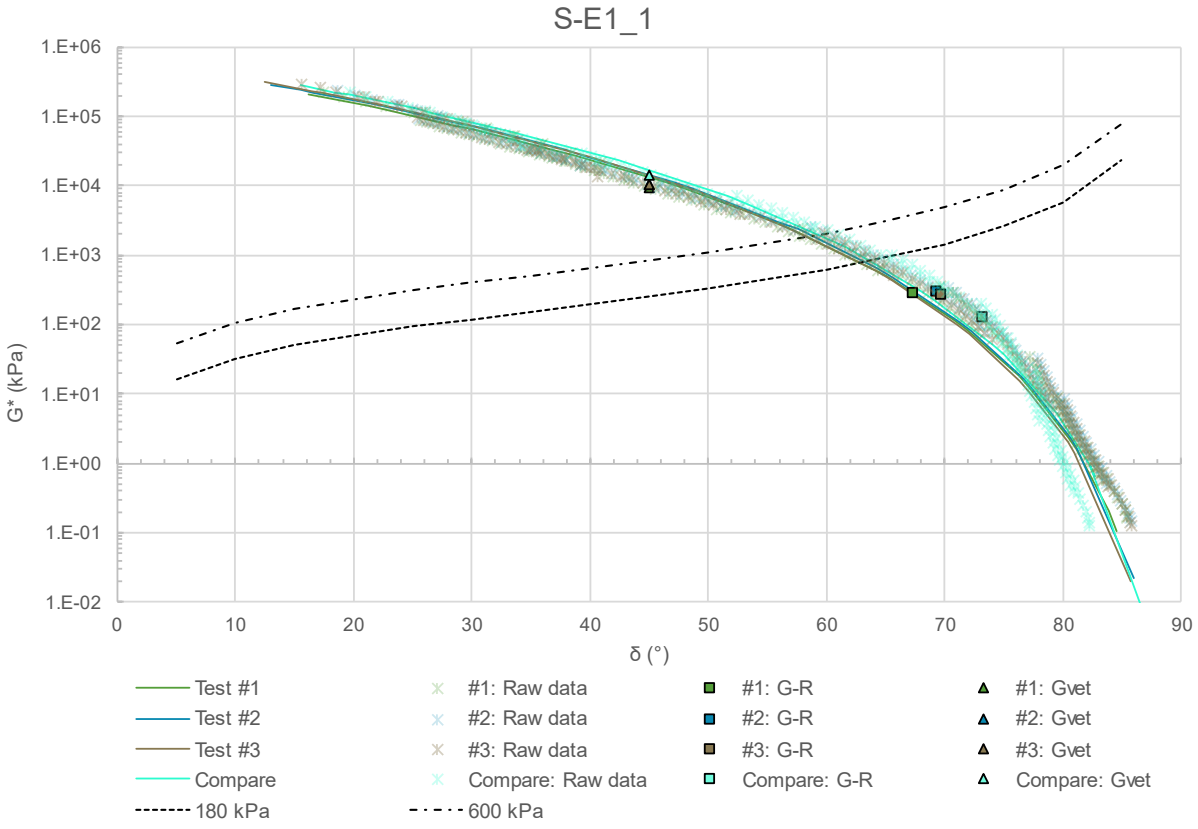

Figure 4.8: Black Space of MR265 km12

The analysis of MR265 km12 has revealed that the accuracy of test 1 in terms of the shift factor model, master curve model, and the value of T_{max}, differ from the other samples, suggesting that the binder from test 1 aged to a greater extent than the other samples. The

value of T_{max} of test 1 is the highest value of T_{max} for all of the binders used in this study, despite this binder only being 1 year old. The notes made during the recovery procedure was consulted to determine whether there are any reasons for the deviation of test 1. Two observations were made. Firstly, MR265 km12 was the first sample to be recovered. It is possible that at this stage, the binder recovery procedure had not been completely refined by the tester. And secondly, the duration of phase 2 of the distillation proses differed. On average, phase 2 took 20 minutes. For test 1, the duration of phase 2 was 55 minutes. It is possible that the high temperature and low pressure that the binder was exposed to during the distillation phase can cause excessive ageing. It should also be noted that a 5 year gap exist between the testing of the compare sample and the test samples. During this time the seal was stored in bags at room temperature. The seal was not stored in an air tight containers, which implies that the binder could have oxidized during this time.

4.7.2 Young, unmodified Cape seal

MR265 km41 is a 70/100 unmodified binder recovered from a 1 year old Cape seal. Figure 4.9 contains the stiffness parameters of MR265 km41. The G-R parameters are subject to noticeable variability. Test 3 has the highest G-R value. This value borders the 180 kPa limit, which suggest damage onset. Apart from test 3, the G_{vet} values correspond well. The compare sample has a slightly higher G_{vet} value, which indicate less hardening. Both G-R and G_{vet} suggest that test 3 does not correlate well with the other three samples.

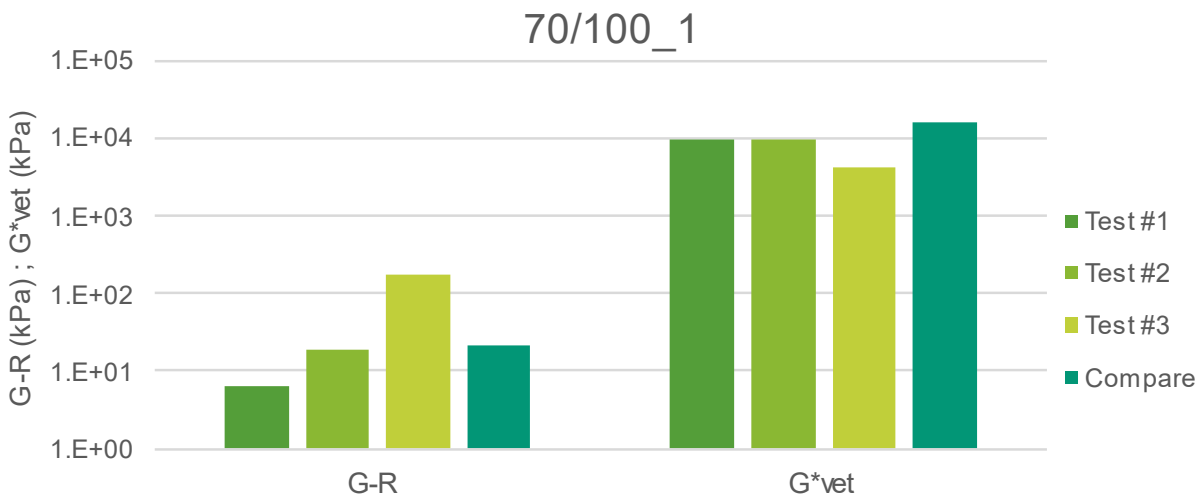

Figure 4.9: Stiffness Parameters of MR265 km41

From Table 4.14, it is noticed that a different shift factor model was used to process the data from test 3. The software was unable to determine a suitable fit using the Modified Kaelble equation. Both the RMS error of the shift factor model and the master curve model of test 3, is higher than the other samples. The shift factor of test 3 is classified as poor, while the master

curve model is classified as fair. The shift factor models, and the master curve models of the other samples are considered to be good.

Table 4.14: RMS Error of Fitted Data of MR265 km41

Name	Shift Factor	RMS Error	Master Curvel	RMS Error
Test #1	Modified Kaelble	0.094	Discrete Modelling	0.060
Test #2	Modified Kaelble	0.156	Discrete Modelling	0.059
Test #3	WLF	0.272	Discrete Modelling	0.127
Compare	Modified Kaelble	0.144	Discrete Modelling	0.057

Table 4.15 contains the recommended repeatability and reproducibility requirements for the stiffness parameters. It can be observed that δ, G* and G-R do not meet the recommended repeatability requirements and G-R also does not meet the recommended reproducibility requirements. Since Figure 4.9 and Table 4.14 both suggest that test 3 is an outlier, it was decided to reconsider the repeatability and reproducibility by omitting test 3. G* still did not meet the repeatability requirement and G-R continued to not comply with the recommended limits for both repeatability and reproducibility. G_{vet} did meet the recommended requirements for both repeatability and reproducibility.

Table 4.15: Repeatability and Reproducibility of Stiffness Parameters of MR265 km41

	Test #1	Test #2	Test #3	Compare
δ (°)	75.972	72.162	58.456	74.353
G* (kPa)	102.770	189.649	559.919	290.384
G-R (kPa)	6.224	18.694	179.809	21.935
Gvet (kPa)	9650.000	9545.000	4160.000	16538.293
	Repeatability		**Reproducibility**	
Δδ	17.516		15.897	
Recommended	6.886		18.964	
Δlog(G*)	0.736		0.451	
Recommended	0.235		0.641	
Δlog(G-R)	1.461		0.914	
Recommended	0.144		0.382	
Δlog(Gvet)	0.365		0.599	
Recommended	0.386		1.066	

From Figure 4.10, it can be seen that values for ΔT_c and T_{max} appear to be within the same range, while the values for T_{vet} are fluctuating. Tests 1, 2, and 3 are m-controlled, since ΔT_c is negative, while the compare sample has a positive ΔT_c, making the sample S-controlled. These values are relatively close to zero, therefore, the different classification could be insignificant. The T_{max} values indicate that the compare sample is slightly harder than the test samples. The T_{vet} values give the impression that test 1 aged to a lesser extent, while test 3 is once again the outlier. Since T_{vet} is calculated from modelled data, the dissimilarity of test 3 could be related to the higher RMS error values from Table 4.14.

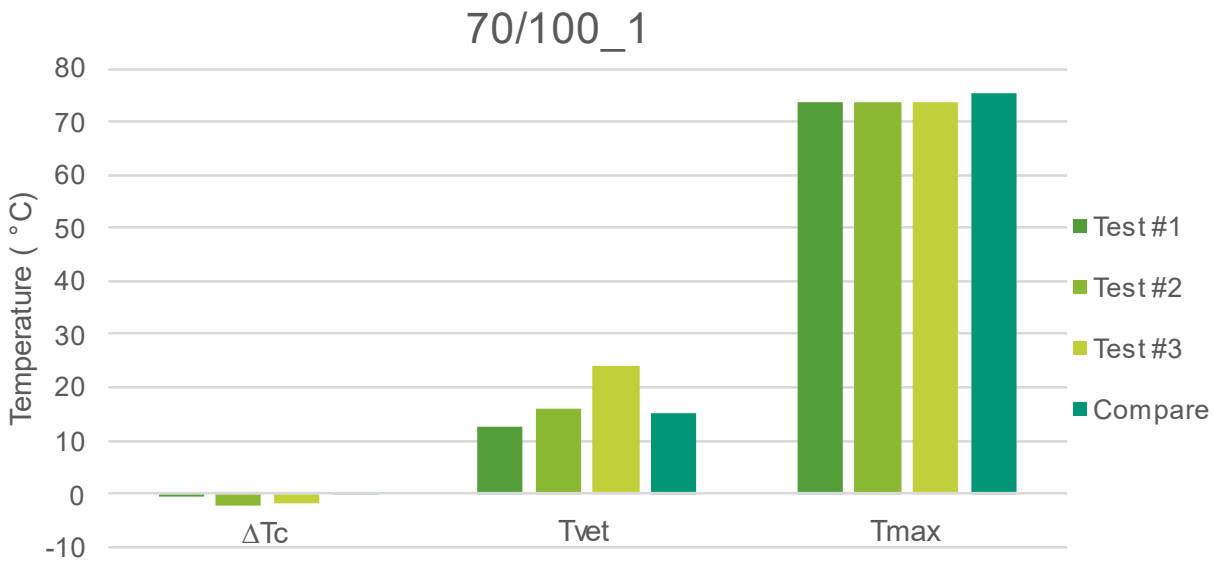

Figure 4.10: Temperature Parameters of MR265 km41

Table 4.16 reveals that ΔT_c and T_{max} meet the recommended requirements for both repeatability and reproducibility. If test 3 is omitted and ΔT_{vet} is recalculated, the value of ΔT_{vet} for repeatability and reproducibility will be 3.355 and 2.432 respectively. Although T_{vet} will still not succeed in terms of the recommended repeatability limit, it will pass the recommended requirement for reproducibility.

Table 4.16: Repeatability and Reproducibility of Temperature Parameters of MR265 km41

	Test #1	Test #2	Test #3	Compare
Tc,s	-29.822	-26.914	-27.049	-23.418
Tc,m	-29.287	-24.730	-25.100	-23.782
ΔTc	-0.535	-2.184	-1.948	0.363
Tmax	73.654	73.654	73.605	75.303
Tvet	12.651	16.006	23.855	15.086
	Repeatability		**Reproducibility**	
ΔTc,s	2.908		6.404	
ΔTc,m	4.557		5.506	
Δ (ΔTc)	1.649		2.547	
ΔTmax	0.049		1.698	
ΔTvet	11.204		8.769	
Recommended	1.9		3.4	

Figure 4.11 shows the Black Space diagrams, including discrete modelling of the data. The raw data points and the model for test 3 deviates from the other samples between 24°<δ<63. It is revealed that this region is populated by data from the 8 mm frequency sweep. There is a horizontal gap between the data from the 8 mm and 25 mm frequency sweeps and overlapping between the data from the 8 mm frequency sweep and the BBR data. The data points obtained from the BBR and 25 mm frequency sweep for all four samples correlate very well, hence the good correlation between the values for ΔT_c and T_{max}. The discrepancies test 3

experiences as seen from G-R, G_{vet} and T_{vet} are rheology related, more specifically related to the rheology obtained from the 8 mm frequency sweep.

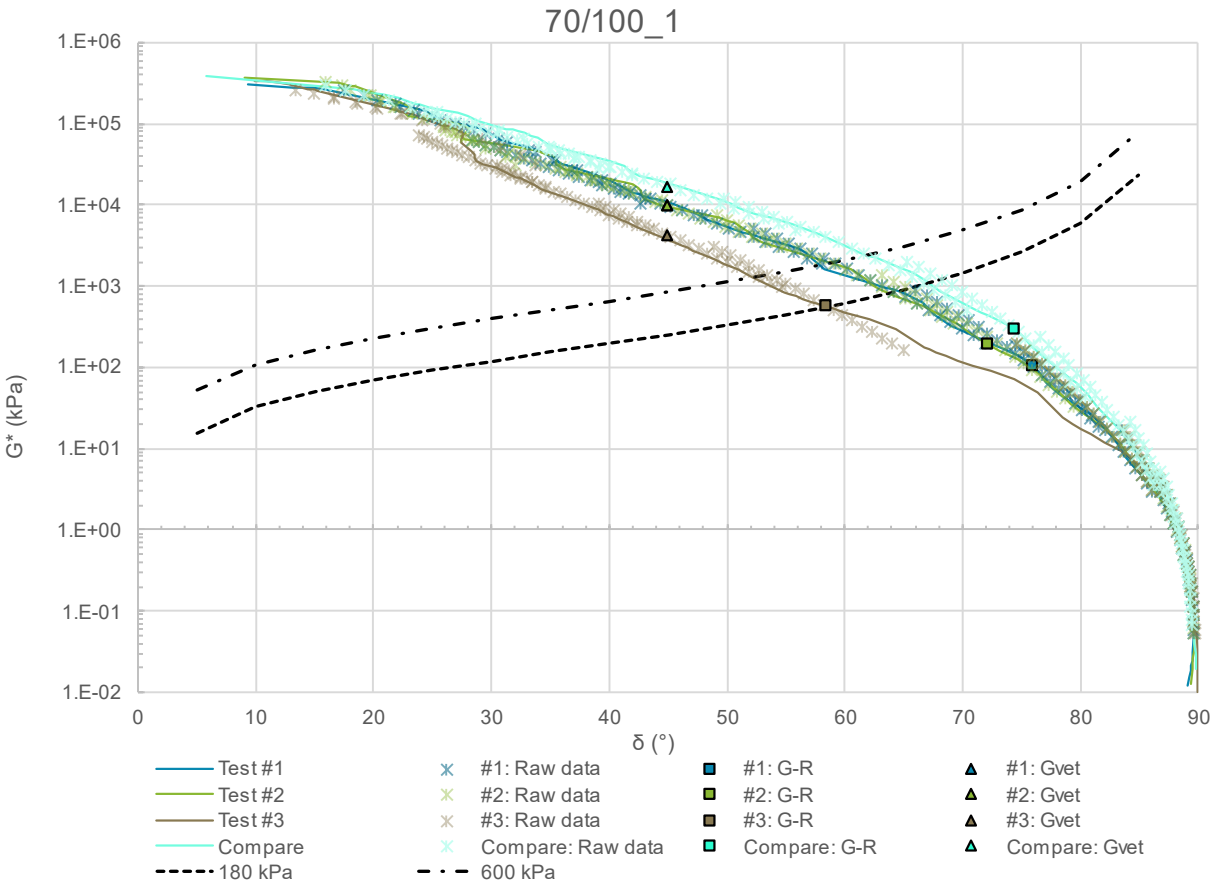

Figure 4.11: Black Space of MR265 km41

It could be argued that the data from the 8 mm frequency sweep was shifted downwards relative to the other samples. G_{vet}, T_{vet} and G-R reveal that test 3 aged to a greater extent than the other samples. However, Figure 4.11 show that test 3 has lower stiffness values. Another option is that the data from the 8 mm frequency sweep was shifted to the left, which suggest that the shift is related to the δ values. Lower δ values indicate a higher degree of ageing, which correlates to the ageing suggested by G_{vet}, T_{vet} and G-R.

The 8 mm frequency sweep test was repeated to eliminate any testing errors. The repetition delivered the same results as seen in Figure 4.11. The notes made during the recovery procedure did not reveal any discrepancies that suggest that the samples were exposed to different conditions during the recovery procedure. Therefore, it is unclear what caused the deviation in the 8 mm frequency sweep data. Apart from test 3, there is a strong correlation between test 1 and 2, while the compare sample is slightly elevated. A chemical analysis can help explain this phenomenon.

4.7.3 Young, modified emulsion Cape seal

R61/6 km88.05 is a SC-E2 modified binder recovered from a 1 year old Cape seal. From Figure 4.12, it can be seen that the compare sample has a lower G-R and higher G_{vet}, which suggest that the compare sample is aged to a lesser extent than the other samples. The G_{vet} values of all three samples are in a similar region, while the compare sample has a much lower G-R value. Since both G-R and G_{vet} of the test samples only differ slightly, there is no clear distinction of the extent of ageing between these samples.

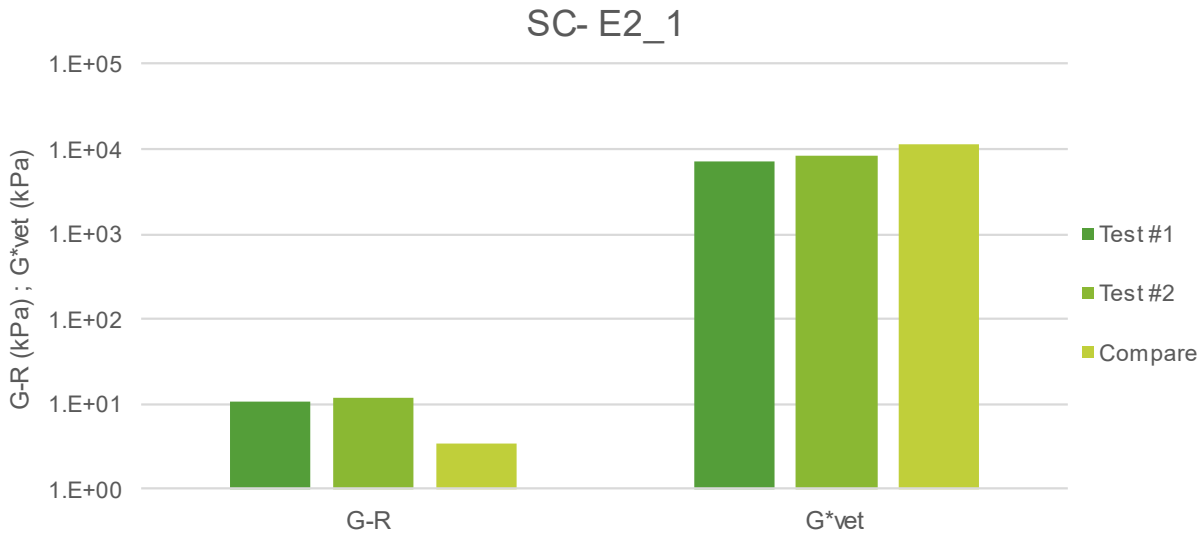

Figure 4.12: Stiffness Parameters of R61/6 km88.05

From Table 4.17, the low RMS error of the compare sample's shift factor suggest that this sample was shifted more accurately than the other samples. However, the discrete master curve modelling of the test samples provides a better fit than the compare sample. The shift factor models and the master curve models of all of the samples are classified as very good and good. Considering that all of the RMS error values are less than 10%, it is unlikely that the variability experienced in the G-R values is related to data processing. This may be confirmed when considering Black Space.

Table 4.17: RMS Error of Fitted Data of R61/6 km88.05

Name	Shift Factor	RMS Error	Master Curve	RMS Error
Test #1	Modified Kaelble	0.073	Discrete Modelling	0.054
Test #2	Modified Kaelble	0.077	Discrete Modelling	0.049
Compare	Modified Kaelble	0.022	Discrete Modelling	0.073

Table 4.18 contains the recommended repeatability and reproducibility requirements of the stiffness parameters. All of the stiffness parameters meet the recommended requirement, except for the recommended reproducibility requirements of G-R. When looking at the input values that G-R comprises of, it is interesting to see that both δ and G* fall well within the

recommended reproducibility criteria but the combination of these values results in a G-R values that do not comply with the recommended criteria. This observation might suggest that the criteria be revised.

Table 4.18: Repeatability and Reproducibility of Stiffness Parameters of R61/6 km88.05

	Test #1	Test #2	Compare
δ (°)	70.447	70.936	74.743
G* (kPa)	90.259	102.767	48.614
G-R (kPa)	10.729	11.600	3.489
Gvet (kPa)	7349.126	8511.845	11640.000
	Repeatability	**Reproducibility**	
Δδ	0.489	4.297	
Recommended	7.069	19.451	
Δlog(G*)	0.056	0.325	
Recommended	0.198	0.509	
Δlog(G-R)	0.034	0.522	
Recommended	0.105	0.2374	
Δlog(Gvet)	0.064	0.200	
Recommended	0.390	1.068	

Based on the G-R values, it appears as that the compare sample aged to a lesser extent than the test samples. Since the RMS error of the compare sample's master curve is slightly higher than the test samples, and the G_{vet} values do not reveal the same ageing pattern as the G-R values, it is expected that G-R's failure to comply with the recommended reproducibility requirement, may be modelling related.

The temperature parameters are provided in Figure 4.13. Similar to the trend indicated by G_{vet}, T_{vet} and T_{max} also suggest that the compare sample aged to a lesser extent than the test samples. Although T_{vet} shows that test 1 aged to a greater extent than test 2, T_{max} reveals the opposite. Furthermore, the ΔTc values imply that test 1 is S-controlled, while test 2 is m-controlled. The study from which the data of the compare sample was obtained, did not perform BBR testing. Therefore, the reproducibility of the samples cannot be compared in terms of critical low temperature parameters. Differences between the test samples and the compare sample is possibly due to the time delay in recovery between the samples. T_{vet} is determined from the models. Since the models of the compare sample have been determined without BBR data, these can also vary significantly.

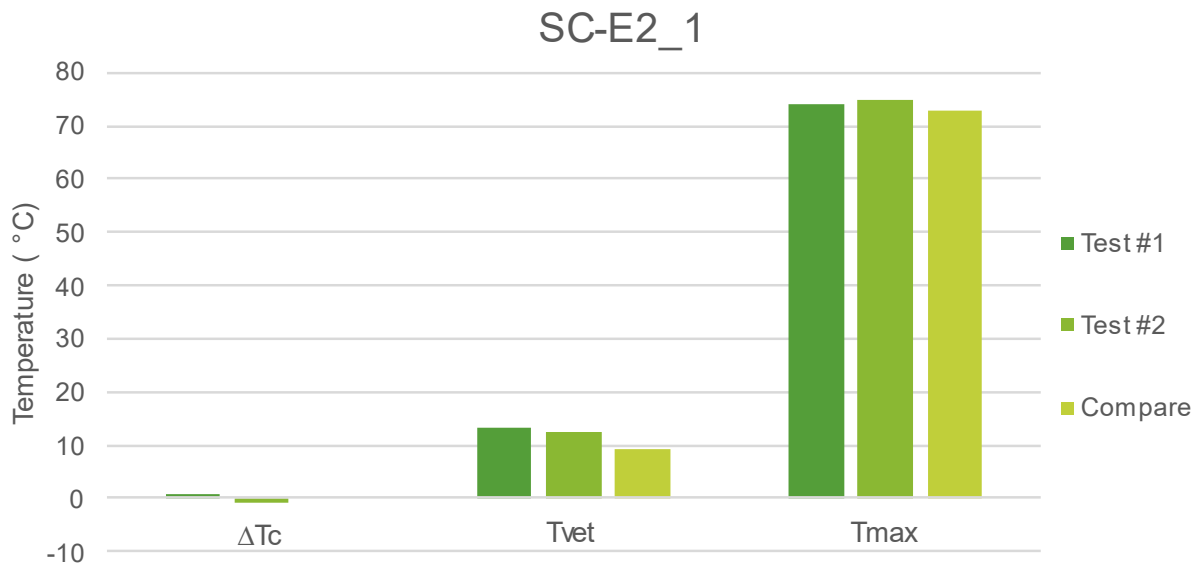

Figure 4.13: Temperature Parameters of R61/6 km88.05

From Table 4.19, it can be seen that test 1 and 2 perform well in terms of the recommended repeatability limit. $T_{c,S}$ is the only parameter that does not comply with the 1.9 limit. For reproducibility, ΔT_{max} complies with the recommended requirement but ΔT_{vet} does not. Since T_{vet}, another parameter that is calculated from modelled data, is subject to variability, it supports the argument for variability due to modelling errors.

Table 4.19: Repeatability and Reproducibility of Temperature Parameters of R61/6 km88.05

	Test #1	Test #2	Compare
Tc,s	-31.233	-30.302	-
Tc,m	-32.082	-29.444	-
ΔTc	0.849	-0.858	-
Tmax	74.205	74.807	72.754
Tvet	13.138	12.626	7.576
	Repeatability		**Reproducibility**
ΔTc,s	0.931		-
ΔTc,m	2.637		-
Δ (ΔTc)	1.707		-
ΔTmax	0.602		2.052
ΔTvet	0.512		5.562
Recommended	1.9		3.4

Figure 4.14 shows the Black Space diagram, including discrete modelling of the data. T_{vet} is linked to the crossover frequency, which is also coupled with δ=45°. At δ=45°, the compare model experiences an upward projection, resulting in a deviation from the raw data points. Since T_{vet} relies on the model, the deviation could be linked to the variability between the T_{vet} values. For δ<30°, the compare model is much lower than the other two samples. This is because no BBR data is available to correct the model. Despite the compare sample's lack of

low temperature data points, all three models remain comparable. There is also a strong correlation between the raw data points from all three samples.

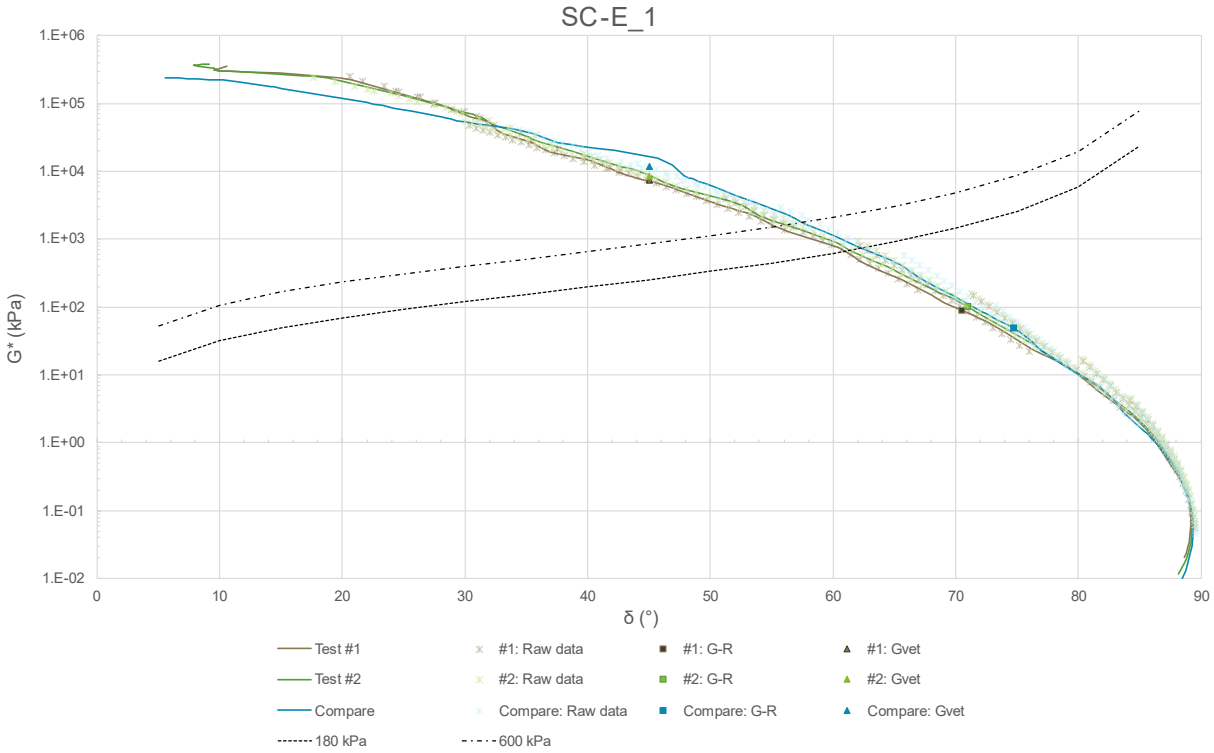

Figure 4.14: Black Space of R61/6 km88.05

Although the δ values, that G-R comprise of, met the recommended reproducibility requirements, the visual inspection of Figure 4.14 suggest that the deviation between the test samples and the compare sample, is unacceptable. The same conclusion is drawn for the G* values of the G-R parameter. It appears that the recommended reproducibility requirement is not suitable for the input values of G-R, since the requirement confirmed that the δ and G* are within range, when in fact, the Black Space diagrams revealed the opposite. The recommended reproducibility requirement seems more appropriate for the values of G-R since the requirements initially revealed that the G-R values do not perform well in terms of reproducibility.

4.7.4 Older, unmodified Cape seal

MR174 km9 is a 70/100 unmodified binder recovered from a 9 year old Cape seal. Figure 4.14 contains the stiffness parameters of MR174 km9. There is a strong correlation between the G_{vet} values, but the G-R parameters suggest that the test sample is aged to a greater extent than the compare sample. The G-R parameters are also very low, considering that the seal is 9 years old.

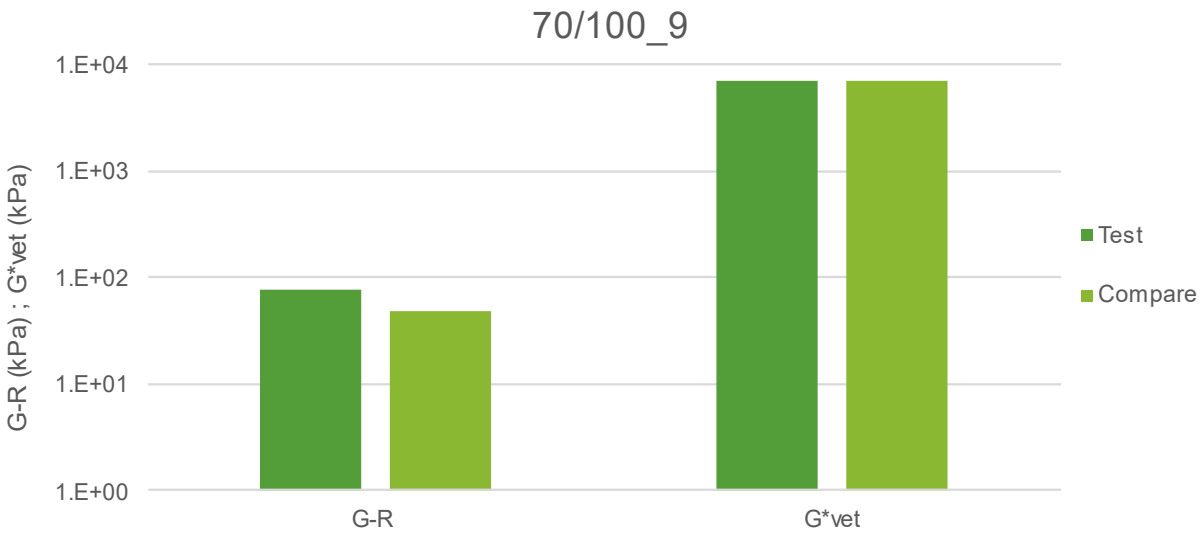

Figure 4.15: Stiffness Parameters of MR174 km9

Table 4.20 contains the RMS error values for the shift factors and the master curve models. Although the shift factor model of the test sample has a slightly higher RMS error value, both shift factor models are classified as very good. The master curve models of both samples are classified as good. It appears that deviations would not be a result of modelling errors.

Table 4.20: RMS Error of Fitted Data of MR174 km9

Name	Shift Factor	RMS Error	Master Curve	RMS Error
Test	Modified Kaelble	0.075	Discrete Modelling	0.054
Compare	Modified Kaelble	0.024	Discrete Modelling	0.059

Table 4.21 contains the repeatability requirements for the stiffness parameters. All of the stiffness parameters comply with the repeatability limit. The Black Space diagram will be used to confirm the repeatability of G-R.

Table 4.21: Reproducibility of Stiffness Parameters of MR174 km9

	Test	Compare
δ (°)	63.408	66.295
G* (kPa)	345.191	270.103
G-R (kPa)	77.351	47.678
Gvet (kPa)	6888.333	7100.000
	Reproducibility	
Δδ	2.887	
Recommended	17.510	
Δlog(G*)	0.107	
Recommended	0.671	
Δlog(G-R)	0.210	
Recommended	0.482	
Δlog(Gvet)	0.013	
Recommended	1.038	

Figure 4.16 illustrates the difference between the two samples' temperature parameters. The study from which the data of the compare sample was obtained, did not perform BBR testing. The test sample has a ΔT_c value less than -5. Considering the age of the surfacing, a low ΔT_c value is expected. There is a strong correlation between the T_{max} values. The T_{vet} values of the two samples appear to differ slightly. Since the RMS error values mentioned in Table 4.20 are relatively low, it is not expected that a data processing error produced the variability between the T_{vet} values.

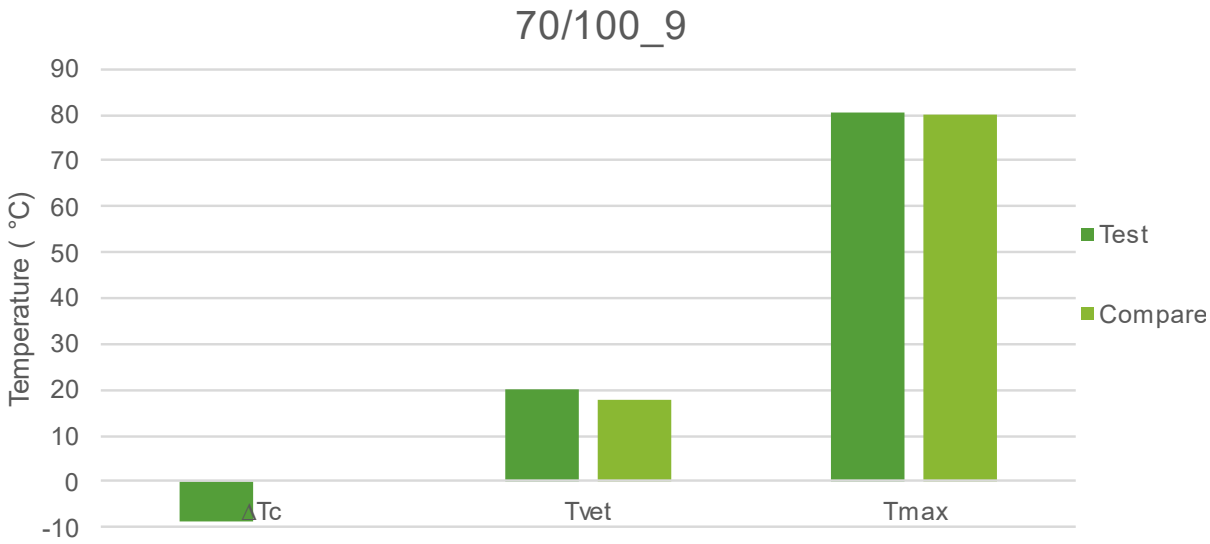

Figure 4.16: Temperature Parameters of MR174 km9

The reproducibility of the two samples is evaluated in Table 4.22. Both parameters comply with the recommended requirement. This suggest that the variability between the two T_{vet} values appear to be acceptable. Unfortunately, it is not possible to compare the two samples in terms of ΔT_c.

Table 4.22: Reproducibility of Temperature Parameters of MR174 km9

	Test	Compare
Tmax	80.489	82.860
Tvet	19.935	17.812
	Repeatability	
ΔTmax	2.371	
ΔTvet	2.123	
Recommended	3.4	

Figure 4.17 shows the Black Space diagrams of the two samples using discrete modelling. There appears to be a strong correlation between the two models, more specifically the 60°C and 70°C isotherms. For 28°<δ<80°, the compare sample has slightly higher stiffness values than the test sample. At δ=28°, the two models intersect. To the left of the intercept, the

compare model predicts lower stiffness values. This stresses the importance of low temperature test data to determine accurate prediction models. The G-R markers also confirm that the samples performed well in terms of repeatability.

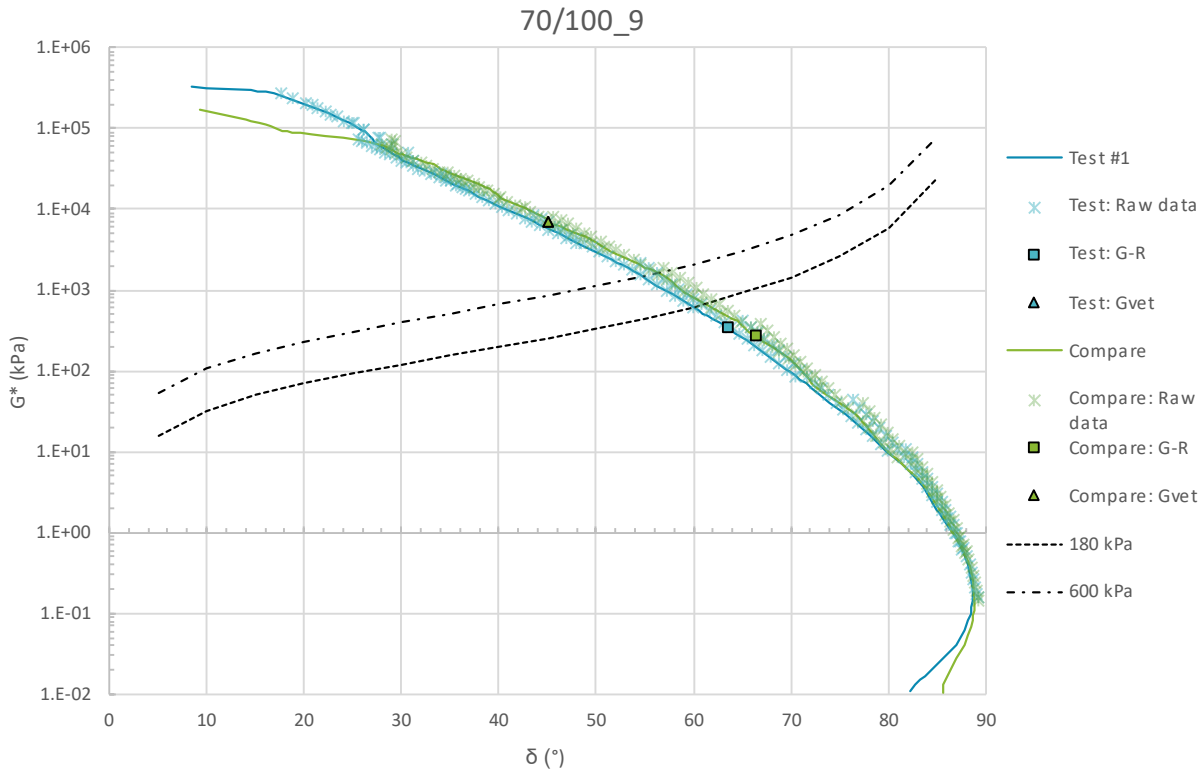

Figure 4.17: Black Space of MR174 km9

4.7.5 Summary of Pertinent Findings

The repeatability and reproducibility analysis revealed five possible reasons for differences between the samples: These reasons include different procedures regarding:

1. Modelling shift factor and master curve models
2. Recovery and extraction of bitumen from seal specimens
3. Rheometry, i.e. DSR and BBR testing
4. Additional storage time between the various studies.
5. Age and modification of the binder

Table 4.23 and Table 4.24 provide a summary of the quality of the raw data, the modelling of the data, and the durability parameters. All three categories will use the same keys, namely low, moderate, or high errors or variability. For the data variability, low would mean that the data sets are almost identical, moderate will suggest slight, but acceptable, variability, while high would imply significant differences between the data sets. For the modelling of the data, low suggest a RMS error less than 7%, moderate refers to a RMS error less than 15%, and

high is used for RMS error greater than 15%. If the durability parameters comply with the recommended repeatability or reproducibility requirements, low will be used, while failure to comply with the recommended requirements will be indicated with high.

From Table 4.23, it can be seen that the DSR data experiences more variability than the BBR data. For the data modelling section, the majority of the samples are classified as low, except for the repeatability of MR265 km41. The durability parameters reveal that T_{max}, ΔT_c and G_{vet} more easily comply with the recommended requirements, compared to T_{vet} and G-R.

Table 4.23: Summary of Seals aged 1 year and younger

	MR265 km12		MR265 km41		R61/6 km88		R61/8 km51	
	Repeat	**Reprod**	**Repeat**	**Reprod**	**Repeat**	**Reprod**	**Repeat**	**Reprod**
Binder Type	S-E1		70/100		SC-E2		SC-E2	
Age	1		1		1		1	
Seal Type	S1		S4		S4		S4	
DATA VARIABILITY								
8mm Quality	low	low	high	moderate	low	moderate	low	low
25mm Quality	low	high	low	moderate	low	low	low	moderate
BBR Quality	low	low	low	low	low	N/A	moderate	N/A
DATA MODELLING								
Shift Quality	low	low	moderate	low	low	low	low	low
MC Quality	low	low	high	low	low	low	low	low
DURABILITY PARAMETERS								
Tmax	high	high	low	low	low	low	low	low
Tvet	low	low	high	high	low	high	low	high
ΔTlow	low	low	low	low	low	N/A	high	N/A
G-R	low	high	high	high	low	high	low	low
Gvet	low	low	low	low	low	low	low	low

From Table 4.24, it can be seen that the 8 mm data experiences the most discrepancies, while the BBR quality experiences the least discrepancies. From the data modelling section, it can be seen that the majority of the samples experience low variability, with N2/32 km21 being the exception. During the data modelling phase, it was also noted that for the older seals, 6 years and above, the entire 5°C isotherms had to be omitted, since it did not fall within the LVE range and some of the 15°C isotherms data points had to be omitted in order for the RHEA software to accept the input data. The durability parameters suggest that as binder age increases, the durability parameters are prone to less deviation.

Table 4.24: Summary of Seals aged older than 1 year

	N2/16 km71		N2/32 km21	N8/8 km5.6	MR174 km9	N2/31 km3.6
	Repeat	Reprod	Repeat	Repeat	Reprod	Reprod
Binder Type	S-E1		S-E1	S-E1	70/100	S-E1
Age	2		6	7	9	12
Seal Type	M		S2	S2	S4	S2
DATA VARIABILITY						
8mm Quality	high	moderate	high	moderate	moderate	moderate
25mm Quality	moderate	high	low	low	low	low
BBR Quality	moderate	N/A	low	low	N/A	low
DATA MODELLING						
Shift Quality	low	low	high	low	low	low
MC Quality	low	low	low	low	low	low
DURABILITY PARAMETERS						
Tmax	high	high	low	low	low	low
Tvet	high	high	low	low	low	low
ΔTc	high	N/A	low	low	N/A	low
G-R	high	high	low	low	low	low
Gvet	low	low	low	low	low	low

The following relationships are observed between the variability of the raw data and the durability parameters:

- If the 8mm shows variability, G-R and Tvet do not comply with the recommended specification;
- If the 25mm shows variability, T_{max} does not comply with the recommended specification;
- If the BBR data shows variability, ΔTc does not comply with the recommended specification;
- G_{vet} generally complies with the recommended specification and appears to be less affected by variances in recovery, testing and modelling.

As for the suitability of the recommended specifications, it appears that the specification provides adequate repeatability and reproducibility tolerance for the majority of the durability parameters. However, the G-R parameter is the exception. The following discrepancies with regard to reproducibility were noted:

- The input values of G-R (G* and δ) would comply with the recommended specification but the G-R parameter would not.
- Δ values would comply with the recommended specification but the Black Space Diagram revealed that the deviation between the δ values should be unacceptable.

It appears that the recommended reproducibility specification for δ should be more stringent. However, the recommended specification appear suitable to judge the repeatability and reproducibility of G-R and the corresponding G* input value.

4.8 FTIR Analysis

Chapter 4.7 provided insight regarding the variability present in the raw data, the modelling of the data, and the durability properties of each seal. In this Chapter, the chemical composition of the binders will be evaluated by comparing the absorbance at three distinct wave numbers. The area of the peaks is used to quantify the discrepancies between the respective peaks. Possible links between the variable ageing suggested by the performance parameters and the corresponding chemical composition, is investigated.

4.8.1 Young, modified single seal

Chapter 4.7.1 revealed that the accuracy of the shift factor model, the master curve model, and the values of T_{max} of test 1 varied from the other samples. It was also disclosed that during the recovery process of test 1, the duration of phase 2 of the binder recovery process was much longer than the other samples. The durability parameters suggest that the compare sample aged to a lesser extent than the test samples, while test 1 aged the most. Figure 4.18 illustrates the FTIR absorbance of all four samples.

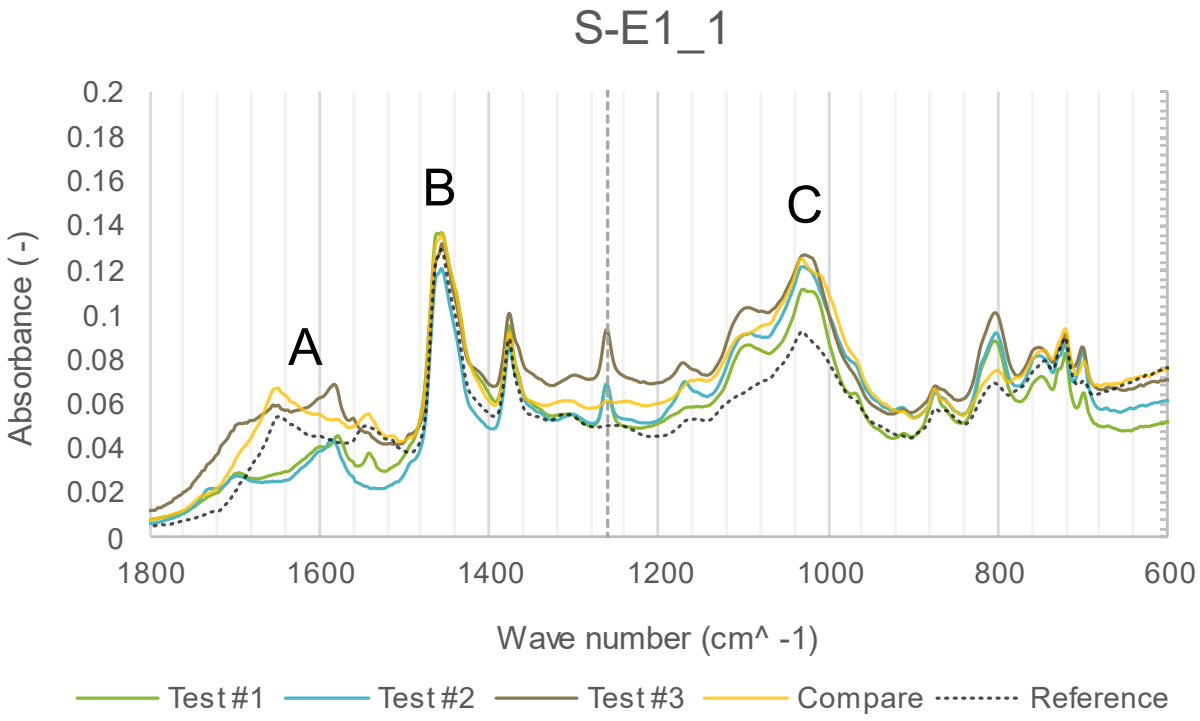

Figure 4.18: FTIR Absorbance of MR265 km12

In Figure 4.18, there are no distinct carbonyl peaks at 1700 cm^{-1}, as suggested by Van Den Bergh (2011). Within region A, the test samples have a more distinct peak at 1580 cm^{-1}, while the compare sample has a more distinct peak at 1650 cm^{-1}. At region B and C, all the samples experience peaks at similar wave numbers. At B, the peak of test 2 is slightly lower than the other samples, while at C, the peak of test 1 is slightly lower than the other samples. There appears to be no distinct indication that test 1 varies from the other samples. When using the reference plot as a benchmark to identify any significant peaks, it can be seen that at 1260 cm^{-1}, all of the test samples have an unexpected peak. At this wave number, neither toluene nor ethanol, the solvents used during the recovery process experience a peak. Therefore, the cause of this peak is unclear.

In Figure 4.19, the peak areas of each range are presented. The compare sample has a negative area within range A. In Figure 4.18, it can be seen that the wave number, where the compare sample experiences a significant peak, differs from the wavenumber where the test samples experience a significant peak. The negative area suggest that range A does not provide an adequate evaluation range within which the compare sample can be analysed. Regardless of the negative value, the variability in peak areas of range A, correlates to the variability of T_{vet}, in Figure 4.7.

Figure 4.19: Peak Areas of MR265 km12

The areas within range B, reveal that test 1 differs significantly from the other samples. The extent of this discrepancy correlates with the discrepancies of T_{max}, as presented in Figure 4.7. Within range C, the areas of the test samples correlate very well, while the compare sample

is slightly higher. The variability of the areas within range C, are similar to the variability of the G_{vet} values in Figure 4.6.

4.8.2 Young, unmodified Cape seal

Chapter 4.7.2 revealed that test 3 aged to a greater extent than the other samples. Test 3 also varied from the other samples in terms of raw data, modelling and durability parameters. The entire 8 mm DSR data set was displaced relative to the other samples, which had an influence on the quality of the performance parameters. Figure 4.20 indicates the FTIR absorbance of all four samples.

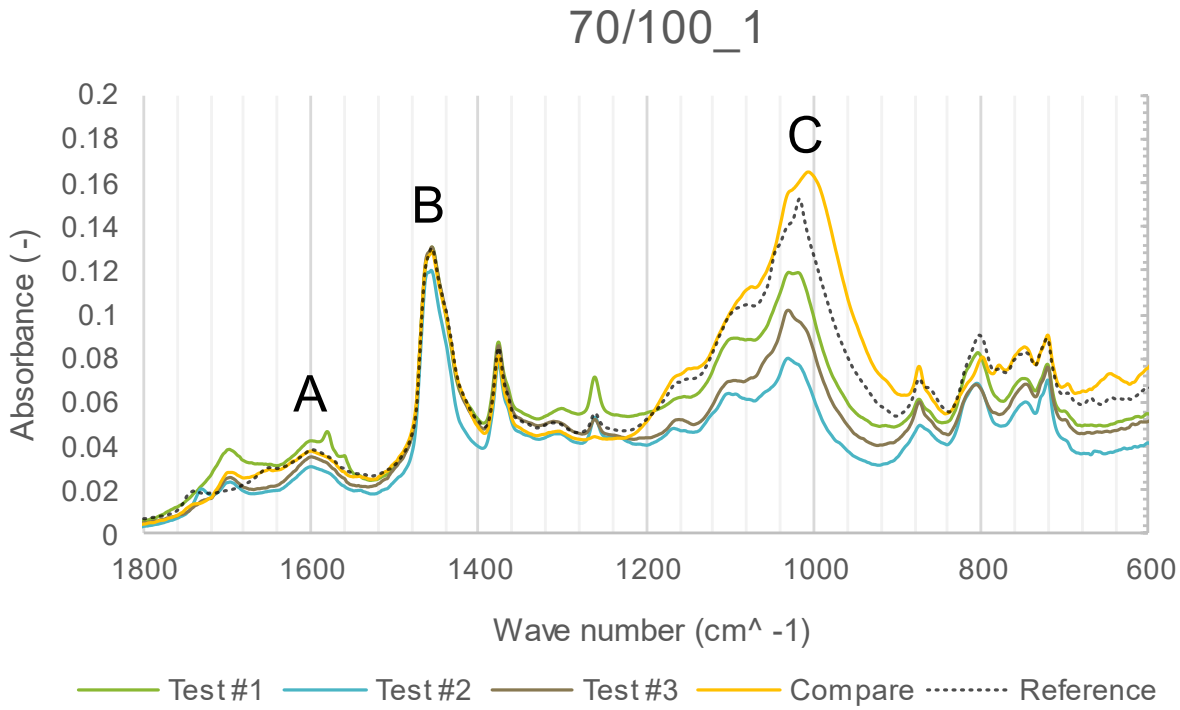

Figure 4.20: FTIR Absorbance of MR265 km41

At 1700 cm^{-1}, all of the samples experience a slight peak, as suggested by (Van Den Bergh, 2011). A more distinct peak is present at region A (1600 cm^{-1}). Here, all of the samples also correlate well. At region B, the peaks are very similar. More variability is present at region C, where the compare sample has a much higher peak than the test samples. The higher peak suggests a harder binder. This correlates with the Black Space Diagram, which revealed that for the majority of the compare sample's DSR data was harder than that the test samples. At 1260 cm^{-1}, all of the test samples experience an unexpected peak. There are no distinct indication to suggest that test 3 differs from the other samples.

The peak areas of each range are presented in Figure 4.21. It is expected that the areas of test 3 would differ from the other samples. However, for range B and C, the areas of test 2

differ from the other samples. Although the differences between the areas of range A are minimal, these differences tend to correlate with the differences of T_{vet} and G-R, as seen in Figure 4.10 and Figure 4.9. Except for test 2, the peak areas of range B are very similar. All of the T_{max} values in Figure 4.10 are also very similar. The peak areas of range C experiences noticeable differences.

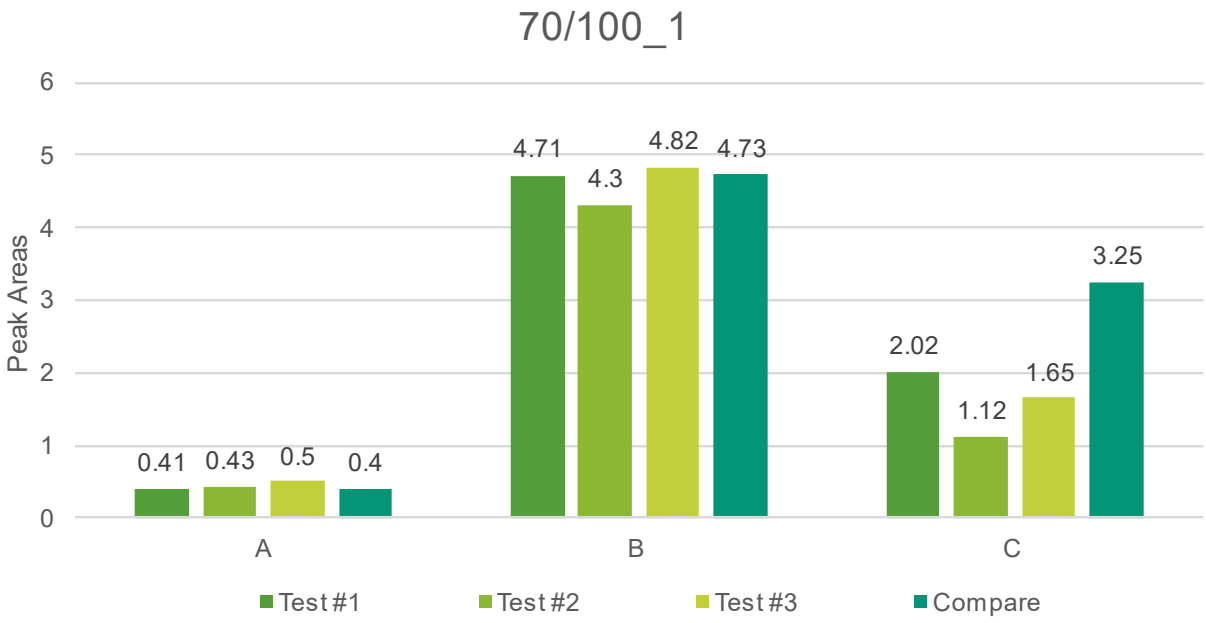

Figure 4.21: Peak Areas of MR265 km41

4.8.3 Young, modified emulsion Cape seal

From Chapter 4.7.3, it was found that the durability parameters of the test samples were very similar. G-R and T_{vet} of the compare sample varied from the test sample. Although these parameters did not perform well in terms of the recommended reproducibility requirement, the Black Space diagram indicated insignificant differences between all of the samples.

Figure 4.22 illustrates the FTIR absorbance of all three samples. The test samples experience a slight peak at 1700 cm^{-1}, with a more distinct peak at region A. The peaks of the compare sample deviates from the test samples, as a slight peak is present at 1740 cm^{-1}, and a more distinct peak at 1650 cm^{-1}. At region B, the peaks of all three samples correlate very well. More variability is present at region C. Although the durability parameters suggested that the compare sample is aged to a lesser extent than the test samples, in Black Space, the 8 mm DSR data is slightly higher than the test samples. Apart from region B, the absorbance of the compare sample is higher than the test samples, suggesting a harder binder. It appears as if the FTIR absorbance at region A and C correlates well with the interpretation from the Black

Space Diagram, especially for the 8 mm DSR data. The compare sample and test 1 experience a slight peak at 1260 cm^{-1}.

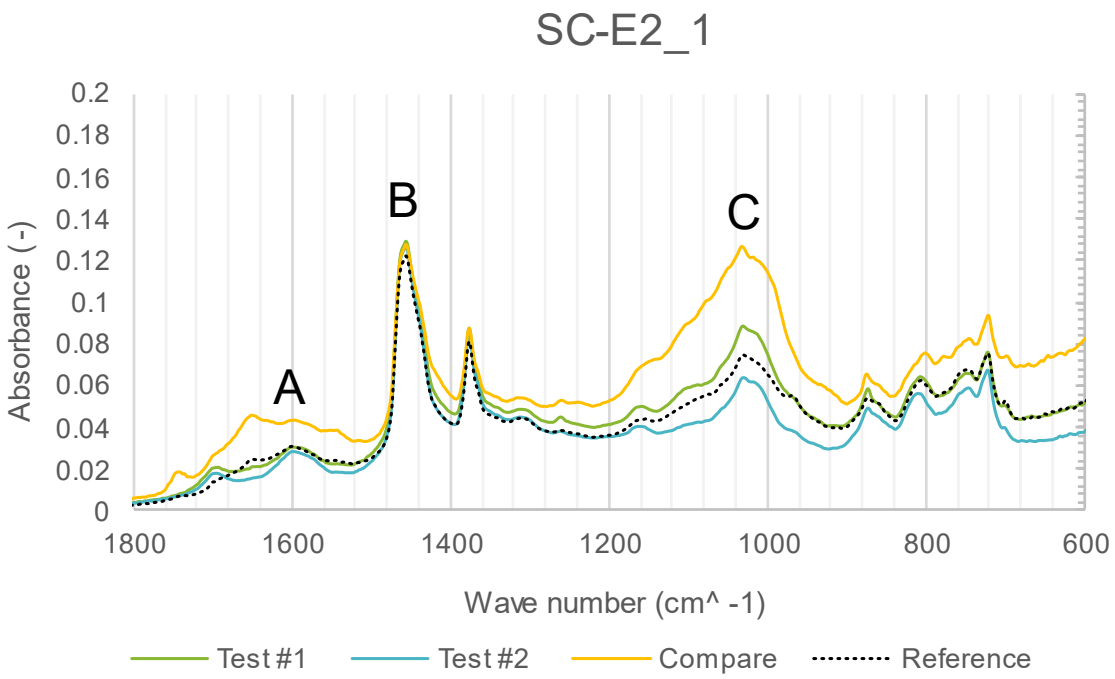

Figure 4.22: FTIR Absorbance of R61/6 km88

In Figure 4.23, the peak areas of each range are plotted. For range A and B, the test samples correlate well. The range A area of the compare sample is much lower than the test samples. This is expected, as Figure 4.22 show that wave number, where the compare sample experiences a significant peak, differs from the wavenumber where the test samples experience a significant peak. The wave number range for the range A areas might have to be adjusted. The differences between the range A areas correlate with the differences T_{vet} and G-R experience, as presented in Figure 4.13 and Figure 4.12.

The values of G_{vet} and T_{max} did not comply with the recommended reproducibility limits, although the values did not differ significantly. The difference between the test sample and the compare sample in terms of the area of range B and T_{max}, correlate. There are distinct differences between the areas of range C. The extent of this discrepancy does not correlate with any of the durability parameters.

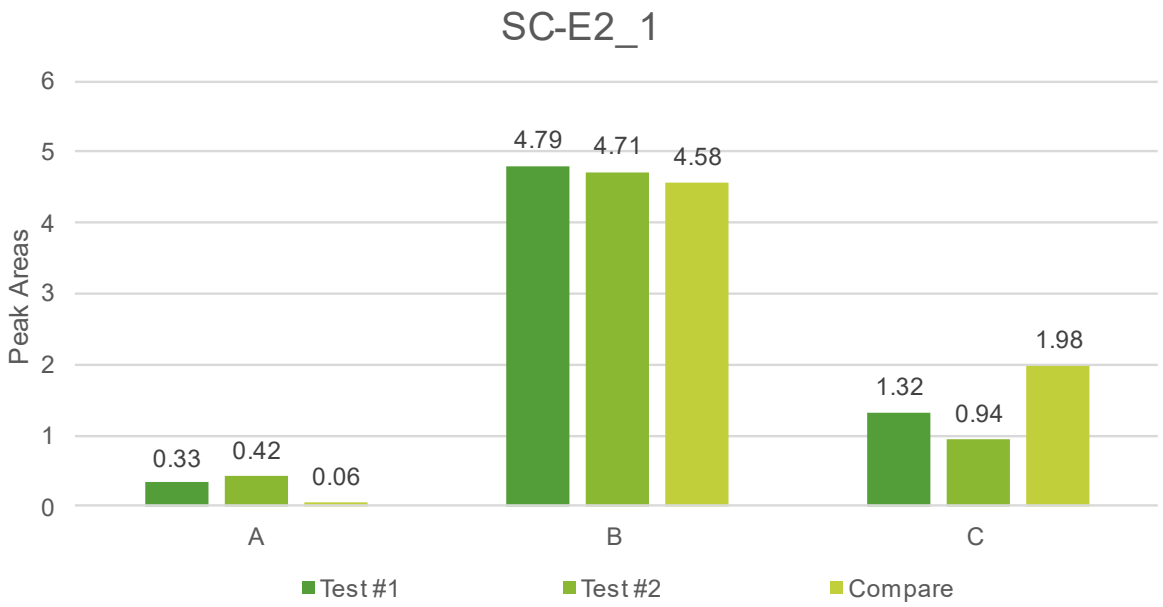

Figure 4.23: Peak Areas of R61/6 km88

4.8.4 Older, unmodified Cape seal

In Chapter 4.7.4, it was shown that all of the durability parameters complied with the recommended reproducibility specification. Slight discrepancies are noted between G-R and T_{vet}. In Black Space, the 8 mm DSR data of the compare sample is slightly higher than the test sample. However, these ageing indicators are very closely related. The FTIR absorbance of both samples are presented in Figure 4.24.

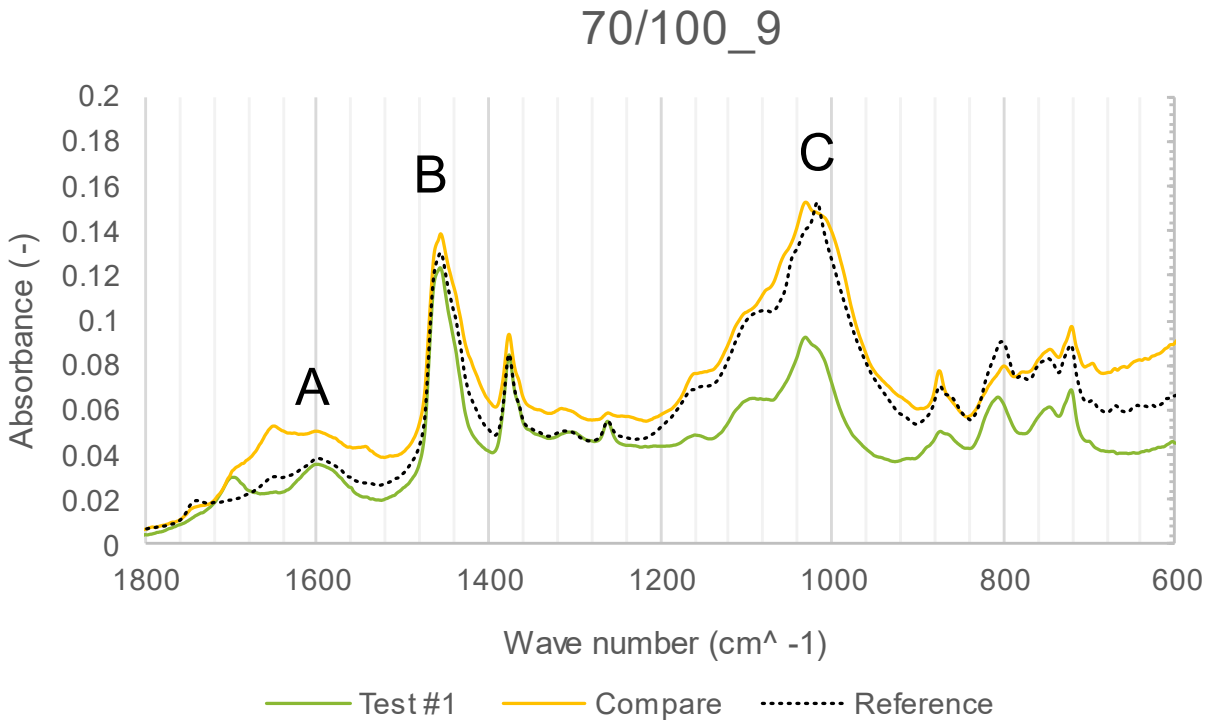

Figure 4.24: FTIR Absorbance of MR174 km9

The compare sample does not form a clear peak at 1700 cm^{-1}. Although the compare sample has a peak at 1650 cm^{-1}, this peak is not as distinct as would be expected. The test sample has a slight peak at 1700 cm^{-1} and a more distinct peak at region A. At region B, the peaks of both samples correlate well, while more variability is present at region C. The difference between the peaks at region C, suggest that the compare sample aged to a greater extent than the test sample. Although this is an older binder, it does not appear that any peaks are significantly higher in comparison to the aforementioned younger seals.

The peak areas of each range are plotted in Figure 4.25. The differences between the areas of range A tend to correlate with the differences of T_{vet} and G-R, as seen in Figure 4.15 and Figure 4.16. Although the differences between the areas of range B correlate with the differences between the areas of range C, these differences do not correlate with any durability parameters.

Figure 4.25: Peak Areas of MR174 km9

4.8.5 Summary of Pertinent Findings

The FTIR analysis revealed that all of the binders had significant peaks at position B (1030 cm^{-1}) and C (1460 cm^{-1}), suggesting that these wave numbers are ideal for binder ageing evaluation. According to Van Den Bergh (2011), 1700 cm^{-1} is also a significant wave number for binder ageing evaluation. Although the majority of the samples have a peak at this position, it appears that a more distinct peak is situated at 1600 cm^{-1}. At position B, the peaks of the samples corresponded with one another, while at position C the peaks of the samples experienced more variability. As for the suitability of the ranges selected to determine the peak

areas, only one sample had a negative area, which suggest that the ranges are suitable to quantify the ageing between different binders.

In Chapter 2.4.4, it was established that the solvents used during the binder recovery procedures, experienced significant peaks at wave numbers less than 930 cm^{-1}. None of the samples experienced unexpected peaks within this range. In Figure 4.26 and Figure 4.27, the binders were considered separately based on the type of solvent used during the binder recovery process. The following observations were made:

- The majority of the binders recovered using the toluene-ethanol blend experience distinct peaks at 1700 cm^{-1} and 1600 cm^{-1}, with the peak at 1600 cm^{-1} being slightly higher.
- The binders recovered using trichloroethylene experience peaks at different wave numbers. These wave numbers vary between 1720 cm^{-1} and 1560 cm^{-1}.
- Various binders recovered using the toluene-ethanol blend experience a visible peak at 1260 cm^{-1}.
- Literature revealed that the solvents used during the recovery procedure experience significant peaks at wave numbers less than 800 cm^{-1}. None of the binders have excessive peaks within this region. This, together with the low mass change percentages indicated in Table 4.2, suggest that no residual binder is present in the recovered binder.
- At position C, the binders recovered using trichloroethylene experience higher peaks than the binders recovered using the toluene-ethanol blend. This suggest that during the recovery process, the solvent might interact with the binder on a molecular level and possibly affect the chemical composition of the binder. It appears that certain wave numbers are more susceptible to variability than others.
- From the FTIR absorbance curves, there is no clear distinction between the binders in terms of age or binder type.

Considering that the peak at position C is consistently higher for trichloroethylene and the unusual peak at 1260 cm^{-1} for the toluene-ethanol blend, the question arises whether solvent interactions may be more significant than contamination. Although the FTIR analysis provides significant additional information regarding binder chemistry, the extent and understanding of its correlation with physical binder properties, specifically following recovery and extraction, requires further analysis and investigation.

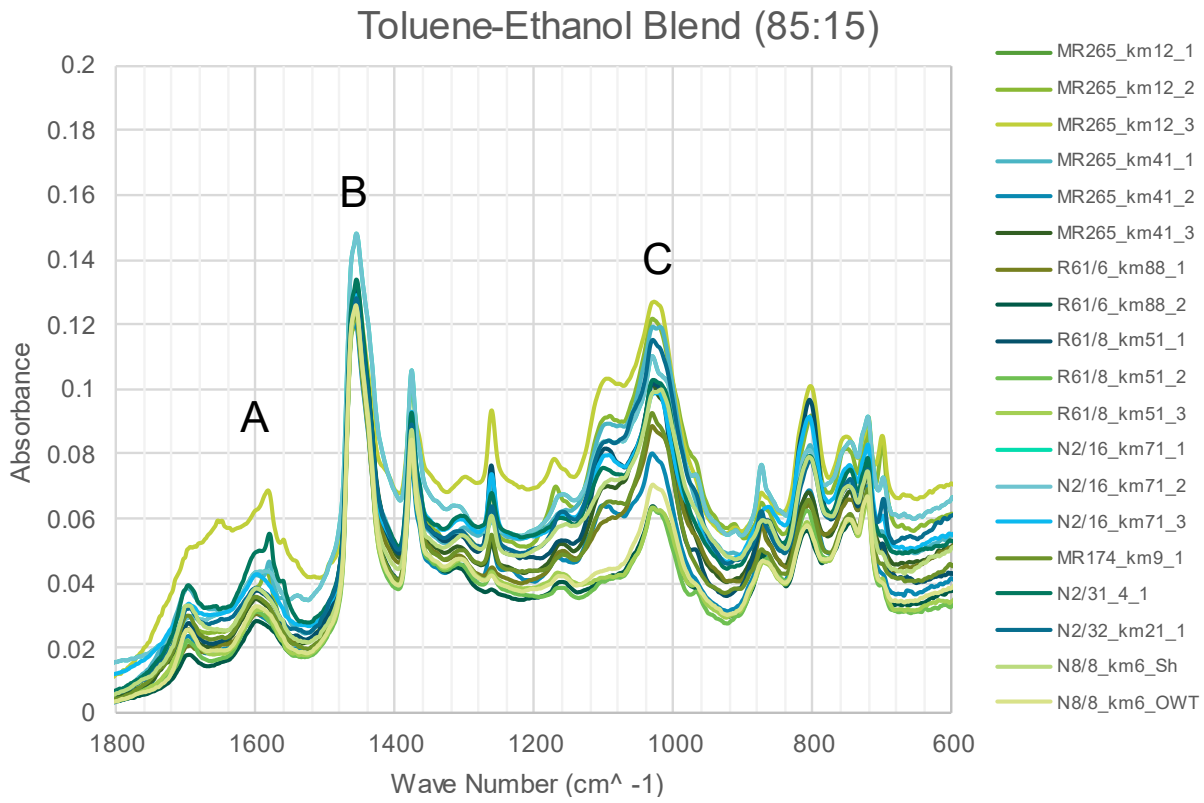

Figure 4.26: FTIR Absorbance of Binders Using Toluene-Ethanol Blend as Solvent

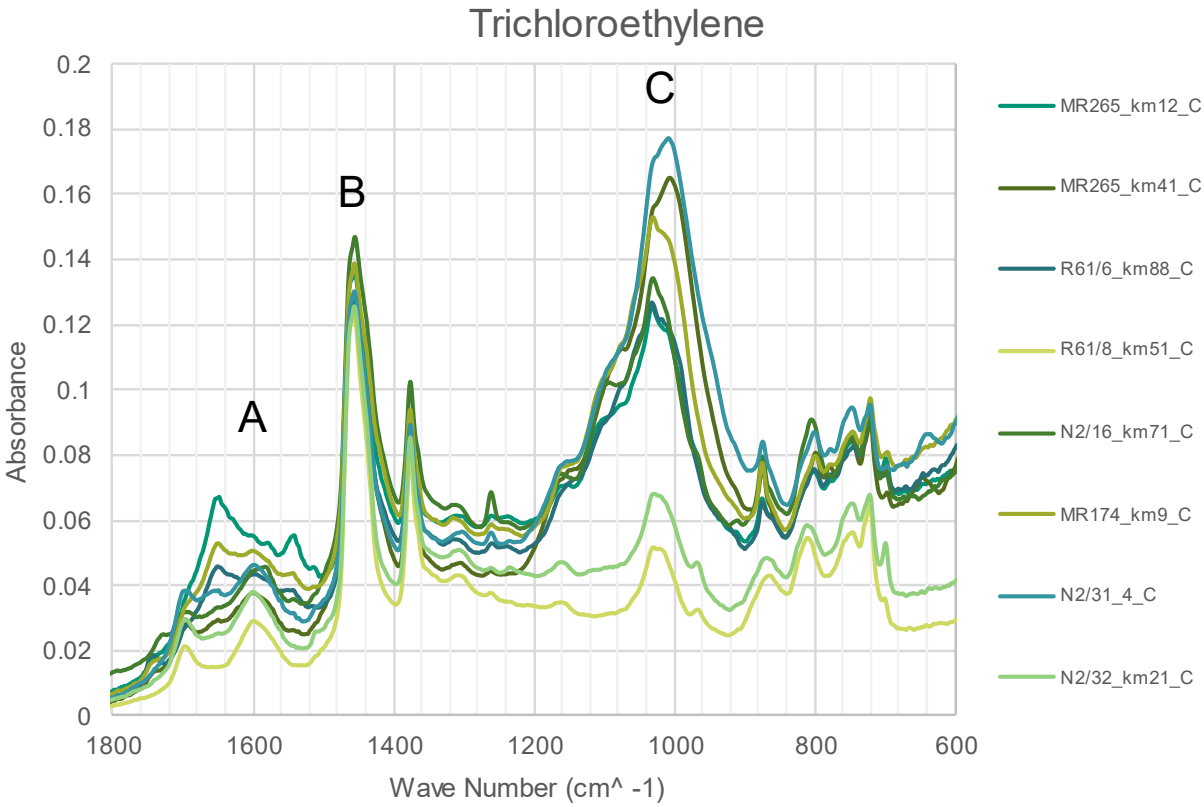

Figure 4.27: FTIR Absorbance of Binders Using Trichloroethylene as Solvent

Chapter 5: Conclusions and Recommendations

In order to evaluate the consistency of the rheological properties of recovered seals binders, seal binders were obtained and tested, as explained in Chapter 3. The results were analysed and discussed in Chapter 4. This chapter will focus on the key findings of the study and provide recommendations for future studies, in order to advance seal binder rheology.

5.1 Conclusions

In accordance with the objectives in Chapter 1.3, seal binders were recovered from existing road surfaces. The procedure, as set out in EN 12697-3 (2013), with adjustments as recommended in Goosen and Jenkins (2019), has been followed. In this study, the procedure was adjusted by implementing a fixed rate of 50 millibar (5 kPa) per minute, when lowering the pressure within the rotary evaporator during phase 2 of the distillation process. It was noted that the duration of phase 2 of the distillation process, appear to influence the rheology of the binder. For the majority of the binders, the duration of phase 2 of the distillation process was less than 30 minutes, which appears to be an ideal duration. A binder that was exposed to the conditions of phase 2 of the distillation process for an extended time, had a T_{max} value that deviated significantly from the other binders.

The following findings regarding the variability of the raw data, modelling of the data, and the durability parameters of the recovered binders, are identified:

- The quality of the performance parameters are influenced by the following factors: the accuracy between the rheological models (shift factor and master curve model) and the raw data values; different procedures regarding the recovery of bitumen from the seal sample; age and modification of the binder; rheometry; and additional storage time between the various studies.
- From the durability parameters calculated in this study, it is found that G_{vet} is least affected by variances in recovery, testing and modelling, since all of the G_{vet} values complied with the recommended specification for both repeatability and reproducibility.
- Data obtained from low temperature (BBR) testing and high temperature (25 mm DSR) testing, experienced less variability than data from testing at intermediate temperatures (8 mm DSR). However, where the 25 mm data varies, T_{max} does not comply with the

recommended specification, while ΔT_c does not comply with the recommended specification if the BBR data shows variability.

- Where the 8 mm data shows variability, G-R and T_{vet} generally do not comply with the recommended specification. Since these parameters are determined from modelled data, the quality of the shift factor model and the master curve model must also be considered.
- The durability parameters of the older binders are less susceptible to variability than the younger binders. It might be that the older binders have a lower ageing potential than the younger binders .
- For the majority of the samples there was a strong correlation between the raw data and optimised models when plotted in Black Space. Black Space diagrams are useful in determining specific regions where δ, G*, and durability parameter differences occur. Black Space was also used in evaluating the suitability of the recommended specifications.
- The recommended repeatability and reproducibility specifications appear to provide suitable tolerance for the evaluation of the durability parameters. However, a more stringent approach should be considered for δ. It was noted in certain cases that the specification allowed δ variability, while additional inspection revealed this extent of variability should not be allowed.
- The ΔT_c specification in SATS 3208 (2019) also appear to be a suitable in evaluating the low temperature performance of young, recovered binders. The binders that exceeded this requirement are relatively old (older than 6 years).

The FTIR analysis provided the following insights regarding the chemical composition of recovered binders:

- It is apparent that 1030 cm^{-1} and 1460 cm^{-1} are ideal wave numbers to consider the impact of the extraction-recovery process on the chemical composition of the recovered binder.
- At 1030 cm^{-1}, discrepancies with regard to height of the peaks was noted. There is a clear distinction between the peaks of binders recovered using a toluene-ethanol blend and binders recovered using trichloroethylene. This implies that during the extraction-recovery process the solvents alter certain chemical molecules of the bitumen.
- The ranges used to calculate the peak areas of the binders appear to be a suitable way to quantify the repeatability and reproducibility of the recovered binder from a chemical perspective.

5.2 Recommendations

Although this study provides valuable insight, various unknowns regarding the efficiency of the seal binder recovery method remain. Based on the analysis of the results, it is believed that the following recommendations be considered for future research:

- Before a definite seal binder recovery method can be finalised, the effect that the extraction-recovery method has on the chemical composition of the binder must be determined.
- Additional seal binder recoveries using different solvents need to be performed to determine whether certain solvents are more suitable to recover seal binders than others.
- With additional development, finalise the method to determine the Ash Content of recovered binders, to further evaluate the efficiency of the seal binder recovery method.
- Recover seal binders from existing road surfaces and consider the effect of traffic and climate with regard to the rate of ageing of bitumen and its influence on changes in rheology.
- Conclude suitable repeatability and reproducibility specifications that can be applied to the performance parameters of recovered binders.
- The DSR testing of recovered binders must be performed at higher temperatures to ensure that T_{max} can be calculated by interpolation.
- To improve the quality of the modelled data, it is suggested that either a 5°C isotherm from the DSR testing or a -6°C isotherm from BBR testing, be used to populate the master curve models. The presence of sufficient data will prevent the model from deviating from the raw data points.
- Determine the SARA (Saturate, Aromatic, Resin and Asphaltene) fractions of recovered binders and verify whether these fractions provide insight with regard to the observations revealed from the FTIR.
- Compare durability parameters of recovered seals with artificially aged binder and evaluate the similarity between these results.

References

Alaamri, R. S. N., Kattiparuthi, R. A. and Koya, A. M. (2017) 'Evaluation of Flexible Pavement Failures-A Case Study on Izki Road', *International Journal of Advanced Engineering, Management and Science*, 3(7), pp. 741–749. doi: 10.24001/ijaems.3.7.6.

Anderson, R. M. *et al.* (2011) 'Evaluation of the Relationship between Asphalt Binder Properties and Non-Load Related Cracking', pp. 615–663.

Asgharzadeh, S. M. *et al.* (2015) 'Evaluation of rheological master curve models for bituminous binders', *Materials and Structures/Materiaux et Constructions*, 48(1–2), pp. 393–406. doi: 10.1617/s11527-013-0191-5.

ASTM D 113 (2007). Standard Test Method for Ductility of Bituminous Materials. American Society for Testing andMaterials, pp. 1–4.

ASTM D 482 (2019). Standard Test Method for Ash from Petroleum Products. American Society for Testing andMaterials, pp. 1–3.

ASTM D 1856 (2009). Standard Test Method for Recovery of Asphalt From Solution by Abson Method 1. American Society for Testing andMaterials, pp. 1–5.

ASTM 7175 (2001) 'Standard Method of Test for Determining the Rheological Properties of Asphalt Binder Using a Dynamic Shear Rheometer (DSR)', *ASTM Interanational*, 3(August), pp. 1–16. doi: 10.1520/D7175-08.2.

ASTM D 6648 (2008). Standard Test Method for Determining the Flexural Creep Stiffness of Asphalt Binder Using the Bending Beam Rheometer. American Society for Testing and Materials, pp. 1–14.

Bagampadde, U., Isacsson, U. and Kiggundu, B. M. (2005) 'Influence of aggregate chemical and mineralogical composition on stripping in bituminous mixtures', *International Journal of Pavement Engineering*, 6(4), pp. 229–239. doi: 10.1080/10298430500440796.

Baumgaertel, M. and Winter, H. H. (1989) 'Determination of discrete relaxation and retardation time spectra from dynamic mechanical data', *Rheologica Acta*, pp. 511–519. doi: 10.1007/BF01332922.

Baumgaertel, M. and Winter, H. H. (1992) 'Interrelation between continuous and discrete relaxation time spectra', *Journal of Non-Newtonian Fluid Mechanics*, pp. 15–36. doi: 10.1016/0377-0257(92)80043-W.

Bredenhann, S. J. *et al.* (2019) 'Implementation of a performance-grade bitumen specification in South Africa', 61(3), pp. 20–31.

Britannica (2018) 'Viscosity'. Available at: https://www.britannica.com/science/viscosity (Accessed: 23 November 2020).

Caro, S. *et al.* (2008) 'Moisture susceptibility of asphalt mixtures, Part 1: Mechanisms', *International Journal of Pavement Engineering*, 9(2), pp. 81–98. doi: 10.1080/10298430701792128.

Christensen, D. W. and Anderson, D. A. (1992) 'Interpretation of dynamic mechanical test data for paving grade asphalt', *Asphalt Paving Technology: Association of Asphalt Paving Technologists-Proceedings of the Technical Sessions*, pp. 67–116.

Connell, J. O. and Steyn, W. (2017) 'an Overview of the Ageing of Bituminous Binders', *36th South African Transport Conference*, (July 2017), pp. 308–324. Available at: http://www.satc.org.za/assets/2a_oconnell_over.pdf.

Craig, R. (2003) *Mechanics of Materials*. Third. John Wiley & Sons.

Da Silva, L. S. *et al.* (2004) 'Study of rheological properties of pure and polymer-modified Brazilian asphalt binders', *Journal of Materials Science*, 39(2), pp. 539–546. doi: 10.1023/B:JMSC.0000011509.84156.3b.

Distin, T., Africa, S. and Association, B. (2008) 'TRAFFIC DISTRIBUTION', pp. 1–19.

EN-12697-3 (2013). Bituminous Mixtures - Test Methods for Hot Mix Asphalt - Part 3: Bitumen Recovery: Rotary Evaporator. European Standard.

Fox, R. ., McDonald, A. . and Pritchard, P. . (2011) *Introduction to Fluid Mechanics*. John Wiley & Sons.

Gerber, A. K. J. (2016) 'Numerical modelling of performance and failure criteria for surfacing seals', (March).

Glover, C. J. *et al.* (2005) *Development of a New Method for Assessing Asphalt Binder Performance Durability*.

Goosen, E. and Jenkins, K. (2019) 'Extraction and Recovery of Bituminous Binders from Chip Seal Samples', 12th Conference on Asphalt Pavements for Southern Africa. Available at: https://www.capsa2019.co.za/wp-content/uploads/2019/10/CAPSA'19 - Papers Accepted For The Conference.pdf.

Goosen, E. S. (2021) 'Modelling of Surfacing Seal Binder Ageing and Rheology', (December), pp. 1–214.

Hoffmann, P. (2007) 'BITUMEN RUBBER CHIP AND SPRAY SEALS IN SOUTH AFRICA', (July), pp. 225–238.

Hunter, R. N., Self, A. and Read, J. (2015) *The Shell bitumen handbook*, *Read, J., & Whiteoak, D. (2003). The Shell bitumen handbook. Thomas Telford.* doi: 10.1680/sbh.32200.

Lee, M. *et al.* (2004) 'Comparison of Results of SHRP and Conventional Binder Tests on Paving Asphalts', *International Journal of Applied Science*, 2(3), pp. 245–256.

Lesueur, D. (2009) 'The colloidal structure of bitumen : Consequences on the rheology and on the mechanisms of bitumen modi fi cation', 145, pp. 42–82. doi: 10.1016/j.cis.2008.08.011.

Lister, A. S. (2005) *Validation of HPLC methods in pharmaceutical analysis*, *Separation Science and Technology*. Elsevier Inc. doi: 10.1016/S0149-6395(05)80051-0.

Lu, X., Talon, Y. and Redelius, P. (2008) 'Aging of bituminous binders – laboratory tests and field data', *The 4th eurasphalt & eurobitume congress*, pp. 1–12.

Mensching, D. J. *et al.* (2015) 'Exploring low temperature performance in black space', *Asphalt Paving Technology: Association of Asphalt Paving Technologists-Proceedings of the Technical Sessions*, 84(December), pp. 459–496. doi: 10.1080/14680629.2015.1077015.

Mikhailenko, P. and Baaj, H. (2017) 'Survey of Current Asphalt Binder Extraction and Recovery Practices Survey of Current Asphalt Binder Extraction and Recovery Practices Peter Mikhailenko , Research Associate , CPATT , University of Waterloo Hassan Baaj (presenter), Associate Professor , ', (September).

Mturi, G. *et al.* (2015) 'A Review Towards a National Bitumen Extraction-Recovery Method', (August), pp. 1–17.

Rowe, G., Baumgardner, G. and Sharrock, M. (2009) 'Functional forms for master curve analysis of bituminous materials', *Advanced Testing and Characterization of Bituminous Materials*, (1951), pp. 81–92. doi: 10.1201/9780203092989.ch9.

Rowe, G. M., King, G. and Anderson, M. (2014) 'The influence of binder rheology on the cracking of asphalt mixes in airport and highway projects', *Journal of Testing and Evaluation*, 42(5). doi: 10.1520/JTE20130245.

Rowe, G. M. and Sharrock, M. J. (2011) 'Alternate shift factor relationship for describing temperature dependency of viscoelastic behavior of asphalt materials', *Transportation Research Record*, (2207), pp. 125–135. doi: 10.3141/2207-16.

Rowe, G. M. and Sharrock, M. J. (2017) 'Cracking of asphalt pavements and the development of specifications with rheological measurements', (June). doi: 10.14311/ee.2016.215.

Saal, R. N. J. and Labout, J. W. A. (1958) *Rheological Properties of Asphalts*, *Rheology*. ACADEMIC PRESS INC. doi: 10.1016/b978-0-12-395695-8.50014-8.

SABITA (2012) *Manual 2: Bituminous binders for road construction and maintenance*.

SABITA (2016) 'THE INTRODUCTION OF A PERFORMANCE GRADE SPECIFICATION FOR BITUMINOUS BINDERS', (January).

SABITA (2019a) 'asphaltNEWS', 33(3).

SABITA (2019b) 'Origin and use of bitumen', pp. 0–1.

SABITA (2020) *TG2 : Bitumen Stabilised Materials*. Available at: http://www.sabita.co.za/wp-content/uploads/2020/08/tg2-august-2020.pdf.

SANRAL (2009) 'Flexible Pavements Road Pavement Repairs - Flexible Pavements', *Routine Road Maintenance Manual*, (2), pp. 1–28.

SANRAL (2014) *SOUTH AFRICAN PAVEMENT ENGINEERING MANUEL Chapter 1*.

SANS 3001 (2011). Part AS20: Determining of the Soluble Binder Content and Particle Size Analysis of an AsphaltMix. South African National Standard.

SANS 4001 (2012). Part BT2: Cutback bitumen. South African National Standard.

SANS 4001 (2014a). Part BT3: Anionic bitumen road emulsion. South African National Standard.

SANS 4001 (2014b). Part BT4: Cationic bitumen road emulsion. South African National Standard.

SANS 4001 (2016). Part BT1: Penetration grade bitumen. South African National Standard.

Shaw, M. . and MacKnight, W. . (2005) 'Introduction to Polymer Viscoelasticity'. John Wiley & Sons.

Texas Department of Transporation (2010) 'Seal Coat and Surface Treatment Manual', (July).

TG1 (2019) *The use of modified bituminous binders in road construction*, *Dictionary Geotechnical Engineering/Wörterbuch GeoTechnik*. doi: 10.1007/978-3-642-41714-6_200286.

Tredoux, C. (2020). Rheological Performance of Seals in South Africa Based on Binder Ageing Considerations. Tech. Rep., Stellenbosch University. Available at: https://scholar.sun.ac.za

TRH 3 (2007) 'Design and Construction of Surfacing Seals', *Technical Recommendations for Highways*, (May), pp. 1–258.

Van Heerden, J. *et al.* (2011) 'The Use of Dynamic Shear Rheometer (DSR) to Predict the Penetration of Bitumen', *10th COnference on Asphalt Pavements for South Africa, KwaZulu-Natal, South Africa*, (October 2018), pp. 1–10.

Van Den Bergh, W. (2011) *The Effect of Ageing on the Fatigue and Healing Properties of BituminousMortars*. Technische Universiteit Delft.

Van Zyl, G. and Jenkins, K. (2015) 'Overview of Long Term Seal Performance', in.

Vega, A. M. M. (2016) 'Exploring the Black Space of Compressive and Shear Modulus'.

Widyatmoko, I., Heslop, M. W. and Elliott, R. C. (2005) 'Viscous to Elastic Transition Temperature and the In Situ Performance of Bituminous and Asphaltic Materials', *Journal of the Institute of Asphalt Technology*, 14(May), p. 7.

Yusoff, N. I. . ., Hainin, M. R. and Airey, G. D. (2005) 'What You Need to Know About Bitumen Rheology', *Supply Chain Management Review*, (September), pp. 29–36. doi: 10.1007/978-3-319-15509-8.

Yusoff, N. I. M. *et al.* (2013) 'Modelling the rheological properties of bituminous binders using mathematical equations', *Construction and Building Materials*. Elsevier Ltd, 40, pp. 174–188. doi: 10.1016/j.conbuildmat.2012.09.105.

Yusoff, N. I. M., Chailleux, E. and Airey, G. D. (2011) 'A Comparative Study of the Influence of Shift Factor Equations on Master Curve Construction', *International Journal of Pavement Research and Technology*, 5.

Yusoff, N. I. M., Shaw, M. T. and Airey, G. D. (2011) 'Modelling the linear viscoelastic rheological properties of bituminous binders', *Construction and Building Materials*. Elsevier Ltd, 25(5), pp. 2171–2189. doi: 10.1016/j.conbuildmat.2010.11.086.

Appendices

Appendix A: Repeatability and Reproducibility Analysis

This appendix is an extension of the discussion presented in Section 4.7.

A.1 Young, modified emsulsion Cape seal

R61/8 km51.01 is a SC-E2 modified binder recovered from a 1 year old Cape seal. During the distillation phase of test 1 and 2, a thick layer of bubbles formed on top of the solvent-binder solution. It is believed that the bubbles are related to the emulsifier. As shown in Figure A.1, the feeder was closed but the bubbles continued to form. A risk was that the bubbles could backwash through the rotary evaporator into the evaporating flask, therefore smaller amounts of the solvent-binder solution was fed into the system. Consequently, discrepancies were noted during the binder recovery procedures.

Figure A.1: Layer of Bubbles

The stiffness parameters are presented in Figure A.2. The G-R value of test 2 is the highest and the compare sample is the lowest. The G_{vet} values are similar. The stiffness parameters show no clear distinction in terms of the extent of ageing.

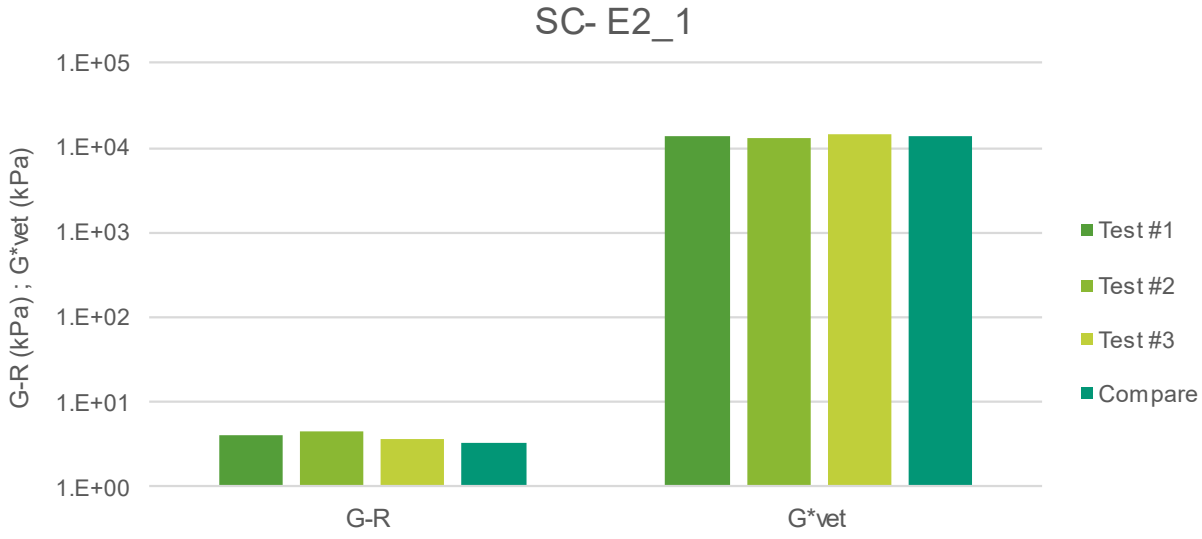

Figure A.2: Stiffness Parameters of R61/8 km51.01

Table A. 1 contains the RMS error values of all four samples. The RMS error values of the shift factors vary. This reveals that the difference between the G-R parameters are possibly not connected to the ageing of the binders, i.e. rheology related, but that it is rather linked to the shifting of the data. The RMS error values of shift factor models of the test samples are classified as very good, while the compare sample is considered good. All of the master curve models are classified as good.

Table A. 1: RMS Error of Fitted Data of R61/8 km51.01

Name	Shift Factor	RMS Error	Master Curve	RMS Error
Test #1	Modified Kaelble	0.087	Discrete Modelling	0.049
Test #2	Modified Kaelble	0.101	Discrete Modelling	0.049
Test #3	Modified Kaelble	0.080	Discrete Modelling	0.042
Compare	Modified Kaelble	0.016	Discrete Modelling	0.050

Table A.2 contains the recommended repeatability and reproducibility requirements for the stiffness parameters. All of the stiffness parameters comply with the recommended requirements, except the repeatability of G-R. Once again, the input values of G-R comply with the recommended repeatability requirement but G-R does not.

Table A.2: Repeatability and Reproducibility of Stiffness Parameters of R61/8 km51.01

	Test #1	Test #2	Test #3	Compare
δ (°)	76.793	76.259	77.030	75.608
G* (kPa)	74.869	76.666	69.039	50.824
G-R (kPa)	4.014	4.453	3.569	3.241
Gvet (kPa)	13848.276	12913.171	14483.871	13414.849
	Repeatability		**Reproducibility**	
Δδ	0.771		1.422	
Recommended	7.352		20.634	
Δlog(G*)	0.046		0.046	
Recommended	0.187		0.187	
Δlog(G-R)	0.096		0.138	
Recommended	0.060		0.156	
Δlog(Gvet)	0.033		0.033	
Recommended	1.117		1.117	

The temperature parameters are presented in Figure A.3. Due to the lack of BBR testing, ΔT_c was not calculated for the compare sample. Based on the ΔT_c values, test 1 is S-controlled, while test 2 and 3 are m-controlled. The T_{vet} values of test samples correlate well but the compare sample has a much lower T_{vet} value. The difference between T_{vet} can be related to a modelling error. The T_{max} values of all four samples are similar.

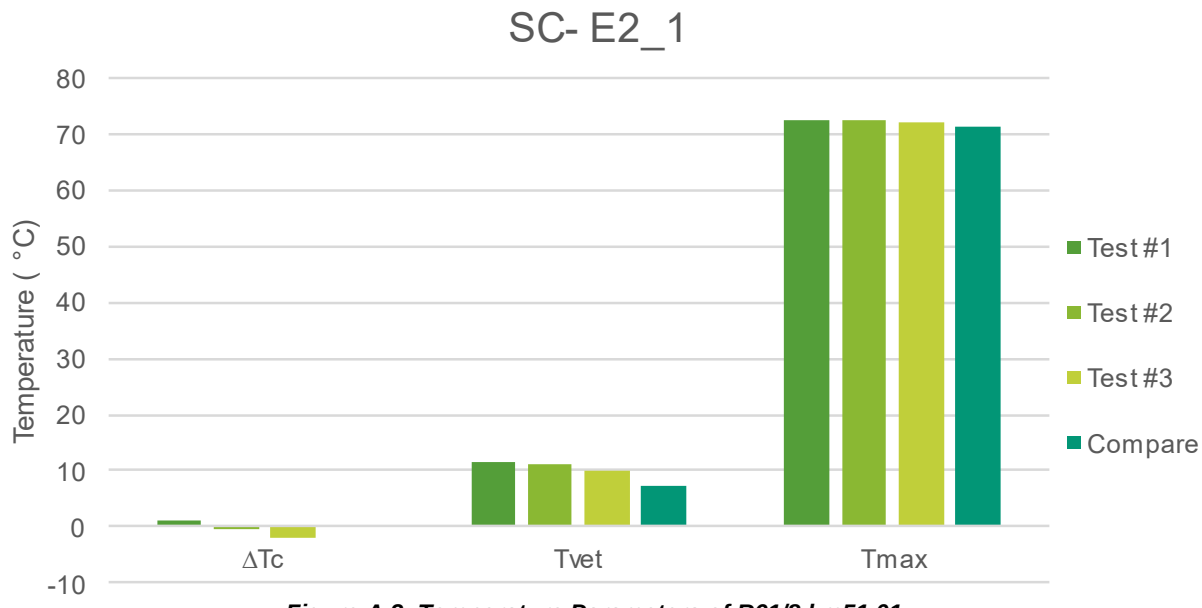

Figure A.3: Temperature Parameters of R61/8 km51.01

Table A.3 considers the recommended repeatability and reproducibility of the temperature parameters. T_{max} and T_{vet} meet the recommended repeatability requirement but ΔT_c does not. The discrepancies between ΔT_c can be rheology related. The geometry of the bitumen beams constructed for BBR testing could also contribute towards the variability seen between the ΔT_c values. In terms of reproducibility, T_{max} falls within the recommended criteria, while T_{vet} does not comply with the recommended requirement.

Table A.3: Repeatability and Reproducibility of Temperature Parameters of R61/8 km51.01

	Test #1	Test #2	Test #3	Compare
Tc,s	-27.842	-28.580	-29.754	-
Tc,m	-28.954	-28.338	-27.880	-
ΔTc	1.112	-0.242	-1.874	-
Tmax	72.604	72.506	71.992	71.418
Tvet	11.462	11.150	10.145	7.212
	Repeatability		**Reproducibility**	
ΔTc,s	1.912		-	
ΔTc,m	1.074		-	
Δ (ΔTc)	2.986		-	
ΔTmax	0.611		1.185	
ΔTvet	1.317		4.250	
Recommended	1.9		3.4	

Figure A.4 shows the Black Space diagram using discrete modelling. For 30°<δ<60°, there is a strong correlation between all four models and their raw data points. At δ=45° there appears to be no obvious deviations between the models. Since the G_{vet} markers are overlapping, there is also no deviation between the raw data, which makes it unclear as to why T_{vet} does not meet the recommended reproducibility requirements in Table A.3. It is possible that the difference is due to shifting.

Outside the 30°<δ<60°region, the compare sample has lower stiffness values. Below 30°, there are no data points to populate the compare model, therefore the lower stiffness values are not problematic. For δ<30°, the data points of each test appear more distinct in comparison with the tight grouping that is experienced throughout the remainder of the graph. This shows that the variability of the ΔT_c values is related to testing or are rheology based. However, this variability does not seem problematic.

Above 60°, the compare stiffness values are lower than the test samples. The G-R parameters are plotted within this region, which explains why the compare sample has a lower G-R parameter. It can also be seen that the G-R parameters of the test samples overlap, which suggest that there is a strong correlation between these values, but based on the repeatability analysis, conducted in Table A.2, the test samples do not meet the recommended repeatability requirement. Therefore, it is believed that a visual representation in Black Space must be considered in combination with the recommended requirements in order to determine whether G-R performs well in terms of repeatability or reproducibility. For this seal, Figure A.4 confirms that the G-R parameters of the test samples do perform well in terms of repeatability.

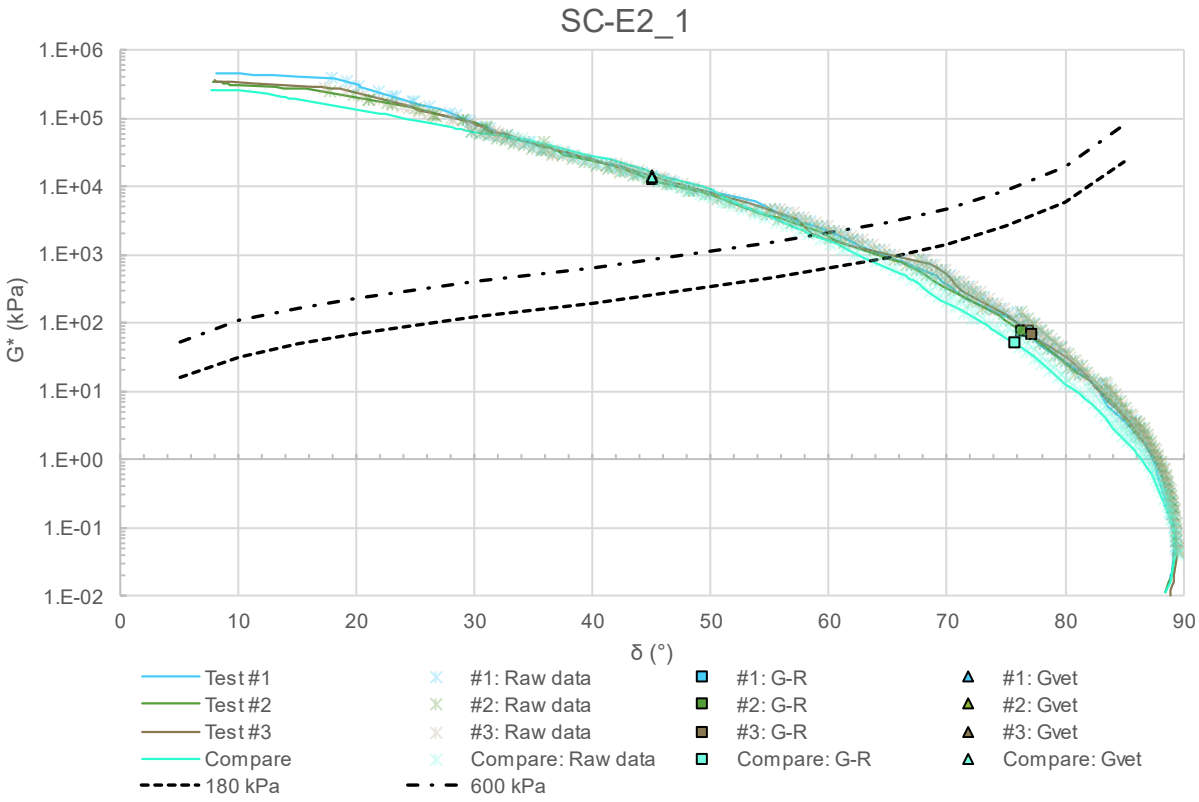

Figure A.4: Black Space of R61/8 km51.01

A.2 Young, modified multiple seal

N2/16 km71.5 is a S-E1 modified binder recovered from a 2 year old multiple seal. The multiple seal comprises of a 20 mm aggregate layer and two 7 mm aggregate layers. The stiffness parameter of N2/16 km71.5 are indicated in Figure A.5.

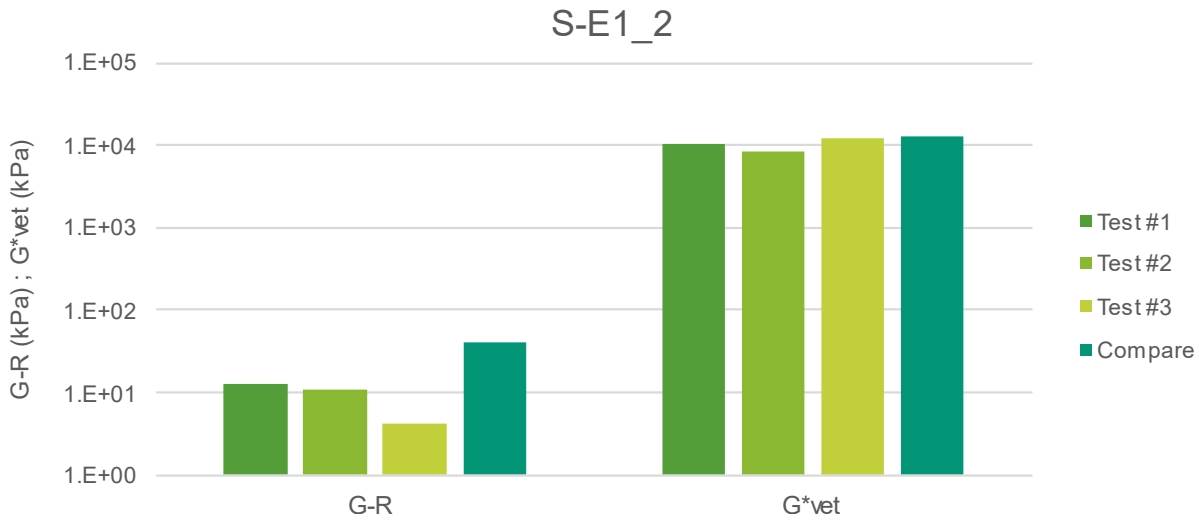

Figure A.5: Stiffness Parameters of N2/16 km71.5

The compare sample has a slightly higher G_{vet}, suggesting that the sample aged to a lesser extent than the other three test samples. Test 2 has the lowest G_{vet}, suggesting that this sample aged to a greater extent. The G-R parameters are significantly more scattered. Based on the G-R parameters, the compare sample is aged the most, while test 3 is aged the least.

Table A.4 contains the RMS error values of all four samples. The RMS error values of the shift factor models varies a lot. The shift factor models of test 1 and the compare sample are classified as very good, while test 2 and 3 are classified as good. The master curve models of all of the samples are classified as good. Despite the highest RMS error values, the stiffness values of test 2 tend to correlate well with test 1, but test 3 that has a lower RMS error values than test 2, tend to deviate from test 1.

Table A.4: RMS Error of Fitted Data of N2/16 km71.5

Name	Shift Factor	RMS Error	Master Curve	RMS Error
Test #1	Modified Kaelble	0.069	Discrete Modelling	0.047
Test #2	Modified Kaelble	0.187	Discrete Modelling	0.072
Test #3	Modified Kaelble	0.178	Discrete Modelling	0.051
Compare	Modified Kaelble	0.028	Discrete Modelling	0.048

Table A.5 contains the recommended repeatability and reproducibility requirements for the stiffness parameters. G* and G-R do not meet the recommended repeatability or reproducibility requirements. This is to be expected, as seen from the variation between the

G-R values, presented in Table A.5. It is believed that the variability of G* is the cause of the variability between the G-R parameters.

Table A.5: Repeatability and Reproducibility of Stiffness Parameters of N2/16 km71.5

	Test #1	Test #2	Test #3	Compare
δ (°)	70.303	70.967	72.658	70.114
G* (kPa)	106.674	97.883	46.039	327.335
G-R (kPa)	12.872	11.012	4.285	40.277
Gvet (kPa)	10292.381	8586.970	11969.231	12568.966
	Repeatability		**Reproducibility**	
Δδ	2.356		2.545	
Recommended	7.131		19.173	
Δlog(G*)	0.365		0.852	
Recommended	0.189		0.553	
Δlog(G-R)	0.478		0.973	
Recommended	0.093		0.296	
Δlog(Gvet)	0.144		0.166	
Recommended	0.401		1.088	

Figure A.6 indicates noticeable variability between the temperature parameters. It was not possible to calculate ΔT_c for the compare sample, as no BBR data was available. The ΔT_c values reveal that test 1 and 3 are S-controlled, while test 2 is m-controlled. Based on T_{max} and T_{vet}, the compare sample aged the most and test 3 aged the least. A similar trend is observed from the differences between the G-R parameters.

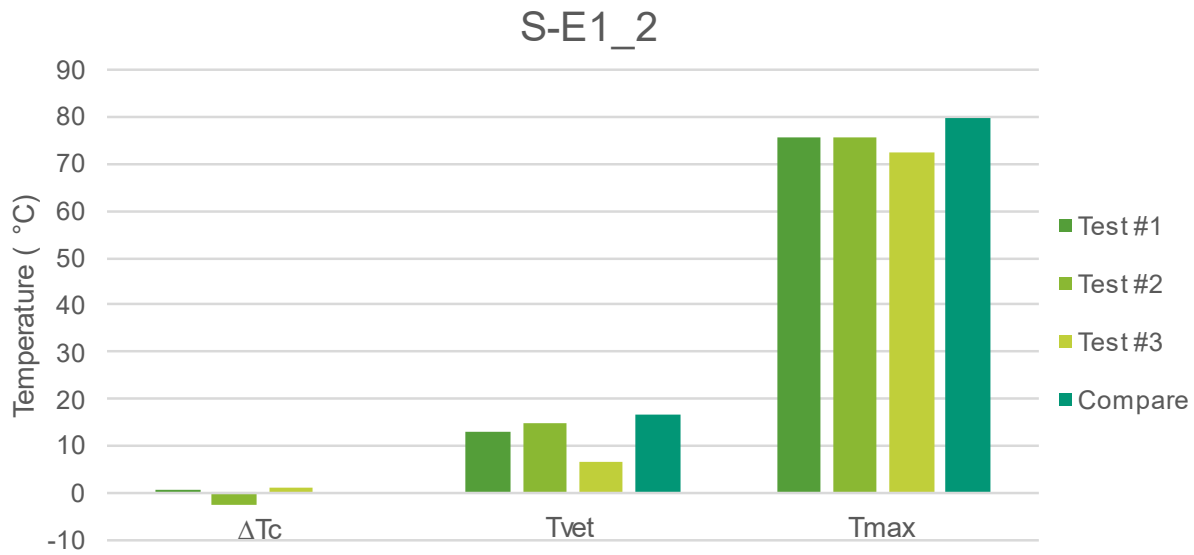

Figure A.6: Temperature Parameters of N2/16 km71.5

From Table A.6 it can be seen that neither the recommended repeatability nor the recommended reproducibility requirements are satisfied. There are also no correlations between the extent to which the temperature parameters differ.

Table A.6: Repeatability and Reproducibility of Temperature Parameters of N2/16 km71.5

	Test #1	Test #2	Test #3	Compare
Tc,s	-29.624	-30.565	-32.871	-
Tc,m	-29.731	-27.829	-34.117	-
ΔTc	0.107	-2.737	1.247	-
Tmax	75.717	75.588	72.586	79.652
Tvet	12.928	14.810	6.530	16.801
	Repeatability		**Reproducibility**	
ΔTc,s	3.246		-	
ΔTc,m	6.289		-	
Δ (ΔTc)	3.983		-	
ΔTmax	3.131		7.066	
ΔTvet	8.281		10.272	
Specification	1.9		3.4	

Figure A.7 shows the Black Space diagrams of the four samples using discrete modelling. Despite the variability suggested by the repeatability and reproducibility analysis, it appears that the Black Space diagrams are not as inconsistent as expected. For δ<30°, there is a strong correlation between the data point for all of the test samples. Within this region, the test 3 model is slightly higher than the other test samples, while the compare model is slightly lower than the test samples. BBR testing of test 3 were conducted at -30°C, -24°C, -18°C, and -12°C. It is possible that the -30°C isotherm elevated the model. The lack of BBR data points prevent the compare-model from being accurate within this region.

Where δ>70°, the compare sample has higher stiffness values than the other test samples. All of the G-R parameters are situated within this region, hence the variability this parameter exhibits. In this case, the visual inspection of the Black Space diagram supports the findings from the repeatability and reproducibility analysis. Despite the variability, the G-R markers correlate well with the raw data and the rheological model.

For 45°<δ<70°, there is a strong correlation between all of the data points. At δ=45°, test 2 deviates, while the strong correlation continues between test 1, test 3 and the compare sample. It can be seen that the steric hardening of the 5°C isotherm and BBR data of test 2 overlap where 30°<δ<45°. It appears as if the 5°C isotherm approaches a horizontal plateau, which is why the model deviates to such an extent. This occurrence explains the high RMS error for both the shift factor and master curve model of test 2. Test 3 is the other sample that had a high RMS error values. From δ<45° test 3's model contains various vertical steps, despite the fact that sufficient data points are available. Between these vertical jumps, the model does not fit the data points very well. It is believed that the vertical jumps are to blame for the high RMS error values of test 3. The values of G-R and T_{vet} for test 3 deviates the most

from the other samples. It is believed that these deviations are caused by the modelling error that created the vertical jumps and not due to rheological discrepancies.

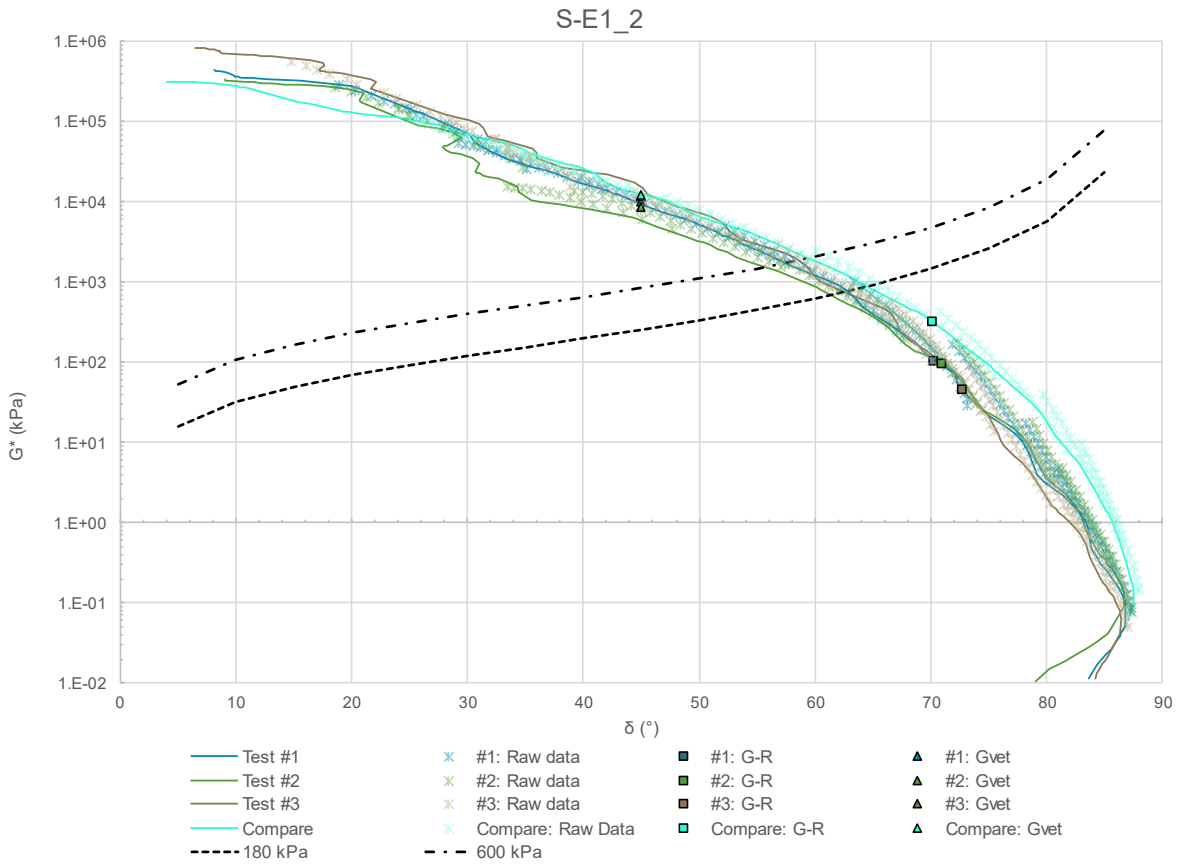

Figure A.7: Black Space of N2/16 km71.5

A.3 Old, modified double seal

N2/32 km21 is a S-E1 modified binder recovered from a 6 year old double seal. For the purpose of this study, this seal is classified as an older surfacing. The stiffness parameters, presented in Figure A.8, are quite indistinct.

Figure A.8: Stiffness Parameters of N2/32 km21

The G-R parameters suggest that the compare sample aged to a greater extent, while the G_{vet} values indicate the opposite. Despite the age of the seal, the G- R values are below 180 kPa, to suggest that the surfacing was still in good condition.

Table A.7 shows a high RMS error values for the Modified Kaelble from the test sample. The shift factor of the test sample is classified as as poor, while the rheological model is considered to be as fair. Both the shift factor model and the rheological model of the compare sample is classified as very good. Discrepancies between the G-R values is likely a result of the test sample's flawed shift factor model. It seems that the G-R parameter of the compare sample is more reliable, since the RMS error values are much lower.

Table A.7 RMS Error of Fitted Data of N2/32 km21

Name	Shift Factor	RMS Error	Master Curve	RMS Error
Test	Modified Kaelble	0.228	Discrete Modelling	0.102
Compare	Modified Kaelble	0.091	Discrete Modelling	0.027

Table A.8 contains the recommended reproducibility requirements for the stiffness parameters. Despite the deviation between the RMS error values, all of the stiffness parameters comply with the recommended reproducibility requirements.

Table A.8: Reproducibility of Stiffness Parameters of N2/32 km21

	Test	Compare
δ (°)	66.954	67.591
G* (kPa)	249.290	475.325
G-R (kPa)	41.518	74.718
Gvet (kPa)	6946.667	11314.815
	Reproducibility	
Δδ	0.637	
Recommended	18.164	
Δlog(G*)	0.280	
Recommended	0.6849	
Δlog(G-R)	0.255	
Recommended	0.471	
Δlog(Gvet)	0.212	
Recommended	1.066	

In Figure A.9, the temperature parameters also do not clearly distinguish between the extent of ageing that the two samples experience. ΔT_C and T_{vet} suggest that the test sample aged more, while T_{max} recommend that the compare sample aged more. Since T_{vet} is based on shifted data, it is also uncertain to what extent the flawed shift factor influenced the authenticity of the test sample's T_{vet} and G-R. In order to calculate $T_{c,s}$ and $T_{c,m}$ for the compare sample, the data had to be extrapolated since there was no binder left to conduct an additional test to

meet all of the requirements. This will definitely contribute towards the variability between the samples' ΔT_C values.

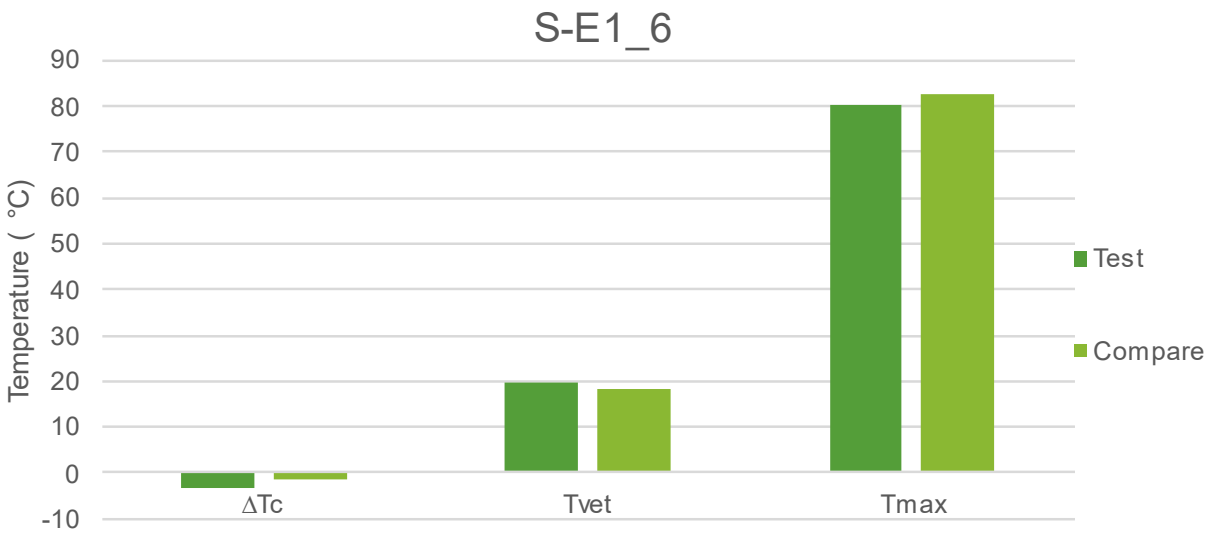

Figure A.9: Temperature Parameters of N2/32 km21

Despite the distorted shift factor, all of the temperature parameters perform very well in terms of the recommended reproducibility specification, as seen from Table A.9. The values for ΔT_C also comply with the -5°C limit provided in SATS 3208.

Table A.9: Reproducibility of Temperature Parameters of N2/32 km21

	Test	Compare
Tc,s	-26.161	-23.119
Tc,m	-22.725	-21.609
ΔTc	-3.437	-1.510
Tmax	80.274	82.860
Tvet	19.881	18.399
	Reproducibility	
ΔTc,s	3.042	
ΔTc,m	1.115	
Δ (ΔTc)	1.927	
ΔTmax	2.586	
ΔTvet	1.482	
Recommended	3.4	

Figure A.10 shows the Black Space diagram for both samples using discrete modelling. The raw data points of both samples are also plotted. It can be seen that there is a strong correlation between the raw data points where δ<28° and δ>74°. For 28°<δ<74°, the compare sample experiences higher stiffness values than the test sample. As previously mentioned, the binder hardening can be related to ageing, fines retention or the test sample could still contain solvent, rendering the binder softer. Either way, it appears that the hardening effect

does not occur uniformly at all temperatures. A visual inspection of the Black Space diagram confirms that the stiffness parameters perform well in terms of repeatability.

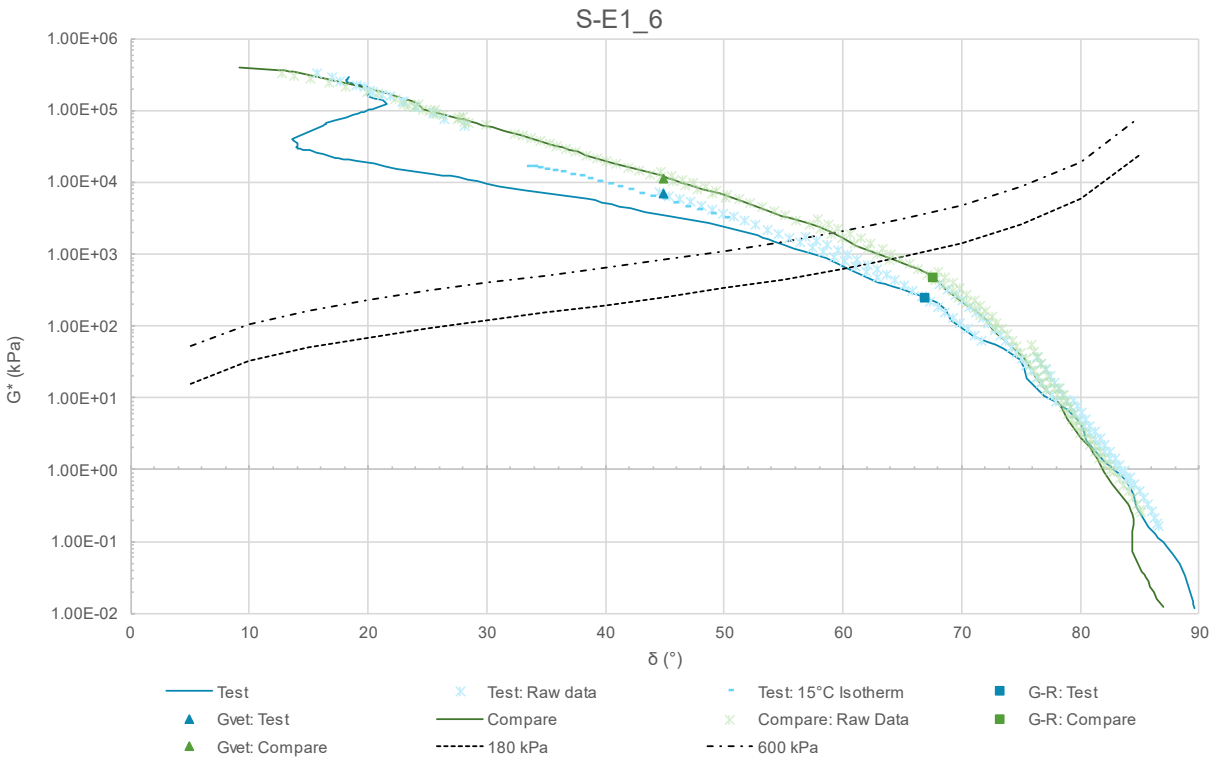

Figure A.10: Black Space of N2/32 km21

There appears to be a gap between the DSR data points and the BBR data points for the test sample. The 5°C isotherm from the test sample was omitted, because it was outside the LVE range. BBR tests were conducted at -24°C, -18°C and -12°C. The compare sample also conducted BBR testing at -18°C and -12°C but the 5°C isotherm was within the LVE, which allowed the 5°C isotherm to populate the region of 28°<δ<33°, where the test sample has the gap. It also appears that the test sample's 15°C isotherm flattens as δ strives to zero. The 15°C isotherm is not influenced by shifting, since a reference temperature of 15°C is used. The horizontal plateau is overemphasized in the model because there are no data points between 28° and 33° to correct the model. Future investigations should definitely consider testing a BBR sample at -6°C if the 5°C isotherm does not fall within the LVE range, to ensure that a continuous graph can be plotted.

A.4 Old, modified double seal

N8/8 is a S-E1 modified binder recovered from a 7 year old double seal. The two seal samples used in this section were located at different positions in the pavement. One sample was retrieved from the shoulder, while the other sample was recovered from the outer wheel track. Typically, the outer wheel track experiences much more traffic loading than the shoulder. Bear

in mind that this is a seal sample from a national road, where the shoulder is frequently utilised by heavy vehicles to accommodate lighter vehicles that travel at higher speed. The seal is 7 years old, therefore it is predicted that the durability parameters will reflect that of an aged binder. For the period between retrieval and testing, these samples were exposed to the same storage conditions. Discrepancies in the rheology of the binder are likely a result of exposure to different in-situ traffic loadings or from the binder recovery procedure.

Figure A.11 shows the stiffness parameters of both test samples. The G_{vet} values are similar but the G-R values vary. The G-R values for the outer wheel track and the shoulder are 150 kPa and 80 kPa respectively. The G-R parameter of the outer wheel track is almost double that of the shoulder and is also approaching the 180 kPa limit, which is associated with damage onset.

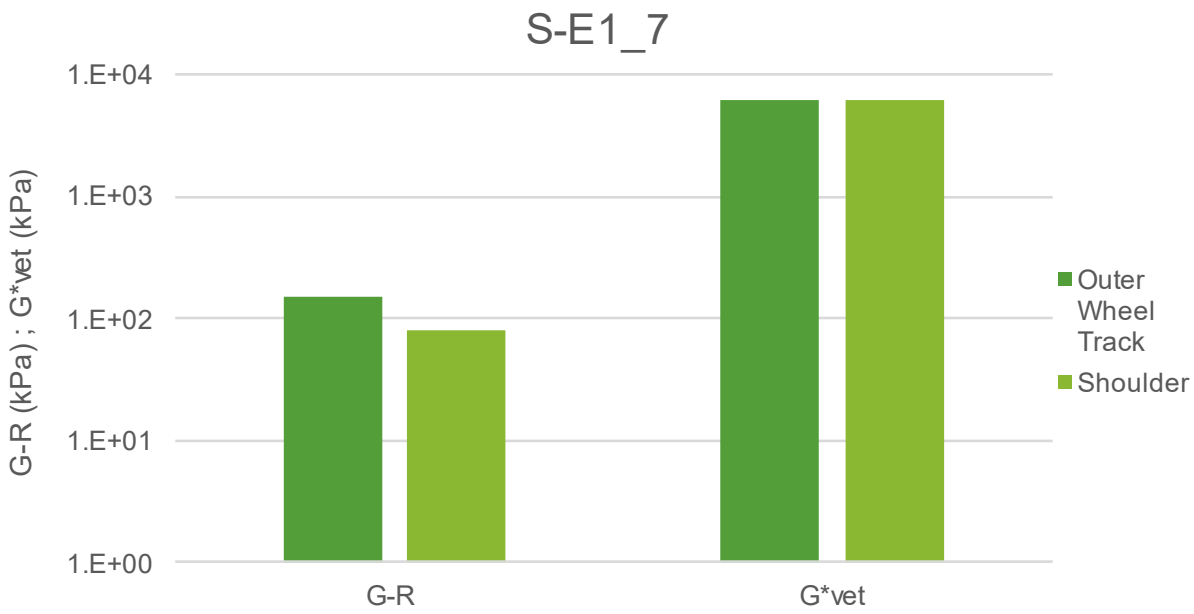

Figure A.11: Stiffness Parameters of N8/8 km5.6

From Table A.10, it can be seen that the shift factor model of both samples is classified as very good, while the master curve model of the outer wheel track is considered good and the shoulder is catalogued as fair. Since the RMS error for both the rheological models of the outer wheel track is less than the values of the shoulder, it is suggested that the results from the outer wheel track are more accurate.

Table A.10: RMS Error of Fitted Data of N8/8 km5.6

Name	Shift Factor	RMS Error	Master Curve	RMS Error
OWT	Modified Kaelble	0.073	Discrete Modelling	0.066
Shoulder	Modified Kaelble	0.082	Discrete Modelling	0.119

Table A.11 contains the recommended repeatability requirements for the stiffness parameters. All of the stiffness parameters comply with the recommended repeatability requirements, except for G-R. The Black Space diagram will be used to provide clarity relating to the repeatability of G-R.

Table A.11: Repeatability of Stiffness Parameters of N8/8 km5.6

	Outer Wheel Track	Shoulder
δ (°)	60.964	62.807
G* (kPa)	560.244	339.769
G-R (kPa)	150.951	79.773
Gvet (kPa)	6139.380	6200.625
	Repeatability	
Δδ	1.843	
Recommended	6.189	
Δlog(G*)	0.217	
Recommended	0.264	
Δlog(G-R)	0.277	
Recommended	0.204	
Δlog(Gvet)	0.004	
Recommended	0.379	

From Figure A.12, it can be seen that the values of both T_{max} and T_{vet} are similar. A similar trend in observed in the values of G_{vet} The fact that the discrepancy in G-R is not detected in T_{vet} suggest that the variability is not related to a modelling error. The ΔT_c values for both samples are negative, which implies that both samples are m-controlled. Considering the age of the samples, it is expected that the relaxation potential of the binder has decreased.

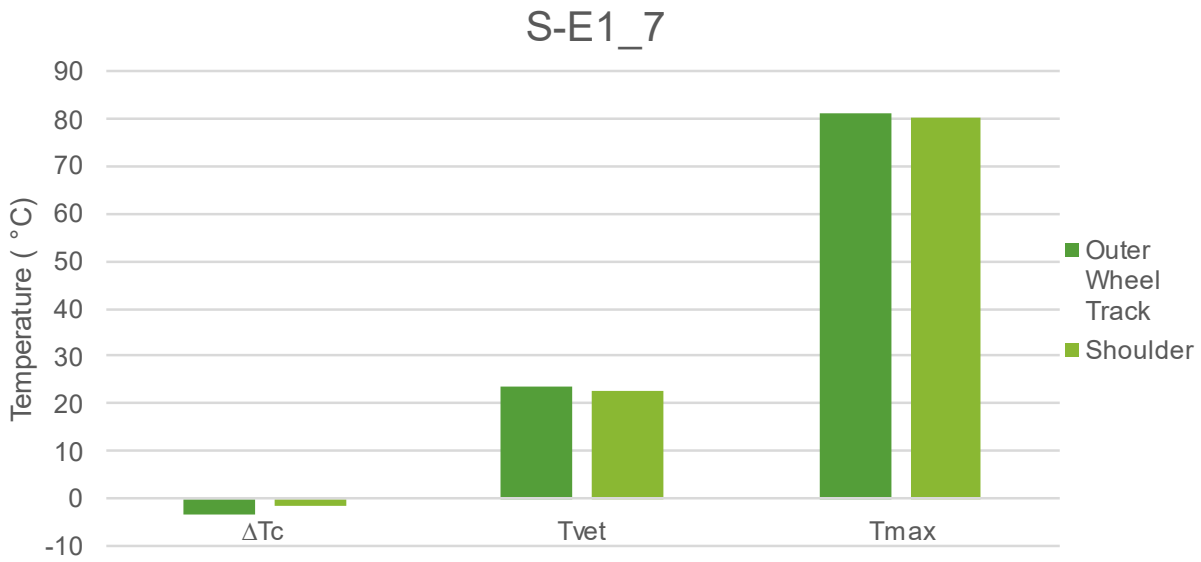

Figure A.12: Temperature Parameters of N8/8 km5.6

The recommended repeatability of the temperature parameters is shown in Table A.12. Apart from $T_{c,s}$ and $T_{c,m}$ not complying with the recommended limits, all of the temperature parameters presented in Figure A.12, are within the recommended range. Despite the age of the binder, the ΔT_C values also comply with the -5°C limit provided in SATS 3208.

Table A.12: Repeatability of Temperature Parameters of N8/8 km5.6

	Outer Wheel Track	Shoulder
Tc,s	-27.173	-29.136
Tc,m	-23.682	-27.491
ΔTc	-3.491	-1.645
Tmax	81.417	80.278
Tvet	23.795	22.659
	Repeatability	
ΔTc,s	1.963	
ΔTc,m	3.809	
Δ (ΔTc)	1.846	
ΔTmax	1.139	
ΔTvet	1.136	
Recommended	1.9	

In Section 3.7, it was mentioned that for the modelling software to prepare master curves, ambiguous data points had to be removed. For both these samples, the 5°C isotherms had to be removed, since these data points interfered with the BBR data points. Figure A.13 shows the Black Space diagram of the samples using discrete modelling. The raw data points for both samples are also included. The two models correlate well, except between 30° and 60°, where the shoulder model deviates. The vertical shift at 30° is especially misleading.

From the shoulder data points, it can be seen that between 33° and 49°, the data points overlap. Further inspection revealed that this region is populated by data from -12°C, -6°C and 15°C isotherms. Data from the 15°C isotherms is plotted separately to show that the DSR and BBR data are not able to converge. Since 15°C is used as the reference temperature, no shift factor is applied to the 15°C isotherm. Therefore, the 15°C isotherm will have a significant influence on the accuracy of the model.

The G-R parameters, as well as the 180 kPa and 600 kPa limits, are also plotted in Figure A.13. Since these parameters are not positioned between 33° and 49°, it is believed that the deviation in the shoulder model is not to blame for the variability experienced in the G-R parameter. Considering that these two samples were not exposed to identical traffic conditions, it is believed that the G-R parameters perform well in terms of repeatability

It is also noted that the variability is not observed in all of the durability parameters. This might imply that the binder recovery process affects certain areas of binder behaviour, such as the

region where G-R is positioned, more than other areas, such as T_{max}. It is believed that the different in-situ traffic loadings the samples were exposed to contribute towards the variability that the G-R parameters experienced.

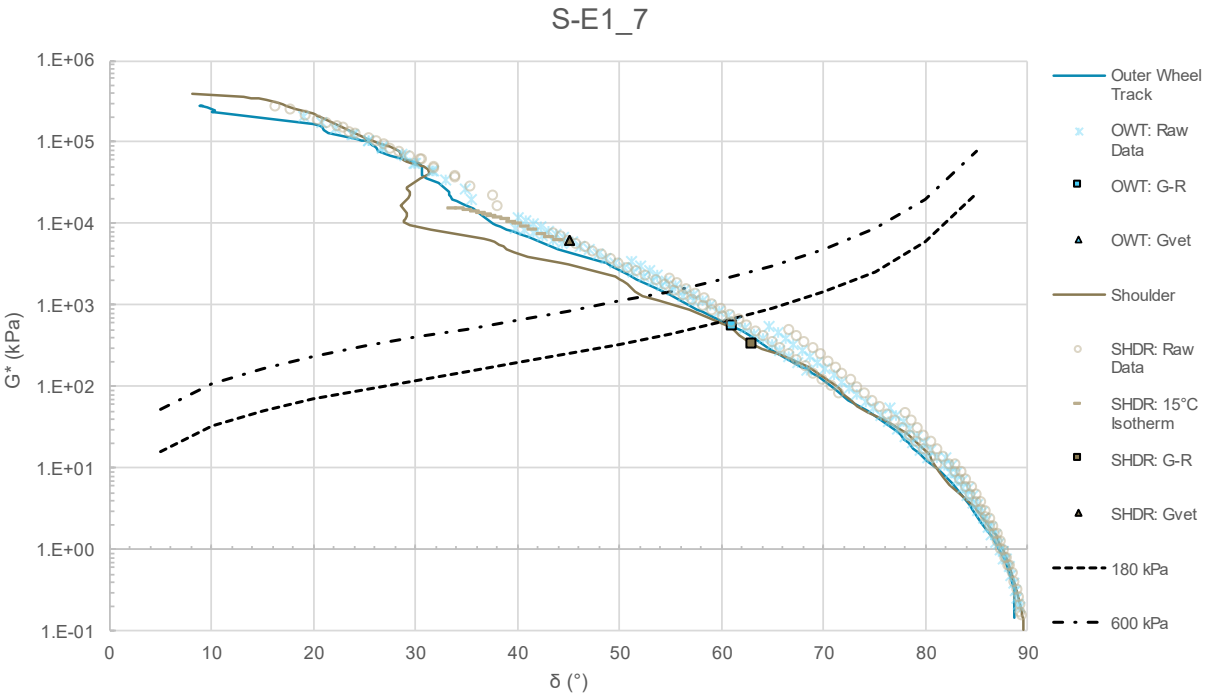

Figure A.13: Black Space of N8/8 km5.6

A.5 Old, modified double seal

N2/31 km3.6 is a S-E1 modified binder recovered from a 12 year old double seal. Apart from the age, the seal was retrieved from a national road. National roads typically experience high traffic volumes, especially heavy vehicles. It is expected that the durability parameters will exceed the limits provided in SATS 3208. It should be noted that a 5-year gap exist between the testing of these two samples.

From the stiffness parameters presented in Figure A.14, it is unclear which binder aged to a greater extent. The test sample has a lower G-R and G_{vet} value. The G-R parameter of both samples exceed the 600 kPa limitation, suggesting that both samples experienced significant hardening.

Figure A.14: Stiffness Parameters of N2/31 km3.6

The RMS error of the shift factor and master curve model for both samples are listed in Table A.13. Overall, the RMS error values are quite low. The shift factor model of the test sample is classified as good, while the compare sample is very good. Both rheological models are catalogued as good.

Table A.13: RMS Error of Fitted Data of N2/31 km3.6

Name	Shift Factor	RMS Error	Master Curve	RMS Error
Test	Modified Kaelble	0.123	Discrete Modelling	0.061
Compare	Modified Kaelble	0.048	Discrete Modelling	0.047

Table A.14 contains the recommended repeatability requirements for the stiffness parameters. All of the stiffness parameters comply with the recommended limits. The Black Space diagram will be used to confirm the repeatability of G-R.

Table A.14: : Reproducibility of Stiffness Parameters of N2/31 km3.6

	Test	Compare
δ (°)	52.535	53.980
G* (kPa)	1788.225	2849.345
G-R (kPa)	833.572	1218.287
Gvet (kPa)	5490.000	8072.105
	Reproducibility	
Δδ	1.445	
Recommended	14.380	
Δlog(G*)	0.202	
Recommended	0.906	
Δlog(G-R)	0.165	
Recommended	0.811	
Δlog(Gvet)	0.167	
Recommended	1.033	

The temperature parameters are arranged in Figure A.15. The T_{vet} and T_{max} values are similar. Based on these two temperature parameters, the compare sample aged to a greater extent than the test sample. The T_{vet} values, ΔT_c suggest the opposite and show that both binders are m-controlled. The ΔT_c of the test sample exceeds the -5°C limit recommended by SATS 3208, while the compare sample in still within the acceptable range. It is possible that oxidation took place during the period between testing, which could explain why the test sample exceeded -5°C, while the compare sample did not.

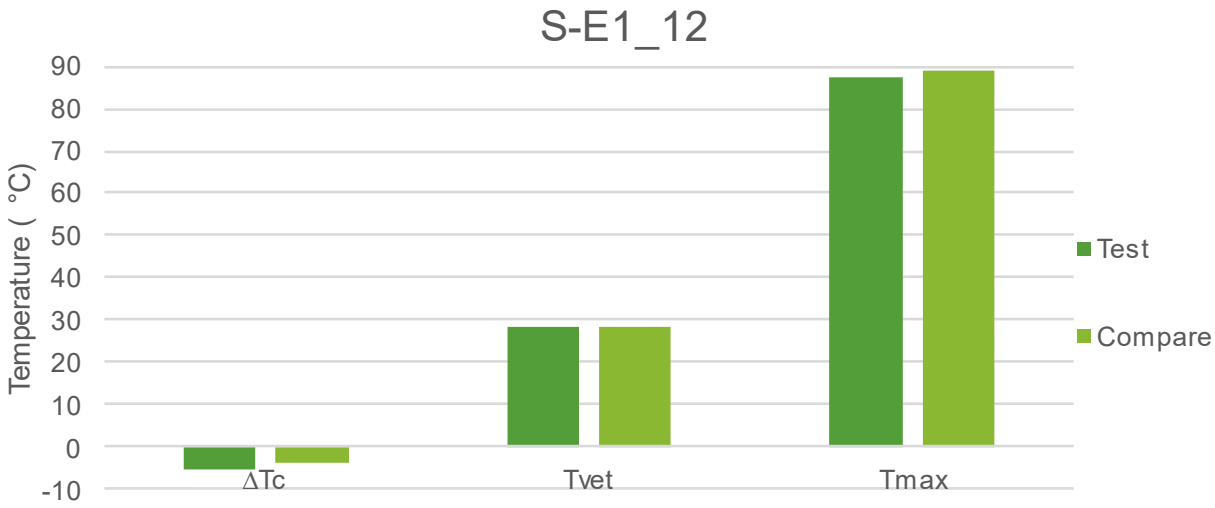

Figure A.15: Temperature Parameters of N2/31 km3.6

The reproducibility of the two samples is conveyed in Table A.15. The only parameters that did not comply with the recommended limit, are $\Delta T_{c,s}$ and $\Delta T_{c,m}$. The analysis of the durability parameters indicates a symmetric state. G_{vet} and ΔT_c suggest that the test sample aged to a greater extent than the compare sample, while G-R and T_{vet} suggest that the compare sample aged more, and T_{max} does not distinguish between the two samples.

Table A.15: Reproducibility of Temperature Parameters of N2/31 km3.6

	Test	Compare
Tc,s	-23.190	-18.239
Tc,m	-17.915	-14.240
ΔTc	-5.274	-3.998
Tmax	87.195	88.884
Tvet	28.496	28.529
	Reproducibility	
ΔTc,s	4.951	
ΔTc,m	3.675	
Δ (ΔTc)	1.276	
ΔTmax	1.689	
ΔTvet	0.033	
Recommended	3.4	

In Figure A.16, it can be seen that the 15°C isotherm and the BBR data of the test sample overlap, resulting in a model deviation between 24° and 40°. If the 15°C isotherm is disregarded, there is a strong correlation between the raw data points between δ<30° and δ>58°. In the δ<30° region, data used to determine ΔT_c is plotted, while in the region δ>58°, data that is used to determine T_{max}, is situated. Based on the strong correlation between the raw data points in these two regions, it can be deduced that the two samples are relatively consistent for both high and low temperatures.

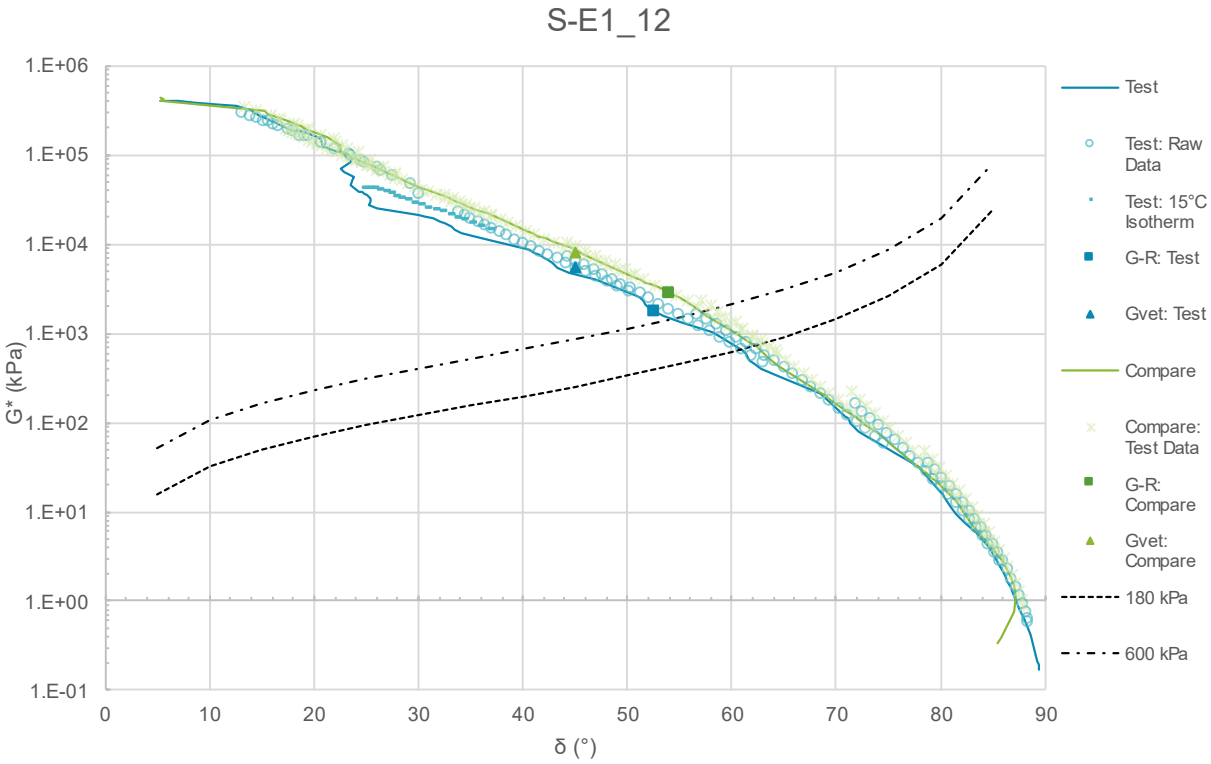

Figure A.16: Black Space of N2/31 km3.6

From Figure A.16, it can also be seen that both stiffness parameters fall within the 30°<δ<58° range, where the majority of the variability occurs. The variability can be traced back to the 15°C and 25°C isotherm. It is possible that the ageing caused by the binder recovery procedure is the reason for the discrepancies or the 8 mm testing. If this is the case, it appears that for older binders, the effect of ageing is proportional to all durability parameters. This reproducibility analysis emphasises the importance of considering a wide range of durability parameters in order to evaluate the viscoelastic behaviour of bitumen. Due to the age of the binder, it would not be expected to see significant additional ageing while the binder was stored in the laboratory. Despite the variability, it appears that G-R performs well in terms of reproducibility.

Appendix B: FTIR Analysis

This appendix is an extension of the discussion presented in Section 4.8.

B.1 Young, modified emsulsion Cape seal

- Seal name: R61/8 km51
- Binder age: 1 year

Variability from Section A.1:

- G-R and ΔT_c does not comply with the recommended repeatability requirement
- T_{vet} does not comply with the recommended reproducibility requirement.
- G_{vet} and T_{max} are very similar.
- The Black Space Diagram indicated a very strong correlation between the samples, although the 25 mm DSR data of the compare sample was slightly lower than the test samples.

Figure B.1:

- All four samples experience a peak at 1700 cm^{-1} and a slightly elevated peak at position A. The compare sample has slightly higher peaks at both these positions.
- At position B, there is a strong correlation between the samples
- More variability is experienced at position C. Here, the compare sample has the highest peak, which corresponds to the higher DSR data from the Black Space Diagram.
- At various positions, the absorbance of the compare sample is higher than the test samples.

Figure B.2:

- The peak areas of test samples for range A are similar. The differences between the peak areas of range A correlate with the differences seen in G-R and T_{vet}.
- For range B, the peak area of test 1 is higher than the other samples. The peak areas of test 2 and test 3 are similar, while the compare sample has the lowest peak area. The differences do not correlate with the variability present in the durability parameters.
- The peak areas for range C follow a similar variability trend.

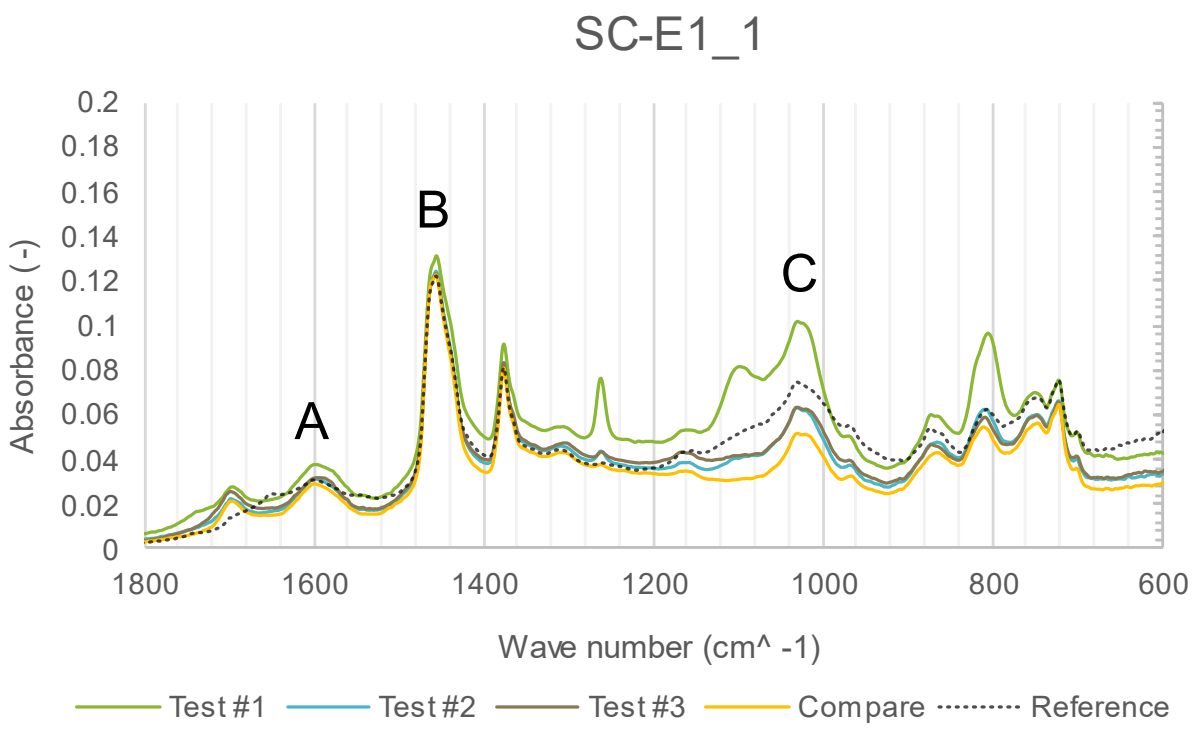

Figure B.1: FTIR Absorbance of R61/8 km51

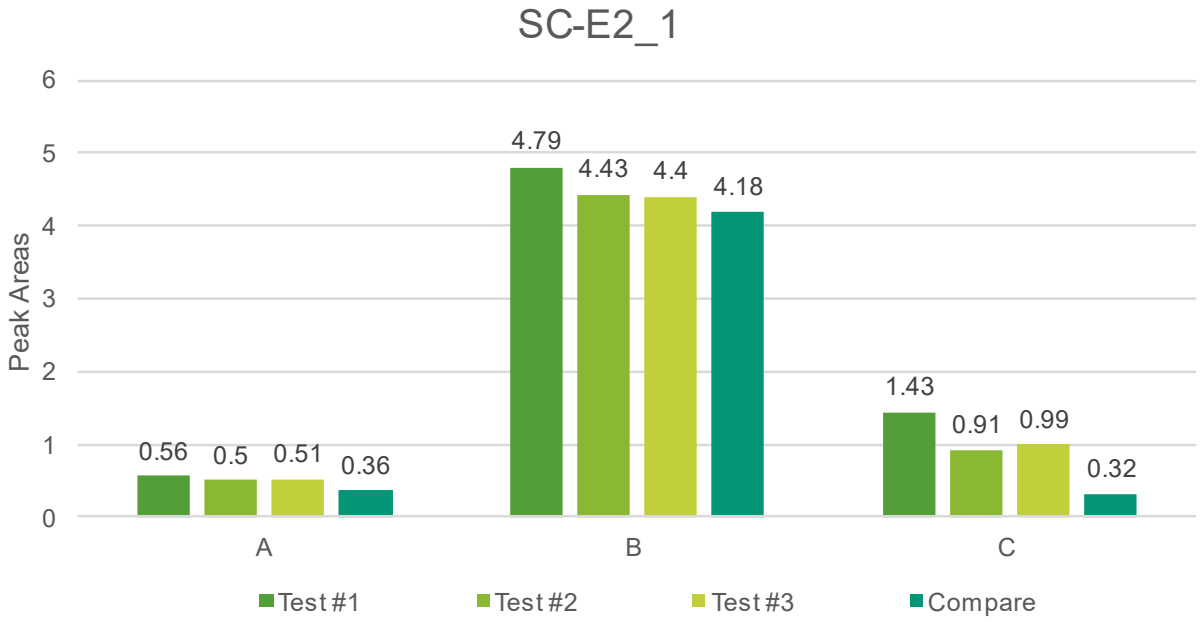

Figure B.2: Peak Areas of R61/8 km51

B.2 Young, modified multiple seal

- Seal name: N2/16 km71
- Age: 2 years

Variability from Section A.2:

- G_{vet} was the only durability parameter that complied with the recommended repeatability and reproducibility requirement.
- The durability parameters (G-R, T_{vet}, and T_{max}) suggest that the compare sample aged to a greater extent than the test samples
- In Black Space, the 25 mm DSR data of the compare sample is higher than the other test samples.

Figure B.3:

- Over the entire range, there is a very strong correlation between the absorbance of test 1 and test 2.
- All of the samples experience a slight peak at 1700 cm^{-1}, followed by a slightly higher peak at position A.
- At position B, the peak of test 3 is lower than the other samples, while the other samples correlate very well.
- The peaks at position C experience more variability. Here the peak of the compare sample is elevated, which suggest that the binder is harder. This observation corresponds to the ageing concluded from the raw data and the durability parameters.

Figure B.4:

- Peak areas of all of the samples are similar for range A. The differences do not correlate with the variability present in the durability parameters.
- Peak areas of test 3 is lower than the other samples. The difference between the areas correlates with the differences seen in G-R and T_{max}.
- The range C peak are of the compare sample is larger than the areas of the test samples. Differences do not correlate with the variability present in the durability parameters.

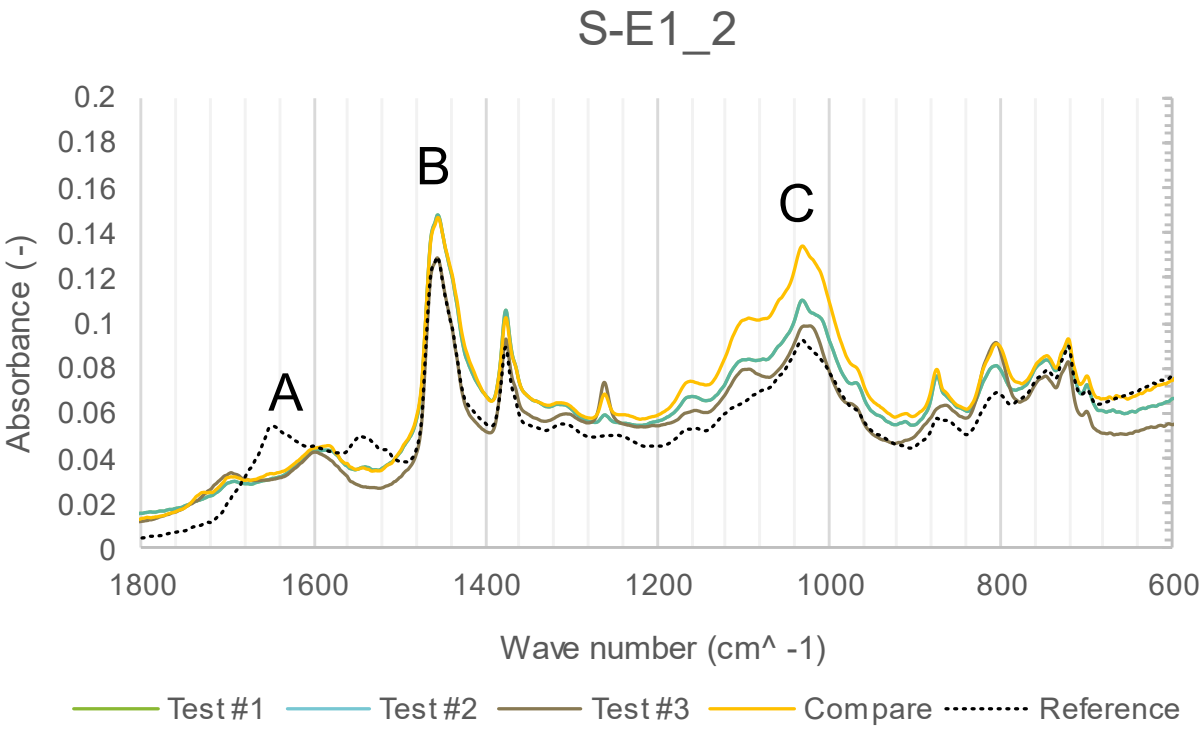

Figure B.3: FTIR Absorbance of N2/16 km71

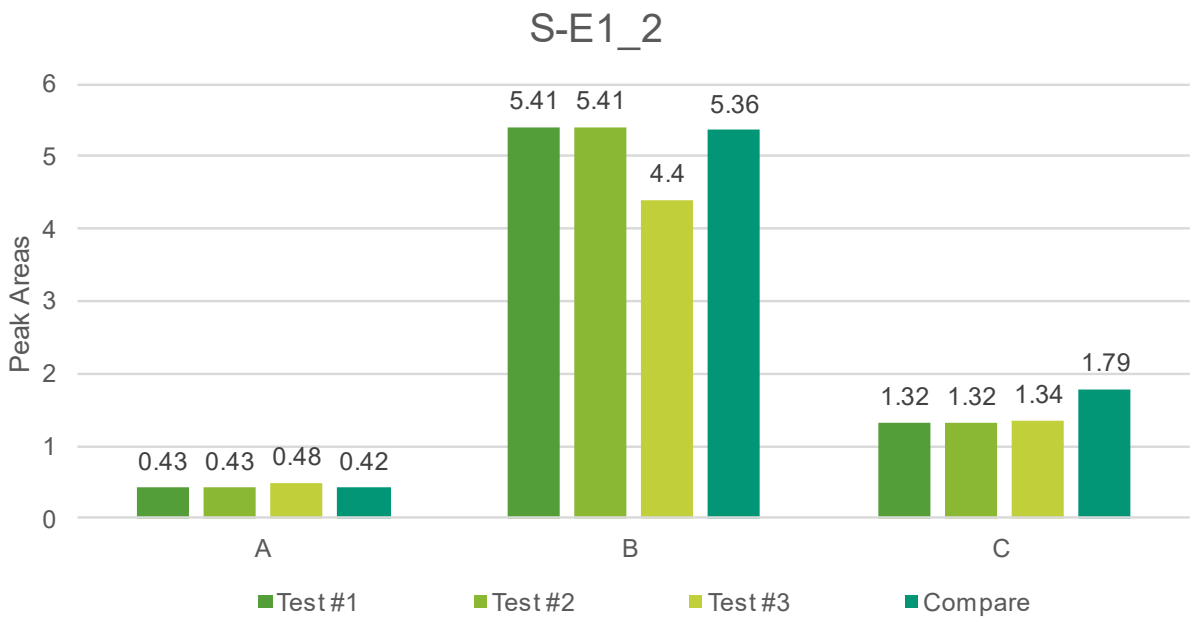

Figure B.4: Peak Areas of N2/16 km71

B.3 Old, modified double seal

- Seal name: N2/32 km21
- Binder age: 6 years

Variability from Section A.3:

- All of the durability parameters complied with the recommended reproducibility requirements.
- The Black Space Diagram revealed discrepancies between the 8 mm DSR data.

Figure B.5:

- Both samples experience a peak at 1700 cm^{-1} and a slightly higher peak at position A.
- At position A and position B, there is a strong correlation between the two samples
- At position C the peaks vary. The test sample has a higher peak, suggesting that the test sample is harder than the compare sample. The Black Space Diagram suggest the opposite.

Figure B.6:

- For range A, the compare sample has a larger peak area than the test sample. This difference correlates with the variability seen in G-R, G_{vet}, and $T_{max.}$
- For both range B and C, the test sample has a larger peak area than the compare sample. The difference between the areas corresponds with the difference between the T_{vet} values.

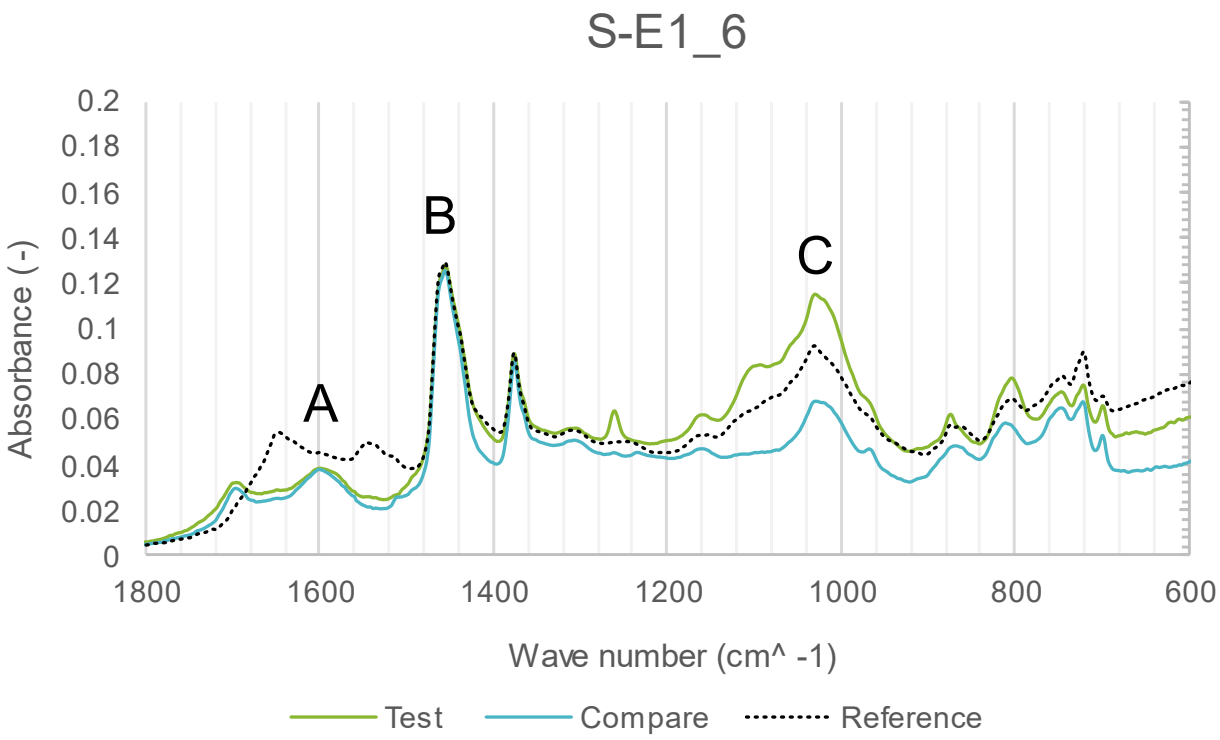

Figure B.5: FTIR Absorbance of N2/32 km21

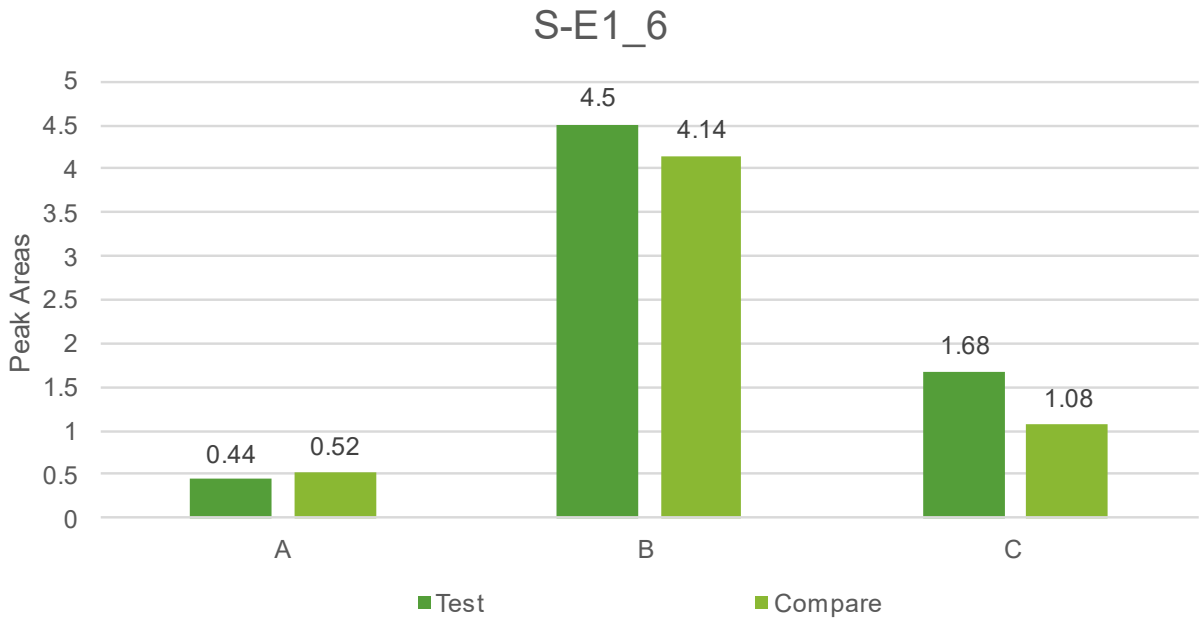

Figure B.6: Peak Areas of N2/32 km21

B.4 Old, modified double seal

- Seal Name: N8/8 km5.6
- Binder age: 7 years

Variability from Section A.4:

- All of the durability parameters comply with the recommended reproducibility requirements.
- G-R and ΔT_c suggest that the outer wheel track aged to a greater extent than the shoulder. The values of the other durability parameters are similar.
- In the Black Space Diagram, the raw data correlated well, expect for the 15°C isotherm of the shoulder-sample.

Figure B.7:

- Both samples experience a peak at 1700 cm^{-1} and a slightly higher peak at position A.
- At position A and B, there is a strong correlation between the two samples.
- At position C, the shoulder has a higher peak than the outer wheel track, which suggest the shoulder aged more than the outer wheel track. This does not correspond to the ageing suggested by the durability parameters.

Figure B.8:

- Both samples have the same peak areas for range A.
- For range B, the outer wheel track has a slightly larger peak area. This difference correlates with the difference seen from the values of G-R.
- For range C, the shoulder has a larger peak area. The difference between the peak areas of range C does not correlate to the differences seen in the durability parameters.

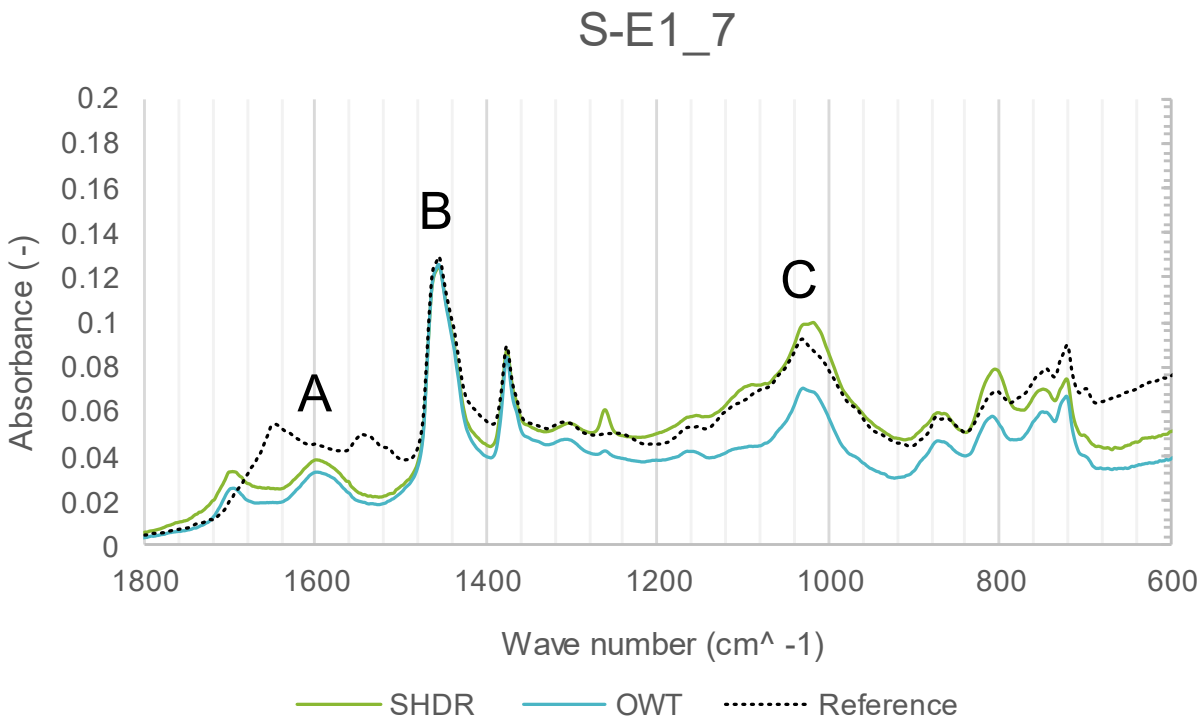

Figure B.7: FTIR Absorbance of N8/8 km5.6

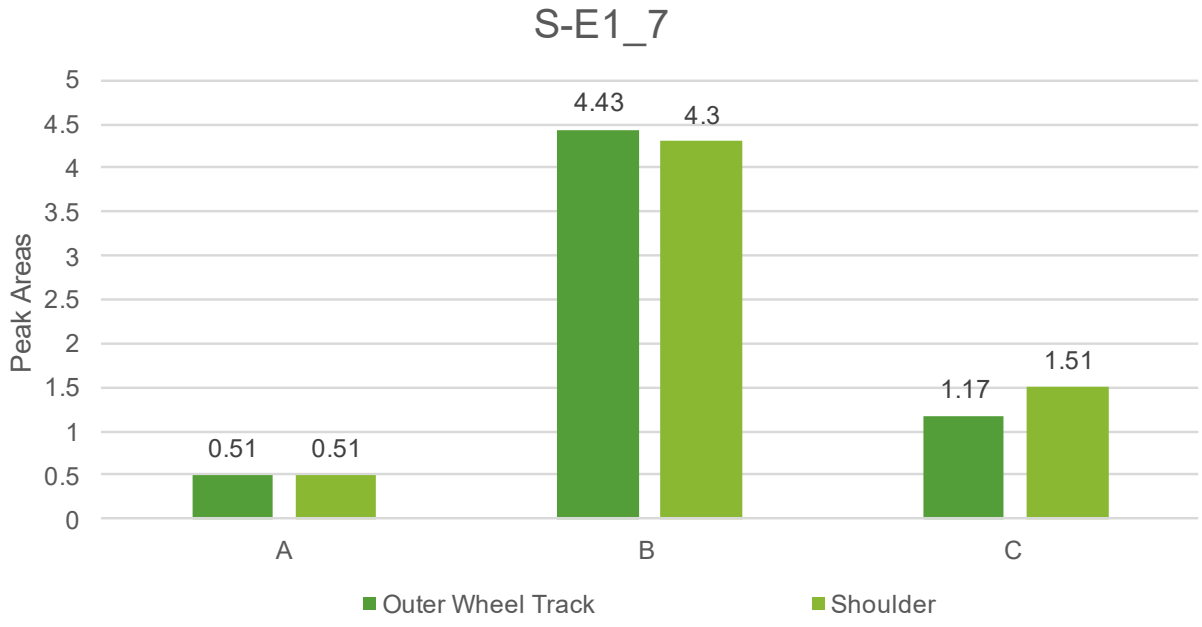

Figure B.8: Peak Areas of N8/8 km5.6

B.5 Old, modified double seal

- Seal name: N2/31 km3.6
- Binder age: 12 years

Variability from Section A.5:

- All of the durability parameters comply with the recommended reproducibility requirements.
- From the durability parameters there is not a clear indication of which sample aged to a greater extent.
- In the Black Space Diagram there is a strong correlation between the raw data points, except for the 15°C isotherm of the test sample. The 8 mm DSR data of the compare sample is slightly higher than the test sample.

Figure B.9:

- At 1700 cm^{-1}, both samples experience a peak of a similar height.
- At position A, the test sample experiences a slightly elevated peak.
- At position B, the peaks of both samples correlate well.
- The peaks at position C differ significantly. The peak of the compare sample is higher than the test sample, which corresponds to ageing presented in Black Space.

Figure B.10:

- For range A, the peak area of the test sample is higher than the compare sample.
- For range B, the peak area of the test sample is also higher than the compare sample.
- For range C, the peak area of the compare sample is noticeably larger than the test sample. Although the differences between the peak areas of range C correlate with the differences seen in G-R and G_{vet}, the extent to which the peak areas vary is more significant.

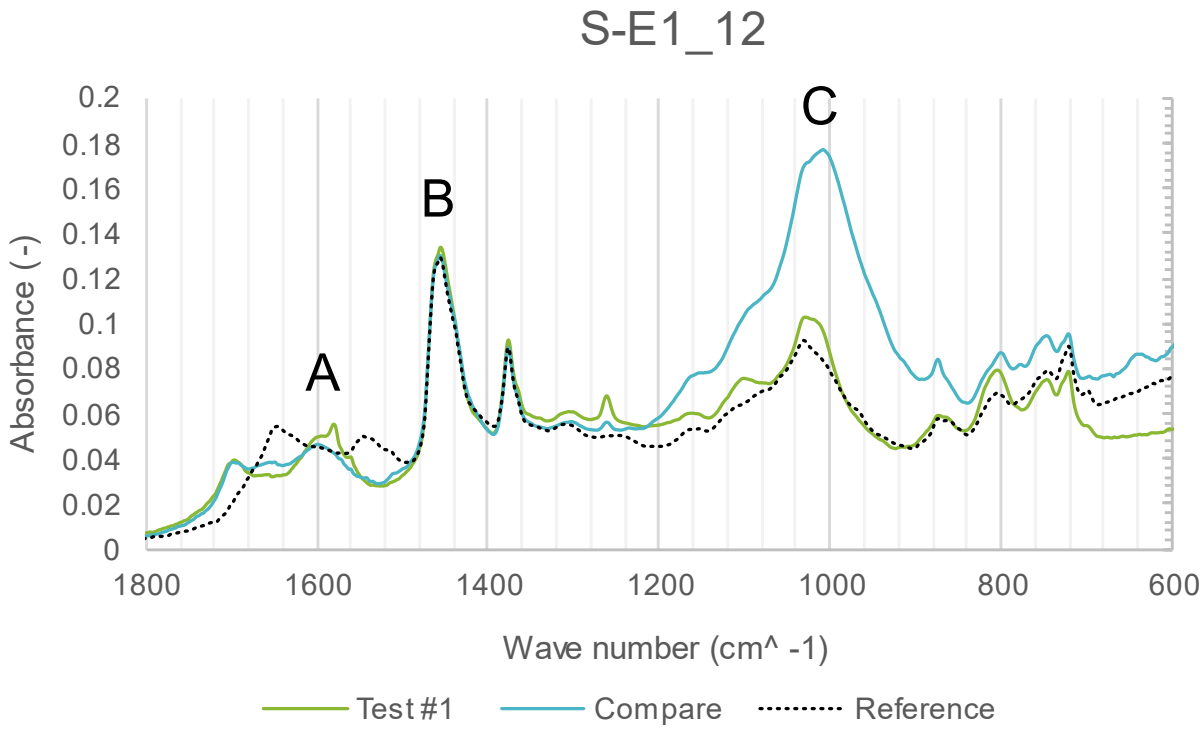

Figure B.9: FTIR Absorbance of N2/31 km3.6

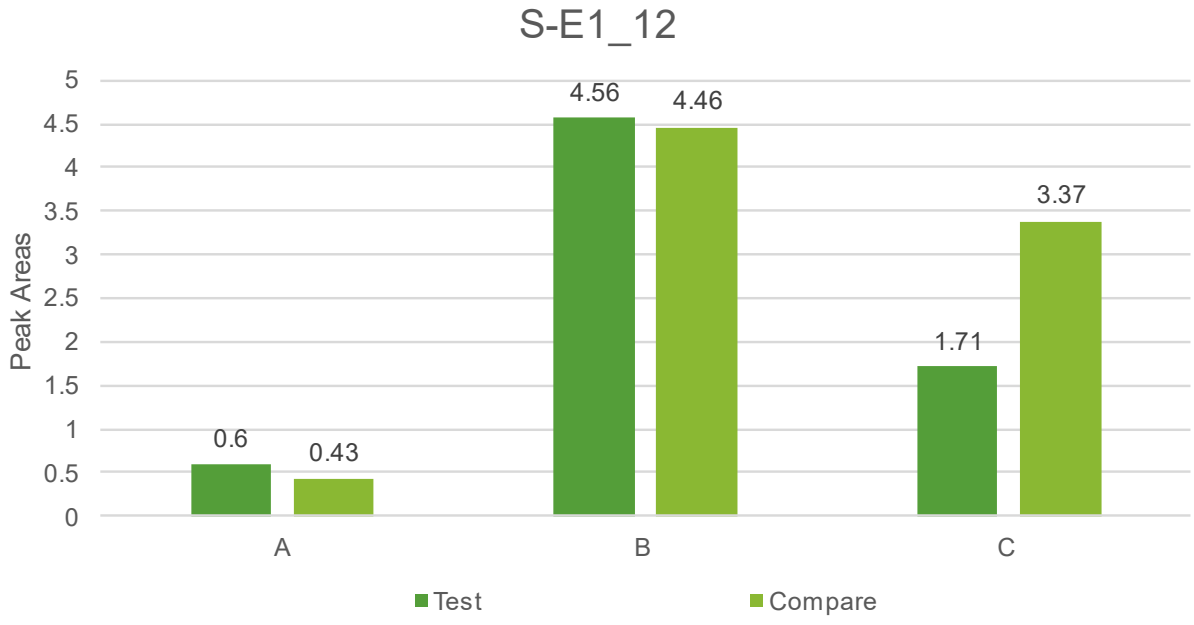

Figure B.10: Peak Areas of N2/31 km3.6

Appendix C: Ash Content

Preliminary testing, as explained in Section 3.4.3, was conducted in an attempt to determine the amount of fines present in the recovered binders. The following procedure was followed:

1. The binder was placed in the oven for 30 minutes at 160°C. During this time, the crucible was placed in the furnace at 700 °C for 10 minutes (Figure C.1). The crucible was removed from the furnace and placed in a desiccator to cool to room temperature for 5 minutes, after which the crucible was weighed. After sufficiently fluid, the binder was poured into the crucible and weighed. See Table C.1.
2. The crucible containing bitumen was placed on a Bunsen Burner (Figure C.2) and heated until the bitumen ignited (Figure C.3). The heat was maintained until a crust formed and the burning ceased (Figure C.4). While the binder was burning, various bitumen droplets were transported in the smoke and accumulated outside the crucible (Figure C.8).
3. The crust was broken (Figure C.5), and the crucible was placed back into the furnace at 800°C for 20 minutes. After 20 minutes the crucible was removed from the furnace (Figure C.6), placed in the desiccator to cool for 5 minutes, and weighed. This process was repeated until the mass of the remaining ash remained constant (Figure C.8). See Table C.2.
4. Calculate the ash content.

The two main challenges were time and test constraints. As seen from Table C.2, eight iterations were performed before the mass stabilised. The iterative process took approximately 4 hours. The ash content procedure would have to be performed on all 30 recoveries used in this study. The test constraint is introduced in step 2 of the ash content procedure. Various bitumen droplets escaped the crucible, while the bitumen was ignited by the Bunsen Burner. It was not possible to re-introduce these bitumen droplets into the crucible. The procedure assumes that all of the carbonaceous material (bitumen) is incinerated, while only impurities will remain. Since some of the bitumen escaped, the calculated ash content may not be accurate. It is believed that this test constraint can be addressed by developing a closed system wherein the ash content procedure can be performed. This system must be able to quantify or prevent bitumen loss that occur during the ash content procedure.

Table C.1: Initial Mass Values

Mass of crucible	45.77 g
Mass of crucible containing bitumen	55.99 g
Initial mass of bitumen	10.22 g

Figure C.1: Place Crucible in Furnace

Figure C.2: Place Crucible on Bunsen Burner

Figure C.3: Maintain Heat Once Ignited

Figure C.4: Crust Forms After Burning Ceased

Figure C.5: Break Crust

Figure C.6: Ash Reduction During Iterative Phase

Figure C.7: Remaining Ash (Mass Stabilised)

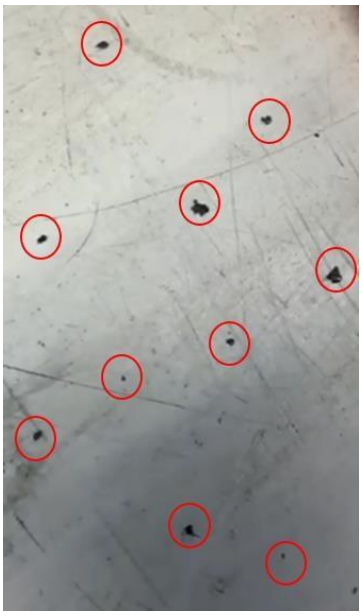

Figure C.8: Dispersion of Bitumen Droplets

Table C.2: Mass Change

Iteration	Mass of Crucible and Ash (g)	Mass of Remaining Ash (g)
1	47.90	2.13
2	47.55	1.78
3	47.01	1.24
4	46.58	0.81
5	46.09	0.32
6	45.83	0.06
7	45.82	0.05
8	45.82	0.05

$$\therefore Ash\ Content\ (\%) = \frac{0.05}{10.22} * 100 = 0.489\%$$

Appendix D: Data Modelling using RHEA Software